Analysis of Edge Problems in Statically-Loaded Fiber-Reinforced Laminated Plates by Linear Elastic Theory

William Michael Lucking

A Thesis

in

The Department

of

Mechanical Engineering

Presented in Partial Fulfillment of the Requirements for the degree of Doctor of Philosophy at Concordia University Montréal, Québec, Canada

January, 1989

ISBN 0-315-49122-1

ABSTRACT

Analysis of Edge Problems in Statically-Loaded
Fiber-Reinforced Laminated Plates
by Linear Elastic Theory

W. Michael Lucking, Ph.D.
Concordia University, 1988

Plates constructed of laminated continuous aligned fiber reinforced composite materials have been observed to delaminate at edges while under static and fatigue loads. Using a linear elastic homogeneous anisotropic material model and solving resulting equations of elasticity, the three dimensional stress states occurring near central circular holes and straight edges of laminated plates are investigated. Shortcomings in the theory and analysis are discussed. For holes, standard three-dimensional finite elements were used in a straightforward procedure to obtain approximate numerical results. For straight edges, a solution procedure is developed within this work based on a weighted residual method.

Specifically, holed plates having $[0/90]_s$, $[90/0]_s$, and [90/0] configurations of Graphite/Epoxy laminates with hole radius/plate thickness over a range of 1-25 under uniaxial uniform normal loading were modeled. Estimates of the maximum stress concentration for thick and thin plates using plane stress and plate theory formulas compared very well with FE results. Reinforcement of the hole with an isotropic ring of varying thickness and rigidity was found

to mitigate the boundary layer stresses and to reduce stress concentration in the plate. Measurements of hole surface deformations using miniature strain gages were done for $[0_7/90_7]_s$ and $[90_7/0_7]_s$ plates. Results indicate that the FE and measurement results agree well except at locations very close to the intersection of the layer interface and the edge where stresses have been surmised to possibly be singular.

For problems where the stress state does not vary along one cartesian axis (e.g. $\partial\sigma/\partial x=0$) a family of exponential functions are derived which satisfy the internal equations of elasticity. Particular solutions are then obtained by a Least Squares Boundary Collocation procedure. Comparison shows that this approach has advantages over methods appearing in literature.

Using the developed approach, the effects of axial, bending and twisting loads on the edge stresses of symmetric, antisymmetric, and asymmetric angle-ply and crossply laminates for shuffled and unshuffled layer sequences are investigated. The results show that the determination of the depth of the edge boundary layer and stress state within it requires solution of the complete boundary value problem for accuracy.

ACKNOWLEDGEMENTS

The author wishes to thank Dr. S.V. Hoa for introducing him to composite materials, and both Drs. T.S. Sankar and Hoa for patience, guidance and financial support in the thesis research and academic work. The financial support, services and equipment support of the Department of Mechanical Engineering of Concordia University are appreciated as well.

The financial and material support of the Canadian Department of National Defence, Defence Research Establishment Pacific in the form of a two year unsolicited contract for the experimental work and the use of Defence Research Establishment Pacific computing facilities in the final stages is gratefully acknowledged. The continued interest of Drs. Street, Barer, and Garrett in the author and this work provided great encouragement.

The author was awarded postgraduate fellowships from the NSERC and FCAR as well as the Transport fellowship from FCAR. The recognition and financial support of these organisations are highly valued.

Members of the Composite Materials Group at Concordia, Antoinette Di Maria, Pierre Drolet, and Ian Lulham deserve thanks and credit for contributing their effort and ideas to the laboratory work and its presentation.

The generous contribution of Dr. Qian Huang in translating a lengthy article from Chinese was very helpful and is appreciated.

Special thanks to Emanuella Beccarelli, Cathy Karkut and Mary Catherine Kropinski for excellent work on the figures.

The author wishes to thank many true friends for their interest, support, and friendship. Appreciated most of all, the faith of my parents was always a source of strength.

TABLE OF CONTENTS

CHAPTER 4

PROBLEMS IN WHICH STRESS DOES NOT VARY AXIALLY

LIST OF FIGURES

<u>Figure</u>

<u>Figure</u>

Figure

Figure

Figure

Figure

LIST OF TABLES

NOMENCLATURE

Symbol	
b	half width of strip
$\bar{C}$	matrix of Hooke's law stiffness coefficients
C_{ijkl}	Hooke's Law effective stiffness tensor in principal coordinate system
C'_{ijkl}	Hooke's Law effective stiffness tensor in rotated coordinate system
$\det(\bar{A})$	determinant of matrix $\bar{A}$
E_c	Young's modulus of isotropic reinforcement material
E_r, E_θ, E_z	Young's modulus of cylindrically orthotropic material
E_x, E_y, E_z	Young's moduli of rectilinearly orthotropic material
$\bar{f}_i$	dimensionless function vector
f_i	boundary condition function
$\bar{g}_i$	dimensionless function vector
G_c	Engineering Shear modulus
h	thickness of laminate ply group
$\imath$	imaginary number $=\sqrt{-1}$
i,j,k,l	integer indices
k_u, k_v, k_w	trial function constants
M_{ij}	edge moment per unit length
ℓ_o, ℓ_f, ℓ	initial, final, and gage length of strain gage
$\Delta\ell$	change in length of strain gage $(\ell_f - \ell_o)$
$\mathcal{L}_i$	linear differential operator
L	length parameter
n	outward normal surface vector
n_j	element of outward normal surface vector
N_{ij}	edge load per unit length

Symbol	
P	total load applied to edge of plate
r	radial distance perpendicular to singular line or point
r	radial coordinate (distance from centerline of hole)
S_{ijkl}	Hooke's law effective flexibility tensor
t	thickness parameter of plate or strip
T_j	surface traction in j direction
$\bar{\lambda}^T$	transpose of matrix $\bar{\lambda}$
U	strain energy
$\bar{u}$	displacement vector $\{u,v,w\}^T$
u,v,w	scalar elements of displacement vector
u_i	scalar elements of displacement vector $i=1,2,3$
u_j^*	imposed boundary displacement
W	plate width parameter
x,y,z	cartesian coordinates
α	ply orientation angle, lamination variable
β	dummy variable for integration if not otherwise defined
δ_i	Dirac delta function
ε_{ij}	strain tensor element
η_o, η_1	strain error constants
η_m	matrix volume content
η_f	fiber volume content
γ_{ij}	engineering shear strain
$\bar{\lambda}$	matrix of direction cosines
λ_{ij}	direction cosine
ν_c	Poisson's ratio for isotropic reinforcement material

Symbol

κ_{ui}, κ_{vi}	ratios k_u/k_w, k_v/k_w
π_i	constants in general solution
$\bar{\sigma}$	stress vector
σ_{ij}	stress tensor element ij
σ_o	gross applied stress
θ	angular coordinate
ψ_y, ψ_z	trial function exponent coefficients
$\bar{\Psi}$	vector of all trial function coefficients
φ_i	roots of characteristic equation
ω	power of singularity
{ }	denotes a vector
[ ]	denotes a square matrix
$-$	overbar denotes vector or matrix

LIST OF ABBREVIATIONS

Abbreviation	
CLT	Classical Lamination Theory
BL	Boundary Layer
BCLS	Boundary Collocation Least Squares
DOF	Degrees of Freedom
EM	Effective Modulus
FE(M)	Finite Element (Method)
IL	Interlaminar
MWR	Method of Weighted Residuals

CHAPTER 1

INTRODUCTION

The combining of two or more distinct phases to obtain a composite material has long been a successful approach to materials design. Composite laminates have emerged as very successful structural material system, not least, in particular, for plates and shells.

Continuous fibers of high stiffness and strength aligned in and bonded to a surrounding matrix are used to make layers in a composite laminate. As part of a mechanical system, each layer of the laminate having its fiber direction aligned with purpose in respect to a global frame, contributes to the system's response. Load-deformation response is tailored and can be such that conventional response (isotropic and homogeneous) is obtained from certain configurations, but this is a subset of the infinite bounded set of responses possible.

In any case, the system's behaviour must be understood and predictable. For innovative radical designs, analytical models may begin to provide useful information for all configuations.

As shown in Figure 1.1, structures may frequently contain holes, ply drops, and various joints. These details generally will cause stresses in their vicinity to be much above that of the surrounding material making them likely sites for initiation of damage.

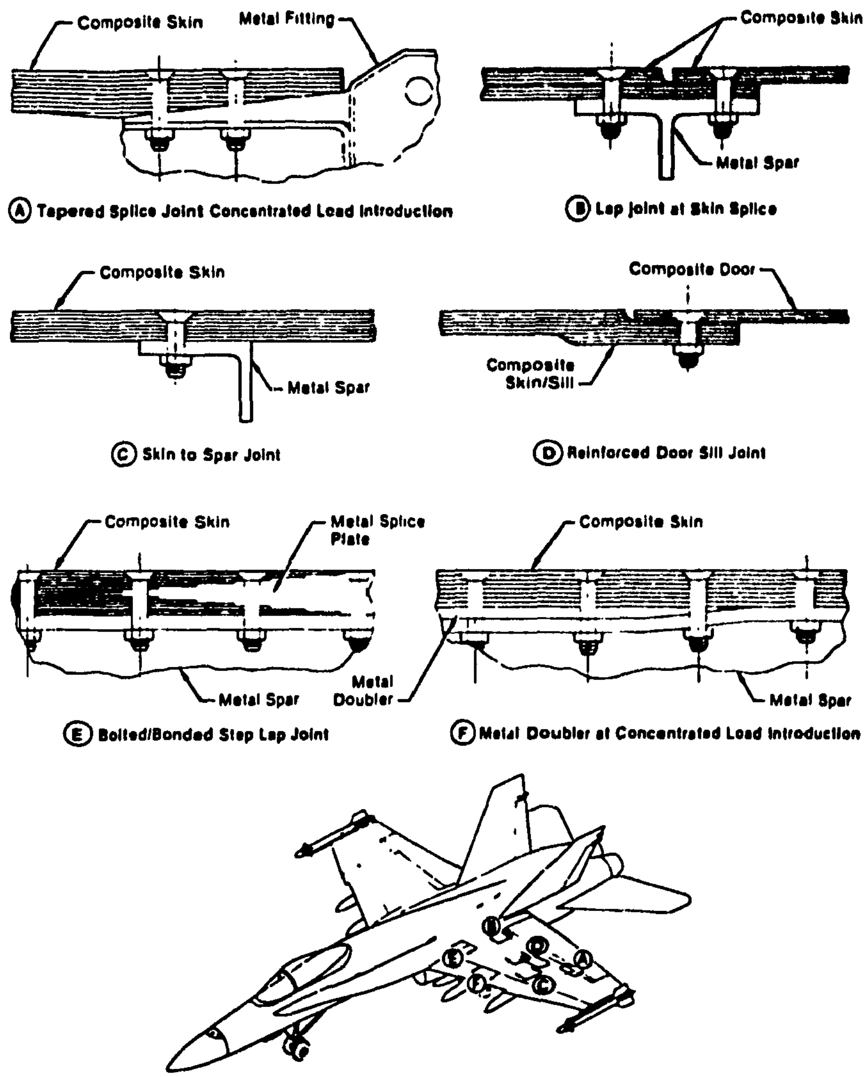

Figure 1.1 Bolted Composite Joints on the F-18.

The main objective in this work is to study the mechanical behaviour (i.e. the initial stress state) of some simple structural problems like circular holes and straight free edges. The work is comprised of investigating this mechanical behaviour by:

i) mathematical modelling based on the classical approach from infinitesimal displacement theory of linear elasticity and the approximate solution of equations from elasticity; and

ii) measurements of deformations.

In so doing, a contribution is made to the understanding of failure processes of composite laminates and the solution procedures. The material is modelled so that the response is linear and elastic. Only the initial geometry, material and loading are investigated.

In Chapter 2 the equations of elasticity are presented and examined. Indefinite aspects of the theory are discussed.

In Chapter 3 laminated plates with a central circular hole are studied both by finite element solution of the elasticity equations and measurements of hole surface strains using miniature foil resistance strain gages. Boundary layer stresses in specially orthotropic laminates are studied for the effects of varying of R/t and of reinforcing the hole with a bonded isotropic ring.

For straight edge problems a mode of solution is developed based on a method which is valid for problems where $\partial\sigma/\partial x=0$ in Chapter 4. The procedure is qualified by comparison with other available solutions. Results are generated to study various straight edge problems of angle-ply and crossply laminates in symmetric, unsymmetric and antisymmetric configurations with shuffled and unshuffled ply groups under normal, bending and twisting loads.

Chapter 5 summarizes the objectives, conclusions, and contributions made and includes recommendations for future work.

CHAPTER 2

THEORETICAL EQUATIONS FOR LINEAR ELASTIC ANISOTROPIC MATERIALS

2.1 Stress, Strain, and Hooke's Law Relation

In this chapter the mathematical theory to be used for the analysis of composite laminates modelled as layered homogeneous anisotropic linearly elastic solid media is presented. Although these same equations may be found elsewhere (e.g. Lekhnitskii(1977)) notations may differ; hence the concerned work is reviewed. In closing, there is a brief discussion on limitations of the theory.

In the mathematical analysis of continua the two quantities of stress and strain may be represented by cartesian tensors (see Jaeger(1966)). The nine components of stress are given by

$$\sigma_{ij} \qquad i,j=x,y,z \tag{2.1.1}$$

and the strains in terms of the displacements are

$$\varepsilon_{ij} = \tfrac{1}{2} \left(u_{i,j} + u_{j,i} \right) \quad i,j = x,y,z \tag{2.1.2}$$

Both the strains and stresses defined in this way constitute symmetric second order cartesian tensors. The strains differ from the commonly used engineering strains in the definition of the shear strains but are related by

$$\gamma_{ij} = 2\ \varepsilon_{ij} \text{ or } \varepsilon_{ij}+\varepsilon_{ji} \qquad i,j=x,y,z\ i\neq j. \qquad (2.1.3)$$

While the engineering strain eliminates redundancy it has a disadvantage in that it is not directly amenable to manipulation by tensor algebra.

From the theory of elasticity the linear relations between stress and strain for an anisotropic homogeneous material under certain conditions are represented by Hooke's law. Hooke's law is expressed, in the most general form, in compact *tensor* notation by

$$\sigma_{ij} = C_{ijkl}\ \ \varepsilon_{kl}\ i,j,k,l=x,y,z\ ; \qquad (2.1.4)$$

where C_{ijkl}, the 81 stiffness coefficients, are the elements of a fourth order tensor. It is understood that for this notation any subscript which appears twice on the right hand side indicates that a summation over its range of possible values must be performed.

The stress,strain and stiffness tensors must be defined in a coordinate system, however, they may easily be transformed to any other coordinate frame which is rotated with respect to the original (see Figure 2.1). Given the components of vectors $\bar{\sigma}$ and $\bar{\varepsilon}$ in the original frame and the direction cosines between the two frames, the components of

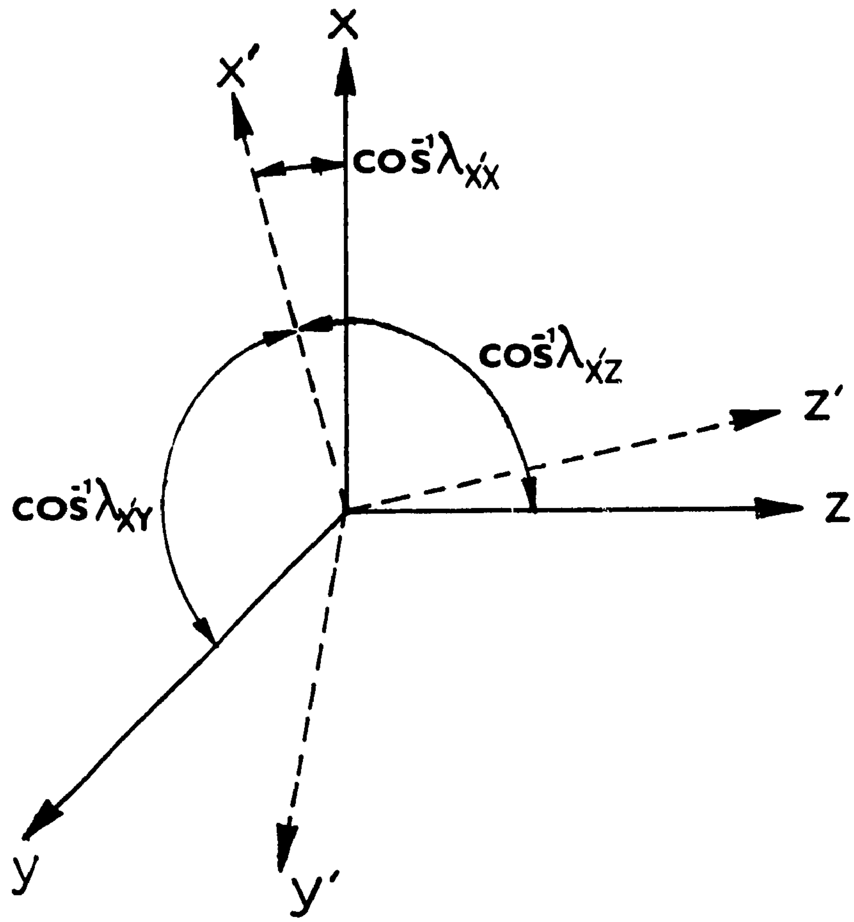

Figure 2.1 Examples of direction cosines for tensor transformation.

$\bar{\sigma}'$ and $\bar{\varepsilon}'$ in the rotated frame are given by

$$\begin{aligned} \sigma'_{ij} &= \lambda_{ik}\ \lambda_{jl}\ \sigma_{kl} \\ \varepsilon'_{ij} &= \lambda_{ik}\ \lambda_{jl}\ \varepsilon_{kl} \end{aligned} \quad i,j = x',y',z' \quad k,l = x,y,z \qquad (2.1.5)$$

where, for example, $\lambda_{z'z}$ is the cosine of the angle between the z axis (in the first frame) and the z'axis (in the rotated frame). In general, the order of suffixes is important; for example,

$$\lambda_{x'y} \neq \lambda_{y'x} \; .$$

The transformations may be presented in matrix form

$$\bar{\sigma}' = \bar{\lambda} \;\; \bar{\sigma} \;\; \bar{\lambda}^{T} \qquad (2.1.6)$$

$$\text{where} \quad \bar{\sigma} = \begin{bmatrix} \sigma_{xx} & \sigma_{xy} & \sigma_{xz} \\ \sigma_{yx} & \sigma_{yy} & \sigma_{yz} \\ \sigma_{zx} & \sigma_{zy} & \sigma_{zz} \end{bmatrix} ,$$

similarly for $\bar{\sigma}'$, $\bar{\varepsilon}$, $\bar{\varepsilon}'$;

$$\text{and} \quad \bar{\lambda} = \begin{bmatrix} \lambda_{x'x} & \lambda_{x'y} & \lambda_{x'z} \\ \lambda_{y'x} & \lambda_{y'y} & \lambda_{y'z} \\ \lambda_{z'x} & \lambda_{z'y} & \lambda_{z'z} \end{bmatrix} .$$

The elements of the C tensor after a rotation of coordinates are represented by

$$C'_{abcd}=\lambda_{ai}\lambda_{bj}\lambda_{ck}\lambda_{dl}\ C_{ijkl}\quad \begin{cases} i,j,k,l=x\ ,y\ ,z \\ a,b,c,d=x',y',z' \end{cases} \qquad (2.1.7)$$

It is impractical to express this in matrix form since it requires a 3x3x3x3 matrix. For a homogeneous material, pure translation of the coordinate system will have no effect on the C tensor.

The strain energy density is a mathematically homogeneous positive definite quadratic scalar function defined by

$$\mathfrak{U} = \frac{1}{2}\ C_{ijkl}\ \varepsilon_{ij}\varepsilon_{kl}\ \ i,j,k,l=x,y,z \qquad (2.1.8)$$

Since $\mathfrak{U}$ is a scalar it is invariant with repect to a change of coordinates; it is related to stress by

$$\sigma_{ij}=\partial\ \mathfrak{U}/\ \partial\ \varepsilon_{ij}=C_{ijkl}\ \varepsilon_{lk}. \qquad (2.1.9)$$

Because the stress and strain tensors are symmetric only 36 coefficients are required to give the six discrete stresses in terms of the six discrete strains. The six stresses may be represented by a vector and obtained by the matrix multiplication

$$\bar{\sigma}\ =\ \bar{\bar{C}}\ \bar{\varepsilon} \qquad (2.1.10)$$

where now we redefine

$$\bar{\bar{C}} = \begin{bmatrix} C_{xxxx} & C_{xxyy} & C_{xxzz} & C_{xxyz} & C_{xxxz} & C_{xxxy} \\ & C_{yyyy} & C_{yyzz} & C_{yyyz} & C_{yyxz} & C_{yyxy} \\ & & C_{zzzz} & C_{zzyz} & C_{zzxz} & C_{zzxy} \\ \text{s y m m e t r i c} & & & C_{yzyz} & C_{yzxz} & C_{yzxy} \\ & & & & C_{xzxz} & C_{xzxy} \\ & & & & & C_{xyxy} \end{bmatrix}$$

$$\text{and} \quad \bar{\sigma} = \begin{bmatrix} \sigma_{xx} \\ \sigma_{yy} \\ \sigma_{zz} \\ \tau_{yz} \\ \tau_{xz} \\ \tau_{xy} \end{bmatrix}, \quad \bar{\varepsilon} = \begin{bmatrix} \varepsilon_{xx} \\ \varepsilon_{yy} \\ \varepsilon_{zz} \\ \gamma_{yz} \\ \gamma_{xz} \\ \gamma_{xy} \end{bmatrix}$$

The matrix $\bar{\bar{C}}$ must be symmetric for reciprocity to occur. That is, given 2 arbitrary states of strain $\bar{\varepsilon}^1$ and $\bar{\varepsilon}^2$ then since $C_{ijkl}\varepsilon^1_{ij}\varepsilon^2_{kl}=C_{klij}\varepsilon^1_{kl}\varepsilon^2_{ij}$ we must have $C_{ijkl}=C_{klij}$. The strain energy U can be represented by

$$U = \tfrac{1}{2}\,\bar{\varepsilon}^T \;\bar{\bar{C}}\; \bar{\varepsilon} \qquad (2.1.11)$$

and so $\bar{\bar{C}}$ is also positive definite since

$$U \geq 0 \text{ for any } \bar{\varepsilon} \neq \{0\}$$

in order for the body to remain stable.

The number of independent elements remaining may be further reduced by considering the elastic symmetry of a material. A material is said to have elastic symmetry when $\bar{C}$ remains invariant under a coordinate transformation. For example, if $-\lambda_{zz'}=\lambda_{xx'}=\lambda_{yy'}=1$ with all other direction cosines zero, then if C remains invariant it has reflexive symmetry across the plane z=0. Hashin(1972) has shown that a uniaxially fiber reinforced composite material with random positioning of the fibers in the yz plane as shown in Figure 2.2 can be represented as being transversely isotropic (one in which $\bar{C}$ is invariant for any rotation about the fiber axis) in the yz plane. The following elements must vanish:

$C_{zzyz}, C_{yyyz}, C_{xxyz}, C_{yzxy}, C_{yzxz}, C_{xzxy}, C_{zzxy}, C_{yyxy}, C_{zzxz}, C_{yyxz}, C_{xxxy}, C_{xxxz}$ and the stiffness matrix then becomes

$$\bar{C} = \begin{bmatrix} C_{xxxx} & C_{xxyy} & C_{xxzz} & 0 & 0 & 0 \\ & C_{yyyy} & C_{yyzz} & 0 & 0 & 0 \\ & & C_{zzzz} & 0 & 0 & 0 \\ \text{s y m m e t r i c} & & & C_{yzyz} & 0 & 0 \\ & & & & C_{xzxz} & 0 \\ & & & & & C_{xyxy} \end{bmatrix}$$

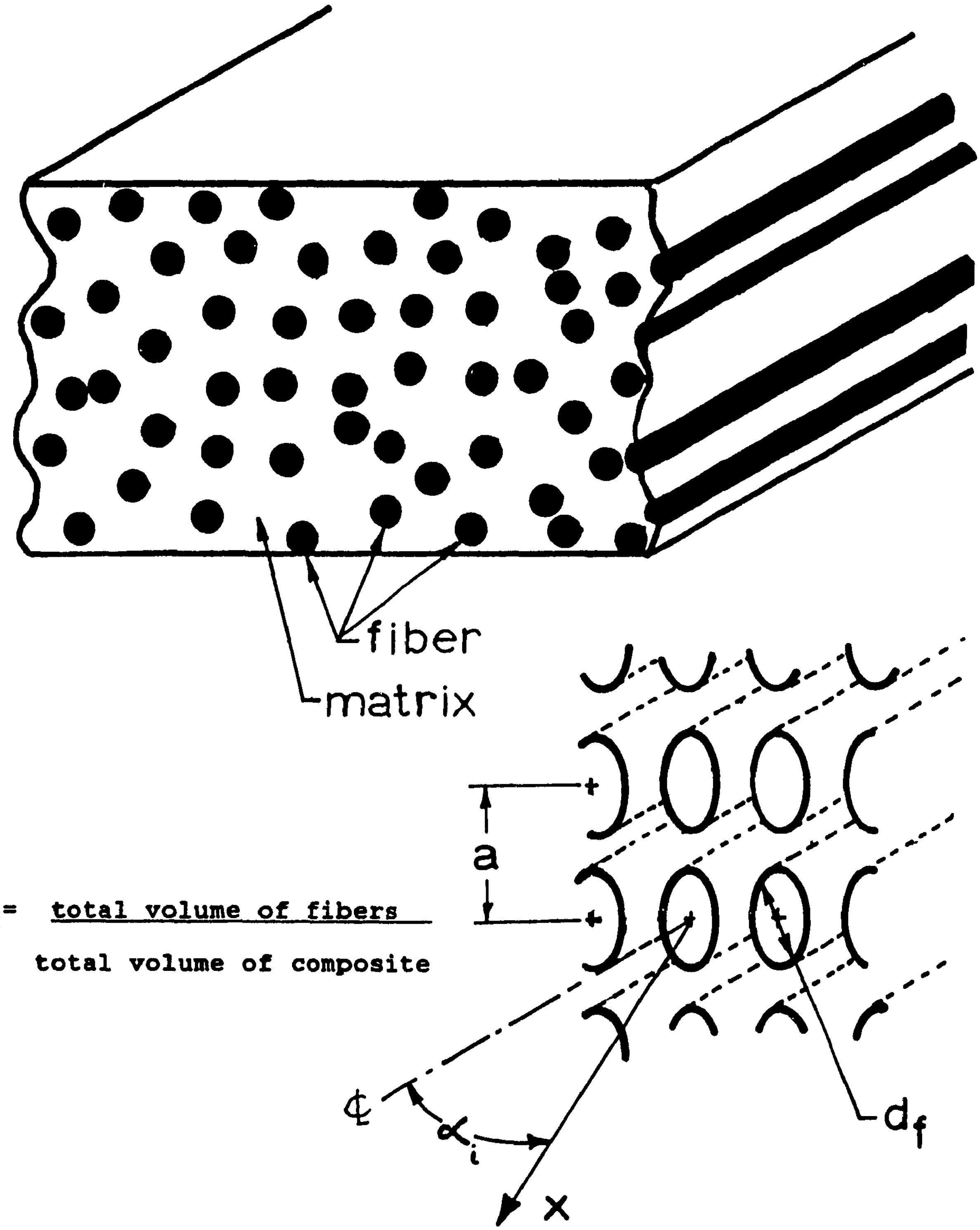

$$\eta_f = \frac{\text{total volume of fibers}}{\text{total volume of composite}}$$

Figure 2.2 Cross section of semi-random fiber reinforced material as described in Hashin(1972).

Further, $C_{yyyy}=C_{zzzz}$, $C_{xxyy}=C_{xxzz}$, $C_{xzxz}=C_{xyxy}$, $C_{yzyz}=\frac{1}{2}(C_{yyyy}-C_{yyzz})$ must hold reducing the number of independent coefficients to five. This stiffness matrix holds for a specifically oriented coordinate system, often called the principal coordinate system where the x axis aligns with the fiber direction.

In general, each layer of a laminate has its principal coordinates differing from some global system for the laminate by a rotation about the z' axis, as shown in Figure 2.3. To express the stiffness matrix coefficients in the coordinate system of the laminate requires that the tensor be transformed and then the independently rotated coefficients be used to populate the matrix. To simplify the notation the suffixes in each term are redefined as follows:

1-xx; 2-yy; 3-zz; 4-zy,yz; 5-xz,zx; 6-xy,yx

In unprimed coordinates the direction 1 is the fiber direction. Using Equation (2.1.7) with the angle between the primed global coordinates and the unprimed principal coordinates equal to α such that

$$\bar{\lambda} = \begin{bmatrix} \lambda_{x'x} & \lambda_{x'y} & \lambda_{x'z} \\ \lambda_{y'x} & \lambda_{y'y} & \lambda_{y'z} \\ \lambda_{z'x} & \lambda_{z'y} & \lambda_{z'z} \end{bmatrix} = \begin{bmatrix} \cos(\alpha) & \sin(\alpha) & 0 \\ -\sin(\alpha) & \cos(\alpha) & 0 \\ 0 & 0 & 1 \end{bmatrix}; \quad (2.1.13)$$

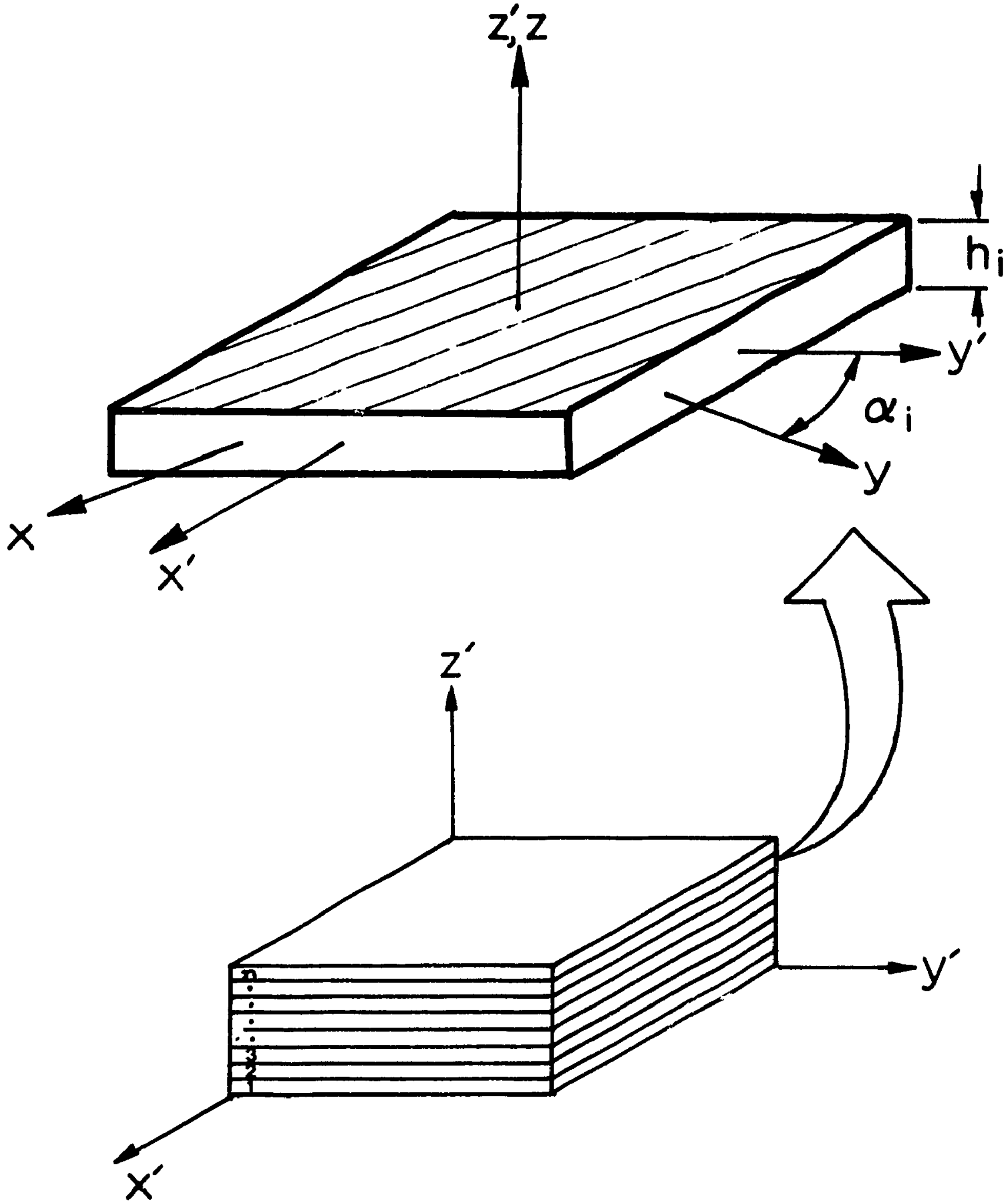

Figure 2.3 Lamination parameters: angle of orientation of layer's principal coordinates in laminate system and the layer thickness.

the non-zero primed coefficients of the $\bar{C}$ matrix in the new notation are:

$$C'_{11}=C_{11}\cos^4(\alpha)+C_{22}\sin^4(\alpha)+ 2(C_{12}+2C_{66})\sin^2(\alpha)\cos^2(\alpha)$$

$$C'_{12}=(C_{11}+ C_{22}-4C_{66})\cos^2(\alpha)\sin^2(\alpha)+C_{12}(\sin^4(\alpha)+\cos^4(\alpha))$$

$$C'_{13}= C_{13}\cos^2(\alpha) + C_{23}\sin^2(\alpha)$$

$$C'_{16}=(-C_{11}+C_{12}+2C_{66})\cos^3(\alpha)\sin(\alpha)$$
$$+(-C_{12}+C_{22}-2C_{66})\sin^3(\alpha)\cos(\alpha)$$

$$C'_{22}= C_{22}\cos^4(\alpha)+ C_{11}\sin^4(\alpha)+ 2 (C_{12}+2C_{66})\sin^2(\alpha)\cos^2(\alpha)$$

$$C'_{23}= C_{13}\sin^2(\alpha) + C_{23}\cos^2(\alpha)$$

$$C'_{26}=(-C_{11}+C_{12}+2C_{66})\cos(\alpha)\sin^3(\alpha)$$
$$+(-C_{12}+C_{22}-2C_{66})\sin(\alpha)\cos^3(\alpha)$$

$$C'_{33}= C_{33} \qquad (2.1.14)$$

$$C'_{36}= (C_{23}-C_{13})\cos(\alpha)\sin(\alpha)$$

$$C'_{44}= C_{55}\sin^2(\alpha)+ C_{44}\cos^2(\alpha)$$

$$C'_{45}= (C_{44}- C_{55})\sin(\alpha)\cos(\alpha)$$

$$C'_{55}= C_{44} \sin^2(\alpha) + C_{55}\cos^2(\alpha)$$

$$C'_{66}=C_{66}(\sin^4(\alpha)+\cos^4(\alpha))+(C_{11}+C_{22}-2C_{12}-2C_{66})\sin^2(\alpha)\cos^2(\alpha)$$

and $C'_{14}=C'_{15}=C'_{24}=C'_{25}=C'_{34}=C'_{35}=C'_{46}=C'_{56}=0$.

The stiffness matrix then becomes populated as follows

$$\bar{\bar{C}}' = \begin{bmatrix} C'_{11} & C'_{12} & C'_{13} & 0 & 0 & C'_{16} \\ & C'_{22} & C'_{23} & 0 & 0 & C'_{26} \\ & & C'_{33} & 0 & 0 & C'_{36} \\ & \text{s y m m e t r i c} & & C'_{44} & C'_{45} & 0 \\ & & & & C'_{55} & 0 \\ & & & & & C'_{66} \end{bmatrix}$$

so that

$$\bar{\sigma}' = \bar{\bar{C}}' \, \bar{\varepsilon}'.$$

The unprimed coefficients in the principal coordinates can be expressed using the engineering notation as

$$\begin{aligned} C_{11} &= E_{11}(1-\nu_{23}\nu_{32})/DET \\ C_{12} &= E_{22}(\nu_{12}+\nu_{13}\nu_{32})/DET \\ C_{13} &= E_{33}(\nu_{13}+\nu_{12}\nu_{23})/DET \\ C_{22} &= E_{22}(1-\nu_{13}\nu_{31})/DET \\ C_{23} &= E_{22}(\nu_{32}+\nu_{31}\nu_{12})/DET \\ C_{33} &= E_{33}(1-\nu_{12}\nu_{21})/DET \\ C_{44} &= G_{23} \\ C_{55} &= G_{13} \\ C_{66} &= G_{12} \end{aligned} \tag{2.1.15}$$

where $E_{22}=E_{33}$, $\nu_{12}=\nu_{13}$, $G_{12}=G_{13}$, $G_{23}=E_{22}/2(1+\nu_{23})$,

$\nu_{13}E_{33}=\nu_{31}E_{11}$, $\nu_{12}E_{22}=\nu_{21}E_{11}$, and $\nu_{23}=\nu_{32}$ (leaving five independent constants as before) and

$$DET=1-\nu_{12}\nu_{21}-\nu_{13}\nu_{31}-\nu_{23}\nu_{32}-\nu_{21}\nu_{13}\nu_{32}-\nu_{31}\nu_{12}\nu_{23} .$$

The relation between G_{23}, E_{22}, and ν_{23} shows transverse isotropy of the material.

2.2 Displacement Equations of Equilibrium

For a body at rest under the influence of only surface tractions the stresses must satisfy the three equations of equilibrium

$$\sigma_{ij,j}=0 \quad i,j=x,y,z \qquad (2.2.1)$$

where the subscript(s) after a comma denotes partial differentiation with respect to that variable. On the surface

$$T_i=\sigma_{ij}n_j \quad i,j=x,y,z \qquad (2.2.2)$$

must be satisfied, where T is the surface traction vector and n is the outward normal vector of the surface.

The general equilibrium equations in terms of the displacements are obtained by substituting Equations (2.1.2) into (2.1.4) and this into (2.2.1) to get

$$(C_{ijkl}(u_{l,k} + u_{k,l}))_{,j} = 0 \quad i,j,k,l=x,y,z \qquad (2.2.3)$$

in compact tensor notation. This yields three linear homogeneous elliptic second order coupled partial differential equations with constant coefficients. The surface tractions are represented in terms of the displacements by

$$T_i = \frac{1}{2} C_{ijkl}(u_{k,l}+u_{l,k})\, n_j \quad i,j,k,l=x,y,z \qquad (2.2.4)$$

For some problems a cylindrical coordinate system may be more suitable. The cylindrical coordinates are r,θ,z. Rotating primed coordinates by θ we get

$$x'=r \;,\; y'=\theta \;,\; \text{and } z'=z.$$

The strain-displacement relations are then given by

$$\varepsilon_r = u_{x',r}$$

$$\varepsilon_\theta = \frac{u_{x'}}{r} + \frac{u_{y',\theta}}{r}$$

$$\varepsilon_z = u_{z',z} \tag{2.2.6}$$

$$\gamma_{r\theta} = \frac{u_{x,\theta}}{r} + u_{y',r} - \frac{u_{y'}}{r}$$

$$\gamma_{rz} = u_{x',z} + u_{z',r}$$

$$\gamma_{z\theta} = u_{y',z} + \frac{u_{z',\theta}}{r}$$

and the equations of equilibrium are

$$\sigma_{r,r} + \frac{\tau_{r\theta,\theta}}{r} + \tau_{rz,z} + \frac{(\sigma_r - \sigma_\theta)}{r} = 0$$

$$\tau_{rz,r} + \frac{\tau_{z\theta,\theta}}{r} + \sigma_{z,z} + \frac{\tau_{rz}}{r} = 0 \tag{2.2.7}$$

$$\tau_{r\theta,r} + \frac{\sigma_{\theta,\theta}}{r} + \tau_{z\theta,z} + \frac{2\tau_{r\theta}}{r} = 0$$

The cylindrical stresses and strains are equal to the rotated cartesian stresses and strains and the equations of equilibrium may be expressed in terms of the rotated displacements. However, the stiffness coefficients of these equations will then be periodic functions of θ obtained by rotating $\bar{C}$ through the angle $\theta-\alpha$ using Equation (2.1.14) rather than constants. It can be seen that if the surface tractions and displacements and the geometry of a body have the same rotational symmetry as the stiffness(i.e. period of 2π) then the displacement functions which are solutions in these coordinates will also be periodic functions of θ with period 2π. This property of the solution may be used as a boundary condition to reduce the size of the domain, a factor which is often important to the effort required in analysis.

2.3 Dimensional Analysis

For every mathematical-physical problem a partial formulation of the solution in dimensionless parameters may be had by dimensional analysis. Further, by making the parameters non-dimensional, their number may be reduced thereby generalizing the results and avoiding investigation of redundant parameters.

Within the theoretical framework already described, the following material, geometry, and loading parameters are relevant to laminated composite plates with holes. As depicted they are R_x, R_y, t, w, l (for a circular hole $R_x=R_y=R$) as the structure's geometric parameters (see Figure 2.4) ; r, z, θ or x, y, z as the coordinates ; N_x, N_y, N_{xy}, M_x, M_y, M_{xy}

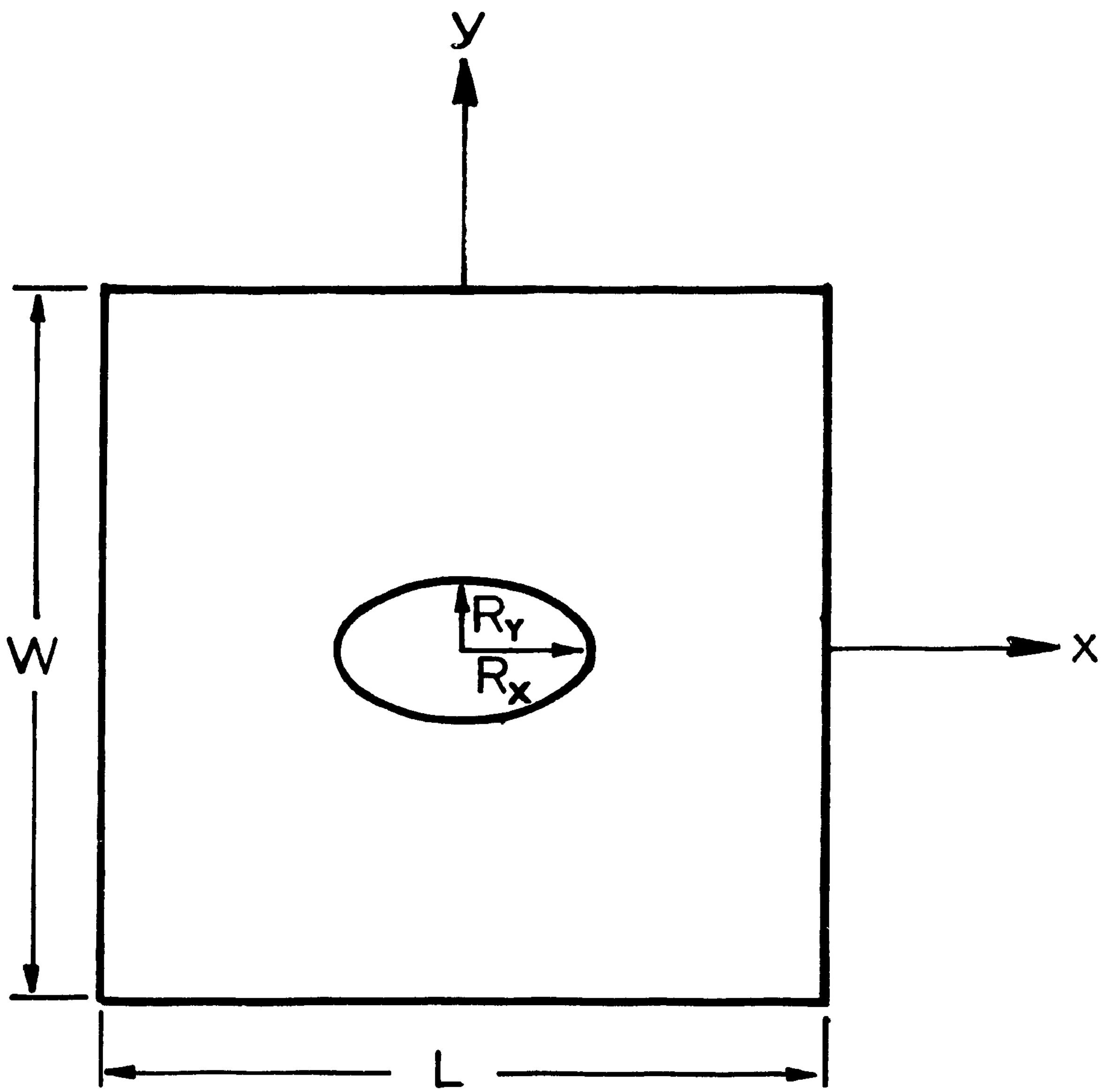

Figure 2.4 Plate geometric parameters.

which are defined as

$$N_{ij} = \int_{-t/2}^{t/2} \sigma_{ij} dz, \qquad M_{ij} = \int_{-t/2}^{t/2} \sigma_{ij} z dz \quad i,j=x,y,z \quad (2.3.1)$$

as the edge loads (Figure 2.5); α_i, h_i as the lamination parameters (Figure 2.3); a and η_f as the microstructural geometric variables (Figure 2.2); and $E_{f1}, E_{f2}, \nu_{f1}, \nu_{f2}, G_f$, as the engineering constants for transversely isotropic fibers as well as E_m, ν_m for the isotropic matrix material.

By using the Effective Modulus (EM) approach, the elastic moduli of the constituents and η_f are replaced by their equivalent effective moduli E_{11}, $E_{22}, \nu_{12}, \nu_{23}, G_{12}, G_{23}$. Because the problem is linearly elastic, using standard methods the solution for any component of the displacement in a plate with an elliptical hole, for example, can be expressed in the form

$$\bar{u} = \frac{N_x}{E_{11}} \bar{g}_1 + \frac{N_y}{E_{11}} \bar{g}_2 + \frac{N_{xy}}{E_{11}} \bar{g}_3 +$$

$$\frac{M_x}{tE_{11}} \bar{g}_4 + \frac{M_y}{tE_{11}} \bar{g}_5 + \frac{M_{xy}}{tE_{11}} \bar{g}_6 \qquad (2.3.2)$$

where $\bar{g}_1, \bar{g}_2, \bar{g}_3 \ldots \bar{g}_6$ are all vectors of dimensionless functions of the variables

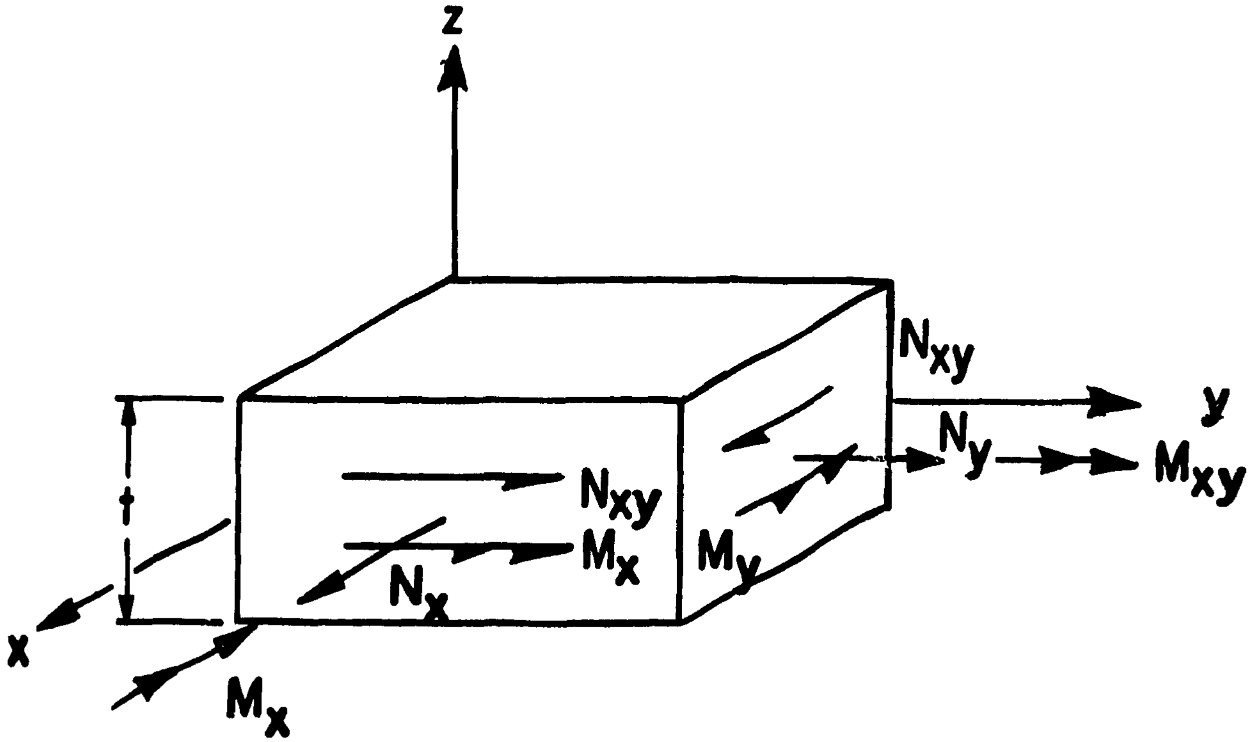

Figure 2.5   Plate loading parameters.

$$\frac{r}{R_x},\ \theta,\ \frac{z}{t},\ \frac{R_x}{R_y},\ \frac{R_x}{t},\ \frac{w}{R_x},\ \frac{l}{R_x},\ \eta_f,\ \frac{R_x t}{a^2},\ \alpha_i,\ \frac{h_i}{t},\ \frac{E_{22}}{E_{11}},\ \nu_{12},\nu_{23},\frac{G_{12}}{E_{11}}$$

In this solution there are 2 fewer variables than there were at the outset. The stresses and strains are expressed similarly since they are linear combinations of the displacement first partial derivatives.

$$\bar{\sigma} = \frac{N_x}{t}\bar{f}_1 + \frac{N_y}{t}\bar{f}_2 + \frac{N_{xy}}{t}\bar{f}_3 + \frac{M_x}{t^2}\bar{f}_4 + \frac{M_y}{t^2}\bar{f}_5 + \frac{M_{xy}}{t^2}\bar{f}_6 \qquad (2.3.3)$$

where $\bar{f}_i$ are vectors of dimensionless functions. These relations exhibit the linear relation between load and response and disclose the possibility of superposing the solutions from linearly independent combinations of the loads.

2.4 Discussion of the Theory

All of the previous material in this chapter, and indeed, all the other works which use the presented model have been presented with the tacit assumption that some mapping exists between field variables in the classical approach and those of models in which the individual phases (microstructure) are accounted for directly. It is beyond the scope of this work to assess the limitations of this theory, but some understanding of the verity of the model is possible without too much detail.

One interpretation discussed by Hashin(1983) is that of replacing field variables in a material having statistically homogeneous material properties by moving averages. In this approach a representative volume element (RVE) is used over which the field variables (e.g. displacement) are averaged. To be statistically homogeneous the average material properties (e.g. the relation between stress and strain) do not change as the RVE is moved through the body. So long as the size of the composite body is much larger than the RVE, and in turn the RVE is much larger than the unit cell (see Figure 2.2) then the classical relation (Equation (2.1.4)) between averaged stress and strain is valid for most practical problems. Therefore, replacing the composite with an equivalent homogeneous body is usually adequate. For example, in Equation (2.3.1) where the constituent material's moduli are replaced by the effective moduli, the geometrical parameter $R_x t/a^2$ does not vanish and still has some effect on the problem. However, so long as this parameter is large then for averaged field variables using a suitable RVE the two models will approximately agree. However, the classical approximation is based on the assumption of negligible strain gradients (see Hashin(1983)) and so is questionable for very high strain gradients.

When is the model invalid? For instance Pagano(1976) modeled a symmetric laminate having finite width and thickness with one reinforced and one unreinforced layer which included discretely modeled regularly arranged fibers surrounding the interface at the free edge. In the homogeneous model stress singularities and so high strain gradients are surmised to occur at the intersection of the interface between layers and the unloaded edge of the laminate. Even near the singular point, averages over a unit cell's dimension in the micro-model were found to agree increasingly with the EM model as the relative fiber diameter decreased (i.e. as Wt/a^2 increased) and all other relative parameters remained constant. Encouragingly, these results show that EM validity can improve as the fibers become relatively small.

CHAPTER 3

ANALYSIS OF PLATES HAVING A CENTRAL CIRCULAR HOLE

3.1 Introduction and Literature Survey

Stress concentration around cutouts in homogeneous plates is a well known phenomena. In regard to laminates, as has been observed in straight edge problems, it is expected that Classical Lamination Theory (CLT) will suffice at some distance from the hole edge i.e. outside the boundary layer. For this region numerous exact and approximate solutions have been compiled for a variety of problems in anisotropic homogeneous plates under edge loading; e.g. Green and Zerna(1954), Lekhnitskii(1968), Lekhnitskii(1977), and Savin(1961). In particular, Savin presents a comprehensive collection of plane stress and plate theory solutions for plates with holes. Using the CLT approach these solutions can be used to approximate stresses in composite laminates; Gresczcuk(1972), for example, obtained the stresses in multilayered laminates symmetric about the midplane (i.e. no bending-membrane coupling).

As for the straight edge problem, boundary layer interlaminar stresses are implied in delamination damage and possibly intralaminar matrix cracking(e.g. Brinson and Yeow(1981)). For ultimate strength the effect of hole radius on ultimate strength of specimens has been reported(e.g. Pipes(1979)) and strength is predicted from a limited number of experimentally determined parameters; most researchers agree that this is an undesirable departure from rational models.

Numerous studies of the elastic stresses within the boundary layer have been done. What follows is a brief synopsis of those most recent and most often referred to in the literature.

For a curved free edge, Tang (1977) used a boundary layer theory formulated in cylindrical coordinates to analyze infinite cross-plied laminates with a circular hole. He presented results for plates with very large ratios of the hole radius to laminate thickness ($R/t>33$) which predict finite values for the all interlaminar stresses on the hole surface.

Many solution methods have been polynomial-based formulations of the Finite Element Method (FEM). Some of these analyses suffered from either poor modeling or the use of too coarse meshes which resulted in incomplete or innaccurate solutions (Rybicki and Hopper(1973), Levy et al (1971), Rybicki and Schmeuser(1978), Dana(1973), and Lee(1982,1980)). These analyses were untimely since the power and availability of computing machines has increased dramatically in recent years.

Raju and Crews (1982a,1982b) studied the behaviour of $[90/0]_s$ and $[0/90]_s$ graphite-epoxy laminates with $R/t=5$ using displacement formulated three dimensional finite elements. They used an extremely dense mesh of finite elements radially surrounding the interface at the hole surface. The solution, requiring 19000 degrees of freedom, showed behaviour consistent with an expected singularity at the interface. Raju and Crews(1981) also obtained solutions for θ=constant planes using the two-dimensional finite element formulation from the uniform extension problem with ε_θ imposed from the exact two-dimensional solution. These solutions showed good agreement with the full three dimensional solution at the singularity, but disagreed elsewhere on the free edge. Since $\partial\sigma/\partial\theta \neq 0$ for the hole problem, the uniform extension solution should not be expected to agree. The order of the singularity was estimated using the equation

$$\sigma = A(\theta)\ r^{\omega-1} + O(r^{(\omega-2)}) \qquad \omega < 1$$

and A and ω were determined from the FE results at small distances r from the singularity. ω was observed to be constant.

Lucking et al(1984) obtained comparable results with standard quadratic isoparametric elements by substructuring the boundary layer in two stages after the initial model of a finite width $[0/90]_s$ plate with a central circular hole. The model had fewer degrees of freedom than that of Raju and was used to show that the interlaminar normal stress σ_z at the hole surface on the midplane depends strongly on R/t.

Altus and Bar-Yoeseph(1983) used a 3-D finite difference code and presented results for a $[\pm 45]_s$ plate with a central circular hole. Bar-Yoeseph(1985) presented a variational-perturbation approach for elliptical holes in angle and cross-plied laminates and studied the effects of lay-up angle and hole aspect ratio for material properties representing boron-epoxy and graphite-epoxy composites claiming accuracy for only very large ratios of diameter to plate thickness.

Wang(1986) used hybrid-stress finite elements which enforced the free edge conditions exactly with the Lagrange Multiplier technique to enforce displacement continuity at the interface. Using a coarse mesh results for $[0/90]_s$ and $[90/0]_s$ Graphite/Epoxy laminates with central circular holes having R/t=.625 were presented.

Many of the different approaches are claimed in some aspect to be superior. Numerical results have been concentrated on practical "benchmark problems" (e.g. balanced (A_{16}=0, see appendix A) symmetric flat laminates with central circular holes) while assessing and developing methods. The problems are simple in geometry but are three dimensional and so have not been as accessible to many approximate methods as the two dimensional problems. Methods of determining the order of possible singularities directly have not been developed for curved free edges.

In this chapter the finite element technique used by Lucking et al(1984) is evaluated. For two crossplied symmetric Graphite/Epoxy composite plates in uniaxial tension, measurements of the strains on the hole surface are taken using miniature strain gages and compared with the model. Using the FE technique the effects of R/t and hole reinforcement are studied for problems having two or three perpendicular planes of reflective symmetry in the geometry, material and loading.

3.2 Formulation and Solution Procedure

3.2.1 Introduction

The FE method is used to obtain approximate numerical strains and displacements from the theoretical model. FE methods, which have largely superceded Finite Difference (FD) methods in recent years enable point by point investigation in the space of input parameters; it easily accepts geometric, material, and loading data, and provides information, which is possibly quite dependent upon computational parameters, in a semi-discrete numerical form. Analysis becomes machine dependent and often cumbersome. There may be little opportunity in the process for mathematical insight.

Despite shortcomings, it does provides information which might otherwise be found only with great difficulty and expense by measurement or other more dialectical mathematical analysis. In the present work, it serves in providing approximate solutions in numerical form to the theoretical equations for comparison with measurement and to explore the model's behaviour for specific problems.

3.2.2 Finite Element Formulation

The problems studied are expected to contain a singularity; they are usually dealt with in several ways. Singular functions could be included in the approximation functions or the singularity can be ignored by using additional mesh refinement in that region and hoping that the non-singular functions will be adequate. Standard isoparametric polynomial-based finite elements are commonly available in well developed packages while singular three dimensional elements for this problem have not yet appeared. Another element or alternative method was not developed, instead a standard package was used and some degree of accuracy was obtained through mesh refinement.

There are many good texts which present and discuss the formulation of the finite elements to be used here,(e.g. Zienkiewicz(1977) and Cook(1974)). Briefly, for aspects of the method to be used here, the formulation is reviewed.

Displacements inside an elemental part of the domain (see Figure 3.2.1) are given by, for example,

$$u = \sum_{i=1}^{n} N_i u_i = \bar{N} \; \bar{a}^e \qquad (3.2.1)$$

where N_i, u_i are the values of N,u at the node i, (N are termed shape, interpolatory, or trial functions) and strain in general is

$$\bar{\varepsilon} = \bar{L} \; \bar{N} \; \bar{a} = \bar{B} \; \bar{a}^e \qquad (3.2.2)$$

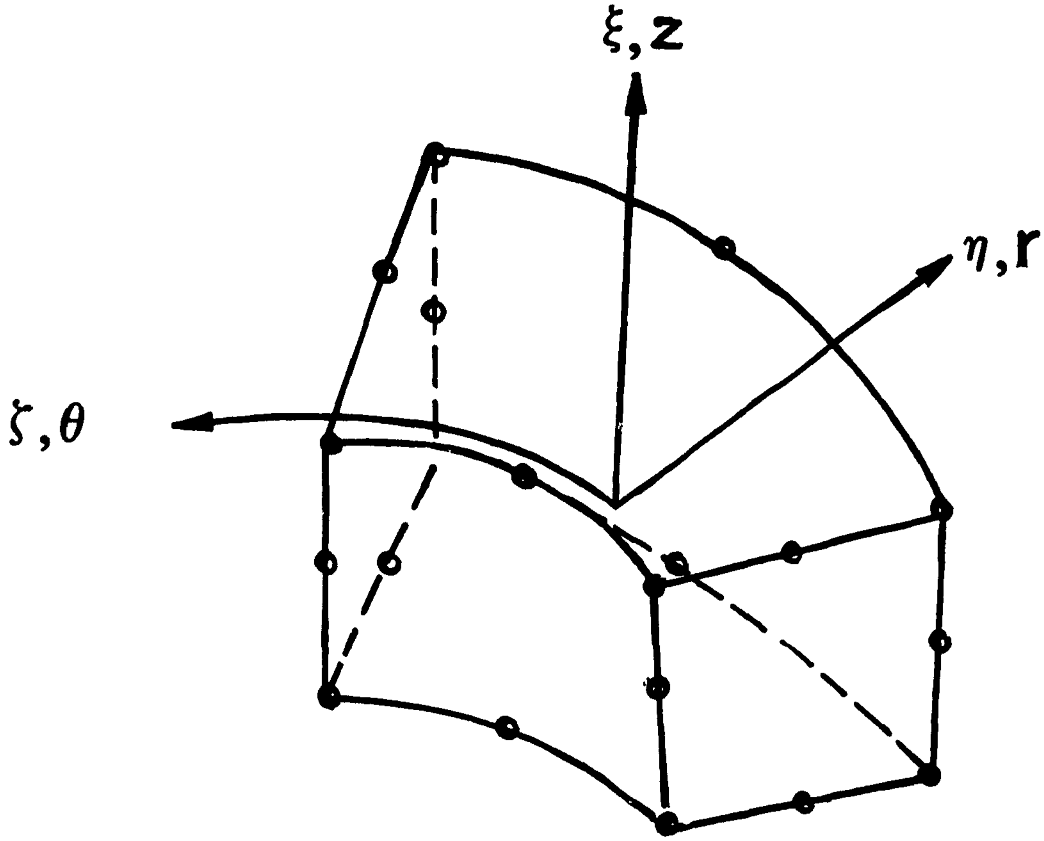

Figure 3.2.1 20 node isoparametric finite element with local and global coordinates

where $\bar{L}$ is an appropriate partial differential operator.

The shape functions, $N_i(\eta,\zeta,\xi)$ for a 20 node element, shown in Figure 3.2.1 are:

for corner nodes ($\zeta=\pm1, \xi=\pm1, \eta=\pm1$)

$$N_i = \frac{1}{8}(1+\xi_0)(1+\eta_0)(1+\zeta_0)(\xi_0+\eta_0+\zeta_0-2);$$

for midside nodes

$$N_i = \frac{1}{4}(1-\xi^2)(1+\eta_0)(1+\zeta_0) \quad \text{for} \quad \xi_i=0 \quad \eta_i=\pm1 \quad \zeta_i=\pm1$$

$$N_i = \frac{1}{4}(1-\zeta^2)(1+\xi_0)(1+\eta_0) \quad \text{for} \quad \zeta_i=0 \quad \eta_i=\pm1 \quad \xi_i=\pm1 \qquad (3.2.3)$$

$$N_i = \frac{1}{4}(1-\eta^2)(1+\xi_0)(1+\zeta_0) \quad \text{for} \quad \eta_i=0 \quad \xi_i=\pm1 \quad \zeta_i=\pm1;$$

where

$$\eta_0=\eta\eta_i \qquad \zeta_0=\zeta\zeta_i \qquad \xi_0=\xi\xi_i .$$

Based on the principle of minimum potential energy, and assuming no body forces, initial stresses or strain, the finite element statement is then

$$\bar{q}^e = \bar{K}^e \bar{a}^e \qquad (3.2.4)$$

where $\bar{K}^e = \int_{\Omega} \bar{B}^T \bar{C}\, \bar{B}\, d\Omega$ and Ω is the volume domain of the element. $\bar{q}^e$, $\bar{K}^e$, and $\bar{a}^e$, are known as the element force vector, stiffness matrix, and displacement vector respectively. The integral is evaluated by Gauss-Legendre quadrature.

The solution for the entire domain is obtained by solving the global set of linear equations

$$\bar{q} = \bar{K}\, \bar{a} \qquad (3.2.5)$$

where $\bar{q}$ and $\bar{a}$ are the nodal force and displacement vectors and $\bar{K}$ is the global stiffness matrix. K and q are obtained by summing the contributions from the element stiffness matrices and force vectors for each node in the global model. $\bar{K}$ is a square matrix that is banded, symmetric, and positive definite.

It is usual to impose force boundary conditions in an approximate manner by setting the nodal forces to

$$\bar{q}^e = -\int_{\Gamma^e} \bar{N}^T \bar{t}\, d\Gamma \qquad (3.2.6)$$

where $\bar{t}$ is the prescribed surface traction and Γ^e is the boundary surface of the element. These equivalent nodal forces are derived by equating the work of the nodal forces through a virtual displacement to that of the surface tractions.

The easiest boundary condition to impose directly on the nodes is the nodal value of displacement. Compatibility is satisfied between elements; on the interface the displacement continuity is satisfied exactly while all stress boundary conditions and continuity conditions (i.e. the stresses required to be continuous may not be) are satisfied approximately. The displacement derivatives could be constrained; but the approximate solution, without special problems, will converge to the unique solution (where the solution exists) without constraints.

3.2.3 Problem Domains

The domain of a problem may be reduced by imposition of symmetry requirements. As was noted in Chapter 2, the elastic symmetry of laminates is such that the $\bar{C}$ tensor varies with period 2π w.r.t. θ. If the loading and geometry share this periodic symmetry then so must the solution and only one half of the total domain need be modelled with periodic boundary conditions. In the special case of a crossplied laminate where all the layers have their principal axes in some sense aligned with the laminate axes (i.e. rotated by zero or $\pi/2$) the material properties also have reflective (or mirror) symmetry about the planes x=0, y=0. If loading and geometry share this property then so do the displacements. In cylindrical coordinates the displacements u and w are even functions of θ and v is odd; further, u and w are even functions of $\theta \pm \pi/2$ while v is odd (the same as if $u,w=\cos(2\theta)$ and $v=\sin(2\theta)$); in a laminate which is symmetric across the midplane, w is odd w.r.t. z while u and v are even.

Such configurations are fundamentally important; their symmetry facilitates and so enhances the analysis. In this chapter only laminates possessing reflective symmetry about the planes x=0,y=0 are analyzed. The problem is depicted in Figure 3.2.2.

3.2.4 Solution Procedure

Finite elements are required in a very dense mesh for accuracy in regions where the solution is poorly approximated by a low degree polynomial, especially near singular points in the solution domain(Strang and Fix(1973)). Mesh density comes at a cost in computer resources.

In the following problems, high stress gradients are expected to occur in a region surrounding the cutout. In order to increase the density of elements in this region the problem was broken down into 3 parts as shown in Fig.3.2.3. Solutions were obtained in stages using a technique that is similar to substructuring (Cook(1974)). By imposing the displacements taken from a cylindrical surface at a constant radius of a coarse mesh on the corresponding surface of subsequently generated finer mesh, greater accuracy in the region of interest, near the hole, can be achieved. In general, the number of elements on the surfaces were different so the nodal displacements imposed on each

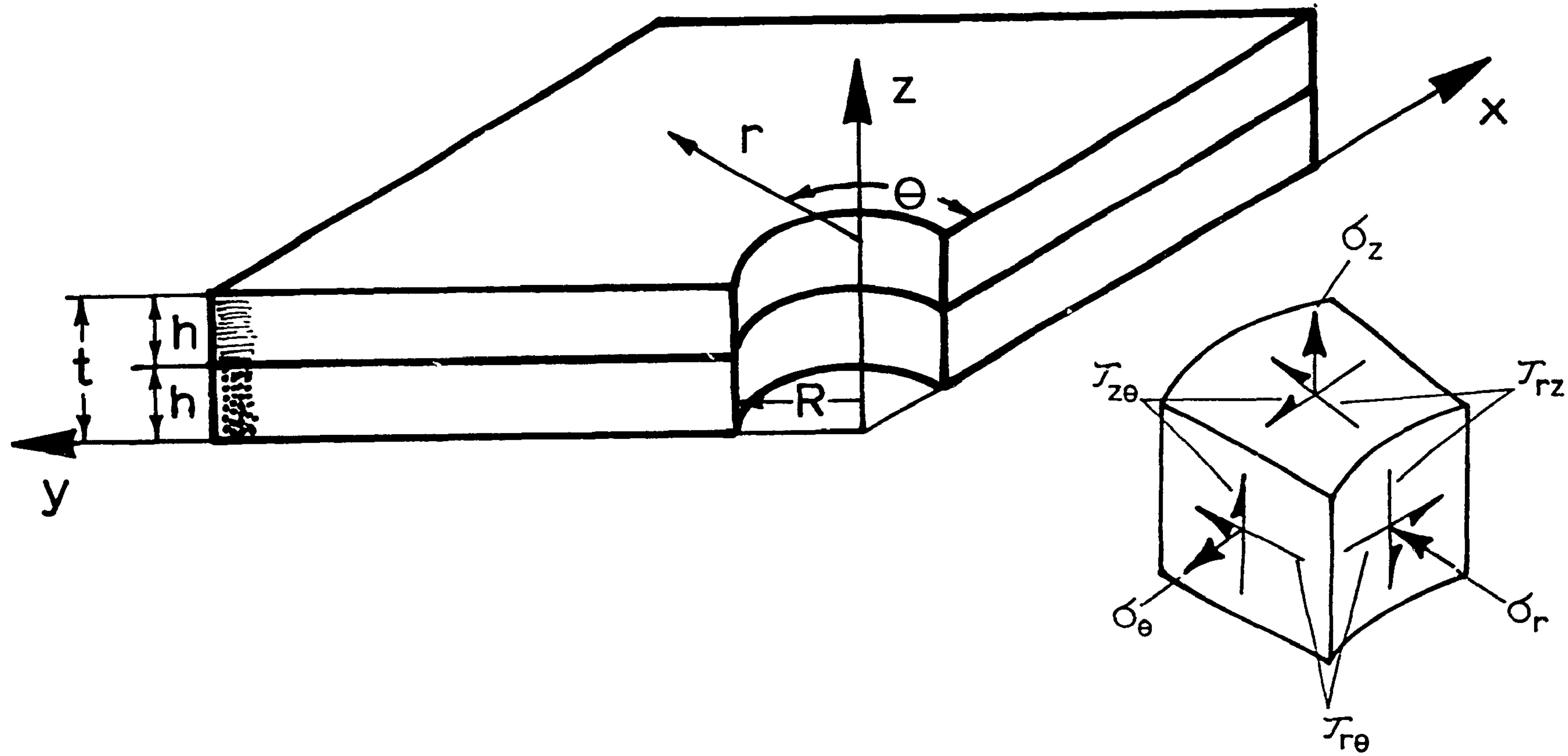

Figure 3.2.2 Portion of structure modeled using boundary conditions from symmetry on x=0,y=0 (and z=0 for symmetric laminates).

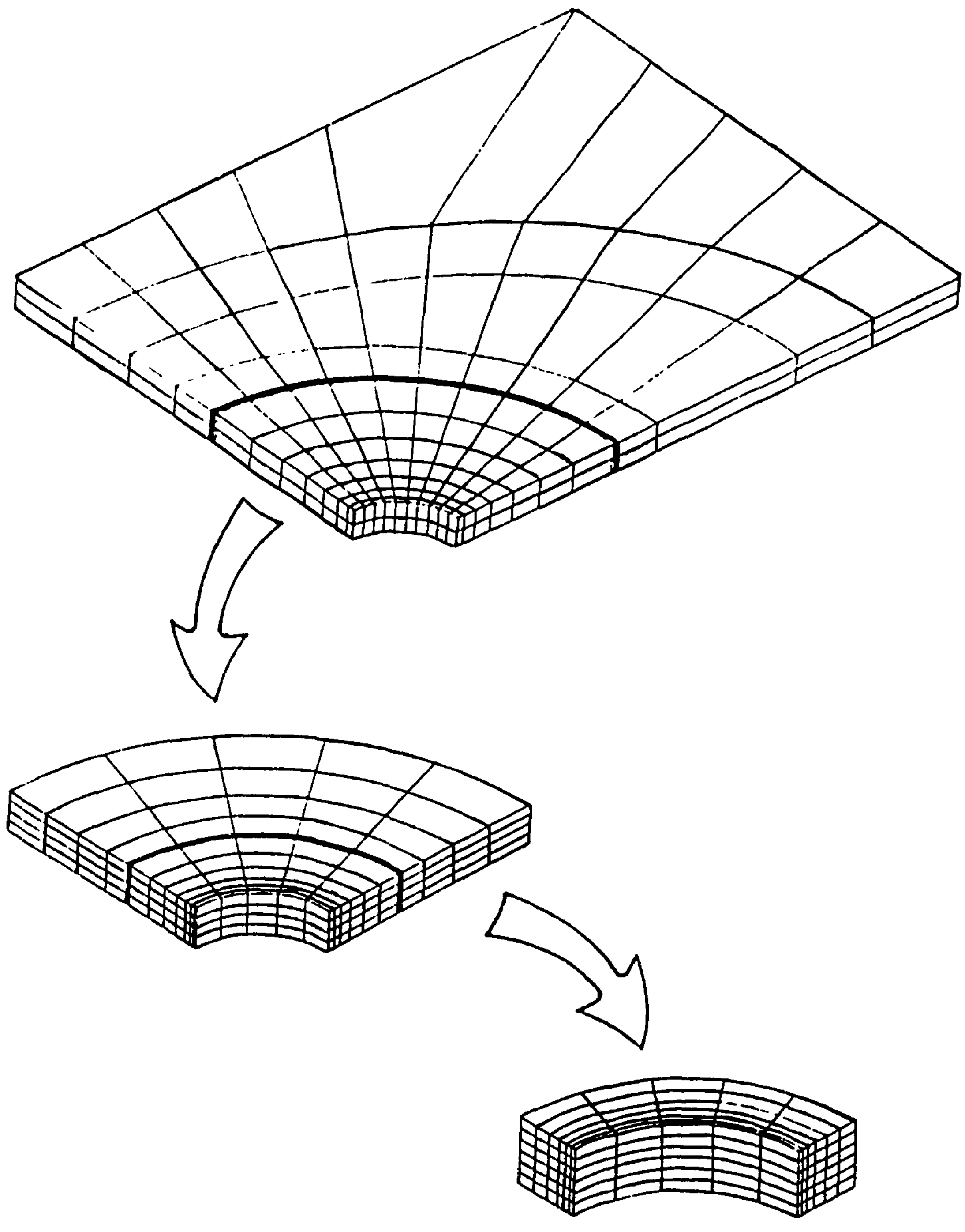

Figure 3.2.3 Depiction of substructuring technique. Displacements from a cylindrical surface at r-R=3t,t are imposed on the next mesh.

subsequent mesh were values interpolated from the previous mesh using a bicubic spline for each layer. The second derivative was set to zero where the slopes were not known from symmetry.

Loading was imposed on the first stage as pressures applied to each ply group on the surface $x = L/2$. The magnitudes of the pressures were determined using Classical Lamination Theory for the case of uniform strain in an infinite laminate with no hole; by the principle of St. Venant, the effect of the hole on the laminate stresses should become negligible away from the hole edge in all directions. Therefore, given that the dimensions of the model are sufficient, this loading is appropriate to approximate the case of an infinite laminate with a central circular hole. Displacement was not imposed because the effect of the hole on the displacements dies away less quickly than for the displacement gradients (the reason for this can be seen in the functional form $f(r^n)$ $n=-1,-2,-3,\ldots$ of the plane stress solutions for plates with holes).

The Finite Element Method as formulated previously is included in a general purpose linear problem computer program encoded in Fortran entitled SAP IV (see Bathe(1974)).

3.2.5 Qualification of Method

The FE results are accurate depending upon how 'close' they are in some sense to a solution which satisfies all conditions of the model exactly. In this subsection accuracy is discussed and results are compared with high accuracy solutions and relevant exact solutions to the plane stress model for individual layers.

Convergence of solutions for the present formulation is expected to be problem dependent (for example, it will depend upon R/t). However, away from the singularity the rate of convergence of the displacements will be $O(h^3)$, and $O(h^2)$ for the stresses(Zienkiewicz(1977)).

In the first of the three stages, the region outside the boundary layer must be accurate for following stages to be accurate. In Figure 3.2.4 for R/t=25 the present FE method for an orthotropic plate using properties shown in Table 3.1 and W/R=10 is compared with the exact solution for an infinite plate. For a single orthotropic layer, a formula for σ_θ on the hole surface is given by Lekhnitskii(1968) as

$$\sigma_\theta = \sigma_o \frac{E_\theta}{E_x} \left[-\sqrt{E_x/E_y}\cos^2\theta + \left(1+(2\,E_x/E_y + E_x/G_{xy} - 2\nu_{xy})^{\frac{1}{2}} \right) \sin^2\theta \right] \qquad (3.2.7)$$

where

$$1/E_\theta = \frac{\sin^4\theta}{E_x} + \left[\frac{1}{G_{xy}} - \frac{2\nu_{xy}}{E_x} \right] \sin^2\theta\cos^2\theta + \frac{\cos^4\theta}{E_y}$$

and $E_x, E_y, \nu_{xy}, G_{xy}$ are the orthotropic elastic moduli(where, for example, $E_x=E_{11}$ when $\alpha=0^\circ$, $E_x=E_{22}$ when $\alpha=90^\circ$). The

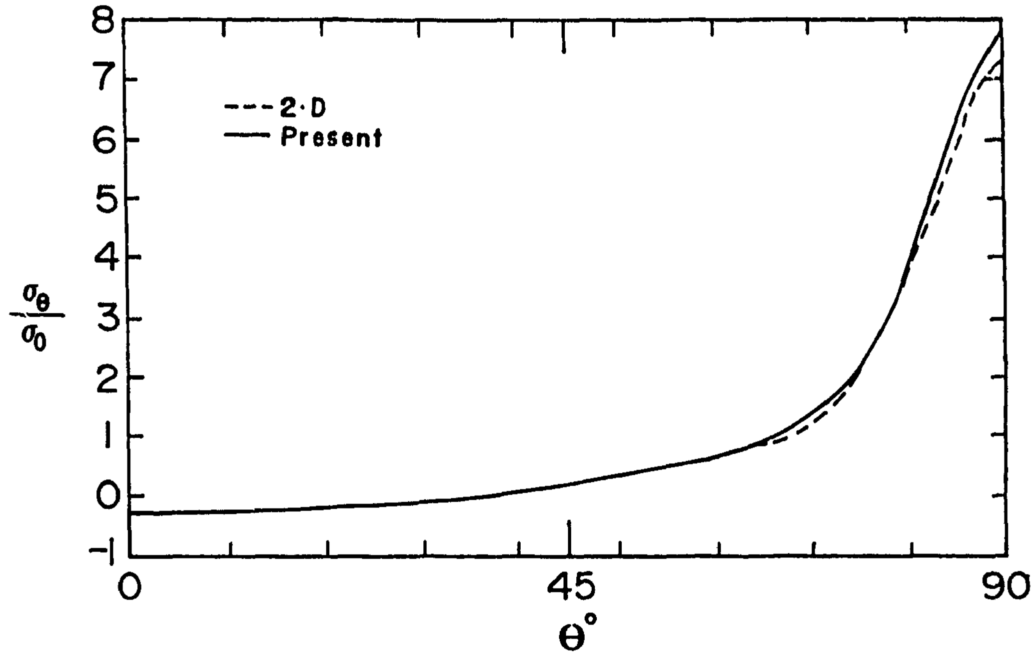

Figure 3.2.4 Comparison of σ_θ at r=R from first FE mesh for $\alpha=0^\circ$ layer with exact plane stress solution.

Table 3.1 Effective Elastic Moduli of Graphite/Epoxy

E_{11}= 145 GPa (21.0 Msi) E_{22}= 10.7 GPa (1.55 Msi)

ν_{12}=.31 G_{12}= 4.5 GPa (.65 Msi) ν_{23}=.49

(from Sandorff(1982))

small difference between the curves in Figure 3.2.4 can be accounted for by the finite width of plate in the FE model. Since stresses are a degree lower in order of convergence the displacements predicted by this mesh should be adequate.

Within the boundary layer in the vicinity of the expected singularity due to the interface intersection, the solution will be dominated by the singularity. Although it is at present unknown, if the asymptotic form of the singularity is surmised to be

$$u = A_1(\theta) r^{\omega} + O(r^{\omega+1}) \quad \omega < 1 \qquad (3.2.8)$$

(where r is the radial distance from the singular line; ω is the order or power, a constant depending only on the material properties for the problems considered here while the strength, or intensity $A_1(\theta)$ of the singularity is problem dependent (i.e. the material and loading). The rate of convergence near the singularity can be dominated by its order ω. The asymptotic expression for the stresses would be

$$\sigma = A_2(\theta) r^{\omega-1} + O(r^{\omega}). \qquad (3.2.9)$$

Tong and Pian(1973) have shown that a reasonable expression for the order of convergence is

$$\sigma - \sigma^{*} = O(h^{\omega-1/2}) \qquad (3.2.10)$$

where σ^{*} is the FE stress, σ is the exact solution. In theory, σ could be found at some small r by refining the mesh to the point where

$$\sigma \approx Ar^{\omega-1} \qquad (3.2.11)$$

then fitting log(σ) vs. log(r) to a straight line as done by Raju(1981) to find A and ω. Alternatively, by fitting data (a nonlinear procedure) from various meshes to

$$\sigma-\sigma^{*}=K(\theta)\,h^{\omega-1/2} \qquad (3.2.12)$$

at some small r to determine K,ω and σ, then A could be found from Equation (3.2.11). However, since K and A are presumed to be problem dependent this might require the procedure for each case. Further, the previous expressions are asymptotic and so are accurate only for values of h smaller than is practical with the present scheme (considering error introduced by the polynomial interpolation between stages and limited computing resources). The nonlinear procedure was not attempted on this basis.

The effect of h on the results can be demonstrated. Results were generated for two cases using R/t=5, W/L=1.4 and W/R=6 with the material properties shown in Table 3.2 for $[90/0]_s$ and $[0/90]_s$ plates. Based on the observation made in previous work by the author and others that the three dimensional boundary layer stresses become negligible outside of one laminate's thickness radially from the hole surface into the plate, the last two meshes in each case were generated for distances of three and one laminate thicknesses from the hole surface. Raju et

Table 3.2 Approximate[1] Effective Elastic Moduli of Graphite/Epoxy

E_{11}= 138 GPa (20 Msi) $E_{22}=E_{33}$= 13.8 GPa (2.0 Msi)

$\nu_{12}=\nu_{13}=\nu_{23}=.21$ $G_{12}=G_{13}=G_{23}$= 5.9 GPa (.85 Msi)

1) In general, shear moduli and Poisson's ratio are not all equal for actual materials.

al(1982a,1982b) obtained solutions for these two cases using a mesh which was highly refined towards the singularity having about 19000 degrees of freedom. The elements bordering the interface had the radial dimension of about h/125 while in the present it is h/10. The mesh had a polar arrangement in the θ-plane progressively refined towards the singularity. The present solution took less than 8500 CPU seconds on a CDC series 179 830D mainframe computer (this number is typical for all solutions in this chapter since, the same or smaller meshes were used throughout).

The results of both solutions are shown in Figures 3.2.5-10. The stresses in the present problems are of most interest on the surface of the hole on the midplane (where due to symmetry $\partial\sigma_z/\partial z=0$) and the interface levels where the singularity is expected. On each θ-plane inplane stress σ_θ will be maximum on the hole surface. In Figure 3.2.5 the distribution of σ_θ through the thickness is compared with Raju et al. The distribution is uniform except near the interface, especially near $\theta=90^{\circ}$. At the interface (see Figures 3.2.6,7) the stress σ_z and $\tau_{z\theta}$ are continuous and so are presented as averages between layers, the results in Figure 3.2.6 show that $\tau_{z\theta}$ in both laminates differs only in magnitude between the two solutions; this can be seen by the identical zero crossing points. In Figure 3.2.7 σ_z at the interface shows similar behaviour but not as definitely as for $\tau_{z\theta}$. From both solutions, it appears that the $\tau_{z\theta}$ singularity is stronger than σ_z and that σ_z is compressive everywhere except near $\theta=90^{\circ}$.

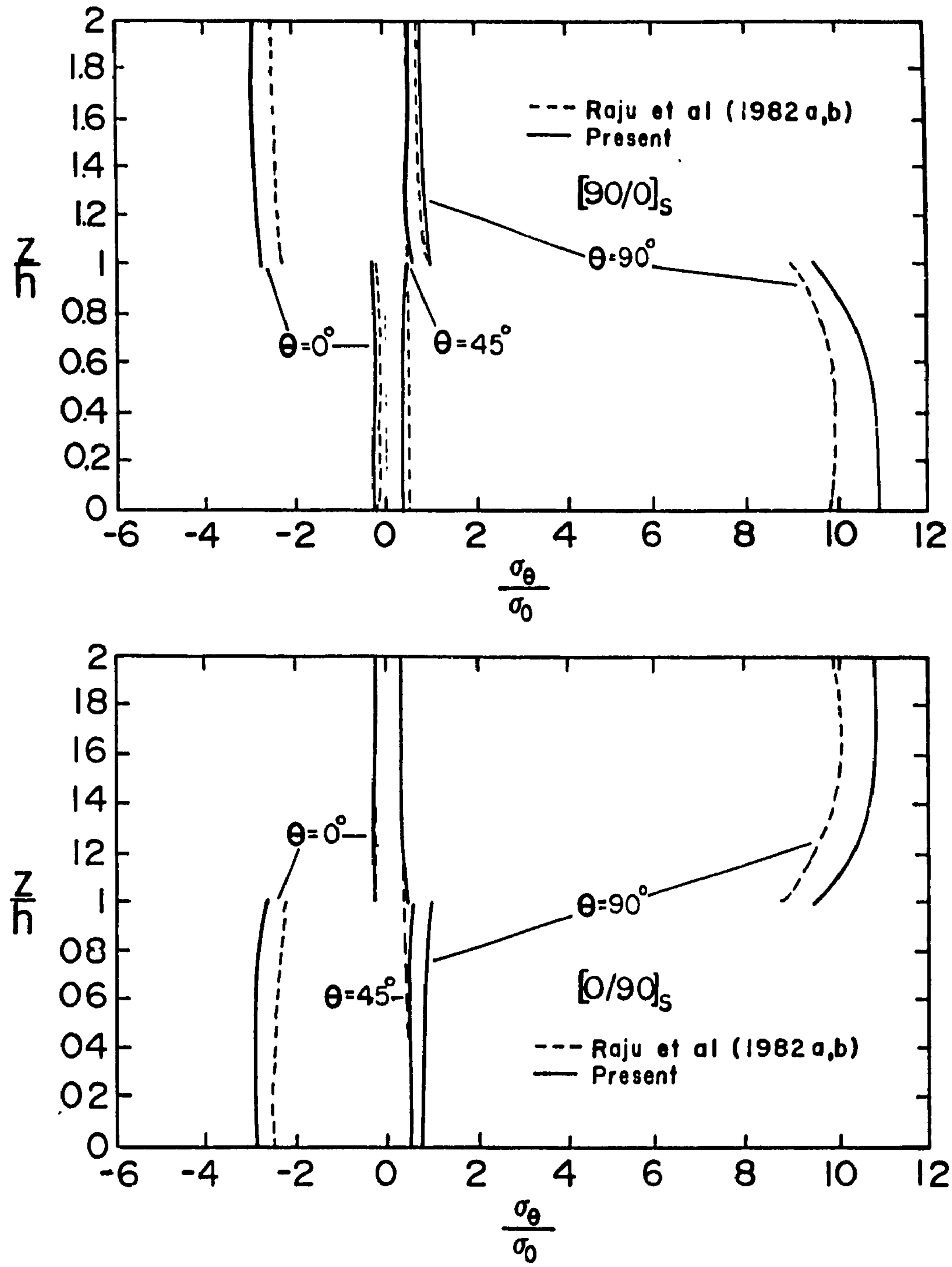

Figure 3.2.5 Normalized circumferential stress at r=R through the thickness from present and Raju et al(1982a,b).

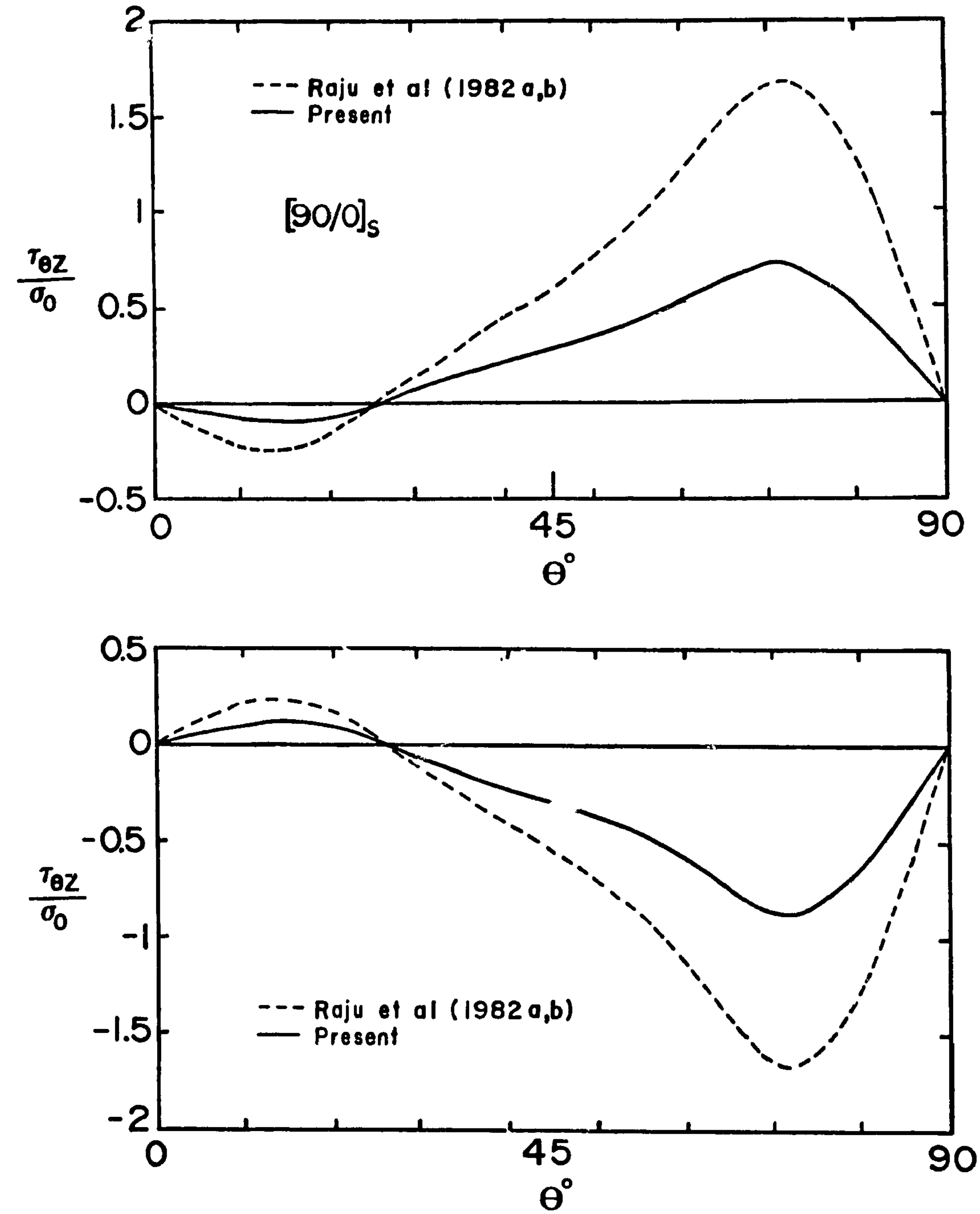

Figure 3.2.6 Normalized interlaminar shear stress at z=h, r=R from present and Raju et al(1982a,b). Comparison shows the effect of mesh density as increasing the strength of the surmised stress singularity.

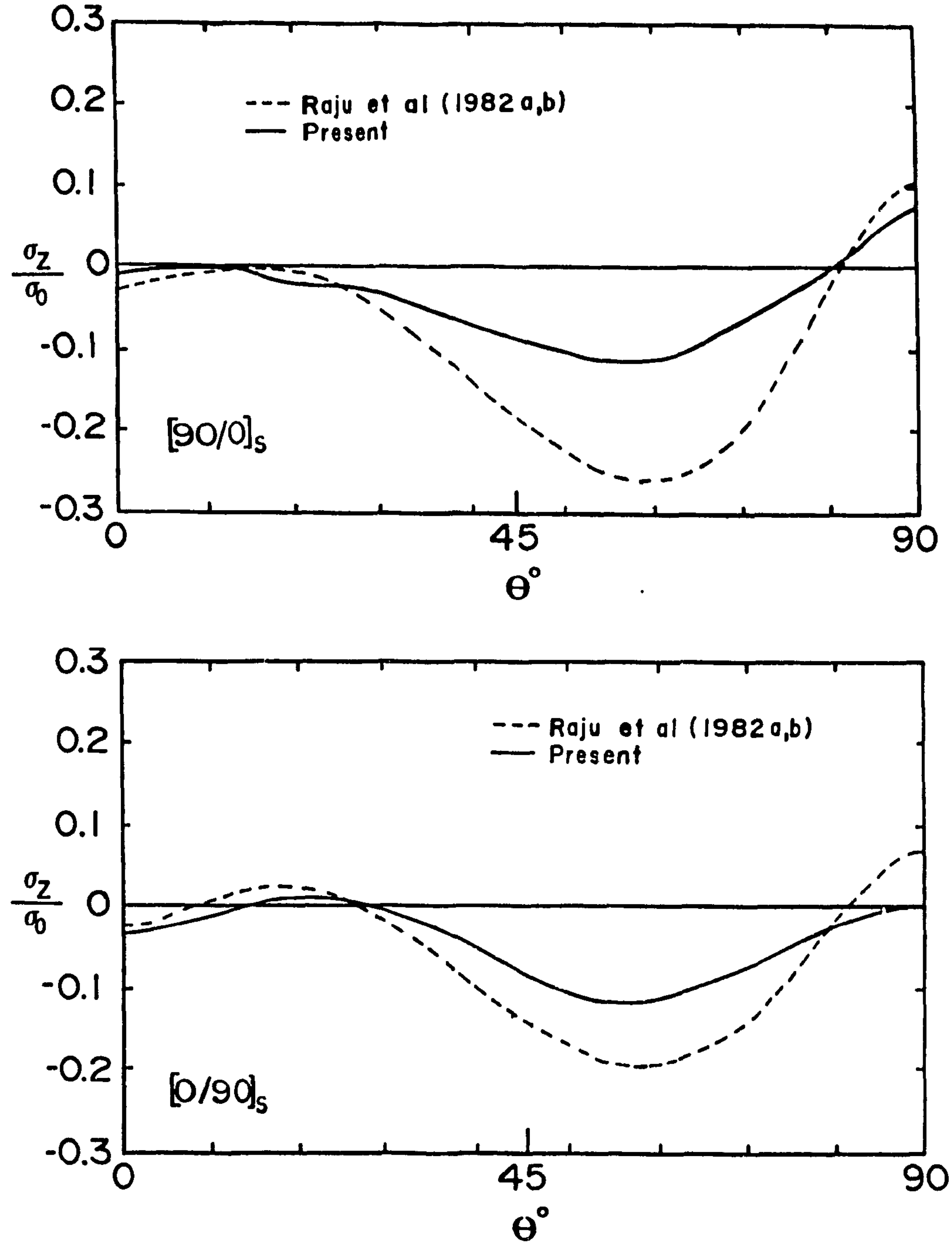

Figure 3.2.7 Normalized interlaminar normal stress at z=h, r=R from present and Raju et al(1982a,b). The higher density of the mesh used by Raju et al yields a similar distribution to the present of greater magnitude.

The interlaminar stress σ_z displays sharp variation through the thickness. Shown in Figure 3.2.8 are comparisons for σ_z through the thickness between the present model and Raju et al. The distributions are similar but are smoothed by decreasing mesh density. This effect appears to be greatest at $\theta=90^{\circ}$. Away from the singularity, the solutions are expected to converge with less refinement than at the interface; there the agreement between the present solutions and Raju et al is much better. Their mesh was more refined towards the interface but still had a more dense mesh near the midplane than the present. Shown in Figure 3.2.9 is σ_z from the present solutions where it is at a maximum in compression.

The effect of mesh refinement on the difference between the interlaminar stresses is apparent only near the expected singularity. Small disagreement elsewhere could theoretically be due to roundoff or discretization error, or the effect of the substructuring in the present method. At the singularity, the magnitude of the stresses are affected without severely altering distribution. Therefore, to its favour, the present method correctly predicts the sign and and shows a very similar distribution near the singularity with far fewer degrees of freedom than was used by Raju et al. In both solutions it was observed that the inplane stresses compare well to results obtained using the plane stress formulas for orthotropic homogeneous plates.

For designers it would be desirable to make use of the very accessible plane stress formulas (Equation 3.2.7)

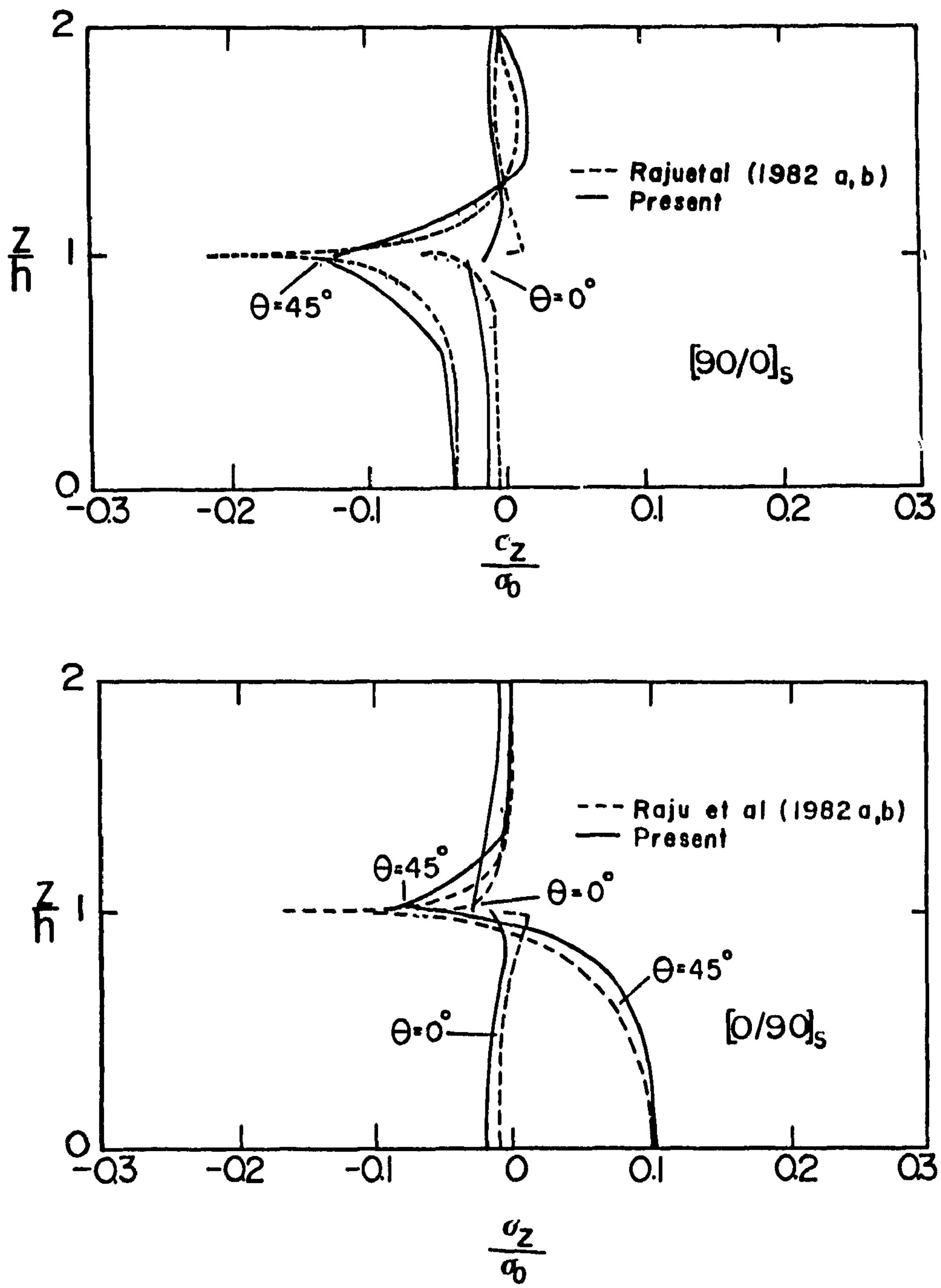

Figure 3.2.8a) Normalized interlaminar normal stress at r=R, $\theta=0^{\circ}, 45^{\circ}$ through the thickness from present and Raju et al(1982a,b). Distributions are similar with greatest disagreement near the surmised stress singularity.

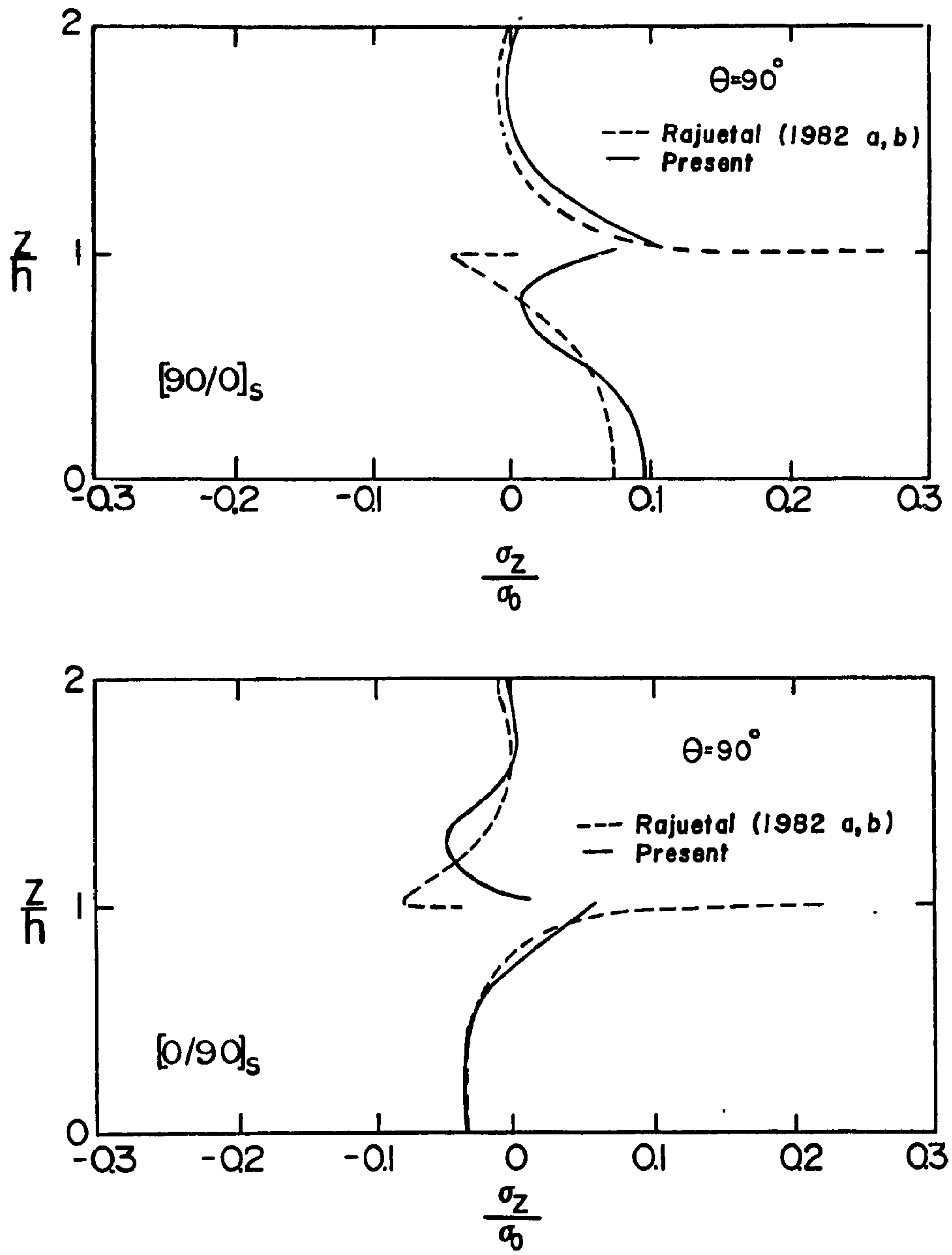

Figure 3.2.8b) Normalized interlaminar normal stress at r=R, $\theta=90^{\circ}$ through the thickness from present and Raju et al(1982a,b). Distributions are similar with greatest disagreement near the surmised stress singularity.

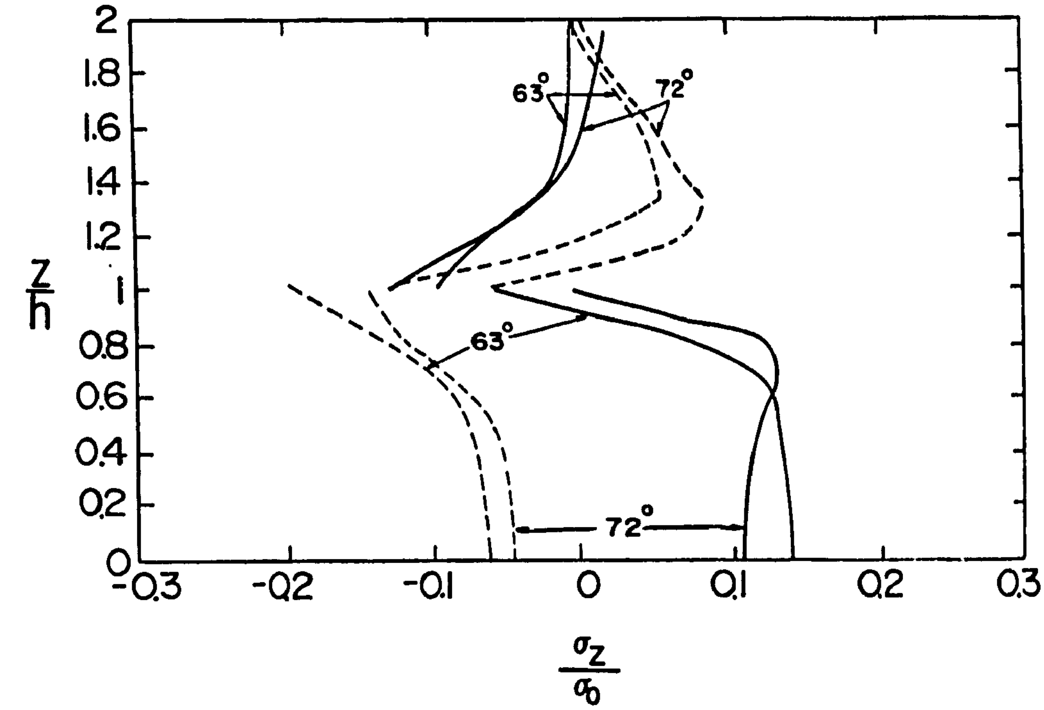

Figure 3.2.9 Normalized interlaminar normal stress at r=R, θ=63°,72° from the present model.

for laminates. There are two apparent methods for obtaining comparable solutions using the two-dimensional solution for an orthotropic plate (the crossplied laminate is not quasi-isotropic although $Q_{11}=Q_{22}$ as for $[0/\pm60]_s$, $[0/\pm45/90]_s$, etc):

1) The far field stresses in the laminate predicted by CLT may be applied as edge loads to each layer; in this case the layers are loaded separately and so can deform independently. This will be referred to as the unbonded method.

2) The laminate is replaced by a single homogeneous plate loaded by the gross applied load having elastic moduli obtained from the laminate stiffness matrix (as done by Greszczuk (1972) and Raju et al) to obtain strain for the laminate from which stress in the layers can be found. The equivalent plate moduli are

$$\nu_{xy}=A_{12}/A_{22} \qquad \nu_{yx}=A_{12}/A_{11}$$

$$E_x = A_{11}(1-\nu_{xy}\nu_{yx}) \quad E_y=A_{22}(1-\nu_{xy}\nu_{yx}) \quad G_{xy}=A_{66}.$$

where A_{ij} i,j=1,2,6 are elements of the laminate stiffness matrix defined in Appendix A. This will be referred to as the bonded method. This approach is basically the same as Classical Lamination Theory. The name is somewhat artificial since surface tractions would have to be applied to the hole surface for it to deform according to Kirchoff's hypothesis. This is one of the ways, as has been pointed out in early work in edge problems, in which Classical Lamination Theory fails near free edges.

Equation (3.2.7) may be used with the principle of superposition to calculate σ_θ by either of the two methods. Shown in Figure 3.2.10 are the σ_θ determined from the two methods and the present FE solutions. It can be seen that the results of the unbonded method agree slightly better with the FE results in the 0^o layers while the bonded method is better in the 90^o layers. Overall, the bonded solution shows better agreement except that it is about 20% less in maximum stress concentration. In part, the difference is again due to the finite width of the laminate in the FE model. It can also be observed that debonding of the plies raises the stress concentration at $\theta=90^o$ in the 0^o layer; this may be relevant to the situation after interface delamination indicating an increased likelihood of complete failure over the integral plate.

3.2.6 Summary and Conclusions

Standard finite elements can be used with a substructuring technique to obtain solutions which compare well with results of a very high density mesh. The interlaminar stresses are dependent on mesh density near the singularity but their sign and distribution on the hole surface were largely unaffected. The computer resources required for a three dimensional problem are relatively high such that ignoring the singularity in the solution may be costly.

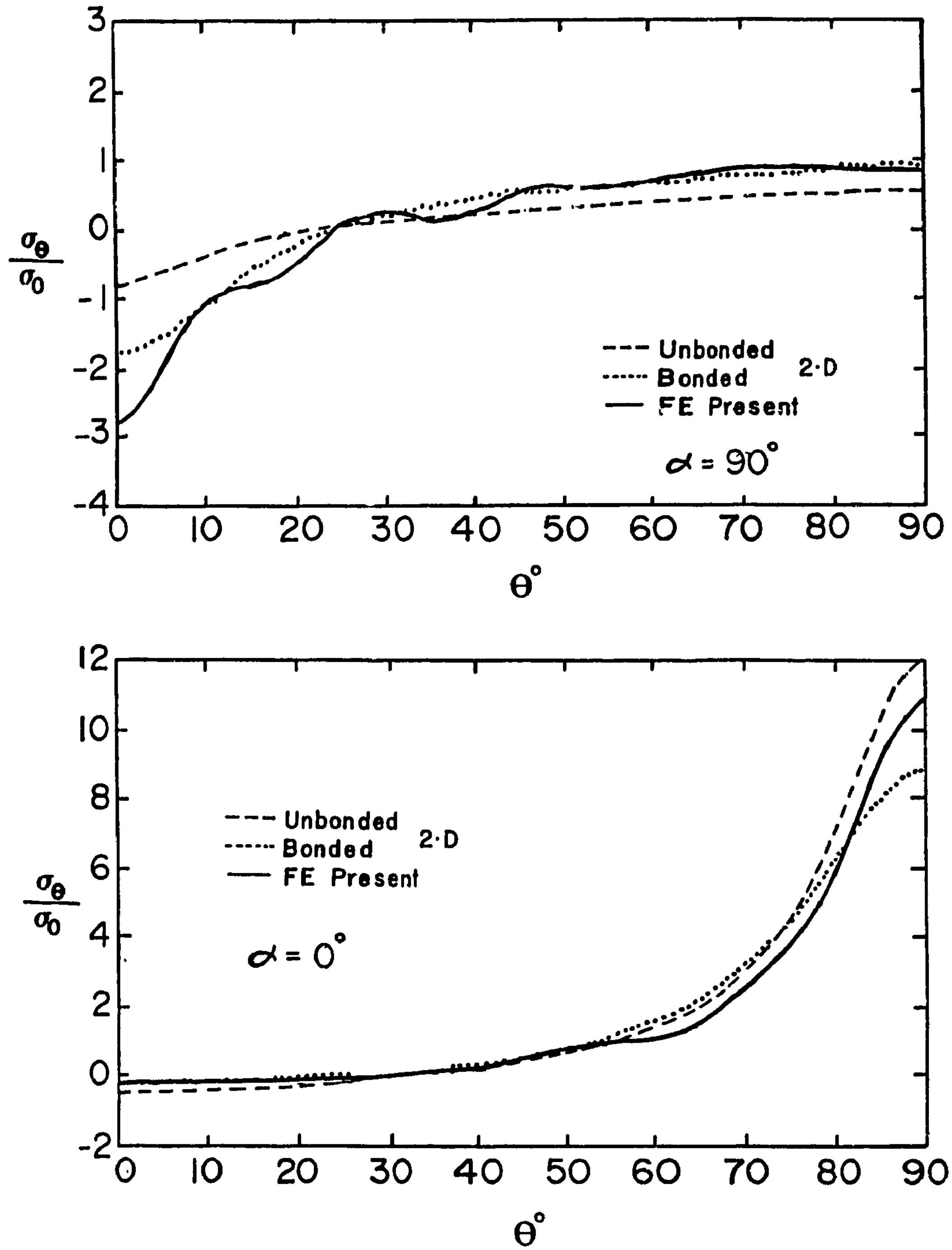

Figure 3.2.10 **Normalized circumferential stress at r=R, z=3h/2, z=h/2 from present FE and two methods using the exact solution for plane stress in single layers.**

Two different schemes to estimate the inplane stresses in a laminate using plane stress formulae for orthotropic layers are presented. The methods yield different results since they roughly model the laminate having bonded and unbonded layers.

3.3 Strain Measurement and Analysis

3.3.1 Introduction

Some confidence in the results of the present model will be justified if they agree with results measured from actual composite laminates of practical utility.

In the past, strain analysis by measurement has been done by Daniel, Rowland, and Whiteside of surface strains on the faces of fiber-reinforced plates using strain gages, Moire grid , and birefringent coatings and compared to two-dimensional linear elastic finite element and exact solutions(e.g. Daniel et al(1973,1974,1978,1980)). There was excellent agreement observed except in the small region surrounding the hole, i.e. the boundary layer. This indicates that the methods used to measure strain, characterize the material, and mathematically model the problem are satisfactory at the level of analysis used outside the boundary layer.

To the author's knowledge, measurements of hole surface strains have not previously been taken with the intent of investigating the boundary layer phenomena. For straight edges it has been the interlaminar shear strain which has been measured while the interlaminar normal strains were not. Note that in all methods, some additional material was bonded to the specimen surface.

3.3.2 Preliminary Problem and Methods Analysis

3.3.2.1 Analysis of Hole Surface Strains and Stresses

Since on the hole surface

$$\sigma_r = \tau_{r\theta} = \tau_{rz} = 0 \qquad (3.3.1)$$

the remaining stresses may be expressed in terms of the strains by using the Hooke's law relations

$$\sigma_z = \frac{\varepsilon_z S_{22} - \varepsilon_\theta S_{23}}{S_{22} S_{33} - S_{23}^2} \qquad (3.3.2)$$

$$\sigma_\theta = \frac{\varepsilon_\theta S_{33} - \varepsilon_z S_{23}}{S_{22} S_{33} - S_{23}^2} \qquad (3.3.3)$$

$$\tau_{z\theta} = \frac{\gamma_{z\theta}}{S_{44}} \qquad (3.3.4)$$

where

$$\begin{aligned} S_{22} &= s^4/E_{11} + c^4/E_{22} + 2(-\nu_{12}/E_{11} + 1/(2G_{12}))c^2 s^2 \\ S_{33} &= 1/E_{33} \\ S_{23} &= -\nu_{23} c^2/E_{22} - \nu_{13} s^2/E_{11} \\ S_{44} &= c^2/G_{23} + s^2/G_{13} \end{aligned} \qquad (3.3.5)$$

and $c = \cos(\theta-\alpha)$ $s = \sin(\theta-\alpha)$.

Using these equations σ_z and σ_θ may be determined from measured values of the two strains ε_z and ε_θ while $\tau_{z\theta}$ requires $\gamma_{z\theta} = \partial w/r\partial\theta + \partial v/\partial z$ be measured. For holes with $R/t>1$ the term $\partial w/r\partial\theta$ was found in the FE results to be less than 5% of the strain $\gamma_{z\theta}$.

Of the two locations considered (i.e. the midplane and interface), the midplane is the most favourable for measurements. At the midplane γ_{rz} and $\gamma_{z\theta}$ are both zero due to symmetry while more importantly ε_z is maximum (so $\partial\varepsilon_z/\partial z=0$). Therefore, ε_z and ε_θ are the principal strains and σ_z and σ_θ are the principal stresses.

Since the strains measured are inevitably affected by extraneous influences to some degree, and considering the complexity of the Equations (3.3.2-5) it seems prudent to investigate what influence differences in the stresses will result from differences (e.g. between FE and measured or actual and measured etc.) in the strains. Beginning with Equation (3.3.2) and assuming the difference between 2 sets of strains ε and ε' to be bounded by

$$| \varepsilon - \varepsilon' | < \eta_0 + \eta_1 | \varepsilon | \qquad (3.3.6)$$

where η_0 and η_1 are constants (η_0 is in strain units). A bound on the error in σ_z may be found from

$$|\sigma_z{}'-\sigma_z| < \frac{\eta_0\ (|S_{22}|+|S_{23}|)+\eta_1(|S_{22}\varepsilon_z|+|S_{23}\varepsilon_\theta|)}{|\ S_{22}S_{33}-S_{23}{}^2\ |} \qquad (3.3.7)$$

Purely for demonstration, the low values η_0=1 $\mu\varepsilon$ and η_1= .05 were used with ε from the FE model at z=0. Figure 3.3.1 shows σ_z/σ_0 and the bounds from equation (3.3.7) for both laminates. While bounds are always conservative they do show tnat small differences in the strains may cause larger errors in σ_z.

3.3.2.2 <u>Measurement by Strain Gages</u>

After surveying the available methods, miniature strain gages were chosen to measure the hole surface strains ε_z and ε_θ. For the normal strains this well-developed technique offers accuracy and convenience without requiring a direct line of access to the hole surface. The usual method of strain rosettes was deemed unfeasible in the presence of large predicted gradients in the region of interest near the interface for the scale of the problem. Unfortunately, strain gages which measure transverse gradients are not apparently available. The strain gage principle of operation requires elongation in the foil direction; using parallel foils to measure a transverse gradient would approximate $\partial v^2/r\partial\theta\partial z$ rather than $\partial v/\partial z$. Shear strain measurement on actual laminates requires a

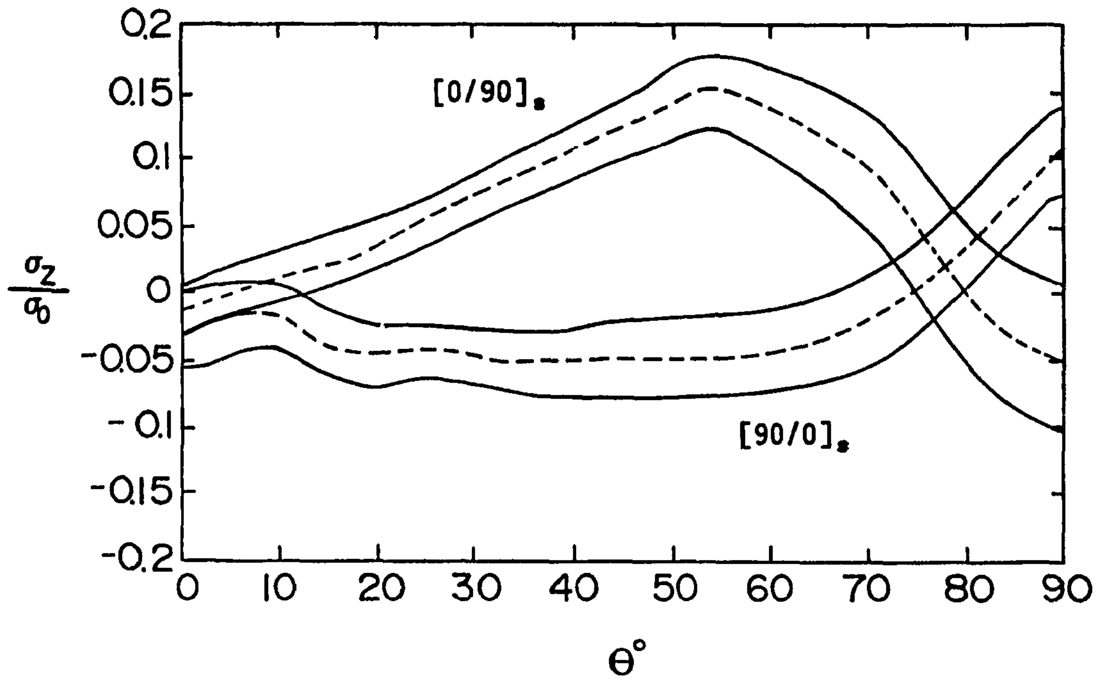

Figure 3.3.1 Interlaminar normal stress at r=R, z=0 from FE models of plates without gages (broken lines) and error bounds from Equation (3.3.7) using η_0=1 $\mu\varepsilon$ and η_1=.05.

different approach.

It would be a mistake to consider strain gages with too much familiarity for the present problems. From other studies (Beatty (1979) and Stehlin(1972)) the materials used in this application of strain gages should not have any special problems such as reinforment effects, but there are other aspects to consider. Although the material interface discontinuity in the FE model is artificial it remained to be seen what behaviour exists in the actual laminate. The singularity arises because the lines of material discontinuity form a sharp corner: placing a third material over the singularity will conceivably have the same effect and alter the behaviour. Further, high gradients expected near the singularity may not transfer well through the two materials and the variation of strain under the gage length will cause the measured value to differ from the point value at the gage center and also may make the measured value sensitive to the gage position.

The gage positioning has three possible errors of which translation in the z direction is most suspect. An approximate expression for the change in the average strain $\bar{\varepsilon}_z$ of a gage centered at $z=z_o$ due to a shift Δz_o is

$$\ell \ \Delta\bar{\varepsilon}_z \approx \varepsilon_z(z)\,\Delta z_o + \frac{1}{2}\,\frac{\partial \varepsilon_z}{\partial z}\,\Delta z_o^{\,2}\Big]_{z_o-\frac{\ell}{2}}^{z_o+\frac{\ell}{2}} \qquad (3.3.8)$$

i.e. the jump of ε_z and $\partial\varepsilon_z/\partial z$ across the gage length.

When considered as a single foil element of initial length ℓ_o perfectly bonded to the surface of the specimen and aligned in the z direction (see Figure 3.3.2), , a 'strain' gage centered at position z would actually measure

$$\varepsilon = \frac{\ell_f - \ell_o}{\ell_o} = \int_0^{\ell_o} \frac{\sqrt{(1+\partial w/\partial z)^2+(\partial v/\partial z)^2+(\partial u/\partial z)^2}}{\ell_o}\, dz - 1$$

$$\approx \int_0^{\ell_o} \frac{\sqrt{(1+2\partial w/\partial z)}}{\ell_o}\, dz - 1 \qquad (3.3.9)$$

where ℓ_o, ℓ_f are the initial and final length ; also note that

$$\lim_{\ell \to 0} \frac{\Delta\ell}{\ell} = \varepsilon_z$$

for continuous ε_z when $\partial v/\partial z$ and $\partial u/\partial z$ are omitted. From the FE results it is observed that gradients in the θ direction are relatively small in relation to the z direction and the dimensions of the gages. In the z direction, the transverse displacement w as well as the circumferential and radial displacements v and u all vary in the z direction. Although these z direction gradients may all exist in large magnitude at the singularity, the approximate expression should be accurate since the squares of the gradients in Equation (3.3.9) should be negligible.

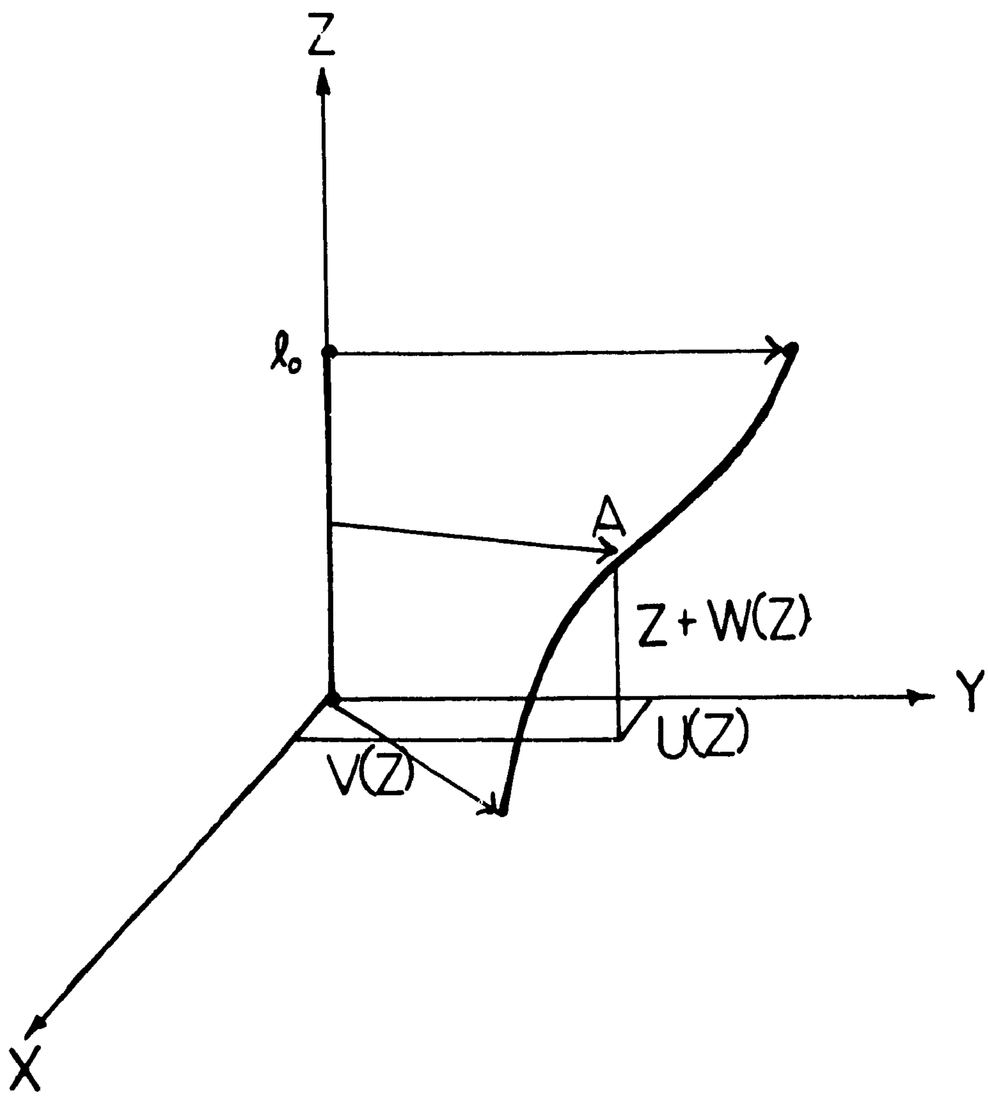

Figure 3.3.2 Single foil element represented as a line. A point A located at (0,0,z) on the undeformed length ℓ_o will have the position (u(z),v(z),z+w(z)) on the deformed length ℓ_f. The final length is then

$$\ell_f = \int_0^{\ell_o} \sqrt{(du/dz)^2 + (du/dz)^2 + (1+dw/dz)^2}\, dz.$$

3.3.2.3 Specimen Analysis

Comparisons between macro and micro models (i.e. on the macro and micro structural levels) are made with volume and surface averages i.e. minivariables. The minimum strain gage length is fixed at a present limit of about 15 graphite fiber diameters. An advantage of this is that random variations due to fiber position are likely to be mitigated. Since the ratio ℓ/a is fixed Rt/a^2 must be set for the specimen. High Rt/a^2 provides a workable surface area and more information on the distribution. Low Rt/a^2 is of interest since the theory is expected to be less accurate as this decreases. The commercial material is a tape of which seven plies were used in each layer of the specimens. Therefore, the measured results are for a relatively thick laminate and should be regarded in this light which is favourable towards the theory.

To model the experimental specimens the FE meshes were generated in the same manner as in the previous section except that for the third stage where two additional elements on the hole surface were placed as depicted in Figure 3.3.3 to represent the strain gages. These elements covered the entire hole surface and had one of three sets of properties: either adhesive, backing or a combination of foil and backing. This coarse mesh crudely models the actual instrumented plates.

The assumptions about the geometry of the plates may have some bearing on the results. The layer thicknesses, in contrast with homogeneous materials, determine the effective moduli. Specifically, for two plates having fiber volume

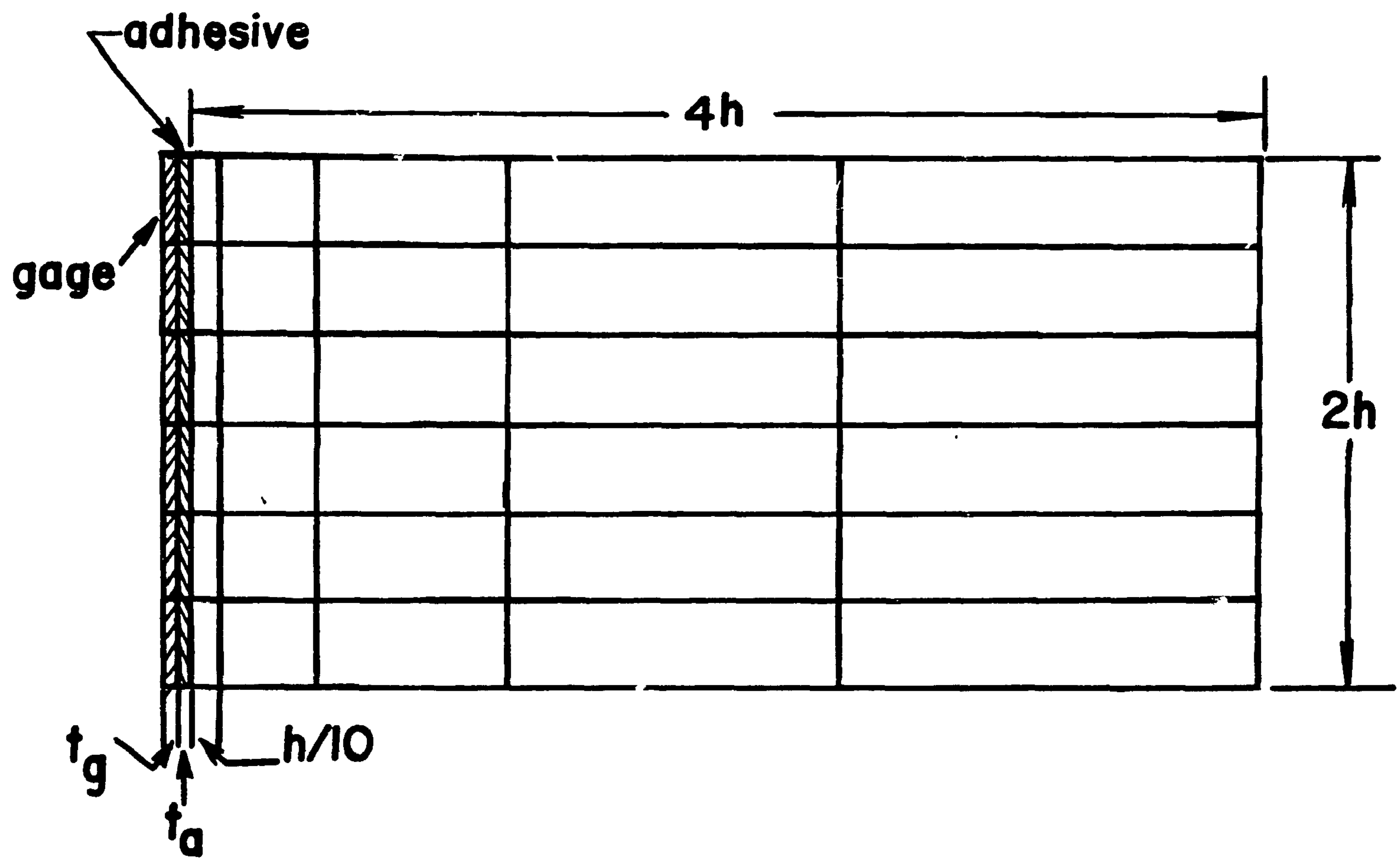

Figure 3.3.3 θ-plane distribution of finite elements used to model experimental specimens. Results were obtained both with and without gage and adhesive elements.

contents η_f and thickness t,

$$\eta_{f1}t_1=\eta_{f2}t_2= \text{ a constant.} \qquad (3.3.10)$$

The layers follow the same relation. If the plate thickness or layer thicknesses varies, so do the material properties. It is assumed in the model that the layer thicknesses are equal and that the plates are symmetric, also that the material is integral. Asymmetry would cause bending deformations to occur. Bending of the plate was measured but was found to be insignificant. In fact, the total thickness of the plates varied about ±8% in a wavy manner. Presumably, the layer thicknesses vary accordingly though not neccesarily such that their relative thicknesses were constant. If the results are very sensitive to the material properties this could be a source of scatter.

3.3.2.4 Summary

Two normal strains on the hole surface can be measured by strain gages to yield the two normal stresses. It was shown by a simple analysis that the calculated stresses may be sensitive to changes in the strains. Strain gages measure the average over the gage length and should not be sensitive to other gradients. Because material is adhered to the hole surface across the singularity, the gages are included in the FE model of the relatively thick specimen.

In this subsection, the problem methods have been analyzed to reveal possible sources of error which have been discussed and some expressed mathematically. While all these errors are possible, it remains to be seen if they are significant in magnitude.

3.3.3 Specimen Preparation and Experimental Procedures

Two specimens were prepared having the dimensions and properties shown in Table 3.3. All plates were cured in an autoclave according to manufacturer's specifications. After trimming the specimen edges and glueing fiberglass tabs to the ends the central and grip holes were drilled with a diamond drill. The holes were finished by boring with a carbide boring tool without fluid at 250 rpm, a feed rate of 12.7mm/minute, and with a depth of cut of .127mm. This left a smooth clean surface on the hole except in quadrants where the tool point travelled directly against the fibers and some tearing occurred, as well some fiber splitting occurred on the exiting side of the plate. Before mounting gages the surfaces were lightly sanded and prepared according to the manufacturer's guidelines (see also Tuttle and Brinson(1984)).

Gages were installed on the hole surface using a special jig (see Figure 3.3.4) in a pattern such as is shown in Figure 3.3.5. The symmetry of the specimens provides up to eight equivalent sights for some measurements. The positioning of the gages through the thickness was in error on average about .127mm from the desired location. Three gage lengths, .203mm, .381mm,.787mm (hereafter referred to only by these numbers without units) were used to measure the transverse normal strain while .381mm gages measured the

Table 3.3 Geometric Dimensions and Material Properties of Test Specimens

	Specimens	
Lay-up:	$[90_7/0_7]_s$	$[0_7/90_7]_s$
Material:	Hercules AS4/3501-6	Hercules AS4/3501-6
[1]Fiber Content:	67.8% by volume	71.2% by volume
Overall Length:	482.6 mm	482.6 mm
Length of Tabs:	25 mm	25 mm
Overall Width :	254.0 mm	254.0 mm
[2]Avg Thickness :	3.66 ± .13 mm	3.48 ±.1 mm
Hole Diameter :	27.94 mm	27.94 mm
	Elastic Moduli[3]	
E_{11} :	137.5 GPa	144.2 GPa
E_{22} :	10.1 GPa	10.6 GPa
ν_{12} :	0.29	0.29
ν_{23} :	0.48	0.48
G_{12} :	5.4 GPa	6.0 GPa

---

(1) A common error in the measurement of η_f using the standard procedure ASTM D-3171-76 is the reduction of weight in water due to bubbles on the specimen. This decreases η_f:

Table 3.3 cont'd

so that for duplicate measurements, the higher η_f was chosen. Evidence that the η_f chosen are correct can be seen in the fact that the product:

fiber volume x thickness

is very nearly equal for both plates.

(2) tolerance is range of variation in thickness, not measurement accuracy.

(3) From symmetry and transverse isotropy it is assumed that $\nu_{12}=\nu_{13}$, $E_{33}=E_{22}$, $G_{13}=G_{12}$, and $G_{23}=E_{33}/2/(1+\nu_{23})$.

Table 3.4: Strain Gage Dimensions and Properties[1]

Adhesive	: E= 2.76 GPa	ν= 0.35
Polyimide Backing	: E= 2.96 GPa	ν= 0.35
Epoxy/Phenolic Backing	: E= 10.34 GPa	ν= 0.35
Constantan Foil	: E= 158.6 GPa	ν= 0.30
[2]Polyimide Backing/Foil	: E= 9.90 GPa	ν= 0.33
[3].203mm Epoxy Backing/Foil	: E= 13.43 GPa	ν= 0.35

Overall Gage Thickness :	.0279 mm
Foil Thickness .	.0025 mm
Adhesive Thickness :	.0254 mm

---

(1) Dimensions and properties were obtained from the manufacturer by private communication.

(2) Assuming isotropy and using rule of mixtures. The foil is assumed to cover 50% of the gage area. Therefore, the foil volume content is (.5 x .0001)/(.001 + .0001)=.04545.

(3) Assuming isotropy and using rule of mixtures. Foil volume content is (.5 x .0001)/.0024=.02083 See note (2).

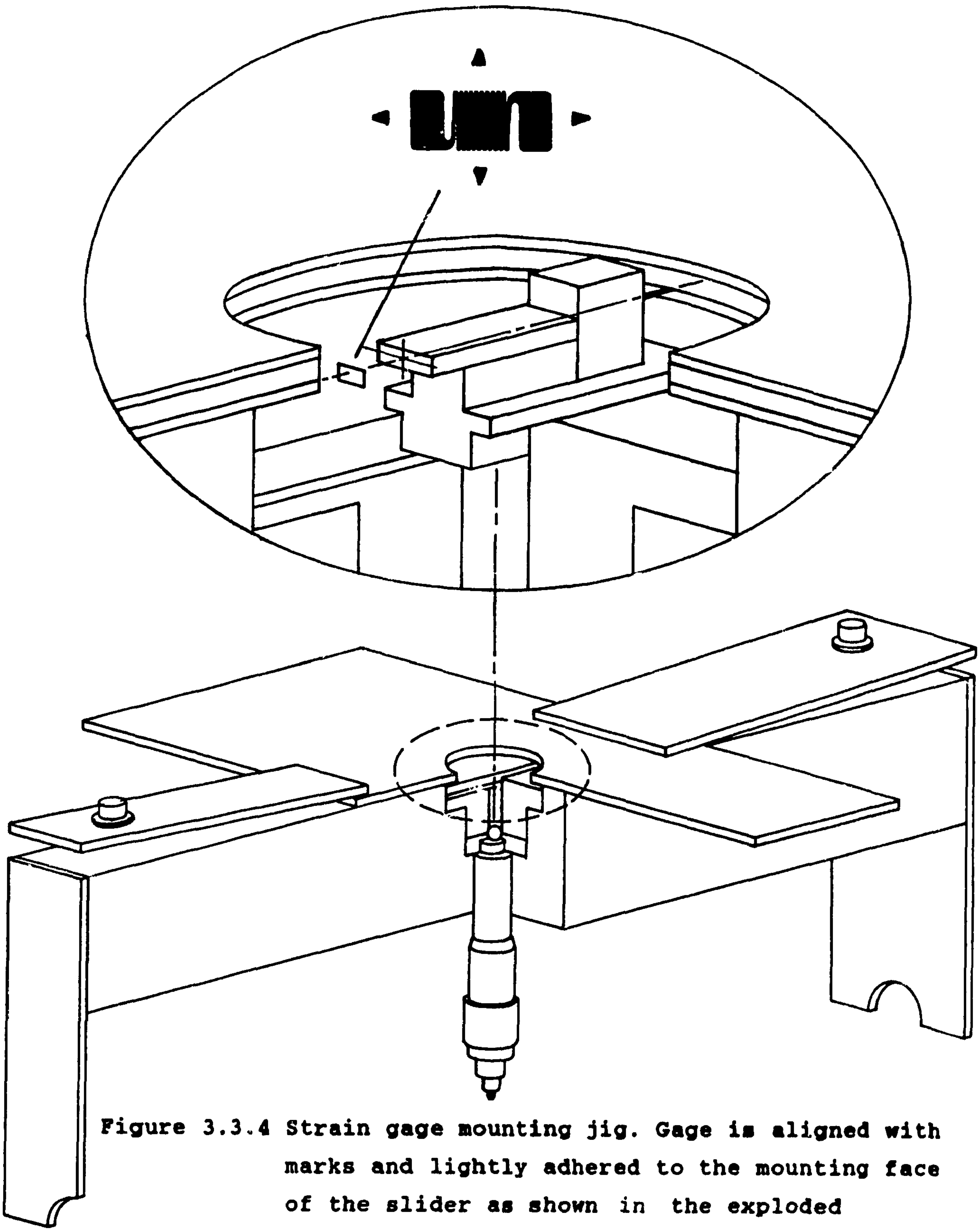

Figure 3.3.4 Strain gage mounting jig. Gage is aligned with marks and lightly adhered to the mounting face of the slider as shown in the exploded section. The needle is level with the horizontal mark and can be referenced at the interface. Positioning is done by rotating the table and the micrometer head.

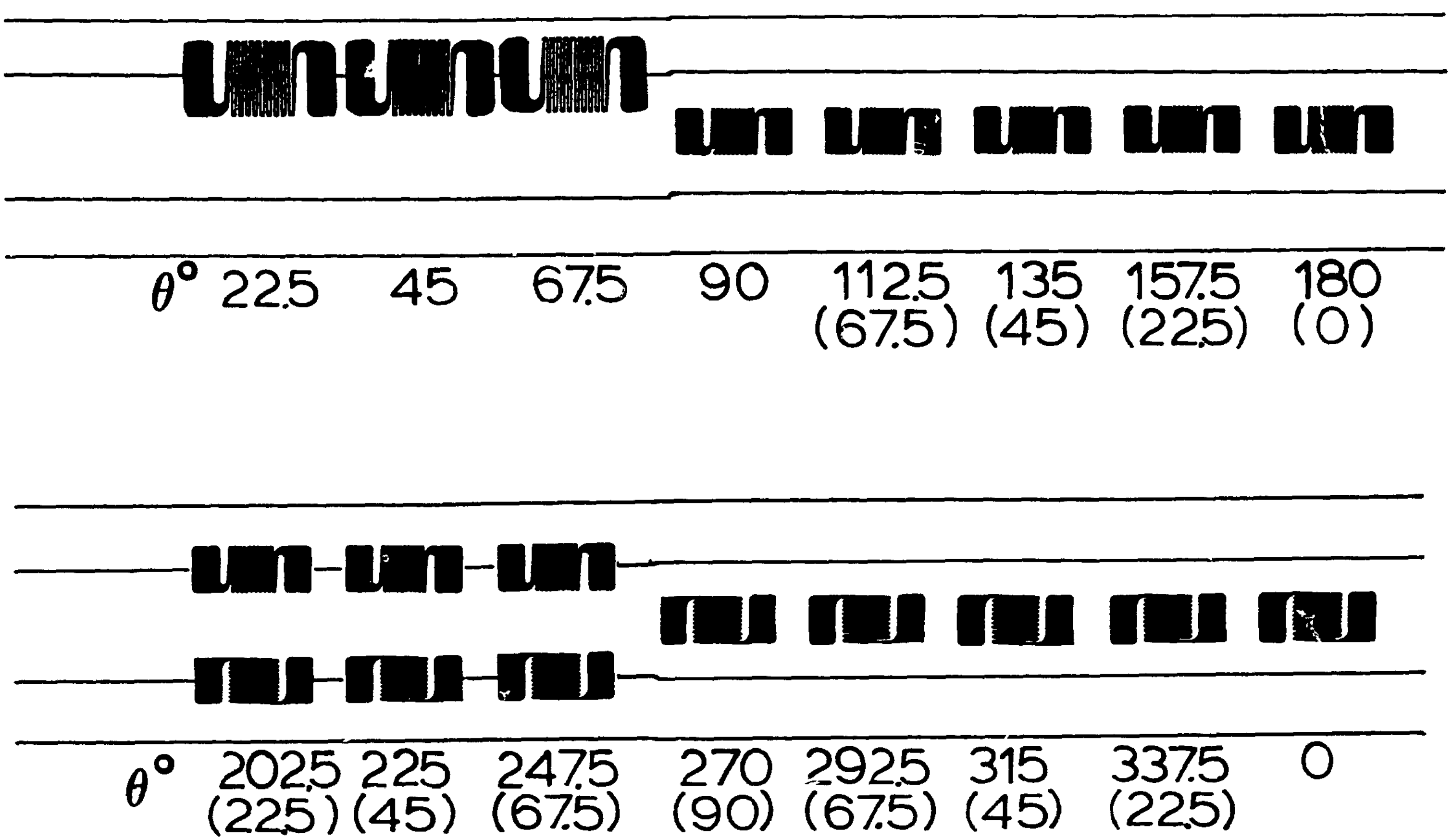

Figure 3.3.5 Typical gage mounting pattern on the hole surface.

circumferential strain in equivalent positions. The .381mm and .787mm gages have very similar construction while the .203mm gages were made with a different backing material. The properties of the gages are listed in Table 3.4. The hole surfaces were instrumented two times to obtain the data presented here. Between runs less than .13mm was machined from the hole radius to clear the surface for reinstrumentation. This small change in R/t is assumed to have a negligible effect on the results and so the data are mixed from the two replications of the experiment.

The specimens were mounted in a load frame as shown in Figure 3.3.6 The 'Whipple-tree' grip mechanisms are designed to apply four equal loads to the specimen; the distribution is somewhat less than uniform. The loading rate was less than 5mm/minute in all cases.

During the tests the gages were excited with 150 mv for the .381mm and .787mm gages and 80 mV for the .203mm gages as is recommended by the manufacturer for optimum accuracy (Micro-Measurements 1979). The specimens were loaded through four cycles while strain data were recorded using a digital acquisition system.

The strain data were analyzed by linear regression (e.g. see Mandel (1964)) to obtain the slope of the stress/strain response curve for each gage. The intercepts and variances were also calculated to detect anomalous behaviour. The final averaged slopes were corrected for the effects of the transverse sensitivity of the gages taking

Figure 3.3.6 Specimen loading and data acquisition equipment.

into account the fact that K_t is different for the three types of gages used (Micro-Measurements (1982)). The .381mm circumferential gages were used to correct all of the transverse gages and to obtain the results listed in Appendix C.

For comparison with the measured results data representing the specimen's material elastic constants, geometry and loading are required. Geometry and loading are straightforward. To obtain sets of effective elastic constants for the two plates, the fiber volume content for each was determined from a sample. Two further plates $[0_8]$ and $[\pm45_2]_s$ were made from the same batch of material used to make the holed plates, and characterized. The fiber volume content of each plate from which specimen's were cut was determined using the ASTM standard procedure D 3171-76. The elastic moduli in Table 3.3 were determined using this data and Hashin's equations in the manner described in Appendix B.

3.3.5 Results and Discussion

The results of the measured strain data from Tables C1,2 are plotted with FE solution results in Figures 3.3.7-9,11,13.

3.3.5.1 Midplane Strains

In Figures 3.3.7,8 are shown the results at the midplane. For both cases the FE model shows little effect of the gages. The measured results are in excellent agreement for both ε_z and ε_θ in the $[90/0]_s$ case; for ε_z in the $[0/90]_s$ case the agreement is fair. In the $[0/90]_s$, the discrepancy increasingly occurs towards the axis perpendicular to the load axis where the strains are, in general, the highest.

One difference between the two laminates is the orientation of the middle plies. The $[0/90]_s$ has a 90^o ply on the midplane so ν_{23} and E_{22} increasingly govern the strain near $\theta=90^o$ where ε_θ is highest, while in the $[90/0]_s$, E_{11} and ν_{13} govern the strain. The determination of the latter two moduli (a simple rule of mixtures) is a much less complex and more accurate process than for the former; ν_{23} required measurement on the edge of a specimen using a miniature gage. The material properties were derived from approximate formulas using measured data. Before questioning the model, the procedures by which the effective moduli were obtained should be investigated.

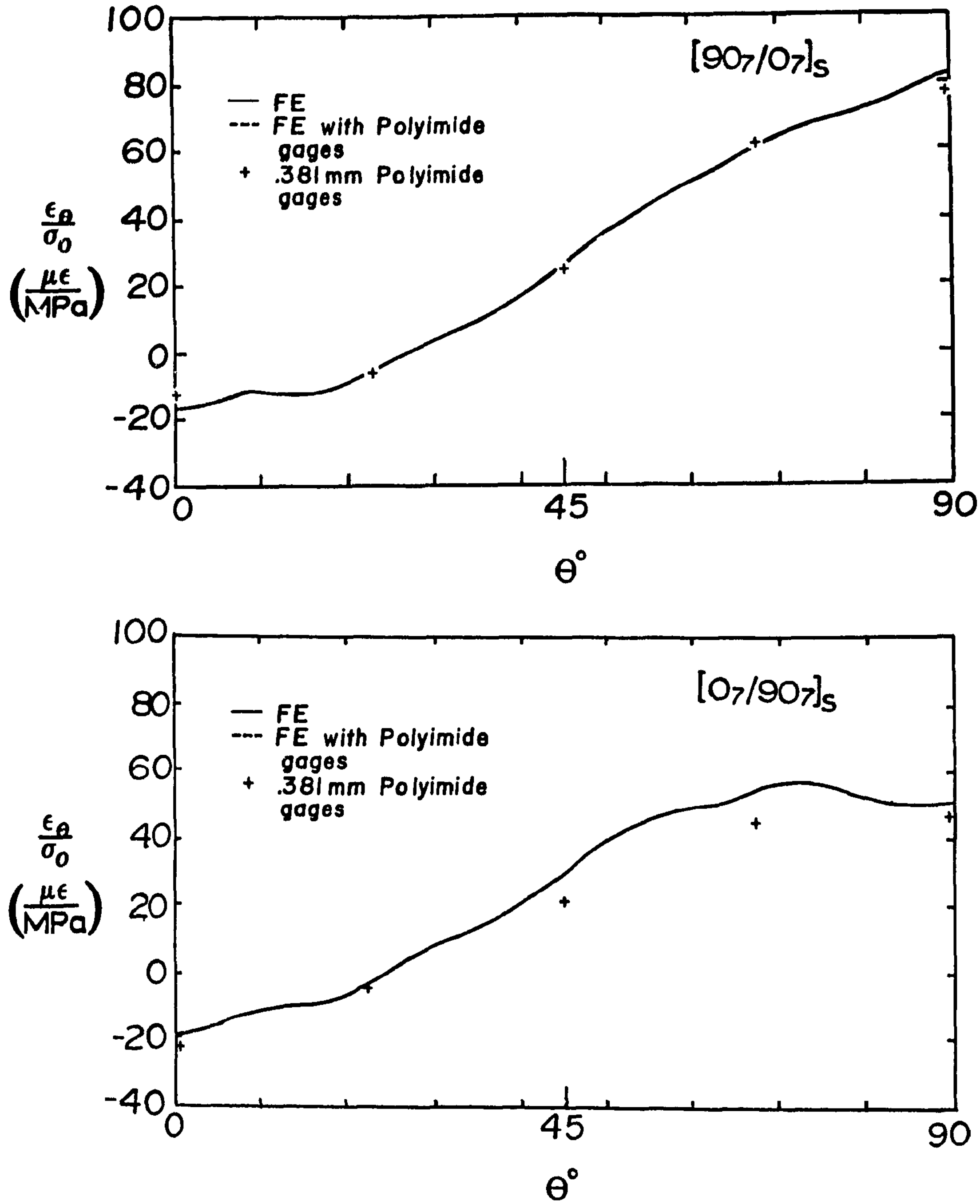

Figure 3.3.7 Circumferential normal strain from midplane of instrumented models at $r=R-t_a-t_g$ and $r=R$ of uninstrumented models and measured values.

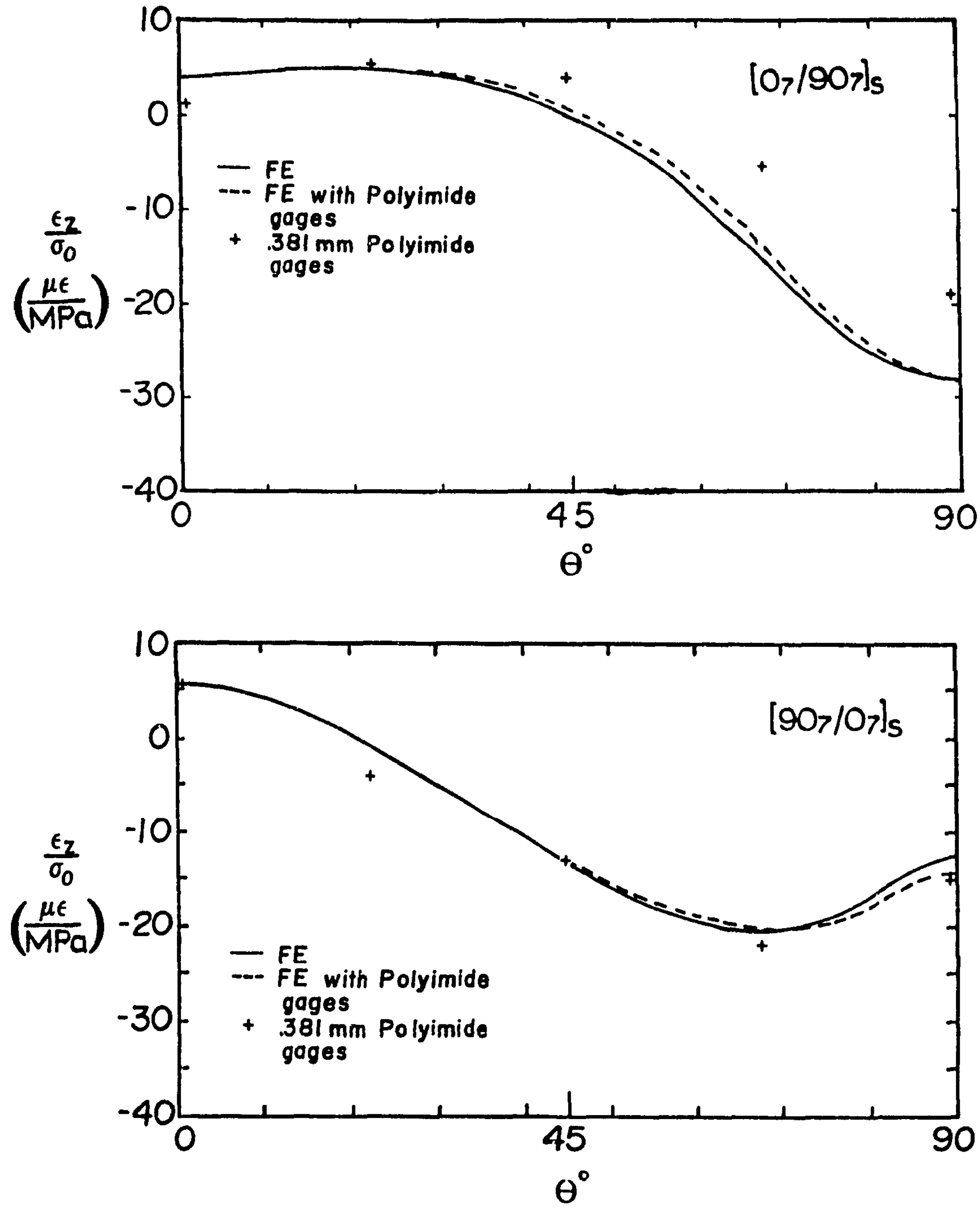

Figure 3.3.8 Interlaminar normal strain from midplane of instrumented FE models at $r=R-t_a-t_g$ and $r=R$ of uninstrumented models and measured values.

3.3.3.3 Interface Circumferential Strains

The circumferential strain from the interface is shown in Figure 3.3.9. Agreement is good except for the one unexplained point for the $[0/90]_s$ case at $\theta=67.5^{\circ}$. At this point, first the higher reading was measured. The gage was then removed and another gage was applied and the measured strain was again high indicating that the cause was in the plate (the measurement system was thoroughly checked). After the hole was resurfaced in preparation for new measurements and a new gage was applied in a different but equivalent location; the lower reading was obtained. Cracking between fibers under the gage may have occurred but was not observed (a closed crack would not be detected visually). Because of the order of procedure, the cause of the first reading is unknown.

3.3.5.3 Interface Transverse Strain

The FE results indicate that the measured transverse strain (or interlaminar strain) at the interface is modified by the presence of gages in the model. This strain, taken from different radii of the model is shown in Figure 3.3.10 (for the uninstrumented plate the ϵ_z is discontinuous and so shown is the average between adjacent elements bordering the interface). The difference in ϵ_z between the instrumented and uninstrumented models at r=R shows that the coating influences the surmised singularity. Further, the differences in the instrumented model between ϵ_z on the hole/adhesive, adhesive/gage, and gage surfaces show that the strain is poorly transferred to the gage surface. Overall these predicted effects significantly alter the strain intended to be measured.

Figure 3.3.11 shows comparison between the measured and FE results. Between 45° and 90°, the results do show definitely better overall agreement between the FE models with the gages included than with the uninstrumented model in both cases. These effects were predicted by the model and are for the present case a shortcoming of the measurement system, but since one important aspect of the work is to investigate the validity of the model the experiments were carried out. The transfer effect on the strain may be reduced by decreasing the relative thickness of the gages and adhesive layer, i.e. using a thicker specimen to reduce the gradients under the gage. It is not shown, but the strain measured by the ideal gage from Equation (3.3.9) evaluated at the interface was negligibly different from ε_z in the FE results, as expected.

Shown in Figure 3.3.12 is the gage surface distribution of ε_z through the thickness of the FE model with a polyimide gage coating for both plates(the distributions from the epoxy gage model are negligibly different). Not shown is ε_θ which is nearly uniform through the thickness except near $\theta=90^{\circ}$ where the strain in each layer differs and so is sloped across the interface. For detail near the interface ε_z is shown discontinuous although in the gage it must be continuous. The average strain measured inside each gage length must fall within the two

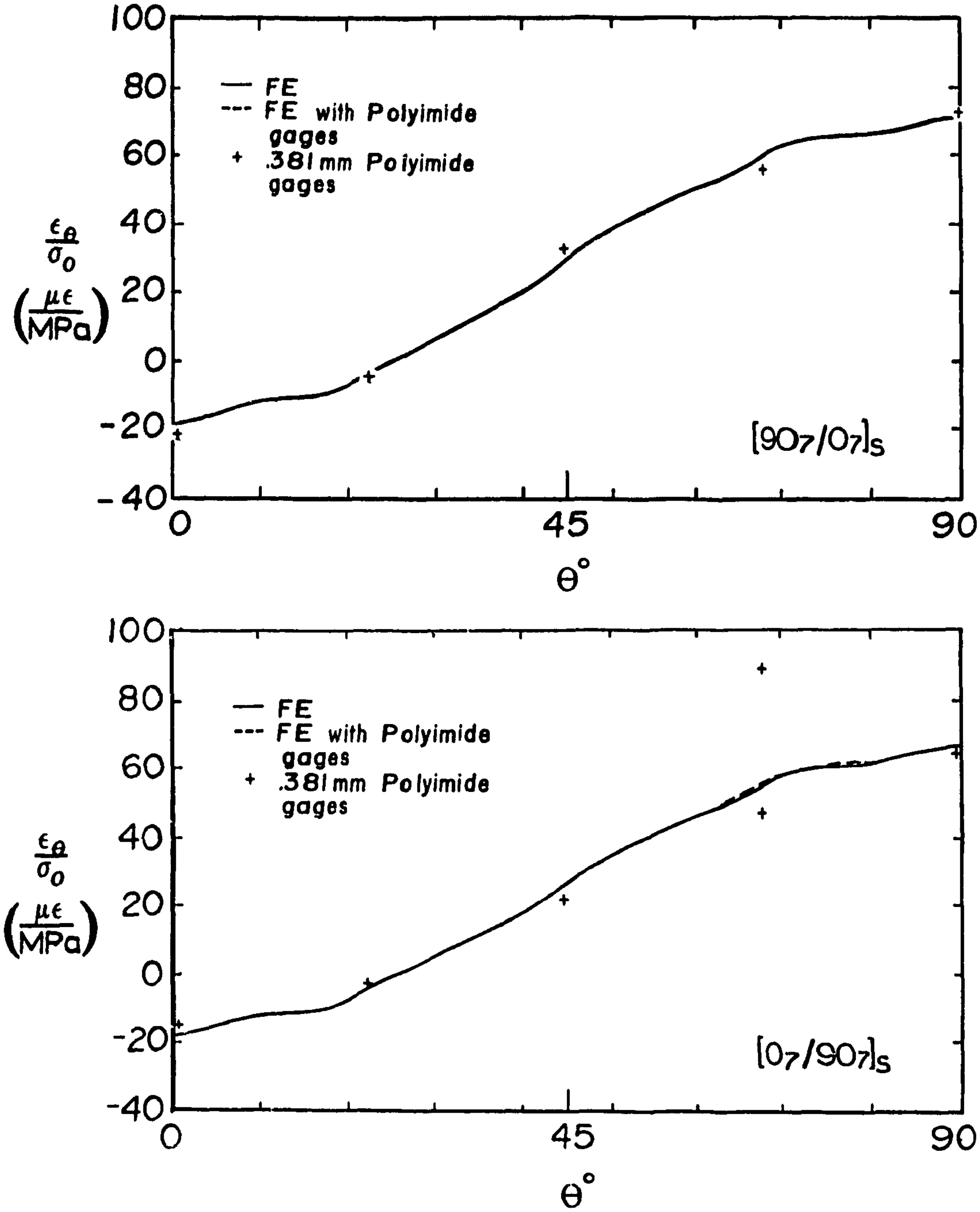

Figure 3.3.9 Circumferential strain from the interface of instrumented FE models at $r=R-t_a-t_g$ and r=R of uninstrumented models with measured values.

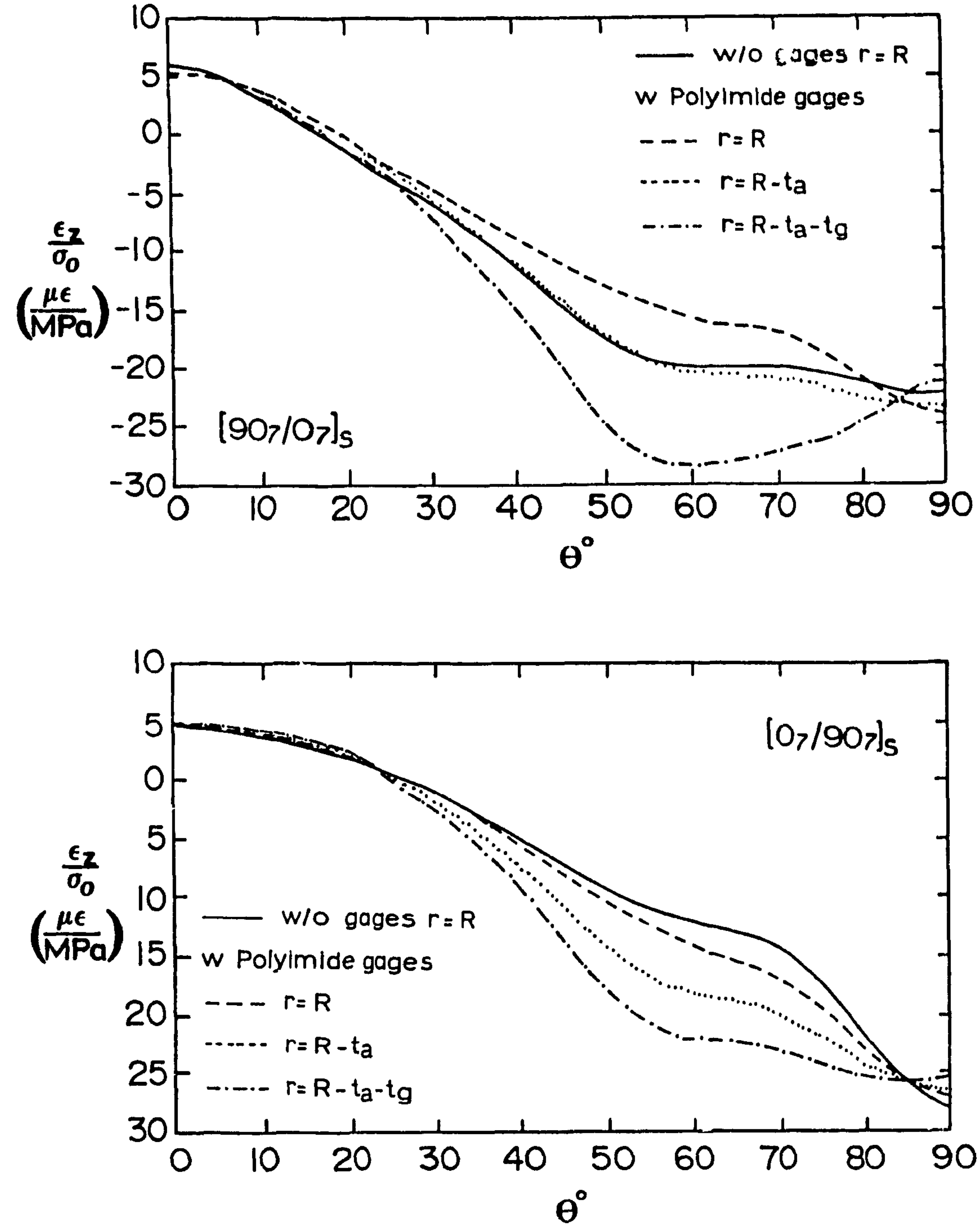

Figure 3.3.10 Interlaminar normal strain at z=h of FE models. These plots show the effect of instrumenting the hole surface on the layer interface of the plate and on the transfer of strain through the adhesive and gage to the foils.

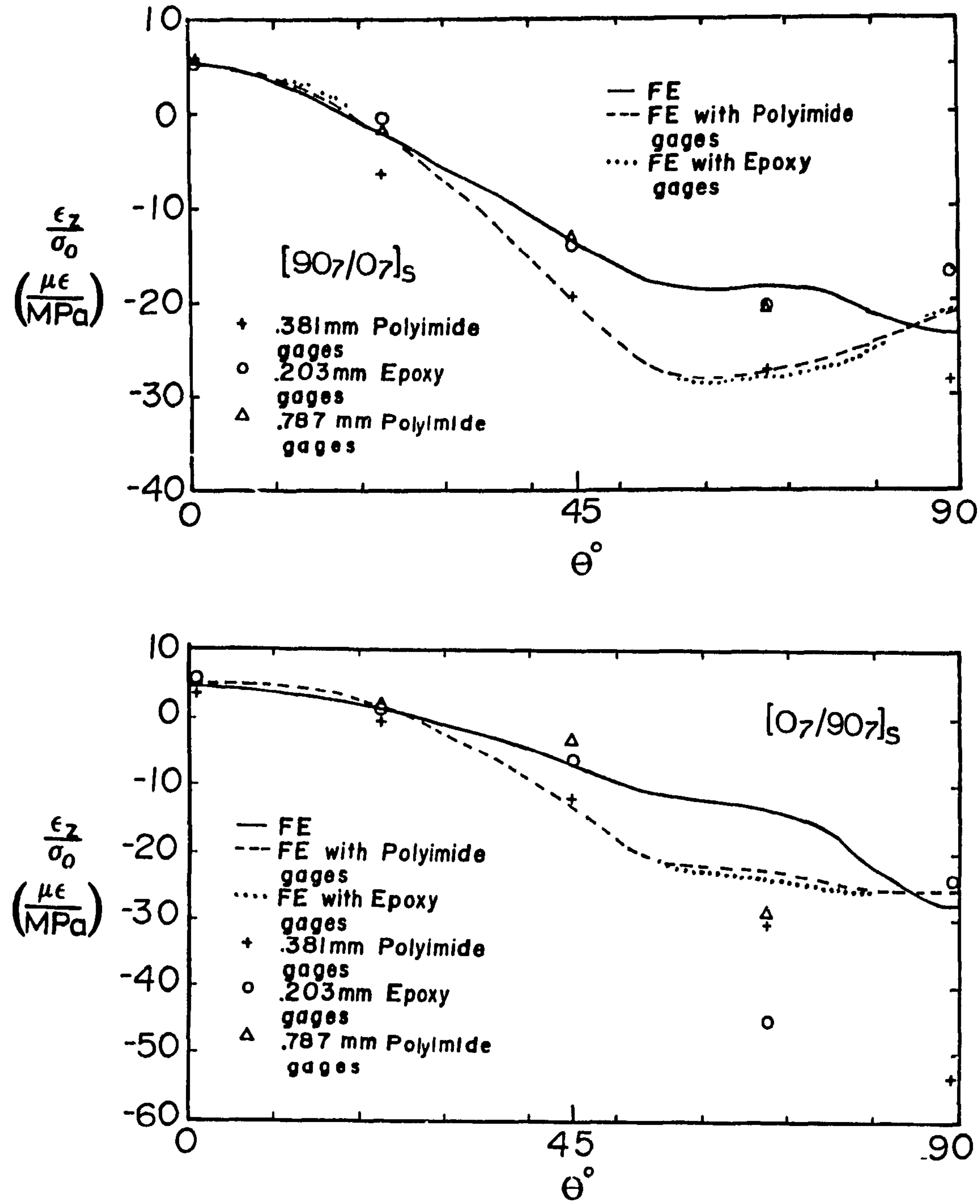

Figure 3.3.11 Interlaminar normal strain from the layer interface of instrumented models at $r=R-t_a-t_g$ and r=R of uninstrumented models and measured strains from three gage lengths.

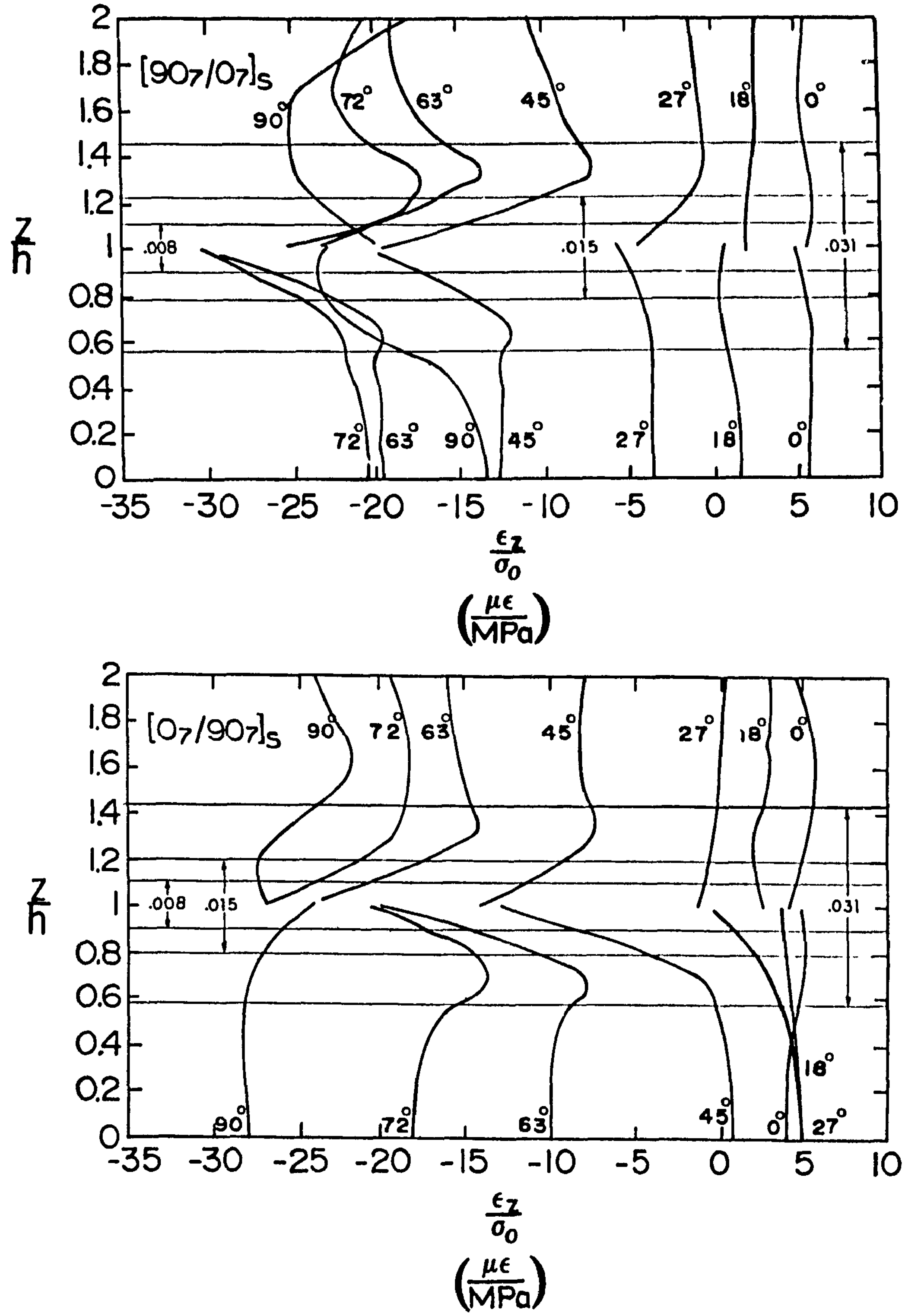

Figure 3.3.12 Interlaminar normal strain at $r=R-t_a-t_g$ of model instrumented with polyimide gages.

extreme values in that interval. The measured strain will be sensitive to the gage position depending upon the distribution of ϵ_z. From the distributions, the .203mm gages are expected to be the most sensitive to positioning. From a visual inspection Δz_o for the .203mm gages are as shown in Table 3.5. The jumps (i.e. difference) in ϵ_z and $\partial\epsilon_z/\partial z$ across the gage length are expected to change near the singularity with mesh refinement. ϵ_z is expected to be complex and error due to positioning makes accurately fitting an approximating function to the limited data unpromising.

At $\theta=0^{\circ}$ the jump is small and the strain is nearly uniform, in agreement with the magnitude and distribution of the measured results in Figure 3.3.11.

The strain is small at $\theta=18^{\circ},27^{\circ}$ but the distribution changes between these two angles. The measured results at $\theta=22.5^{\circ}$ agree very well in both cases except the .381mm gage in the $[90/0]_s$ case. The .381mm gage is wider than the .203mm and so would be more sensitive to the greater change with θ in this case.

The .381mm gage measured a lower average than the .203mm gage in both plates at $\theta=45^{\circ}$; this is not compatible with FE results. Since the distribution is nearly symmetric, if the magnitude near the surmised singularity is greatly increased any shift of the .203mm gage will lower its average; this is much less so for the .381mm gages. This explanation is correct in trend but it is doubtful if the magnitudes even in a refined mesh will confirm this. The .203mm gages were well positioned. The FE results give no indication of a sign change near the singularity while it is clearly indicated in the measured results. This could be evidence of influence of the microstructure. Angles between fibers do not change, the influence of the microstructure could depend upon the angle at which fibers intersect the edge.

At $\theta=63^\circ, 72^\circ$ $\Delta\bar{\varepsilon}_z$ can be large, increasing or decreasing the average from a shift in position, and it increases as the gage length decreases. For example, for the $[0/90]_s$ case (using ε_z from Figure 3.3.12)

$$\Delta\bar{\varepsilon}_z \approx -39\ \frac{\Delta z_o}{h} - 275\ \frac{\Delta z_o^2}{h^2} \text{ and}$$

$\frac{\Delta z_o}{h} = \pm.117$ inches yields $\Delta\bar{\varepsilon}_z \approx -6, +3$ from Equation (3.3.8). The average is increasing inversely to gage length which the $[0/90]_s$ measured results agree but not the $[90/0]_s$. Very poor positioning of the .203mm gage explains the $[90/0]_s$ case. The strain at the actual shifted position is about -20 $\mu\varepsilon$/MPa which is just what the gage measured. In the $[0/90]_s$ case, the strain measured by the well positioned .203mm gage is very large and in agreement with the present FE distribution if the effects of mesh refinement are allowed.

$\Delta\bar{\varepsilon}_z$ is small but the slope changes in sign at $\theta=90^\circ$ approaching the interface from either side in the same

Table 3.5 Positioning error of .203mm Strain Gages in mm

	Δz_o	
θ^o	$[90_7/0_7]$	$[0_7/90_7]_s$
0	−.025	−.025
22.5	+.102	−.076
45	−.025	+.025
67.5	+.127	−.025
90	+.051	+.025

manner as for σ_z. The .203mm gages which measured this strain were well positioned. In both cases can be seen that the average ε_z measured is a much larger negative value for the longer .381mm gage. The change is much larger than the distribution from the present FE results show. The sharper distribution which is surmised to occur with higher mesh density would be more compatible.

To summarize the results for ε_z at the interface, the measured ε_z agree within reasonable limits with the present results from the model. The distribution through the thickness at $\theta=45^\circ$ does not, in either case, agree in a manner which can, beyond the assumptions considered to be salient, be accounted for here. In support of the present results from the model the measured distributions are compatible elsewhere; moreover agreement improves when the surmised influence of mesh density is allowed.

The situation *very* near the interface is apparently more complex than the present methods can predict with great numerical accuracy ; more detailed work is necessary before any conclusion can be made about the adequacy of the model in this region.

3.3.5.4 <u>Stresses from Strains</u>

Finally, shown in Figure 3.3.13 are comparisons of the stresses calculated from FE and measured strains. As expected, σ_θ shows excellent agreement at the midplane while σ_z is sensitive to the difference in strains.

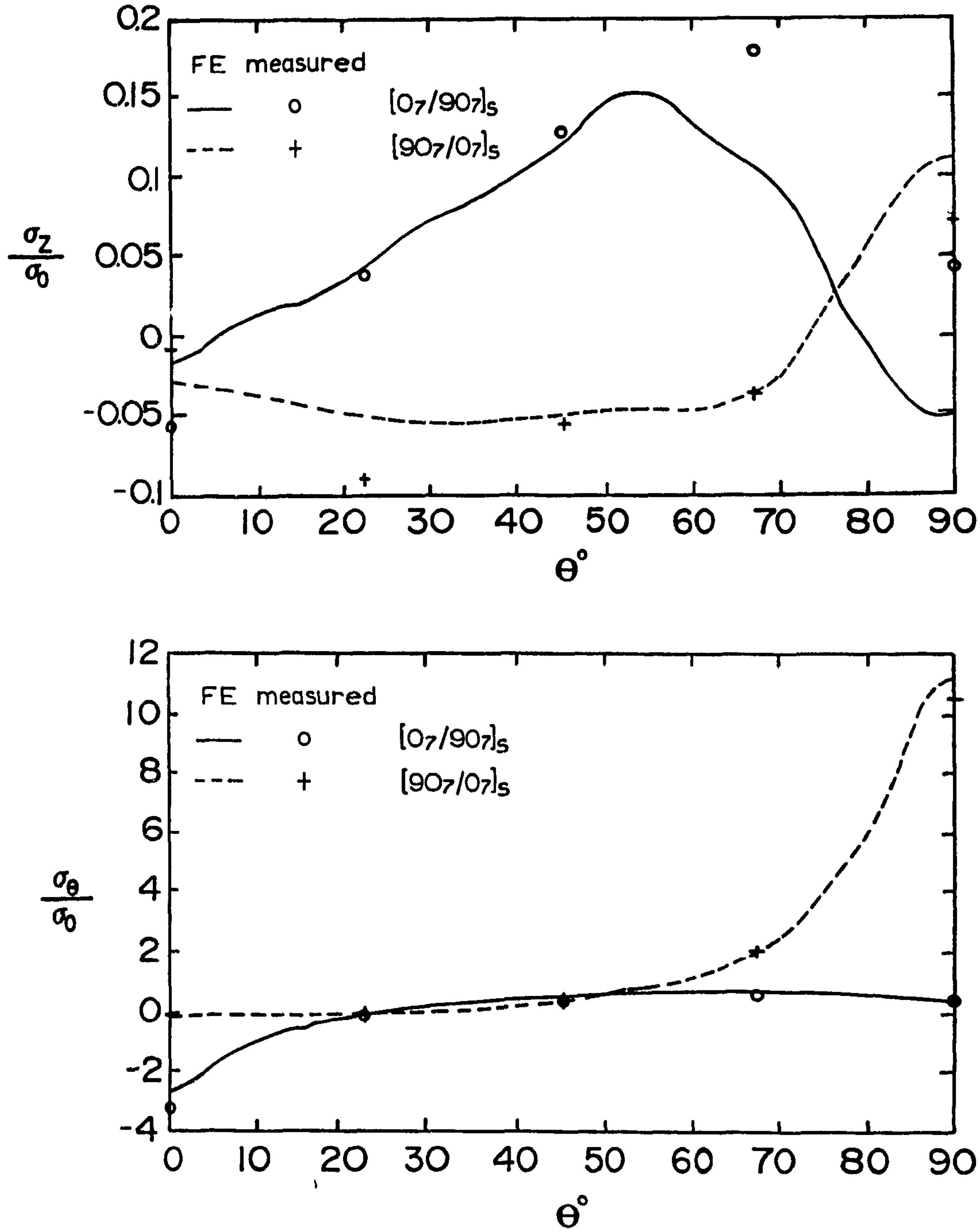

Figure 3.3.13 Interlaminar normal stress (top) and circumferential stress from the FE model and measured strains at r=R, z=0.

3.3.5.5 <u>Discussion</u>

Regarding the overall success of the analysis it must be emphasized that due to the predicted behaviour of the measurement system for ϵ_z at the interface agreement was achieved only after that effect was accounted for and not directly as was desired. Some evaluation of the measurement system and general approach in light of the results is appropriate.

The measurement system suffers from problems of scale. The results indicate that due to high macro-strain gradients positioning accuracy of the gages became a significant factor and the strain would not transfer unaltered through a relatively thick gage. Also, the minimum gage length available will not measure over a single fiber diameter as would be desirable to guide and verify the theory. Because of these effects the gages were approximately represented in the model. This is cumbersome, contributes further to error, and further discourages more rigorous methods of obtaining solutions. While awaiting further theoretical developments in analysis at the microstructural level of composites or measurement techniques of higher resolution which do not interfere and could be applied to this problem, it would be useful to construct enlarged models for measurements.

By increasing the absolute diameter of the fiber, for example by a factor of ten, while maintaining the relative material (by using a cheaper linear elastic material), loading and geometric parameters constant for relevant problems, the observed effects of scale could be mitigated without great expense. This recommendation is based not only on the results observed here, but also on the reading done in preparation for the present work. As was mentioned in the introduction to this section such work has been conducted, but none sufficiently relevant to the material system of concern in this work.

3.3.6 Conclusions and Recommendations for Future Work

Strain gages can give accurate measurements of the circumferential strain, and the interlaminar normal strain away from the interface. At the interface, the discrepancies in ϵ_z between the instrumented model and measurements are attributed to h-dependence of strain in the FE results and effects of scale in the measuring system. Comparison improves after accounting for these factors.

From what has been learned in the present analysis, to obtain more detailed measurements without influence of the measurement system near the interface, enlarged fiber-reinforced models could be used.

For a straight edge, Kriz(1977) determined using a perturbation solution that the interlaminar stress distributions of Gr/Ep $[\pm 45]_s$ laminates were particularly sensitive to the G_{23} modulus. While this study used a questionable method of solution it was feasible because the computational efficiency of the method facilitated the work. In future work on the present problem, some analysis of the sensitivity of the boundary layer behaviour to the material properties using a more efficient method of solution should be performed to determine if errors in the experimentally determined elastic moduli will significantly influence the behaviour and effect comparison with measured results.

3.4 FE Analysis of Selected Problems

3.4.1 The Influence of R/t on $[0/90]_s$, $[90/0]_s$ Laminates

It can be seen in the literature survey in Section 3.1 that all prior analyses apart from Lucking et al (1984) which had reasonable solution accuracy were done for a fixed or very large value of R/t. In this subsection the model is used to study $[0/90]_s$ and $[90/0]_s$ laminates having the material properties listed in Table 3.1 for R/t varied over a range of 1-25.

To vary R/t the thickness parameter was varied while R remained fixed. The same number of elements were used for each mesh with the distribution of elements in the θ-plane of the third stage for each case as shown in Figure 3.4.1; this mesh models the 3-D interlaminar stress boundary layer. In comparing the results using this scheme, because the mesh density varies and the effect on solution accuracy near the singularity is significant but unquantified, the interlaminar stresses near the singularity cannot be compared between solutions. Specifically, on a θ=constant plane h/t is constant but h/R varies directly with R/t being lowest for R/t=25; therefore the mesh density relative to the radial dimension of the *inplane* stress boundary layer varies directly with R/t. This precludes definite comparison between the interlaminar stresses at the interface for different R/t values.

The interlaminar stresses at the interface on the

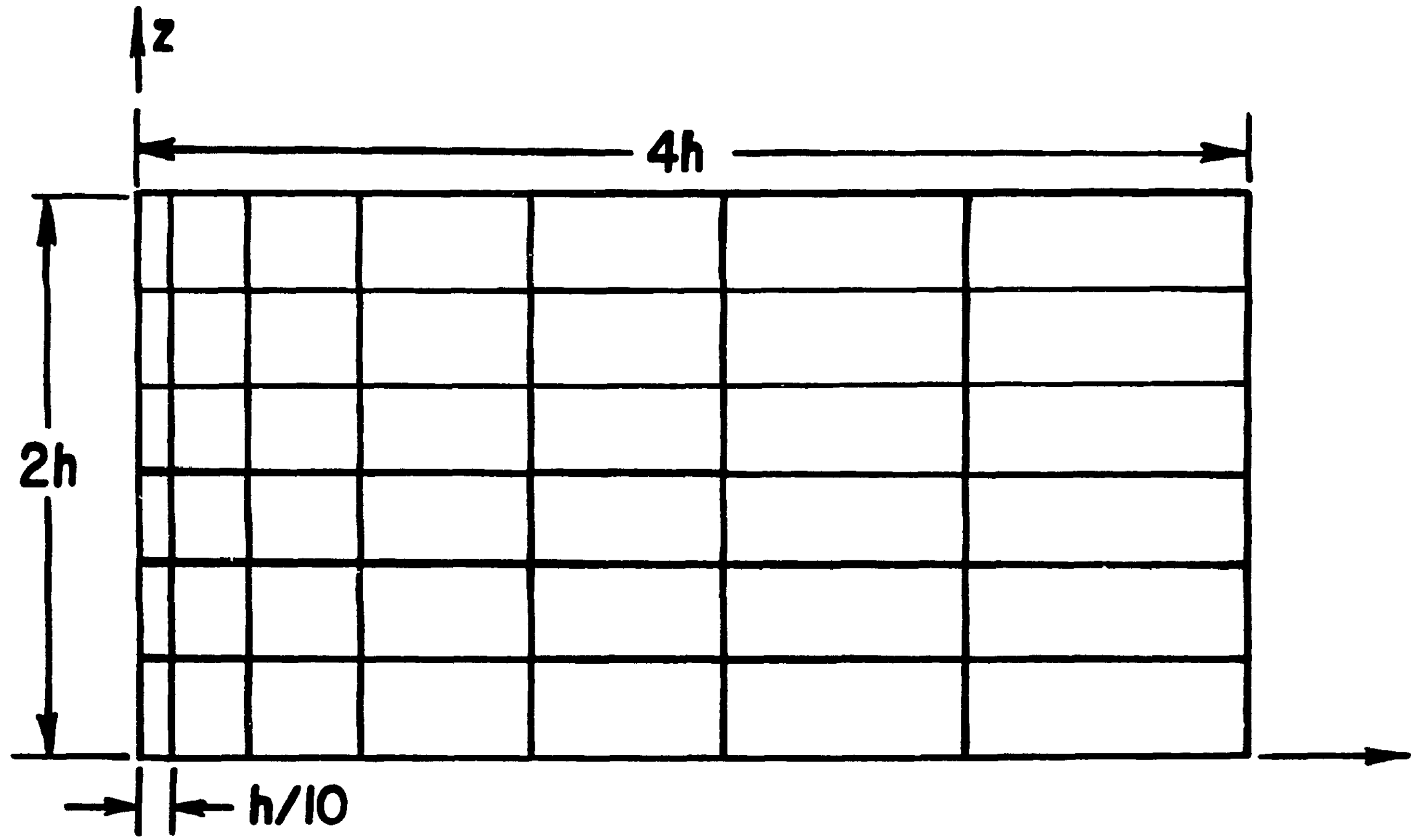

Figure 3.4.1 θ-plane distribution of finite elements in the final stage of model used for R/t study.

hole surface are shown in Figure 3.4.2 and 3.4.3. In the solutions $\tau_{z\theta}$ increases with R/t. Stacking sequence reverses the sign but otherwise has a negligible effect so only the $[0/90]_s$ case is shown. σ_z averaged between layers in Figure 3.4.3 is small and shows little change with R/t. In Figure 3.4.4 the distribution through the thickness for the extreme R/t values is shown. $\tau_{z\theta}$ is the stronger of the two interlaminar stresses for all R/t shown. τ_{rz} (not shown), which must vanish on the hole surface, did not exceed 10% of the applied stress.

In Figure 3.4.5 σ_z on the hole surface at the midplane is plotted for varying R/t. These results are expected to be accurate since little change was observed between each stage of the solution and the midplane is furthest from the singularity on the hole surface. The distribution is greatly affected by R/t and is radically different for the two stacking sequences. σ_z on the midplane may be maximum in tension depending upon R/t and stacking sequence; for maximum in tension the two stacking sequences show reversed trends with R/t. It should also be remembered that the signs of the stresses will be reversed for applied compressive stress and that stresses from the two stacking sequences can be superposed for biaxial loading.

In Figure 3.4.5 the change in σ_z between increasing increments of R/t is decreasing. For example, in both cases it changes far more between 1.00 and 12.5 than it does between 12.5 and 25. A similar trend, although affected by

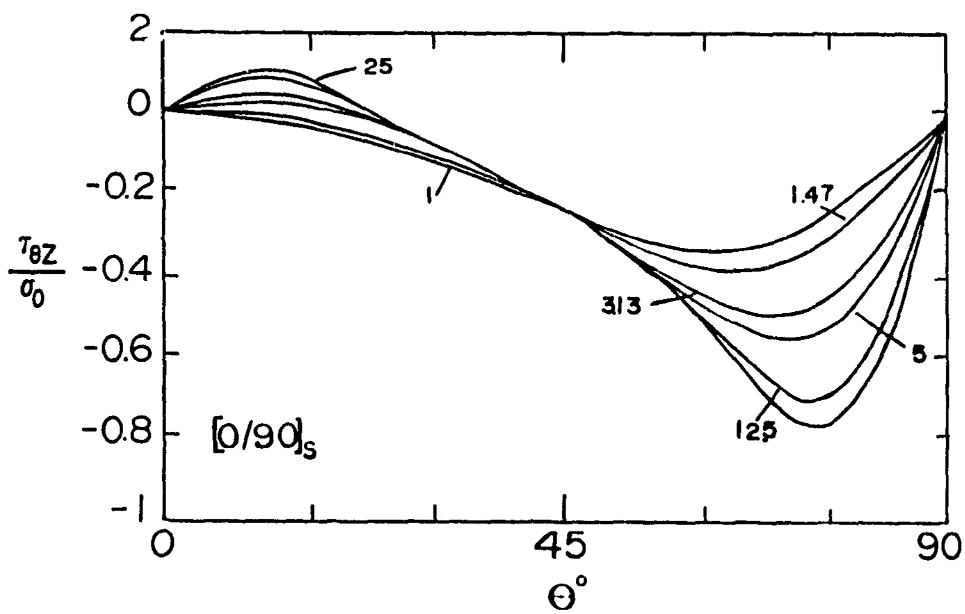

Figure 3.4.2 Interlaminar shear stress at r=R,z=h from FE model of $[0/90]_s$. The distribution for the $[90/0]_s$ case is nearly identical except in sign.

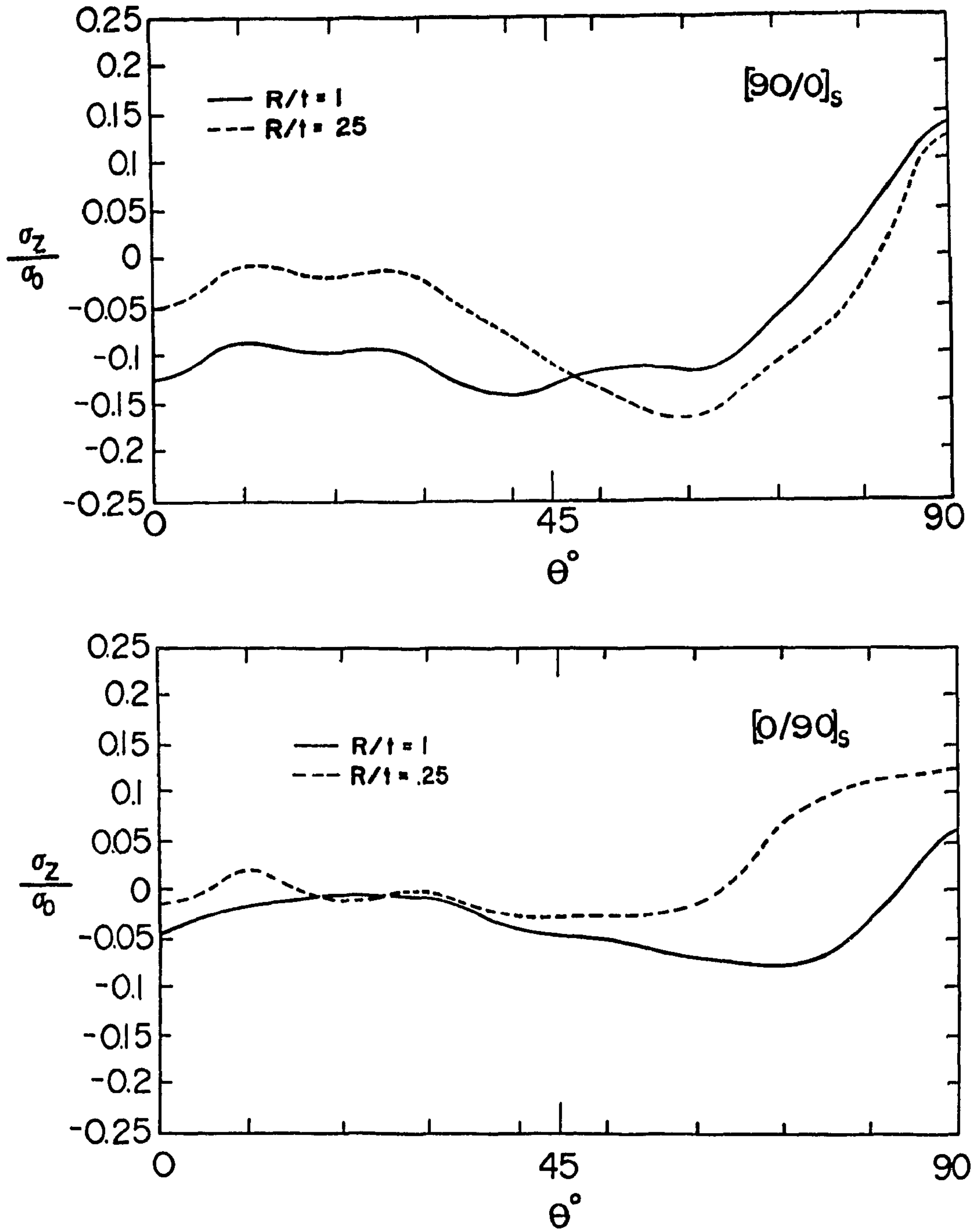

Figure 3.4.3 Interlaminar normal stress at r=R, z=h for thick and thin laminates (R/t=1,25) shows little difference in magnitude between these two extreme cases.

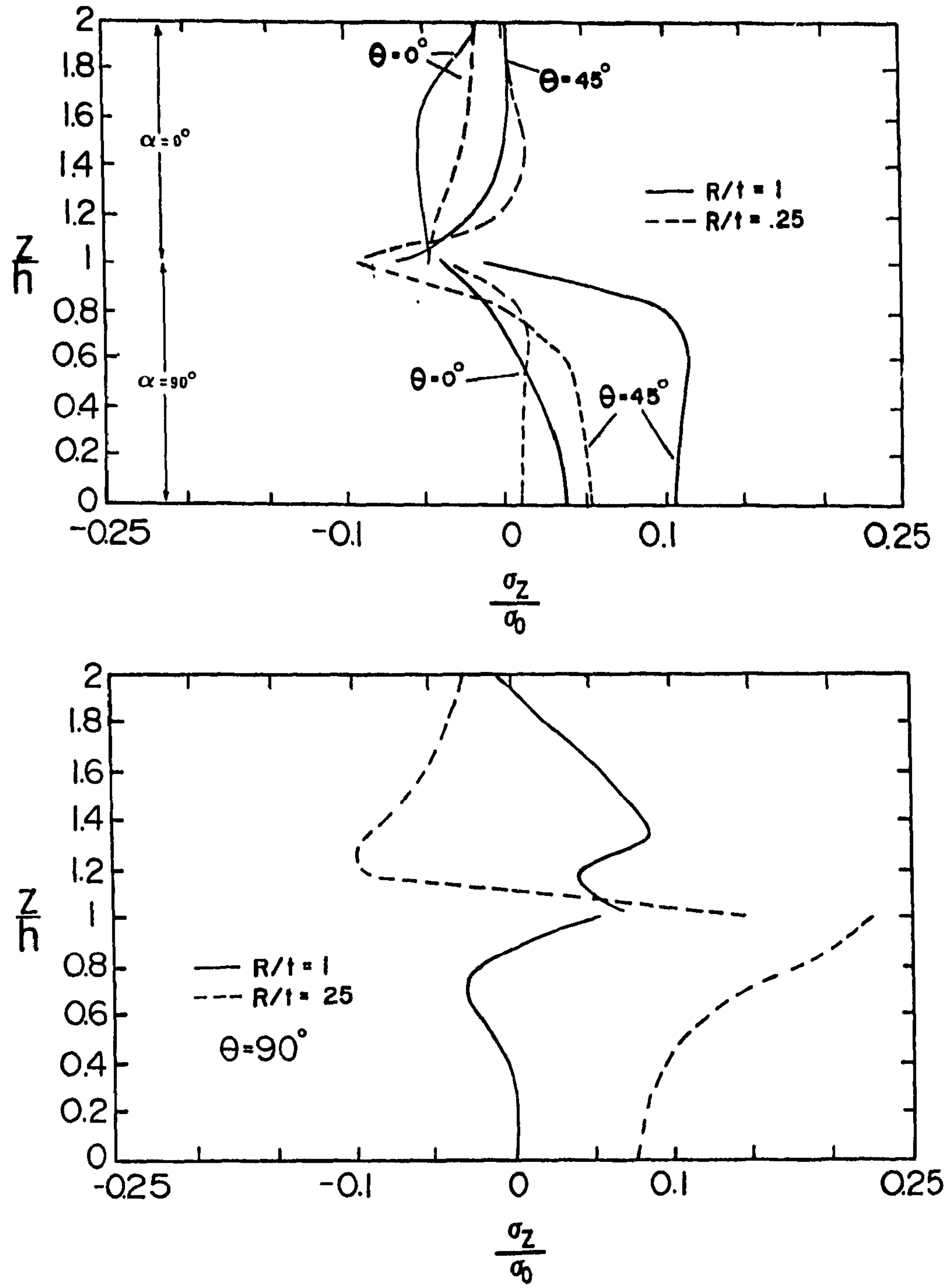

Figure 3.4.4a) Interlaminar normal stress at r=R through the thickness of the $[0/90]_s$ case for thick and thin laminates.

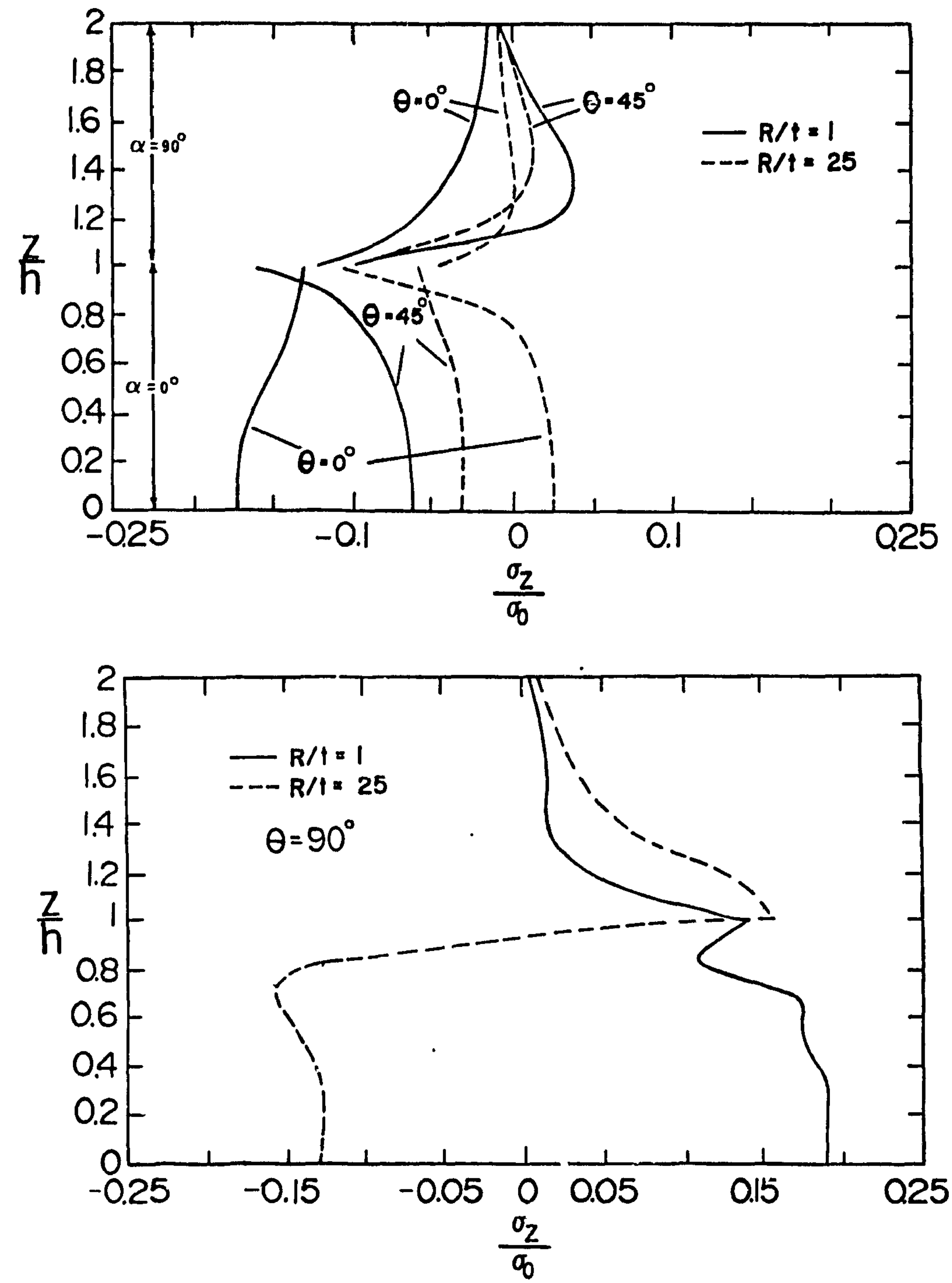

Figure 3.4.4b) Interlaminar normal stress at r=R through the thickness of the $[90/0]_s$ case for thick and thin laminates.

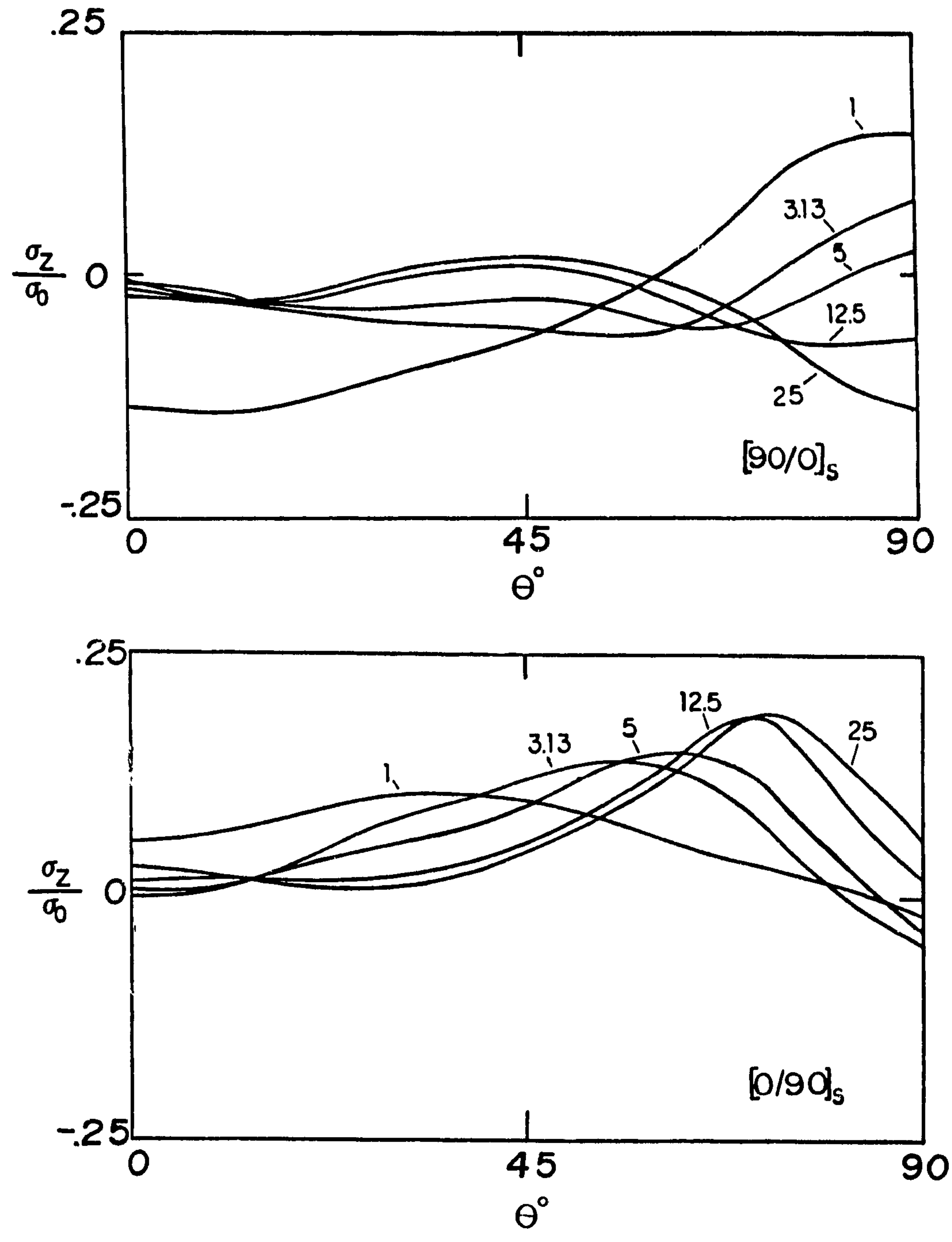

Figure 3.4.5 Interlaminar normal stress at r=R, z=0 for R/t varying from 1-25.

h-convergence, appears in $\tau_{z\theta}$. It appears that a three dimensional state is approached asymptotically.

The distribution of σ_z through the thickness is shown in Figure 3.4.6. The characteristic slope reversal in the $\alpha=0^{\circ}$ is evident at $\theta=90^{\circ}$ in both laminates for R/t=25.

Overall, σ_z is low, i.e. less than 20% of the applied stress. Although the values predicted here are low for composite laminates or even unidirectional plates this stress acts on one of the planes of lowest strength. For isotropic plates Sternberg(1949) found that σ_z was dependent upon the Poisson's ratio and rapidly approached the plane strain value of $\sigma_z/\sigma_o=2\nu$ as R/t decreased. σ_θ was affected negligibly by R/t.

The inplane stresses show an interesting comparison with the two methods of using the orthotropic layer formulae (Equation (3.2.7)) described Section 3.2. In Figure 3.4.6 it can be seen that all curves are close except at $\theta=0^{\circ}$ in the $\alpha=90^{\circ}$ layers and at $\theta=90^{\circ}$ in the $\alpha=0^{\circ}$ layers. At $\theta=90^{\circ}$ it appears that the unbonded formula is closest for low R/t while the bonded formula is closest for high R/t. In either case the bonded method agrees better at the interface where the layers are bonded; the thicker layers may deform without high interlaminar shear strain required in the thinner layers. By this heuristic reasoning, for very low R/t plane strain solutions for individual layers may be required, although the plane strain stresses may not be significantly different. At $\theta=0^{\circ}$ the $\alpha=90^{\circ}$ layer appears to be more

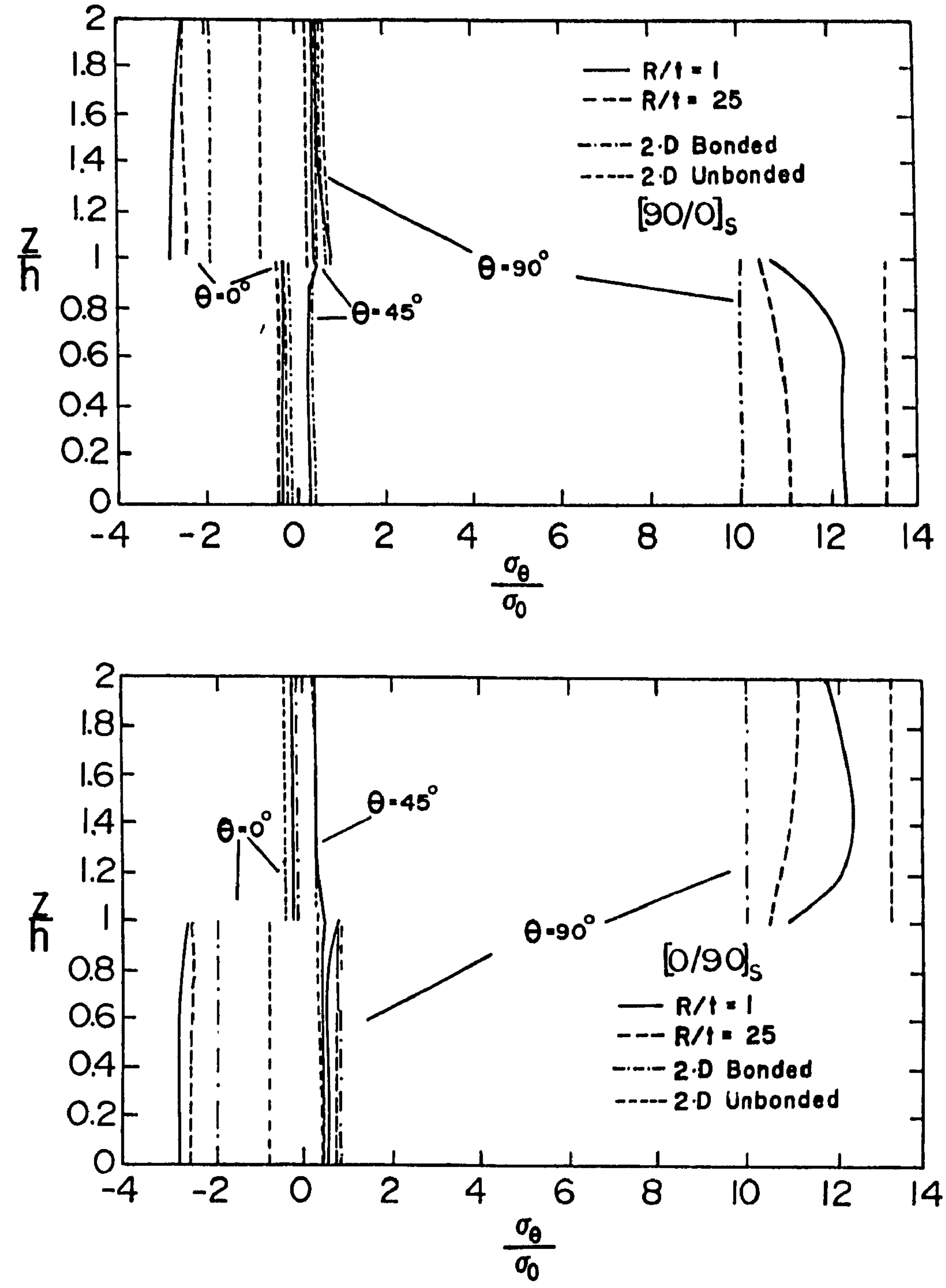

Figure 3.4.6 Circumferential stress at r=R for thick and thin laminates (R/t=1,25) from the FE model and two methods using the plane stress formula.

influenced by the deformation of the $\alpha=0^{\circ}$ layer than by its own loading and is stressed closer to the bonded case. For designers, this method could be a practical way of estimating bounds for the maximum inplane stress concentration which depends on R/t.

In summary, an FE solution having a constant number and distribution of elements within the boundary layer was used to investigate the effect of R/t on $[0/90]_s$ and $[90/0]_s$ laminates under uniform uniaxial loading. $\tau_{z\theta}$ was the strongest interlaminar stress in all cases. σ_z has extrema on the hole surface at the midplane where its distribution is greatly affected by R/t and stacking sequence but its maximum magnitude is less than 20% of the applied load. Interlaminar stresses near the singularity are h-dependent while h varied with R/t for the scheme used. At the interface σ_z is again small and did not appear to be significantly affected by R/t and stacking sequence. The maximum stress concentration at the hole surface appears to be bounded w.r.t. R/t by the bonded and unbonded plane stress formulae.

3.4.2 The Influence of R/t on [90/0] Laminates

In this subsection plates similar to those in the previous section are investigated in the unsymmetric configuration. Unsymmetric laminates, due to their layered heterogeneity, deform in part by curving in response to membrane loading. That is, in terms of Classsical Lamination Theory

$$\bar{B} \neq [0].$$

For a [90/0] configuration ([0/90] is the mirror image) when N_x, $M_x \neq 0$ the model is changed from the symmetric case only in that $\sigma_{iz}=0$ replaces the symmetry boundary condition along z=constant. Results were generated for R/t=2,10,50.

The FE model was largely unchanged from the symmetric case. The boundary layer in which the inplane stresses are affected by the hole in a plate in bending is roughly the same size as for a plate in extension (see Savin (1961) pg. 349) so W=10R was used as for the symmetric plates. Far field σ_x from CLT which varies linearly across the thickness of each layer (see Figure 3.4.11) was applied at x=L/2. The same substructuring scheme was used. A first observation on the results was that the depth of the boundary layer in these laminates is again occurring only to a depth of one laminate thickness (2h in this case) radially from the hole surface so the meshes used were less dense in relation to the boundary layer dimension than for the symmetric laminate. Again the interlaminar stresses were maximum on the hole surface and τ_{rz} was negligibly small.

$\tau_{z\theta}$ is plotted through the thickness on the hole surface in Figure 3.4.7. The distribution and magnitude of $\tau_{z\theta}$ at the interface shown in Figure 3.4.8 is near what was found in the symmetric laminates although it is slightly stronger at the interface than in the symmetric case.

σ_z on the hole surface is shown in Figures 3.4.9,10. As seen in Figure 3.4.9 the shape of the curves through the thickness is similar to what was observed in the symmetric plates but since σ_z must vanish at z=0,2h it is of most interest at the interface. In Figure 3.4.10 σ_z along the interface does not exhibit much change in distribution between R/t=10 and 50. However, while the distribution of σ_z on the hole surface along the interface is very similar to that of the symmetric plates, the magnitude is nearly doubled for the same mesh. Because σ_z is broadly distributed with θ having a maximum on the interface near $\theta=55^{\circ}$ a biaxially loaded plate would have a maximum, for example when R/t=50, of near $-\sigma_o$; although buckling would obviously also be considered, delamination would be a concern for compressive σ_o.

Similar to the symmetric case, comparable results for σ_θ on the hole surface may be obtained from superposing the exact plane stress solutions for orthotropic plates in uniform tension and an approximate solution for a thin holed

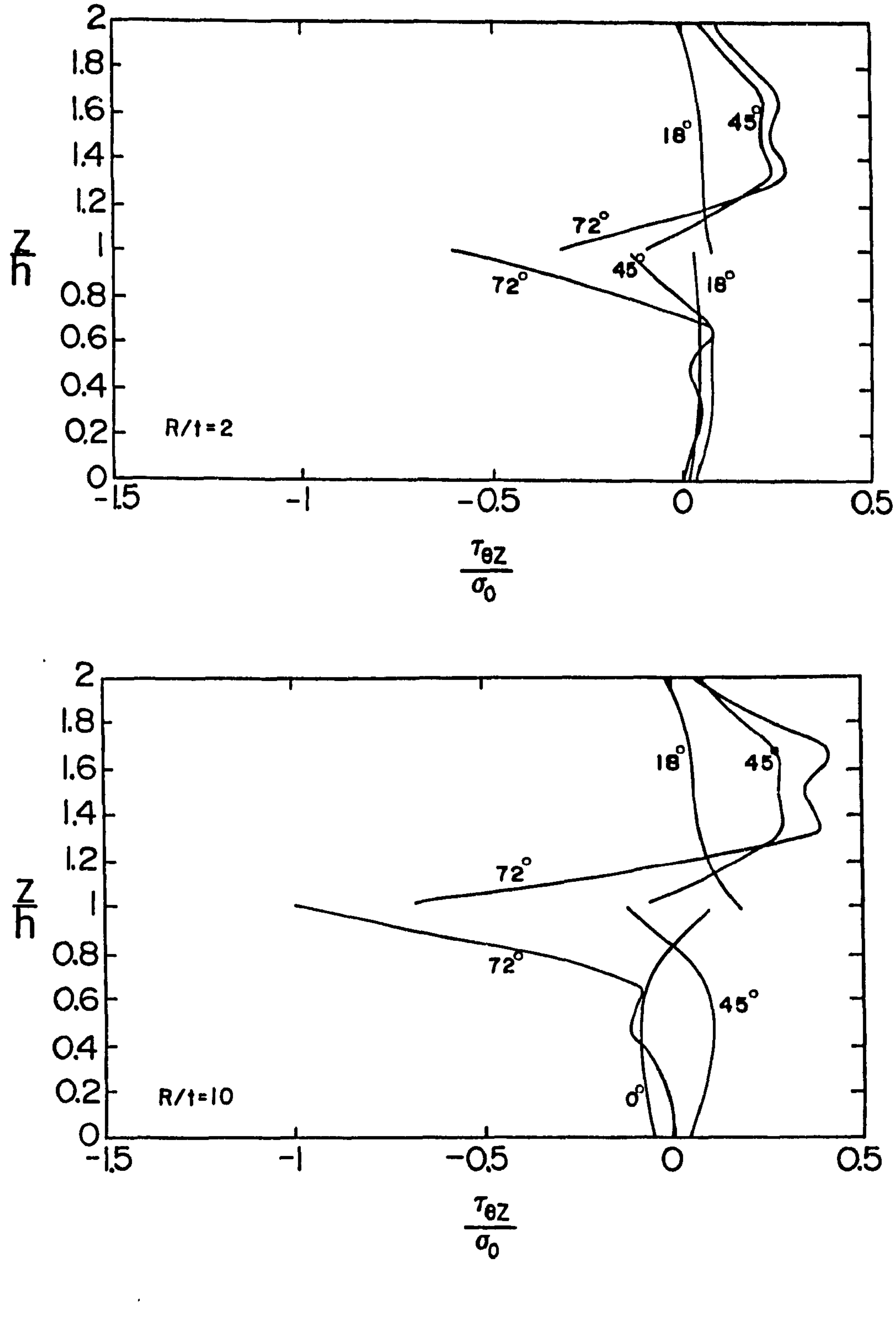

Figure 3.4.7 a,b) Interlaminar shear stress at r=R through the thickness for R/t=2,10.

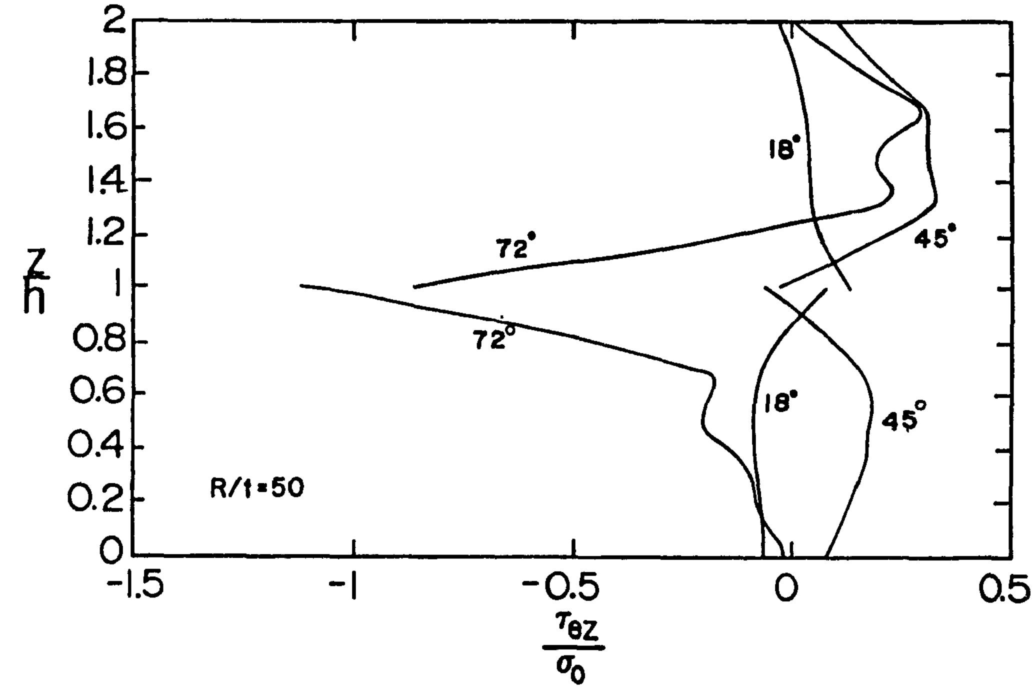

Figure 3.4.7 c) Interlaminar shear stress at r=R through the thickness for R/t=50.

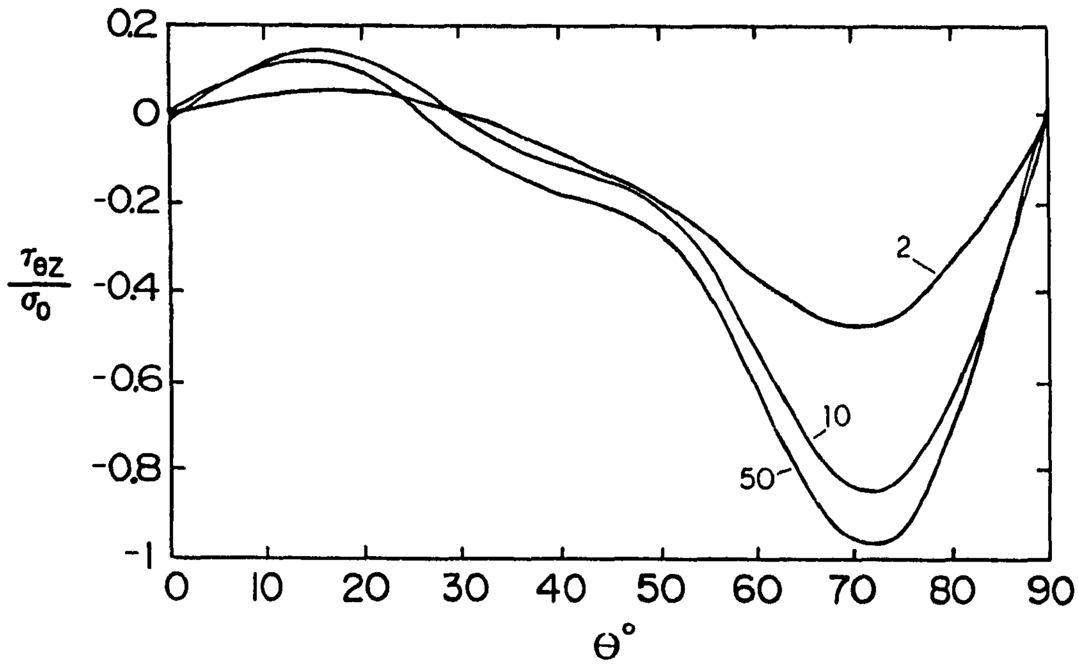

Figure 3.4.8 Interlaminar shear stress at r=R, z=h for R/t=2,10,50. The difference between curves decreases with increasing R/t.

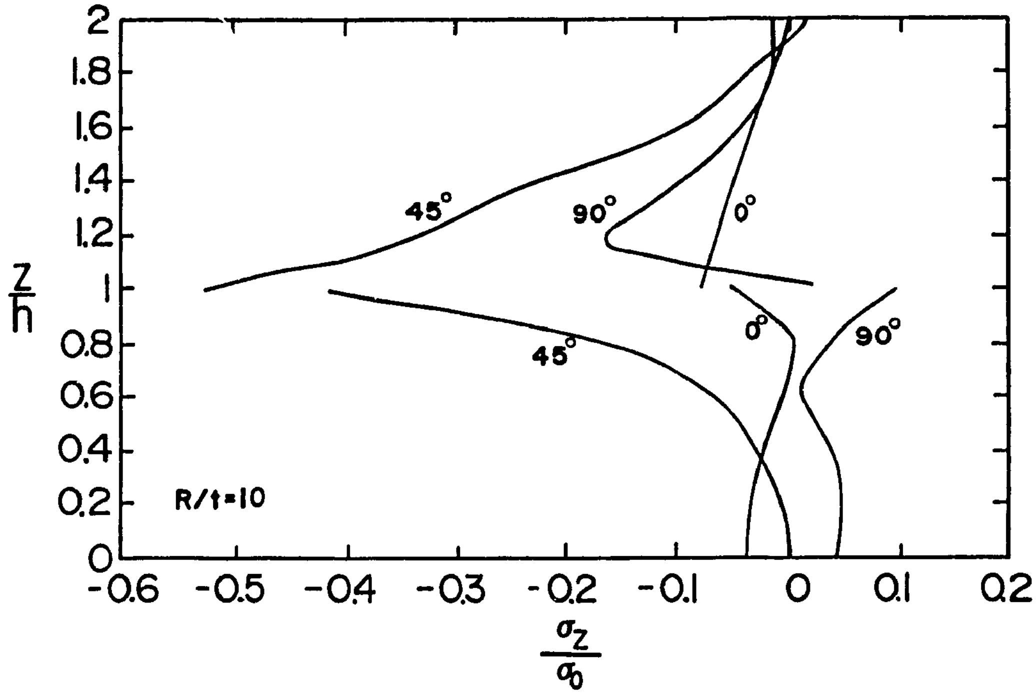

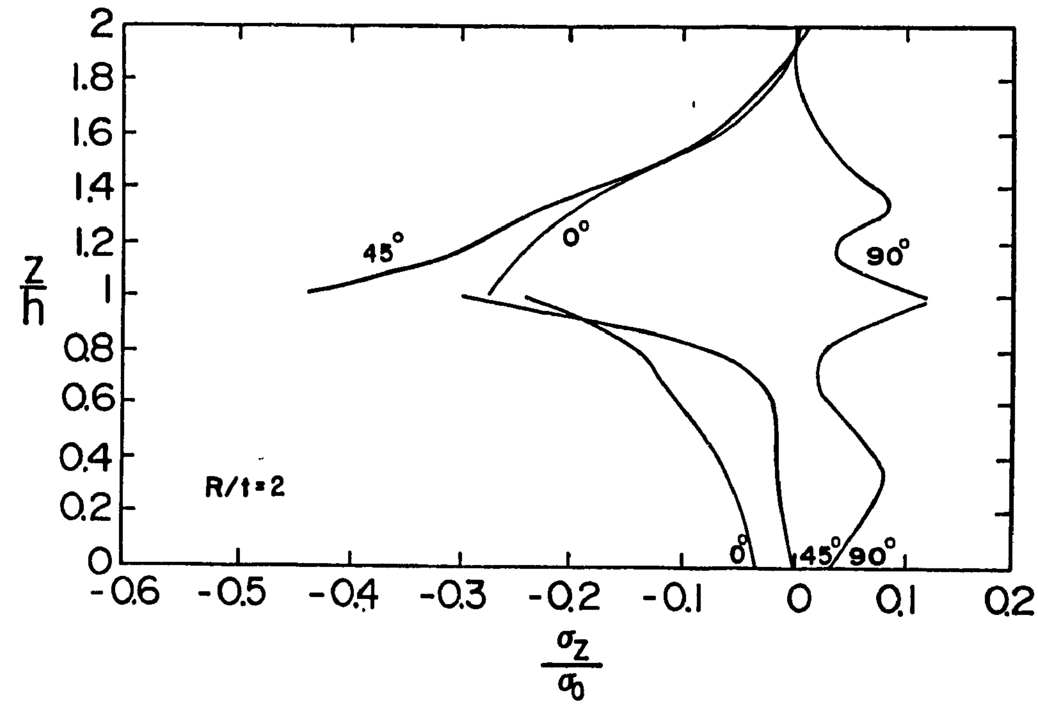

Figure 3.4.9 a,b) Interlaminar normal stress at r=R, $\theta=0°, 45°, 90°$ through the thickness for R/t=2,10. The distribution changes dramatically between these two values of R/t.

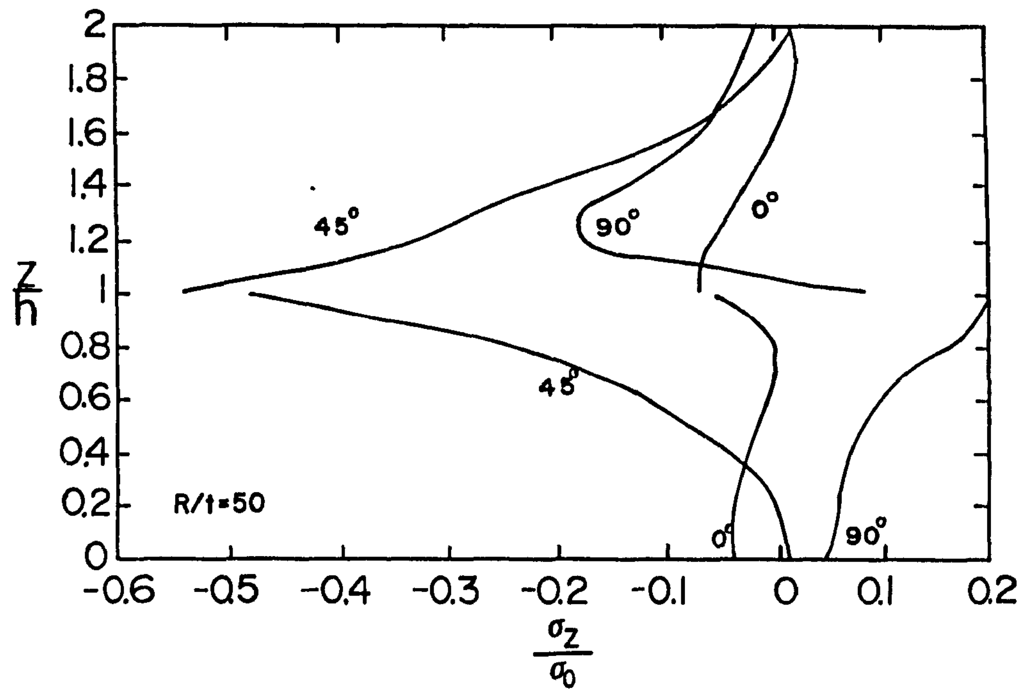

Figure 3.4.9 c) Interlaminar normal stress at r=R, $\theta=0^{o}, 45^{o}, 90^{o}$ through the thickness for R/t=50. The change in distribution diminishes with increasing R/t.

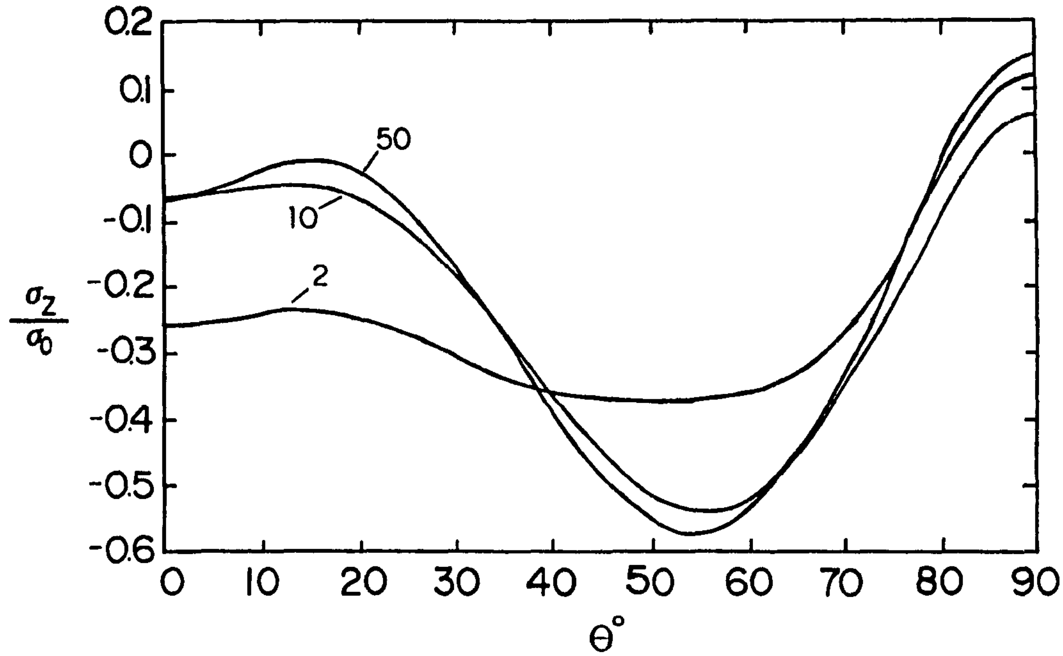

Figure 3.4.10 Interlaminar normal stress at r=R, z=h for R/t=2,10,50. The difference between curves decreases with increasing R/t.

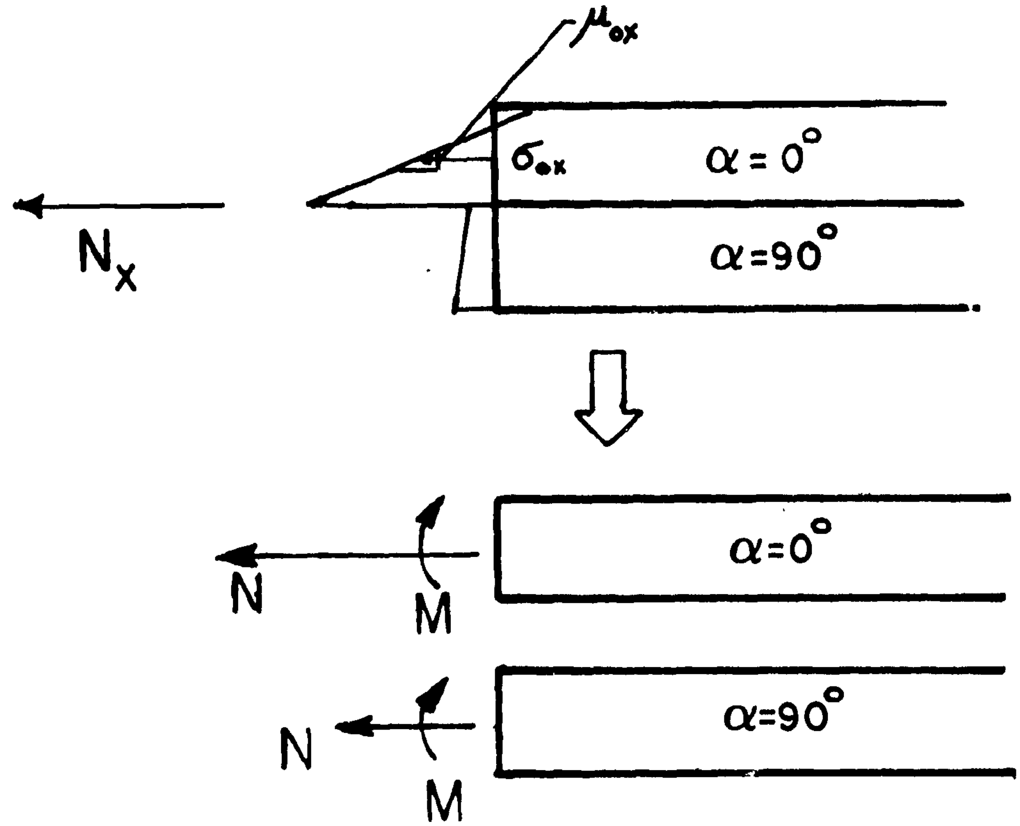

Figure 3.4.11 Far field CLT stresses in [90/0] laminate. The normal stress in each layer can be given by $\sigma_x=\sigma_{ox}+\mu_{ox}z$ so that the net force and bending moments are $N=\sigma_{ox}h$ and $M=\frac{\mu_{ox}h^3}{4}$ respectively.

plate in cylindrical bending due to Lekhnitskii(1968). The net bending moments for the laminate M_x and M_y are zero but the far field CLT distributions of σ_x and σ_y may be resolved into a net applied uniform stresses σ_{ox}, σ_{oy} and linearly varying stresses μ_{ox}, μ_{oy} *in each layer* such that

$$\sigma_x = \sigma_{ox} + \mu_{ox}(z-z_o) \qquad \sigma_y = \sigma_{oy} + \mu_{oy}(z-z_o) \qquad (3.4.1)$$

where z_o is the center of the layer and

$$h/2 > z-z_o > -h/2.$$

So the moment per unit length in the center of each layer is

$$M_{ox} = \frac{\mu_{ox}h^3}{12} \qquad M_{oy} = \frac{\mu_{oy}h^3}{12} \qquad (3.4.2)$$

(see Figure 3.4.11)).

From σ_{ox} and σ_{oy}, σ_θ on the hole surface can be determined for each layer using Equation (3.2.7). The bending moment on the hole surface is given by Lekhnitski(1968):

$$M_\theta = M + M \frac{\sqrt{D_1 D_2}}{D_r} (a_o \sin^4\theta + a_1 \sin^2\theta \cos^2\theta$$
$$+ a_2 \cos^4\theta)/(k+4g) \qquad (3.4.3)$$

where M is the applied moment; and

$$D_1 = \frac{E_x h^3}{12(1-\nu_{xy}\nu_{yx})}, \quad D_2 = \frac{E_y h^3}{12(1-\nu_{xy}\nu_{yx})}, \quad D_3 = \frac{G_{xy}\ h^3}{6} + D_1 \nu_{yx}$$

$$D_r = D_1\cos^4\theta + 2D_3\sin^2\theta\cos\theta + D_2\sin^4\theta$$

$$k = \sqrt{D_1/D_2}\ , \qquad g = G_{xy}/E_y \quad \text{where}$$

E_x, E_y, ν_{xy}, ν_{yx}, G_{xy} are the elastic moduli; and

$$a_o = n, \quad a_1 = k-n-n^2-1+4g(1+\nu_{yx})(1+n), \quad a_2 = k(1-k-4g(1+\nu_{yx}))$$

$n = -\iota(s_1+s_2)$ and s_1, s_2 are roots of the equation

$$D_2 s^4 + 2D_3 s^2 + D_1 = 0. \qquad (3.4.4)$$

Simplified expressions are

at $\theta=0^\circ$
$$M_\theta = M_y = M_{ox}\ \frac{(E_y - 4\nu_{yx}G_{xy})}{(\sqrt{(E_x E_y)} + 4G_{xy})} \qquad (3.4.5)$$

at $\theta=90^\circ$
$$M_\theta = M_x = M_{ox}\ \frac{\sqrt{(E_x E_y)}(1+2\beta) + 4G_{xy}}{\sqrt{(E_x E_y)} + 4\ G_{xy}} \qquad (3.4.6)$$

where β is the imaginary part of the roots of the equation

$$Q_{22}s^2 + 2(Q_{12}+2Q_{66})s^2 + Q_{11} = 0 \qquad (3.4.7)$$

since

$$s_1 = \varphi + \iota\beta \quad s_2 = -\varphi + \iota\beta \quad s_3 = \varphi - \iota\beta \quad s_4 = -\varphi - \iota\beta.$$

Using these equations the distribution of σ_θ can be found through the thickness of each layer. This method is termed the unbonded method.

For a bonded method an equivalent homogeneous plate will not display bending-membrane coupling as does the heterogeneous plate. For this reason no stress moment is predicted on the hole surface by this method. As for symmetric plates the elastic moduli of the equivalent plate are derived from the laminate stiffness matrix to be used in the plate formulas.

The inplane stress σ_θ on the hole surface from all results are plotted in Figures 3.4.12,13. In Figure 3.4.12 σ_θ plotted against θ from the $\alpha=0^\circ$ layer shows that the concentration is highest at the interface at a value of about 17; more than twice what was observed in the symmetric case. In the $\alpha=90^\circ$ layer, the maximum stress concentration is nearly five in compression for R/t=10, so the progression with R/t is not monotonic.

In Figure 3.4.13 σ_θ varies linearly through the thickness towards the maximum stress concentration at $\theta=90^\circ$ in the $\alpha=0^\circ$ layer for high R/t and slightly less so for lower R/t towards the interface; as R/t decreases σ_θ near the interface tends slightly towards that of the higher R/t and bonded cases as was observed in the symmetric laminates.

As was observed in the symmetric plates, the unbonded and bonded methods bound the maximum stress concentration over the range of R/t and show fair agreement for all R/t elsewhere. As bounds are in direct agreement, the plane

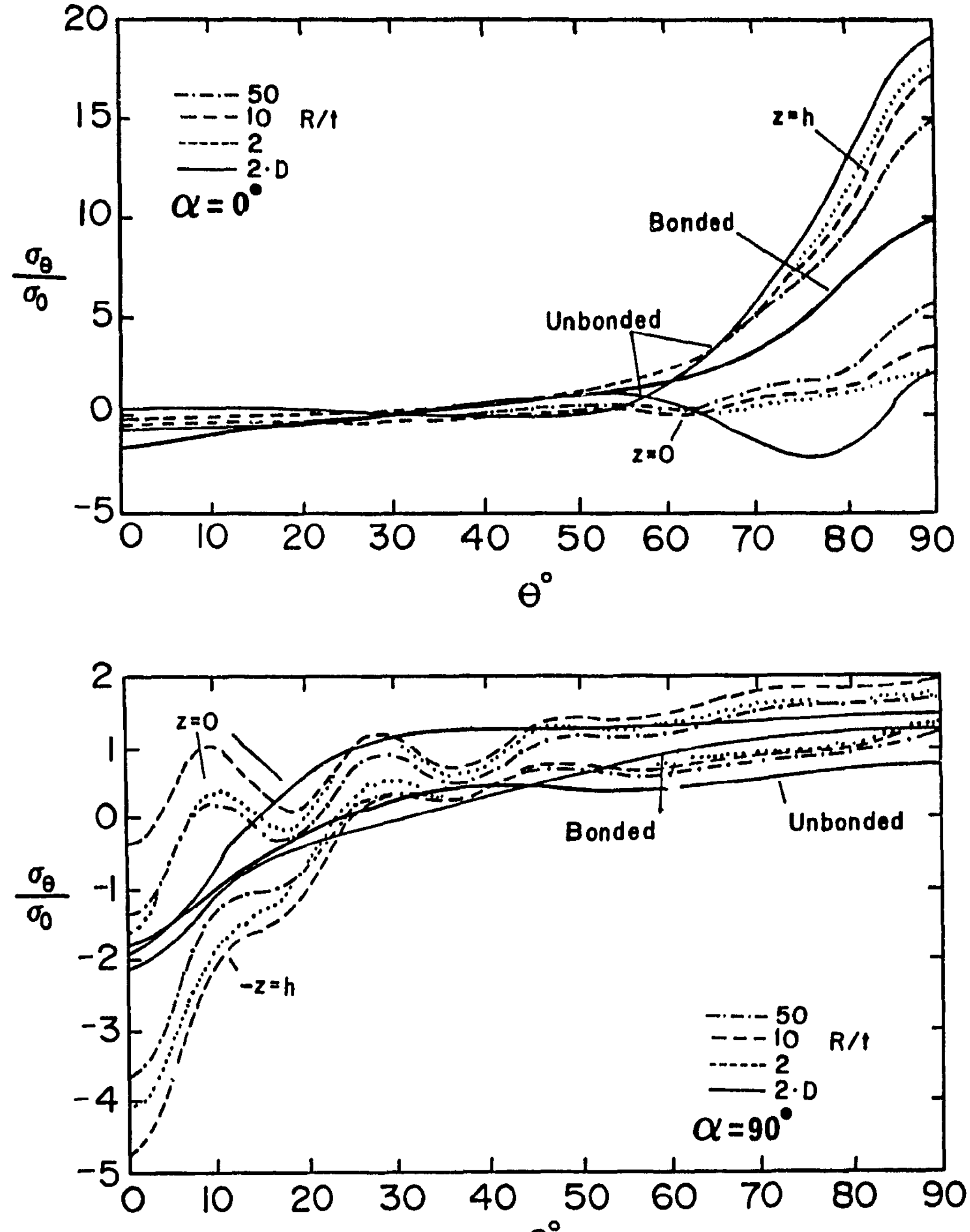

Figure 3.4.12 Circumferential stress at r=R from FE models with R/t=2,10,50 and unbonded method of using the plate theory and plane stress formulas.

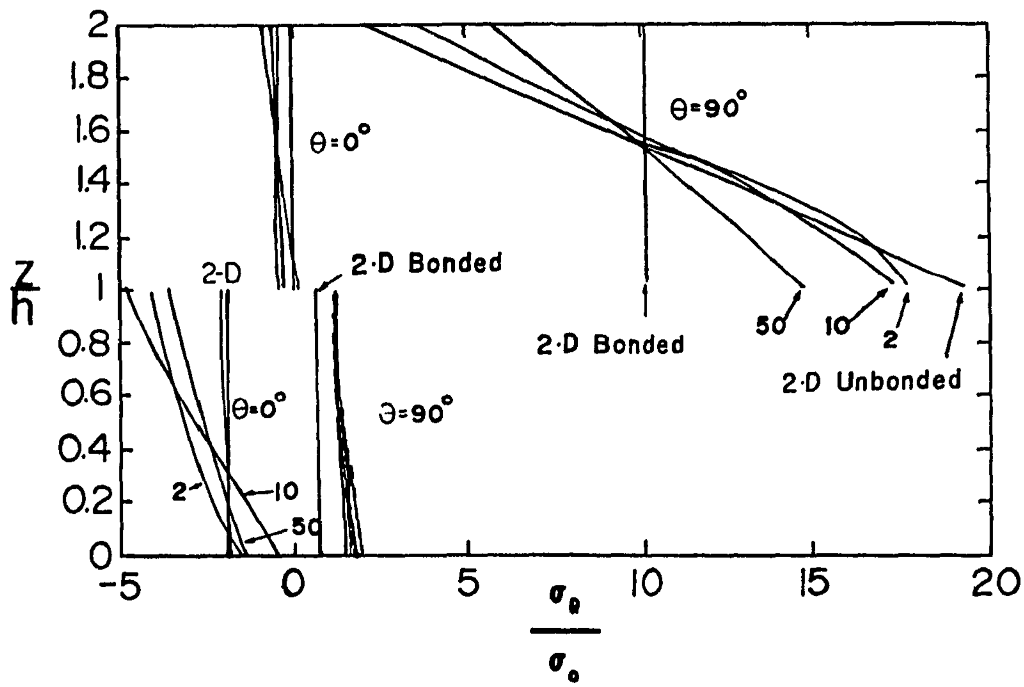

Figure 3.4.13 Circumferential stress at r=R from FE models with R/t=2,10,50 through the thickness with unbonded method of using the plane stress and plate theory formulas.

stress/plate theory results are worst at $\theta=0^{\circ}$ in the $\alpha=90^{\circ}$ layer. For very low R/t thick plate and plane strain solutions would be more appropriate for the unbonded case.

In summary, the unsymmetric configuration of the plates in the previous subsection were investigated. Asymmetry resulted in a much higher maximum concentration of the stresses on the hole surface. Interlaminar stresses σ_z and $\tau_{z\theta}$ show very similar distribution and variation due to R/t at the interface to the symmetric laminates but are stronger, especially σ_z. The distribution through the thickness is such that the interface stress state is very severe. The FE and plane stress/plate theory results show fair agreement overall and the bonded and unbonded methods are observed to bound the FE results over the range of R/t as for the symmetric cases.

3.4.3 Reinforced Hole in a $[0/90]_s$ Laminate

A small influence of an adhesively bonded third material on the interface behaviour of the plate was observed in Section 3.3. Beyond the implications the effect had on the measurement of interlaminar strains, it invites a study of coatings to determine the effect on stresses in the boundary layer. Hole reinforcement, which has been investigated for conventional plates, is compelling for composites since it is congruous with the philosophy of tailoring structural properties by combining phases.

To the author's knowledge, no three-dimensional study of laminates with reinforced holes has been reported in the literature. In Savin's book "Stress Concentration around Holes" (1961) plates with circular holes reinforced by welded isotropic elastic rings under membrane loading are treated as plane problems with the following among the conclusions:

- it is possible to choose a ring of such rigidity that σ_θ in the perforated plate is considerably lower than in the continuous plate(without a hole);

- with increasing radial thickness of the ring the stress σ_θ will diminish in both the ring and plate;

- the σ_θ stress concentration from intermediate ring materials will fall between those of no ring and an absolutely rigid ring.

To investigate these statements for laminates and further see what effect reinforcement has on the interlaminar stresses $[0/90]_s$ plates with R/t=5 and the properties in Table 3.1 were modeled. In the FE model the third mesh had five elements in the plate and two in the ring (coating) as shown in Figure 3.4.14. The isotropic rings had the elastic properties to cover the complete range of rigidities:

$$E_C/E_{11} = 0,\ .48,\ 1.43,\ \sim 5\times10^4;\ \text{and}\ \ \nu_C = .35.$$

Also, the ring thickness was varied so

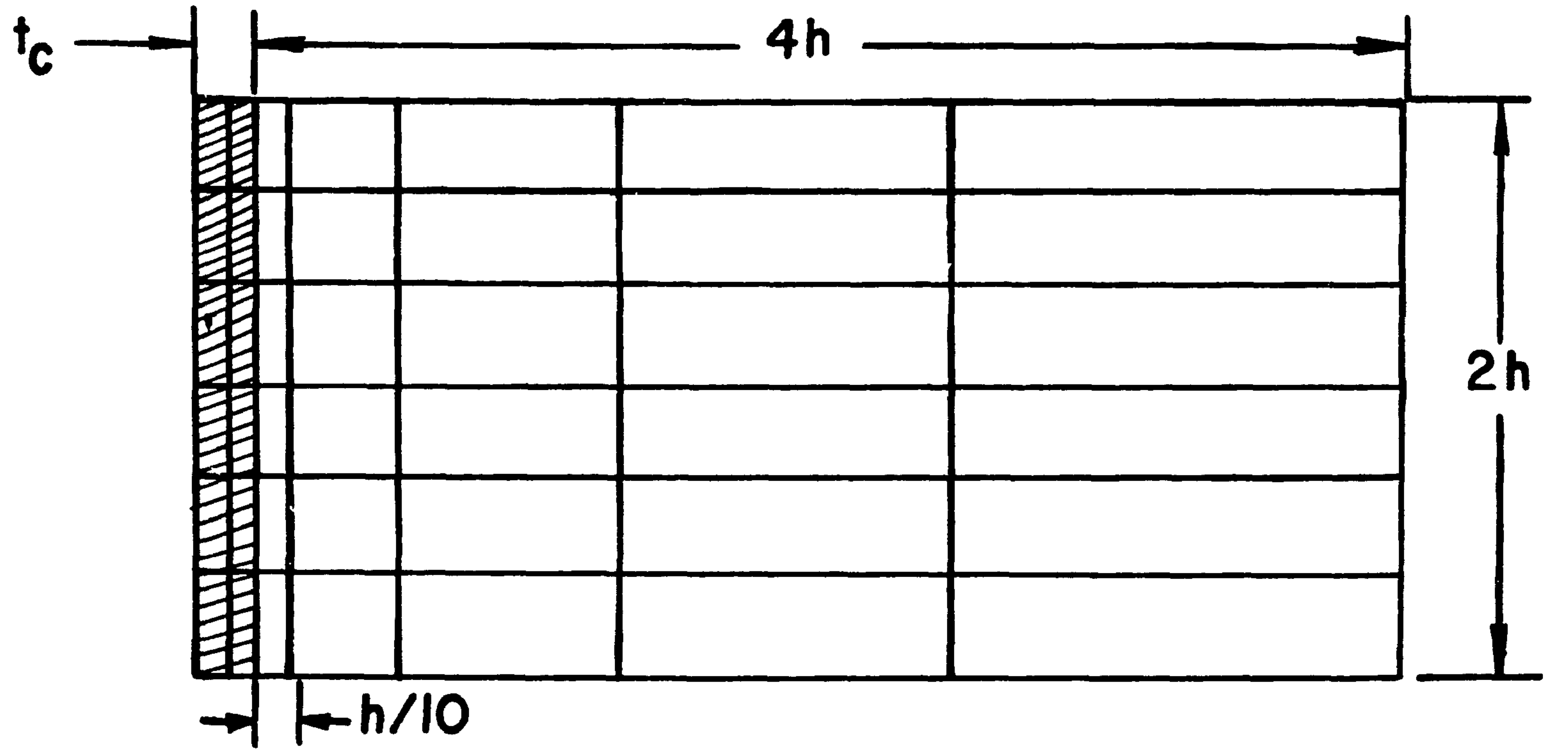

Figure 3.4.14 θ-plane distribution of finite elements for hole reinforcement model.

$t_c/t = 0, .05, 1$.

σ_θ on the plate/ring interface (r=R) for thick rings is shown in Figures 3.4.15; the thin rings had a negligible effect. It can be observed that for σ_θ the maximum is rapidly reduced as the rigidity of the ring increases to where σ_θ is low but still slightly more than σ_o even for the very rigid ring (E_c/E_{11}=5x10^4); these results do not contradict statements by Savin since σ_x in the $\alpha=0^o$ layer is greater than σ_o away from the hole where stresses are uniform. In the $\alpha=90^o$ layer σ_θ was eliminated for a very rigid ring, but the progession with varying E_c/E_{11} contradicts Savin's third statement. However, the shift in σ_θ to tension at $\theta=0^o$ for the intermediate rings is such that the fibers bear the load.

Stresses may develop on the plate-ring interface of a plate with a reinforced hole. τ_{rz} is low but σ_r and $\tau_{r\theta}$ develop on the ring/plate interface for thick rings. Maximum σ_r occurs in the $\alpha=0^o$ layer for the very rigid ring at $\theta= 0^o$ which stresses along the fibers. $\tau_{r\theta}$ in Figure 3.4.16 shows that this stress will have an extremum with respect to rigidity of the ring.

A detail that is overlooked in the plane stress approach is that the situation at the intersection of the ring/plate interface and the plate surface z=2h is similar to that in the plate at the interface on the edge. It was

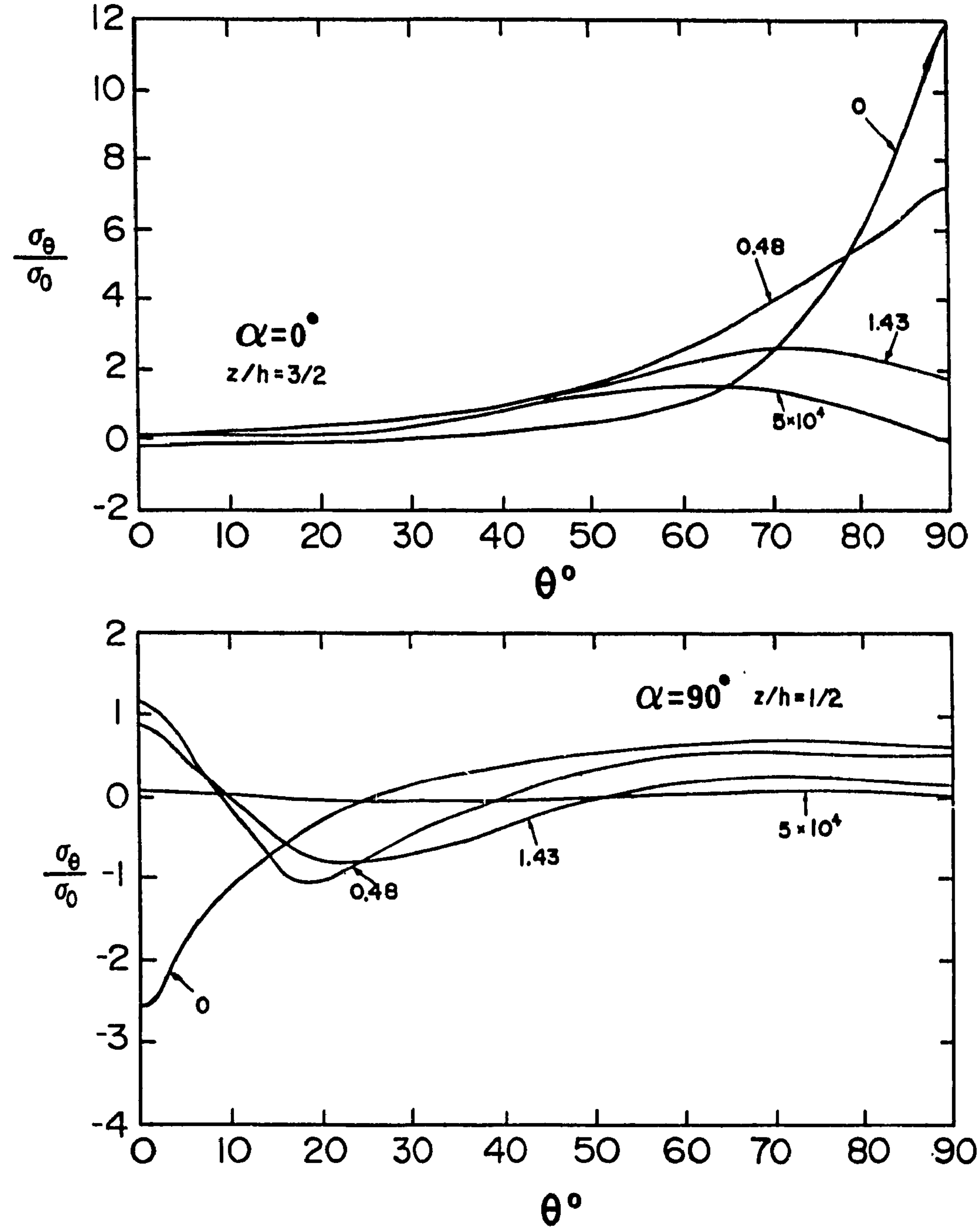

Figure 3.4.15 Circumferential stress at r=R in plate with a thick reinforcing ring ($t_c/t=1$) for varying rigidity (E_c/E_{11}).

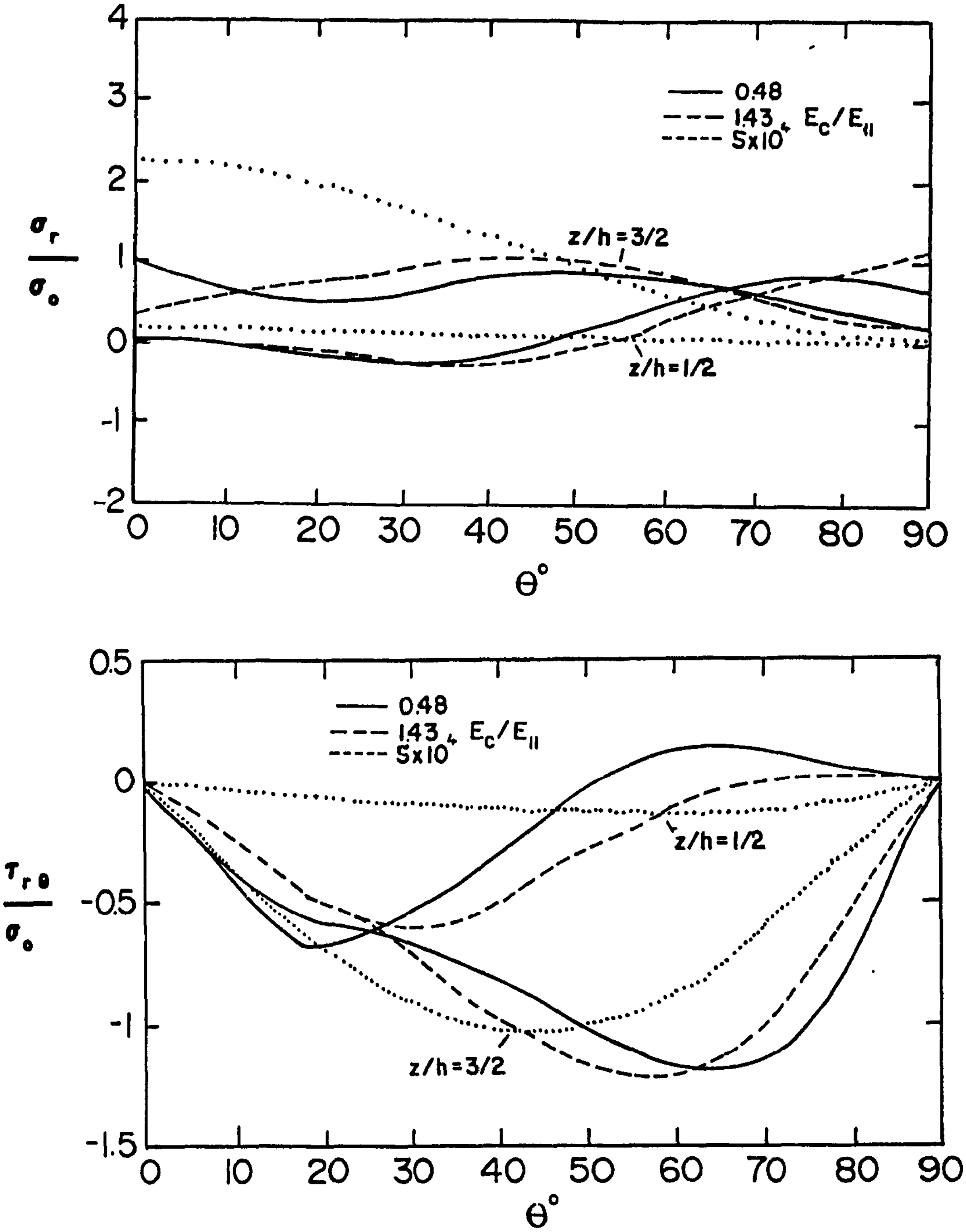

Figure 3.4.16 Inplane radial stresses in plate with a thick reinforcing ring of varying rigidity (E_c/E_{11}). Both normal and shear stresses increase rapidly at low E_c/E_{11}.

observed in the results that σ_r and $\tau_{r\theta}$ show some local stress concentration at this location for thick rigid reinforcement.

For both thick and thin rings the interlaminar stresses at the ring/plate interface intersection line (z=h,r=R) show evidence of only a very weak singularity. For a perfectly rigid ring, on the plate/ring interface

$$\varepsilon_\theta=\varepsilon_z=\gamma_{z\theta}=0. \qquad (3.4.8)$$

Immediately from this we know $\tau_{z\theta}$ is very small since C'_{45} is typically small. σ_z is uniform throughout most of the thickness for thick rings due to the constraint on ε_z,

so $\qquad \sigma_z \approx C'_{13}\varepsilon_r$ since typically $C'_{36}\approx 0$.

For the very rigid ring a small tensile σ_z develops. For thin rings σ_z is low and stepped across the interface until the ring becomes very rigid.

In Figure 3.4.17 it can be seen that $\tau_{z\theta}$ at the interface is rapidly mitigated as rigidity increases relatively independent of the ring thickness. This result indicates $\tau_{z\theta}$ can be avoided by the use of thin flexible coatings.

It is concluded from these results that the maximum stress concentration can be reduced in the plate with the emergence of radial inplane stresses on the plate/hole

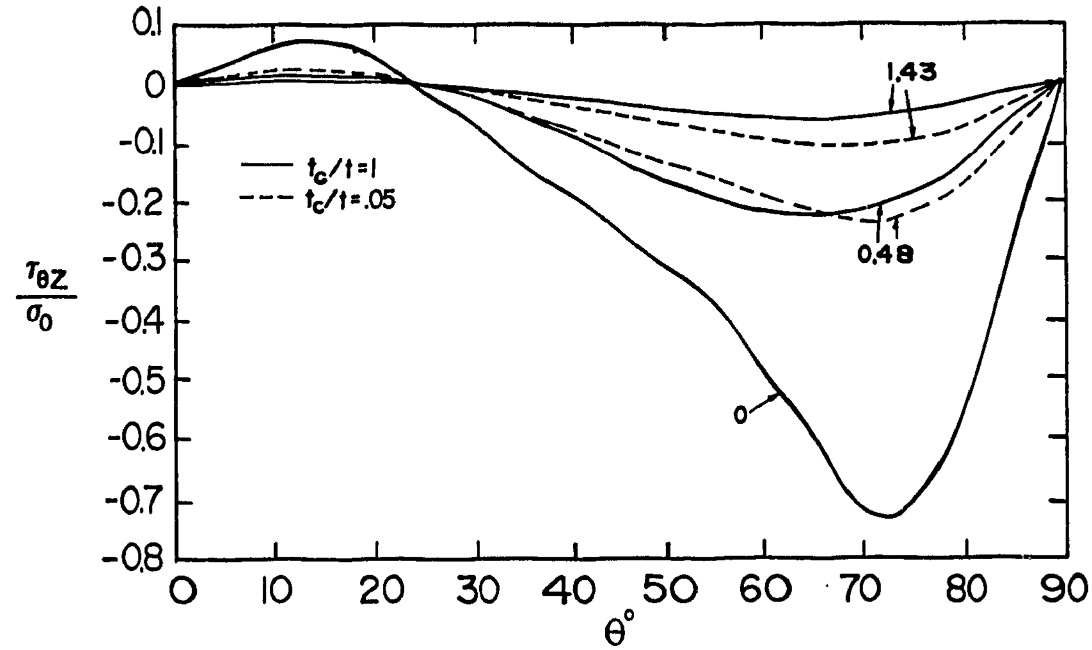

Figure 3.4.17 Interlaminar shear stress at r=R, z=h of plate with reinforcing ring of varying rigidity and thickness. This stress rapidly decreases as the ring rigidity increases for both thick and thin rings.

interface. The singular interlaminar stresses can be mitigated by even thin non-rigid rings. The optimum reinforcement material in the case of a laminate will be determined by the directional strength tensor of the composite material; reinforcement could be tailored to optimize strength of the composite.

3.5 Summary and Conclusions

The effect of a central circular hole in a relatively large laminated plates has been studied. Problems with two or three planes of symmetry, because of importance facilitating and improving the analysis in several ways, were analyzed.

Finite elements provided approximate solutions to the classical model; comparisons with other solutions and measured results showed that the present solutions are reasonably accurate at least to the extent of predicting trends in behaviour; results on several problems of interest were generated.

The measurement of hole surface strains, many aspects of which share much in common with any laminate edge, was attempted. A relatively unsophisticated technique was chosen and results overall were good apart from, unfortunately, in the region of most interest where this method, and for the same reasons other methods, will fail due to the interference of the measurement system on the behaviour of the specimen and systematic error in the results. A simple solution, namely the elimination of scale problems by enlarging the scale of the specimen, is proposed.

Beyond the scope of this work are the development of measurement or tractable mathematical methods which work accurately on the microstructural level; because the randomness of the present analysis is limited to the distribution of the fibers analytical methods are most desirable. Measurements will answer some questions now and may stimulate development in future.

The effects of R/t, unsymmetric lay-up, and hole surface reinforcement were studied. The plane stress solutions for orthotropic plates showed at least fair agreement with the present model in both of the first cases but were unavailable for the last. In general for symmetric laminates σ_z is everywhere low relative to the applied gross stress; it has been shown to depend greatly upon R/t and stacking sequence at the midplane on the hole surface. $\tau_{z\theta}$ is generally the much stronger stress at the interface. The interlaminar stresses were most severe in the case of the unnsymmetric laminate where the magnitude of σ_z was double what was observed in the symmetric cases. The interlaminar stress τ_{rz} was observed to be small and is of least interest since it vanishes on the hole surface and as a shear stress is less likely to cause fracture of a brittle matrix. All the hole surface stresses may be altered by reinforcement to improve strength; application of suitable failure criteria and subsequent experimentation should follow this work.

CHAPTER 4

PROBLEMS WHERE STRESS DOES NOT VARY AXIALLY

4.1 Introduction and Literature Survey

Analysis of laminate edges using linear elasticity has been concentrated on the problem which is relatively simplest: the straight free edge. Salamon(1980) prepared a comprehensive summary of work on free edge problems up to 1980; what follows is a brief survey of work to the present which is relevant to this chapter.

Most attention has been focused on the square free edge problem for which

$$u = \varepsilon_0 x + U(y,z)$$

$$v = V(y,z)$$

$$w = W(y,z)$$

is the functional form of the displacements; this was termed "uniform extension". For symmetric laminates when ε_o is set the problem corresponds to the middle region (x=0) of a very long strip under a net axial load.

Pipes and Pagano(1970) used a finite difference method to solve the displacement equilibrium equations for several laminate configurations. Unfortunately, the solution accuracy was low because the uniform grid of points was not dense enough. Later, based on observations of the FD solutions, a Fourier series solution based on an approximate formulation (it was assummed that $\sigma_z, \tau_{yz}, \sigma_y = 0$ and $C_{45}=0$) specifically for $[\pm\theta]_s$ laminates was presented by Pipes(1972). As in many papers which followed, equal shear moduli were used so that C_{45} vanished. However, because it was subsequently shown that τ_{xz} is the strongest singular stress this solution has some validity; but σ_z, which has nearly the strength of τ_{xz}, is neglected in this solution and so it may not be acceptable in practice.

In another solution for $[\pm\theta]_s$ laminates, using a perturbation method with non-singular exponential functions Hsu and Herakovich(1977) obtained approximate stresses along the interface. Kriz(1977) modified their solution so that unequal shear moduli and Poisson ratios could be used and studied the effects of material properties on $[\pm 45]_s$ laminates. It was found that the interlaminar stresses in the solutions were sensitive to G_{23} so the commonly used approximation $G_{12}=G_{13}=G_{23}$, which is not realized, is questionable. Further, a fiber volume content of 80% produced the highest interlaminar stresses for realistic properties. The perturbation method solutions predicted a tensile value of σ_z for $[\pm 45]_s$ graphite/epoxy not in agreement with solutions from most other methods.

Bar-Yoesph(1981,1983) developed a perturbation-variational solution for uniform extension free edge problems of $[\pm\theta]_s$ laminates using non-singular functions. Both these solutions depend upon a vanishing value of h/w for accuracy. Although the free edge problem has a simple domain shape in two dimensions and is accessable to more analytical methods, numerous solutions to investigate the interlaminar stresses using quasi-three dimensional displacement formulated finite elements have appeared in the past literature and are still appearing (e.g. Wang and Crossman(1977), Raju et al (1981), Herakovitch et al(1985)). In the region of the singularity FE solutions show slow h-convergence. Tong and Pian(1973) showed that the rate of convergence of a polynomial-based finite element solution is often controlled by the order ω if there is an $r^{-\omega}$ singularity, ie.

$$u-u_o=O(h^{\omega}) \quad \text{not} \quad O(h^{p+1})$$

where h is an element dimension, p is the order of polynomial used for a two dimensional domain. To obtain accuracy complex FE meshes having many DOF are generated.

Raju and Crews(1981) used a mesh of quadratic elements (p=2) distributed radially about a lone singularity having about 3600 degrees of freedom (DOF) to obtain reasonable results. They fit their results for τ_{xz} (the strongest singular stress) from $.001<r/h<.01$ to the expression $\tau_{xz}\approx A(\theta)r^{-\omega}$ to get ω=.17 (later, Wang(1982) and Zwiers(1982) obtained ω=.02558 by direct calculation). As predicted by Tong, the FE solutions appear to converge very slowly in the vicinity of singularities. In order to reduce the size of the two elements nearest a singularity one must resort to complex meshes or substructuring techniques avoiding large element aspect ratios or distortion and computational error. Only for very few DOF optimal meshes for minimum stationary potential energy have been generated by Wang(1983a). The problem of convergence and complex mesh generation increases with the number of singularities and the dimension of the domain.

Comparing results from different methods Whitcomb et al(1982) noticed a discrepancy primarily in sign of σ_z predicted between the various methods used in prior results for $[\pm 45]_s$ laminates. They undertook an investigation of the accuracy of standard eight node isoparametric finite elements for laminate free edge problems. h-convergence of quadratic elements was determined by comparison with exact solutions for problems having stress discontinuities and singularities. Based on these experimental results they made the conclusion that finite elements are accurate despite very slow convergence except in a region of two elements around the singular point and point out that this region can be made arbitrarily small. In regard to the boundary conditions near the singularity they showed in a very simple calculation that for the uniform extension problem when the traction free edge and displacement continuity conditions are satisfied exactly using a symmetric stress tensor (with nonsingular functions), σ_z must be tensile at the singular point in the approximate solutions. They claimed that the stress tensor is asymmetric at this point and the enforcement of symmetry along with the exact enforcement of the boundary conditions is the downfall of several methods. Further, they claim that finite elements succeed because displacement continuity is exactly satisfied while stress continuity and the traction free edge are left approximately satisfied.

Wang(1982) presented an eigenfunction expansion solution to problems for which $\partial\sigma/\partial x=0$ based on Lekhnitskii's stress function formulation. A set of functions which satisfied the traction free edge condition as well as the interface continuity conditions yielded the power ω of an $r^{-\omega}$ singularity at the interface; this is an important analytical quantity and is included in the solution. The results showed that the singularity of the square laminate free edge is generally weak in comparison to that at a delaminated edge with $\omega=-.05$ typical for graphite/epoxy. Wang's solution proceeds in two stages. Obtaining the eigenvalues requires that a 12x12 system of equations having terms with ω in transcendental form must be solved by a numerical method for every interface between plies of unlike orientation and depends upon the intersection geometry and material properties. Particular solutions are then obtained using boundary point collocation on the remaining boundaries with added polynomial functions to approximate the far field solution. This is a tedious approach; especially for multilayer laminates or when material properties are varied.

Zwiers et al(1982) showed that Wang's solution is not complete in general since $\ln(r)$ and possibly other singular terms (i.e. $(\ln r)^2$, $(\ln r)^3$, etc.) belong to the complete solution for adjacent layers having orientation angles other than 0/90,$\theta/-\theta$,90/0 and $\pm\theta/\pm\delta$ where δ is small. The lnr singularity was strongest for 90/15 and 90/-15 pair for graphite/epoxy. Further, Zwiers showed that while individual stresses may or may not be singular for $r^{-\omega}$ solutions, depending on the complete boundary conditions of the specific problem, when present all stresses have the lnr singularity. Notably, Raju and Crews(1981) using their highly refined finite element model found for $[\theta/90-\theta]_s$ laminates, that the $[15/-75]_s$ configuration developed the highest τ_{xz} values. This is compatible with Zwiers(1982) since the strength of the ln r singularity is near maximum for this lay-up. Presumably Wang's singular solution would be approximate for these cases.

Wang demonstrated his method on example problems of delamination fracture(Wang(1984)), the central plane of adhesive bonded joints and hygroscopic stresses in $[\pm\theta]_s$ laminates(Wang(1982)). The effect of the geometric angle at the intersection was studied for material fiber angles of $\pm45^0$and a 45^0 ply intersecting with aluminum and results were given for $[\pm\theta]_s$ laminates and not for other configurations. A paper proposed to study the influence of lamination variables never appeared (Wang(1983b)).

A finite element was developed by Wang(1983c) containing the $r^{-\omega}$ singularity and shown to agree with the eigenfunction collocation solution when used with non-singular surrounding elements. Determining the singular functions in the solution requires effort and calculation. Afterwards, for utility it is still required to solve the boundary value problem in order to determine the actual stresses since the presence of singularities in the general solution does not imply their contribution to the specific solution.

On a new tangent, Bar-Yoeseph and Siton(1984) used an asymptotic-variational approach with non-singular functions to solve problems of $[\pm\theta]_s$ laminates with material nonlinearity in transverse and shear moduli. The model showed that material nonlinearity can have significant but not radical effect on the interlaminar stresses.

From the aspect of laminate configuration and loading most serious work appearing in the literature has been done on several "benchmark" problems for straight edges in attempting to sort out the difficulties involved with the singularity in computation. Other configurations and loadings have not been presented even though the interlaminar stresses are known to be problem dependent.

Examples are recently more apparent in the literature for problems with more than 4 layers in the solution domain. Pagano(1974) was able to predict the normal stress on the midplane only of symmetric laminates. Later, a global-local model which replaced parts of the laminate with an equipollent system was presented by Pagano and Soni(1982); the results were sensitive to the substructuring scheme used however. Kassapoglou and LaGace(1986) presented a method for rough estimates of stresses in symmetric laminates in uniform extension; it requires prior knowledge of the stress state to select assumed exponential functions for the stresses. In most practical studies, low accuracy solutions are obtained using standard finite elements attempting only to determine the sign of the interlaminar stresses in the layers or the strain energy release rate by the Rybicki-Kanninen(1977a) method(e.g. Whitcomb and Raju(1984)). The bearing the calculated results have on the real micro-deformations of fiber reinforced materials is not apparently an issue.

Few attempts at measuring the deformations relevant to the free edge effect of fiber reinforced laminates have been made. Small fiber laminates are typically very thin (.005 inches per ply) for graphite/epoxy making measurement of the high gradient deformations and strains difficult. Pipes and Daniel(1971) obtained patterns of axial displacement on the *face* of $[\pm\theta]_s$ laminates using Moire grids and showed good correlation with the FD solution. Oplinger et al(1974) used Moire interferometry on the thin *edge* and the face of $[\pm\theta]_s$ laminates. Later, Herakovitch et al(1985) used a similar method in comparison with results from a linear elastic solution using standard isoparametric finite elements in a highly refined (1028 degrees of freedom) mesh. However, the comparisons were not concrete; rather, the measurements were used to determine the FE mesh density for best agreement at the singularity without questioning the accuracy of measurements. Both of these methods used thin plastic coatings on the surface of the edge but did not consider what effects this may have had upon their measurements. Depositing a third material on the edge face will alter the response to some degree since it is a an intersecting wedge problem with three dissimilar intersecting materials instead of two. Also, transfer of the strain through the coating will depend upon the distribution of strain on the objective surface; worsening as strain curvature increases. Post(1987), using a new moire technique on $[0/90/\pm45]_{6S}$ graphite/PEEK beam under 3 and five point loading showed very sharp peaks in γ_{xz} on the edge. The possible attenuation due to the coating is termed shear lag but is not accounted for in the results. In general, results show that the very high and localized strain γ_{xz} does exist in a manner predicted by the EM solutions.

Various other relevant studies have appeared in the literature including the use of cord rubber models (Ford et al (1982), Lou and Walter(1978)) and enlarged models of photoelastic materials(Alderholdt and Berhaus(1976), Berghaus and Alderholdt(1975)) but did not produce results relevant to current research in composite laminates.

In summary, a survey of the literature shows that much attention has been devoted to the effective modulus model for investigating the elastic behaviour of composite laminates. The $[\pm\theta]_s$ configuration has received by far the most attention with many solutions developed specifically for this problem. For more general methods such as finite elements using polynomial approximating functions seems to account for the slow convergence observed in the vicinity of singularities. Methods containing singular functions require knowledge of the type of singularity which depends upon material properties and global orientation of each adjacent pair of plies. After determining the functions it is still required to solve the boundary value problem to determine the actual stresses. Largely neglected are multilayered laminates, even though low-accuracy solutions are frequent in the literature, and configurations and loadings outside of uniform extension, i.e. most of the laminate system. Also, very little work has been done on measurements with the intention of verifying the complete stress state.

What follows in this chapter is the development of a procedure for obtaining approximate numerical solutions to laminate problems for which $\partial\sigma/\partial x=0$. A displacement formulation and exponential non-singular trial functions are used with a weighted residual method. To avoid complex grids, a boundary method is used. The method developed is flexible with respect to specifying problem materials, geometry, loading and boundary conditions. Further, there is flexibility in specifying the continuity and stress boundary conditions at the singular point. Numerical results are presented for rectangular strips in a variety of configurations and loadings. Finally, multilayer laminates are handled.

4.2 Formulation and General Solution Procedure

4.2.1 Equations of Linear Elasticity

From Section 2.2 the equilibrium equations when the stresses do not vary in one direction, i.e. let $\partial\bar{\sigma}/\partial x=0$, are

$$\sigma_{ij,j}=0 \quad \text{for } i=x,y,z \quad j=y,z \tag{4.2.1}$$

or in terms of the displacements (see Equation(2.2.3))

$$\tfrac{1}{2}C_{ijkl}(u_{k,l}+u_{l,k})_{,j} = 0 \quad j=y,z \tag{4.2.2}$$

These are the general equations, for the special case of laminates with rotated orthotropic layers having the C tensor properties discussed in Chapter 2 the general equations expressed in three linear differential operators become

$$\mathcal{L}_1(\bar{u})=\mathcal{L}_2(\bar{u})=\mathcal{L}_3(\bar{u})=0 \tag{4.2.3}$$

where

$$\mathfrak{L}_1(\bar{u}) = C_{66}v_{,xy}+C_{55}w_{,xz}+C_{16}u_{,xy}+C_{26}v_{,yy}+(C_{45}+C_{36})w_{,zy}$$

$$+C_{66}u_{,yy}+C_{45}v_{,zz}+C_{55}u_{,zz}$$

$$\mathfrak{L}_2(\bar{u})=C_{12}u_{,xy}+C_{22}v_{,yy}+(C_{23}+C_{44})w_{,yz}+C_{26}u_{,yy}+C_{26}v_{,xy}$$

$$+C_{45}w_{,xz}+ +C_{45}u_{,zz}+C_{44}v_{,zz} \tag{4.2.4}$$

$$\mathfrak{L}_3(\bar{u})=C_{13}u_{,xz}+(C_{23}+C_{44})v_{,zy}+C_{33}w_{,zz}+(C_{45}+C_{36})u_{,yz}$$

$$+C_{36}v_{,xz}+C_{45}w_{,xy}+C_{44}w_{,yy}$$

The conditions on the surface of the body are likewise

$$\sigma_{ij}n_i = T_j$$

and

$$u_j = u_j^*.$$

For a unique solution each of the three elements of the vector on the surface must be prescribed, corresponding to the three chosen coordinates, as either a displacement or surface traction.

4.2.2 Homogeneous Solutions-Trial Functions

4.2.2.1 Derivation for Quasi-Three Dimension

To obtain approximate solutions, using the method of Weighted Residuals (also known as error distribution principles (Collatz(1960))), the trial functions used to approximate the solution may satisfy certain conditions exactly. Trial functions which satisfy the equations in the interior of each layer are used for the so called boundary methods. The boundary equations will generally not be satisfied exactly so there is a residual difference to be minimised.

Because the internal solution satisfies the internal equations identically and since every linear boundary value problem has a unique solution, the approximate solution is the exact solution for a problem with the residual boundary and interface conditions. This fact may give further meaning to the residual as an indicator of error. At least intuitively in cases such as boundary error which resembles a point load, that region would be in question.

The internal equations for this class in terms of displacements are

$$\frac{\partial \bar{\sigma}}{\partial x} = \bar{\bar{C}} \frac{\partial \bar{\varepsilon}}{\partial x} = 0 \; . \qquad (4.2.5)$$

Since the determinant of $\bar{\bar{C}}$ cannot be zero this equation must have the trivial solution

$$\frac{\partial \bar{\varepsilon}}{\partial x} = 0 \quad \text{or} \quad (u_{k,lx}+u_{l,kx}) = 0 \qquad k,l=x,y,z$$

The general solution for these 6 differential equations can be expressed in the form

$$u_x = u = U_0(y,z) + \pi_1 xy + \pi_2 xz + \pi_4 x$$

$$u_y = v = V_0(y,z) + \pi_3 xz - \tfrac{1}{2}\pi_1 x^2 + \pi_5 x + \pi_7 \qquad (4.2.6)$$

$$u_z = w = W_0(y,z) - \tfrac{1}{2}\pi_2 x^2 - \pi_3 xy + \pi_6 x + \pi_8$$

where U_0, V_0, and W_0 are arbitrary functions; π_i, $i=1,2,3..8$ are arbitrary constants; and rotations which cause no strain are neglected. The uniform extension problem sets the value $\pi_4=\varepsilon_0=\varepsilon_x$; this is set as input.

The three functions $u-U_0$, $v-V_0$, and $w-W_0$ do not immediately satisfy the three operator equations $\mathcal{L}_i(\bar{u})=0$ exactly when substituted into the $\bar{u}$ vector unless the π_i are suitably defined; this will be dealt with later. If it is assumed true then since the operators are linear, if

$$\mathcal{L}_1(\bar{\bar{U}})=\mathcal{L}_2(\bar{\bar{U}})=\mathcal{L}_3(\bar{\bar{U}})=0 \qquad (4.2.7)$$

where $\bar{U}^T=[\ U_0, V_0, W_0]$ then $\bar{u}$ is a solution to the displacement equations of equilibrium for this problem.

The selection of the trial functions $\bar{U}$ is at the heart of the method. Polynomial functions are avoided because they show very poor convergence in approximating non-analytic functions. Exponential functions are usual for linear problems, so we begin by seeking exponential functions as follows.

Let

$$
\begin{aligned}
U_o &= k_u\ e^{(\psi_z z+\psi_y y)} \\
V_o &= k_v\ e^{(\psi_z z+\psi_y y)} \\
W_o &= k_w\ e^{(\psi_z z+\psi_y y)}
\end{aligned}
\qquad (4.2.8)
$$

where $\psi_y, \psi_z, k_u, k_v, k_w$ are all arbitrary constants. We can operate on $\bar{U}$ with $\bar{\mathcal{L}}$ to get

$$\bar{\mathcal{L}}(\bar{U}) = e^{(\psi_z z+\psi_y y)}\ \bar{L}\ \bar{k} = \{0\}$$

where $\qquad \bar{k}^t=[\ k_u\ ,\ k_v\ ,\ k_w\ ].$

The equations $\mathcal{L}_i=0$ are elliptical so the 3x3 matrix $\bar{L}$ is symmetric and positive definite and has as its elements

$$L_{11}=C_{66}\psi_y^2+C_{55}\psi_z^2$$

$$L_{12}=C_{26}\psi_y^2+C_{45}\psi_z^2$$

$$L_{13}=(C_{36}+C_{45})\psi_y\psi_z$$

$$(4.2.9)$$

$$L_{22}=C_{22}\psi_y^2+C_{44}\psi_z^2$$

$$L_{23}=(C_{23}+C_{44})\psi_y\psi_z$$

$$L_{33}=C_{44}\psi_y^2+C_{33}\psi_z^2$$

If these equations do not have the trivial solution $\bar{k}=\emptyset$ (the null vector) then $\det(\bar{L})=0$. Defining $\varphi=[\psi_y/\psi_z]$ and dividing all the elements of $\bar{L}$ by ψ_z^2 the determinant results in a polynomial in $\varphi^2$of degree three (i.e. φ^2 is raised to the highest power of 3, φ is raised to 6 and there are no odd powers of φ)

$$L_{11}L_{22}L_{33}-L_{11}L_{23}^2-L_{12}^2L_{33}+2L_{12}L_{13}L_{23}-L_{13}^2L_{22}=0 \quad (4.2.10)$$

Solving for the three roots of this polynomial yields three values of φ^2 for which $\mathcal{E}(\bar{U})=0$.

Some knowledge of the roots φ_i^2 can be obtained. Most obvious, there must be at least one real root; if there are two complex roots, they must be conjugate. We can prove that $\varphi_i^2 \neq 0$. If $\varphi_i^2 = 0$ then

$$\bar{L} = \begin{bmatrix} C_{55} & C_{45} & 0 \\ C_{45} & C_{44} & 0 \\ 0 & 0 & C_{33} \end{bmatrix} \tag{4.2.11}$$

and because the $\bar{C}$ matrix must be positive definite and $\bar{L}$ is a principal submatrix it too must be positive definite in this case so $\det(\bar{L}) \neq 0$ (see Ayres (1974)). We can also prove that if φ_i^2 is real then $\varphi_i^2 < 0$. First, we break $\bar{L}$ into the sum of two matrices

$$\bar{L} = \bar{A} + \bar{B}$$

where

$$\bar{A} = \begin{bmatrix} C_{66}\varphi^2 & C_{26}\varphi^2 & C_{36}\varphi \\ C_{26}\varphi^2 & C_{22}\varphi^2 & C_{23}\varphi \\ C_{36}\varphi & C_{23}\varphi & C_{33} \end{bmatrix}$$

$$\bar{B}=\begin{bmatrix} C_{55} & C_{45} & C_{45}\varphi \\ C_{45} & C_{44} & C_{44}\varphi \\ C_{45}\varphi & C_{44}\varphi & C_{44}\varphi^2 \end{bmatrix}.$$

The three principal minors of $\bar{A}$ are

$$p_1=[C_{66}]\varphi^2 \quad p_2=\varphi^4 \det\begin{bmatrix} C_{66} & C_{26} \\ C_{26} & C_{22} \end{bmatrix}$$

and

$$p_3= \varphi^4 \det\begin{bmatrix} C_{66} & C_{26} & C_{36} \\ C_{26} & C_{22} & C_{23} \\ C_{36} & C_{23} & C_{33} \end{bmatrix}.$$

The determinants on the right hand sides are all principal minors of $\bar{C}$ and so are always positive definite. Since $\bar{C}$ is positive definite all principal minors are positive, therefore $\bar{A}$ is positive definite if $\varphi^2 > 0$. In the same way B is singular with rank 2 but the first and second leading principal minors are positive so $\bar{B}$ is positive semi-definite. Now since, by definition,

$$\bar{k}^T \bar{A} \bar{k} > 0 \text{ and } \bar{k}^T \bar{B} \bar{k} \geq 0 \text{ if } \bar{k}\neq 0$$

then

$$\bar{k}^T \bar{L} \bar{k} = \bar{k}^T(\bar{A}+\bar{B})\bar{k} > 0$$

meaning $\bar{L}$ must be positive definite since matrix multiplication is distributive. Therefore $\det(\bar{L})>0$ if $\varphi^2>0$ and so no roots φ_i^2 are non-negative. This inequality is useful in checking numerical results.

When $\varphi^2 = \varphi_i^2$ and $\det(\bar{L})=0$ there are an infinite number of $\bar{k}$ vectors which satisfy $\bar{L}\,\bar{k} = 0$. The elements of $\bar{k}$ are related by

$$\kappa_u = \frac{k_u}{k_w} = \frac{L_{12}L_{23}-L_{13}L_{22}}{L_{11}L_{22}-L_{12}^2}$$

$$\kappa_v = \frac{k_v}{k_w} = \frac{L_{12}L_{13}-L_{11}L_{23}}{L_{11}L_{22}-L_{12}^2} \tag{4.2.12}$$

These ratios are functions of the material properties (i.e. the components of $\bar{C}$ and the roots φ_i^2 of the polynomial while one of the elements of $\bar{k}$ is arbitrary. If $\varphi_i^2<0$ both φ_i and the values of κ_u and κ_v are imaginary numbers; the sign of φ_i makes no difference in the value of the displacements.

To demonstrate, if we choose the trial functions as sums of products of exponentials

$$U_0 = k_u \sin(\psi_y y)\sin(\psi_z z)$$

$$V_0 = k_v \sin(\psi_y y)\sin(\psi_z z) \qquad (4.2.13)$$

and

$$W_0 = k_w \cos(\psi_y y)\cos(\psi_z z)$$

then corresponding to the three roots $\varphi_1^2, \varphi_2^2, \varphi_3^2$ and the three k vectors having ratios $\kappa_{u1}, \kappa_{u2}, \kappa_{u3}, \kappa_{v1}, \kappa_{v2}, \kappa_{v3}$. Setting $k_w=1$ there are three solution *vectors*

$$\bar{U}^i = \begin{bmatrix} \kappa_{ui}\sin(\varphi_i\psi_z y)\sin(\psi_z z) \\ \kappa_{vi}\sin(\varphi_i\psi_z y)\sin(\psi_z z) \\ \cos(\varphi_i\psi_z y)\cos(\psi_z z) \end{bmatrix} \quad i=1,2,3 \qquad (4.2.14)$$

Because each vector is a solution and $\mathfrak{L}_i$ are linear then a vector $k_1\bar{U}^1+k_2\bar{U}^2+k_3\bar{U}^3$ where k_i are arbitrary constants is also a solution. So long as the 3 roots are distinct and $\kappa_{ui}+\kappa_{vi}\neq 0$ for i=1,2,3 it can easily be shown that the 3 vectors are linearly independent and so form a basis at any point in y,z where none of the three are zero. Moreover, vectors formed from such linear combinations will be linearly independent over y,z for different values of ψ_z. Therefore, since ψ_z is arbitrary linear combinations from this family of solutions will also be solutions and will be linearly independent.

A special case occurs when α in Equations (2.1.14) is equal to $n\pi/2$ $n=0,1,2......$ since then $L_{12}=L_{13}=0$; the first equation becomes $L_{11}k_u=0$, and $\kappa_{vi}=-L_{23}/L_{22}$ for $i=2,3$. Three solutions for the vector $\bar{k}$ are

$$\bar{k}=\begin{bmatrix} k_u \\ 0 \\ 0 \end{bmatrix}, \begin{bmatrix} 0 \\ \kappa_{v2} \\ 1 \end{bmatrix} k_w, \begin{bmatrix} 0 \\ \kappa_{v3} \\ 1 \end{bmatrix} k_w$$

where k_u, k_w are arbitrary.

One root corresponds to $L_{11}=0$ and is $\varphi_1^2=-C_{55}/C_{66}$. In this case the solution is $\{k_u\ 0\ 0\}$. The other two roots are found by satisfying

$$\det \begin{bmatrix} L_{22} & L_{23} \\ L_{23} & L_{33} \end{bmatrix} = 0 \quad \text{and yield } \kappa_{v2}, \kappa_{v3}.$$

If the laminate has all specially orthotropic layers then with proper loading $x=0$ is a plane of reflective symmetry and the solution does not include displacements in the axial direction and so we can say $k_u=0$. If the material is isotropic then $\varphi_1^2=\varphi_2^2=\varphi_3^2=-1$ so that the solutions vectors are no longer independent.

In laminates containing plies so oriented there may be axial displacement. In these cases k_u will be arbitrary as well as k_w. Therefore, complete solutions can be obtained in the same general manner as before except that now the U_o component of the displacement solution is independent of V_o and W_o.

The above solution set satisfies the internal, or governing equations of the problem. The constants ψ_z, k_w and in special cases k_u may be arbitrary. In the next section methods of evaluating these parameters to obtain approximate particular solutions are discussed.

4.2.2.2 Extension to Fully Three-Dimensions

Following nearly the same procedure for the complete governing equations would lead to a similar solution set.

Choosing

$$U_o = k_u \, e^{\psi_x x} \, e^{\psi_y y} \, e^{\psi_z z}$$

$$V_o = k_v \, e^{\psi_x x} \, e^{\psi_y y} \, e^{\psi_z z}$$

$$W_o = k_w \, e^{\psi_x x} \, e^{\psi_y y} \, e^{\psi_z z}$$

would lead to an Γ matrix such that, for example, there would be three roots for each pair ψ_x/ψ_y selected. If we set $\psi_x=\psi_y$ then a solution set would be generated, etc. As for two dimensions the solutions would be linearly independent. This method would be potential be useful for holes, beams, etc. It would be worthwhile investigating this boundary method.

4.2.3 Particular Solutions-Weighted Residual Methods

4.2.3.1 General

For a particular problem the boundary conditions may be expressed

$$B_i(\bar{u})=f_i \quad i=1,2...m \tag{4.2.15}$$

(f_i is a defined function) on portion(s) Γ_i of the boundary; if we use an approximation for $\bar{u}$ defined over the whole domain including Γ

$$\bar{u}(\bar{k},\bar{\Psi}) = \sum_{j=1}^{n} k_{wj}\, \bar{U}_j(\psi_{zj}) \tag{4.2.16}$$

where $\bar{k}^T=[\, k_{w1},\ k_{w2},.......k_{wn}]$ $\bar{\Psi}^T=[\, \psi_{z1},\ \psi_{z2},.......\psi_{zn}]$ then on Γ_i Equation (4.2.15) will not, in general, be exactly satisfied so

$$B_i(\bar{u})-f_i=R_i \quad i=1,2...m$$

where R_i, called the residual or error, is not zero unless $\bar{u}$ is the exact solution. Weighted residual methods yield approximate solutions by minimizing the magnitudes of all R_i in some way with respect to arbitrary parameters. The solution obtained is exact for a problem with the necessary residuals applied as boundary conditions; viewed from this aspect intuition and experience can be used to judge the deviation from the desired solution due to the residuals imposed. For example, a sharp change in stress on the boundary would be expected to cause a local disturbance in the interior.

For minimizing the residual w.r.t. $\bar{k}$ there are many methods which fall under the heading of weighted residual methods. Findlay(1966), Collatz(1960), Crandall(1956). and Ci-Da(1985) presented reviews of the methods. Among these methods The least squares method is easily formulated and leads to symmetric matrices. In the following paragraphs various least squares methods are reviewed.

4.2.3.2 Integrated Least Squares Method

For an approximate solution which satisfies

$$\sum_{i=1}^{m} \int_{\Gamma_i} R_i^2 \, d\Gamma_i = \text{a minimum}; \qquad (4.2.17)$$

the well known condition(s) for a minimum w.r.t. $\bar{k}$ are

$$\sum_{i=1}^{m} \int_{\Gamma_i} \frac{\partial R_i^2}{\partial k_{wj}} d\Gamma_i = 0 \quad \text{for } j=1,2\ldots n;$$

this is satisfied if

$$\sum_{i=1}^{m} \int_{\Gamma_i} \frac{\partial R_i}{\partial k_{wj}} R_i \, d\Gamma_i = 0 \quad \text{for } j=1,2\ldots n. \qquad (4.2.18)$$

In this method R_i is weighted by $\partial R_i / \partial k_{wj}$. Given the residual for the ith boundary condition in the matrix form (it will be shown how later)

$$\bar{G}_i \bar{k} - r_i = 0 \qquad (4.2.19)$$

where $\bar{G}_i^T(\bar{\Psi})$ is a vector having n elements, then the weighted residual statement becomes

$$\sum_{i=1}^{m} \int_{\Gamma_i} G_{ij}(\bar{G}_i\bar{k}-r_i)d\Gamma_i=0 \text{ for } j=1,2...n \quad (4.2.20)$$

(elements of the present family of trial functions are easily computed and operated on by differentiation and integration). After summation, this leads to a set of n linear algebraic equations

$$\bar{G}\,\bar{k} = \bar{R}$$

where

$$\bar{G}(\bar{\Psi}) = \sum_{i=1} \int_{\Gamma_i} \bar{G}_i^T\,\bar{G}_i d\Gamma_i \quad \text{and} \quad \bar{R}(\bar{\Psi}) = \sum_{i=1} \int_{\Gamma_i} \bar{G}_i^T\, r_i d\Gamma_i$$

$\bar{G}$ is a symmetric square matrix. This requires that all products $G_{ij}G_{il}$ $j,l=1,2,...n$ be integrated. Unfortunately, although this appears to be a good approach, as the dimension of square matrix $\bar{G}$ increases beyond about 10 this matrix rapidly becomes algorithmically singular(e.g. see Lawson(1974)).

The minimum w.r.t. $\bar{k}$ of the integrated residuals can be sought directly using optimisation techniques rather than by equating the derivatives to zero. Given the residual Equation (4.2.19) the total square residual is

$$R_2 = \sum_{i=1}^{m} (\bar{k}^T \int_{\Gamma_i} [\, \bar{G}_i^T \;\; \bar{G}_i] \, d\Gamma_i \; \bar{k}$$

$$-2 \, r_i \int_{\Gamma_i} [\, \bar{G}_i \, d\Gamma_i] \, \bar{k} + r_i^2) \qquad (4.2.21)$$

and an element of the gradient vector of R_2 w.r.t. k_1 is

$$\partial R_2/\partial k_1 = 2 \sum_{i=1}^{m} (\int_{\Gamma_i} [\, \bar{G}_i^T \; \bar{G}_i \,] \, d\Gamma_i \; \bar{k}$$

$$- \; r_i \int_{\Gamma_i} G_{i1} d\Gamma_i) \qquad (4.2.22)$$

Finding the $\ddot{k}$ vector for which this positive definite quadratic equation is a minimum is a straightforward task using readily available computer optimisation routines such as the conjugate gradient method. It requires low storage for the square symmetric matrix in R_2. However, an initial estimate of $\bar{k}$ is required and the time to find a minimum can depend heavily upon this. Further, $\bar{k}$ often requires scaling by constants to accelerate convergence. In its favour this method conveniently yields the exact total residual.

4.2.3.3 Collocation Least Square Methods

A simple alternative to the weighting factor $\partial R_i/\partial k_{wj}$ used in Equation (4.2.18) is the delta function δ_1. which has the value

$$\delta_1 = \begin{cases} 1 & \text{when } x = x_1 \\ 0 & \phantom{\text{when }} x \neq x_1 \end{cases} \quad . \qquad (4.2.23)$$

This is equivalent to setting

$$\bar{G}_i \bar{k} - r_i = 0$$

at points on the boundary to yield one linear algebraic equation per boundary condition per point on the boundary. There must be at least n equations to solve uniquely for the n unknowns which will constrain the residual to vanish at all the points. If more than n equations are used, say m, $\bar{k}$ may be found which minimizes the L_2 norm w.r.t. $\bar{k}$

$$\| \bar{G}\,\bar{k} - \bar{R} \|_2 = \sum_{i=1}^{m} (\bar{G}_i \bar{k} - R_i)^2 \qquad (4.2.24)$$

where a row of $\bar{G}$ is Equation (4.2.19) evaluated for some boundary condition at some point on it's domain. This method shall be referred to as the least squares boundary collocation (LSBC) method. The minimum norm of the overdetermined set of equations corresponds to the solution of the square symmetric positive definite set of equations

$$\bar{G}^T \bar{G} \bar{k} = \bar{G}^T \bar{R} \qquad (4.2.25)$$

which again for n>10 becomes algorithmically singular. Scaling rows or columns may improve the stability somewhat; scaling columns changes the problem. However, by using transformation methods on the original set of equations the solution may be found without significant computational problems (Lawson(1974)) or error.

Subdomain collocation can be used similarly. The domain of B_i is broken in subdomains Γ_{ij}. The residual is then evaluated over the segment and set to zero i.e.

$$\int_{\Gamma_{ij}} R_i \, d\Gamma_{ij} = \int_{\Gamma_{ij}} \bar{G}_i d\Gamma_{ij} \, \bar{k} - r_i = 0 \ . \qquad (4.2.26)$$

The advantages of the LSBC methods are that only the functions in $\bar{G}$ need to be evaluated and not integrals of their products, and that complex geometries and boundary conditions are as easily represented as the functions which describe them. A potential disadvantage is that the distribution of points affects the solution. However, complication from discretization is often present in other methods such as finite elements and finite differences and may not be a problem if it can be handled systematically. Also, the final system of equations is generally overdetermined and no longer symmetric requiring more storage for the initial equations than the normal equations.

Because the homogeneous solutions apply within the individual layers and interface conditions are approximated the matrix $\bar{G}$ is populated in a block diagonal pattern as depicted in Figure 4.2.1. Using a transformation method $\bar{G}$ is transformed to the block diagonal upper triangular matrix $\bar{R}$. The algorithm is simple, to eliminate G_{ki} where k>i then

For j=1,2.......q

$v=G_{ij}$

$w=G_{kj}$

$G_{ij}= Cv + Sw$

$G_{kj}=-Cv + Sw$

where there are q columns in $\bar{G}$

If $G_{ki}=0$

then

C=1 and S=0

else

if $|G_{ki}|\geq|G_{ii}|$

then

$\mathcal{T}=G_{ii}/G_{ki}$ $S=1/(1+\mathcal{T}^2)^{1/2}$ $C=S\mathcal{T}$

else

$\mathcal{T}=G_{ki}/G_{ii}$ $C=1/(1+\mathcal{T}^2)^{1/2}$ $S=C\mathcal{T}$

Elements below the diagonal are elimnated row by row from the second row. In this way the transformation is done without any intermediate fill-in. That is, only the union

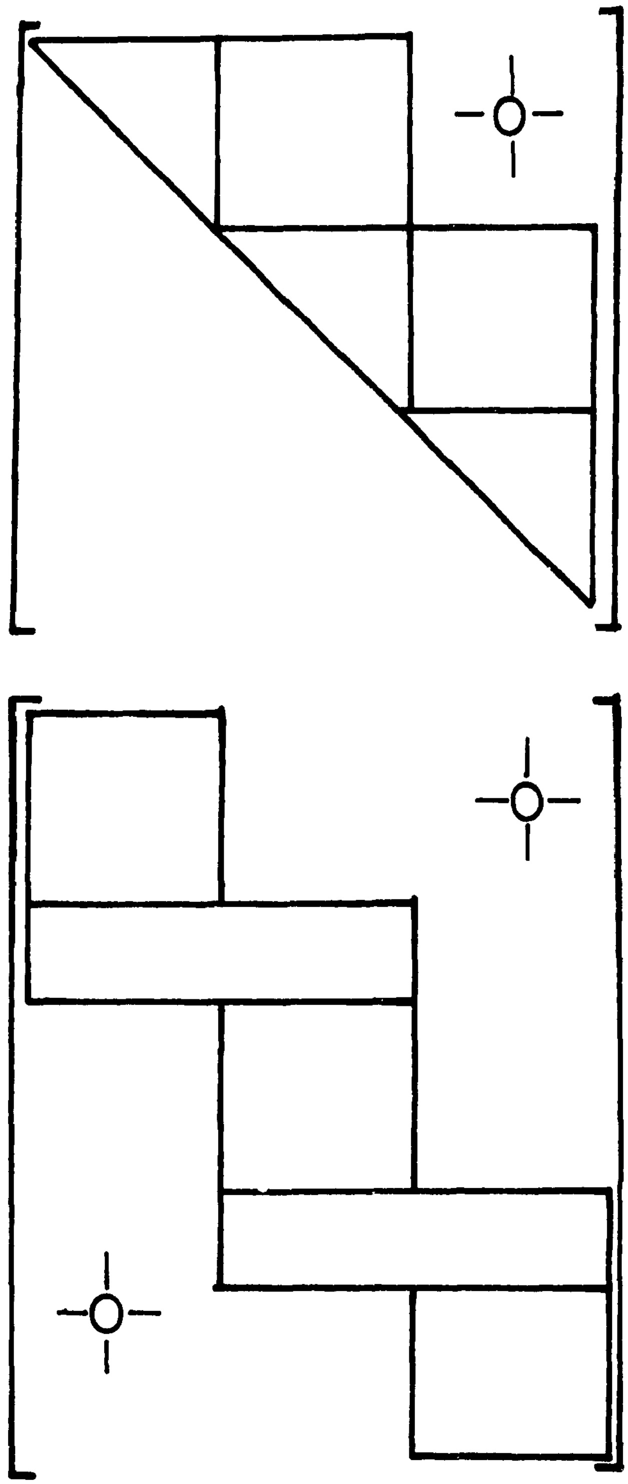

Figure 4.2.1 Matrix $\bar{G}$ (below) for a three layer domain is transformed from block diagonal form to upper triangular block form $\bar{R}$ (above). Storage required is the union of these two matrices.

of populated areas of $\bar{G}$ and $\bar{R}$ are required for storage as depicted in Figure 4.2.1. The housekeeping operations are minimal and the program is simple, stable and efficient. Further, as the number of layers increases, the block sizes do not necessarily increase if the number of DOF in each layer is held constant.

4.2.3.4 Discussion

There are many variations of LS methods devisable. For example, multiplying a residual by a weight value such as the length of the boundary between points will change its relative contribution to the total residual and so the degree to which it is satisfied in the final result. Weights could be spatial functions and could be applied to any of the residual equations.

Overall, the BLSC method using transformation methods is most attractive for large systems and it is desired that the method be flexible w.r.t. boundary conditions and geometry.

4.2.3.5 Selection of $\bar{\Psi}$

The arbitrary parameters ψ_z must be known or set before G can be determined to minimize the residual w.r.t. $\bar{k}$. The object is to determine $\bar{\Psi}$ to yield the best LS approximation. $\bar{\Psi}$ may be found algorithmically from some initial $\bar{\Psi}_o$, assuming the absolute minimum can be found, and there will be no more degrees of freedom than if $\bar{\Psi}$ were set to the best possible. The limitation to searching for $\bar{\Psi}$ is the "curse of dimension" (Fletcher 1980)ie. the time to search increases rapidly with the dimension of $\bar{\Psi}$ if each element is sought. In order to reduce the number of unknowns a sequence dependent upon fewer unknowns can be used to generate $\bar{\Psi}$. In a later section, this approach is taken successfully.

4.2.4 Summary

A simple, flexible method of solution for a large class of laminate problems has been presented in this section. The two conditions which define this class are $\partial\bar{\sigma}/\partial x=0$, and that the rotation of the principal axes for each material be about only one of the two axes perpendicular to the x axis. This places no restriction on the geometry and loading in the problem domain i.e. the plane section normal to the x axis. The object is to obtain a minimum LS residual evaluated on the boundary by evaluating k and Ψ for specific problems. Particular solutions are to be obtained using a BLSC method and Given's method (Given (1958)) on the final system. After solving, the residual is used as the basis for evaluating convergence.

In the next section a procedure for obtaining solutions to specific problems by this method is presented.

For benchmark problems convergence w.r.t. computational parameters is examined and results are compared with those from other successful methods appearing in the literature.

4.3 Solution Prodedure and Qualification

4.3.1 Solution Procedure

The steps in formulating a BLSC solution are:

i) select the trial functions in each layer,

ii) select Ψ,

iii) set a distribution and weighting scheme for the collocation points.

A unique series of the trial functions is chosen in each layer, so that each layer has a unique set of k. On boundaries with certain symmetry (u,v odd and w even; or u,v even and w odd) only functions with the same symmetry are required. The conditions on the laminate boundaries and layer interfaces are satisfied exactly by the selection of the trial functions or approximately by minimizing the sum of the residuals of these equations.

When the residual involves displacements directly, as along the interface, boundary weighting is required. The conditions of compatability and continuity along the interface are

$$u_i^+=u_i^- \qquad \sigma_{iz}^+=\sigma_{iz}^- \qquad i=1,2,3.$$

while the other stresses may be discontinuous across this plane. The magnitude of a displacement's contribution to the residual (i.e. $(u_i^+ - u_i^-)^2$) will be relatively small unless the displacements are suitably weighted. Matching of the interface displacements was achieved by weighting the displacement's residual such that its magnitude is the same order as the stress residuals. The same weight is used in all solutions of about half the elastic modulus: $E_{11}/2$.

The frequencies ψ_z have nonzero finite values. By trial a simple distribution was found to be suitable; i.e.

$$f_z t\psi_z = \pi,\ 2\pi,\ 3\pi,\ \ldots\ldots\ldots n\pi \qquad (4.3.1)$$

where the value of π is used merely to show that $f_z=1$ may not be optimal.

The distribution of collocation points is chosen to avoid what is often called the aliasing error. For example, when the number of collocation points is

$$t\psi_z\ /\pi\ +1$$

over the interval along the free edge then the residual can have zeroes at the collocation points as in Figure 4.3.1. To avoid this kind of error, the condition

$$\#\text{ points} > t\psi_{z\ max}\ /\pi + 1 \qquad (4.3.2)$$

is satisfied; $2t\psi_{z\ max}/\pi+1$ or more may be necessary in practice. Along z=constant boundaries a density of collocation points sufficient to prevent oscillations in the

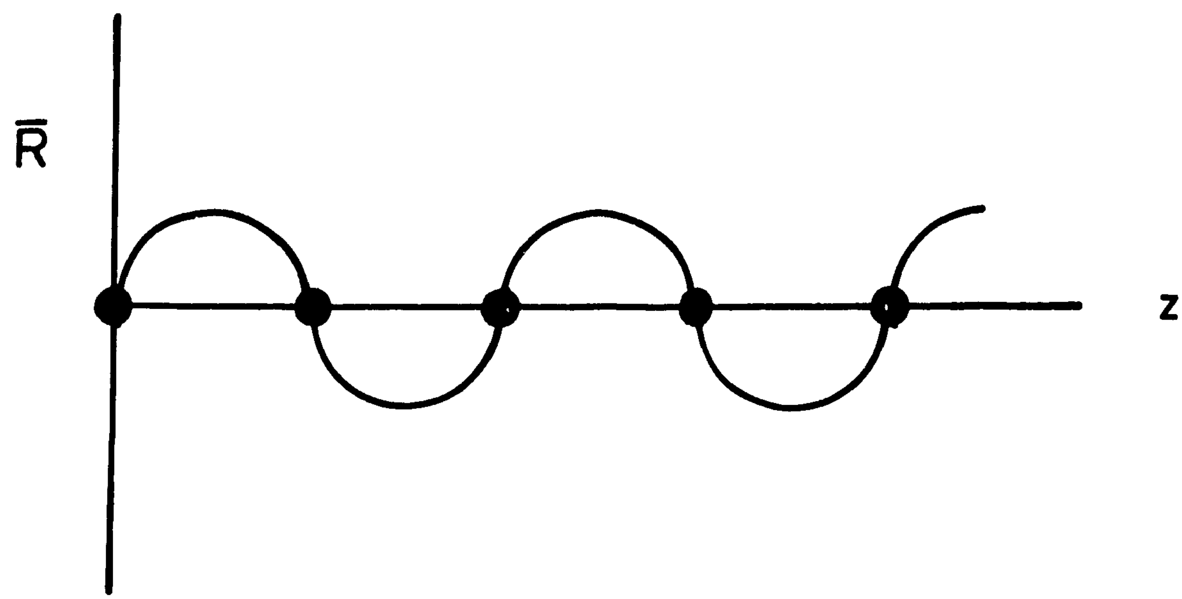

Figure 4.3.1 Zero collocation residual due to inadequate point spacing.

solution is adequate; further, from observations spatially varying the density within the boundary layer (eg. grading the point spacing towards the singularity) eventually causes oscillations away from the singularity; in general, a near uniform density is required which prevents oscillation and is high enough to estimate the residual with sufficient accuracy. A satisfactory scheme was found to be a uniform distrution according to the inequality(4.3.2) along y=b and half as many points with slight grading along z=constant boundaries as in Figure 4.3.2.

The CLT strains for a desired loading are used to evaluate the π_i in Equation(4.2.6). The complete CLT solution for each case is imposed (including ϵ_z) by setting the appropriate π_i so that Equations(4.2.4) are satisfied exactly. This is based on the assumption that for edge phenomena the CLT solution is regained away from the edge.

Given an adequate representation of the integrated residual error by the collocation values the best value of f_z in Equation(4.3.1) can be found by seeking the minimum of the sum of squared residuals (for a low #DOF for efficiency). The integrated residual is necessarily monotonically nonincreasing w.r.t. increasing n for a constant value of f_z.

In the final analysis solutions to the simple free edge problem can be evaluated by several checks beyond the residual average. Since CLT stresses are assumed outside the boundary layer to satisfy equilibrium it must be true that

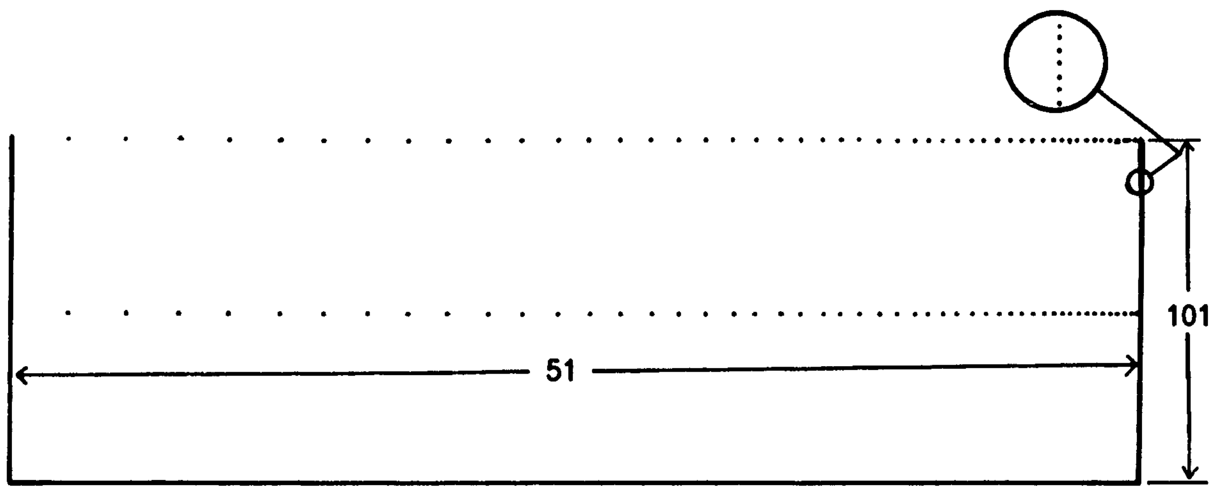

Figure 4.3.2 Collocation point distribution for four layer symmetric laminate.

$$\int_0^b \sigma_z dy=0 \quad ,$$

$$\int_z^t \tau_{xy}\, dz= \int_0^b \tau_{xz}\, dy \quad ,\text{and} \qquad \int_z^t \sigma_y\, dz= \int_0^b \tau_{yz}\, dy.$$

As well, point checks on the satisfaction of boundary conditions may disclose error.

4.3.2 Qualification of the Method and Procedure

In this section solutions obtained by the above procedure are examined for convergence and are compared with results in the literature from other qualified methods. As mentioned in Section 4.1 the problems which have to this time received most attention in the literature, are $[\pm 45]_s$, $[90/0]_s$, and $[0/90]_s$ laminates in uniform extension.

The domain and boundary conditions for these problems are shown in Figure 4.3.3. For the present method the displacement boundary conditions on the surfaces y=0 and z=0 are satisfied exactly by the choice of trial functions in which u and v are even exponential functions of y and odd exponential functions of z while w is the opposite. In the upper layer both odd and even functions of z for the displacements are necessary since the boundary condition is matching the lower layer.

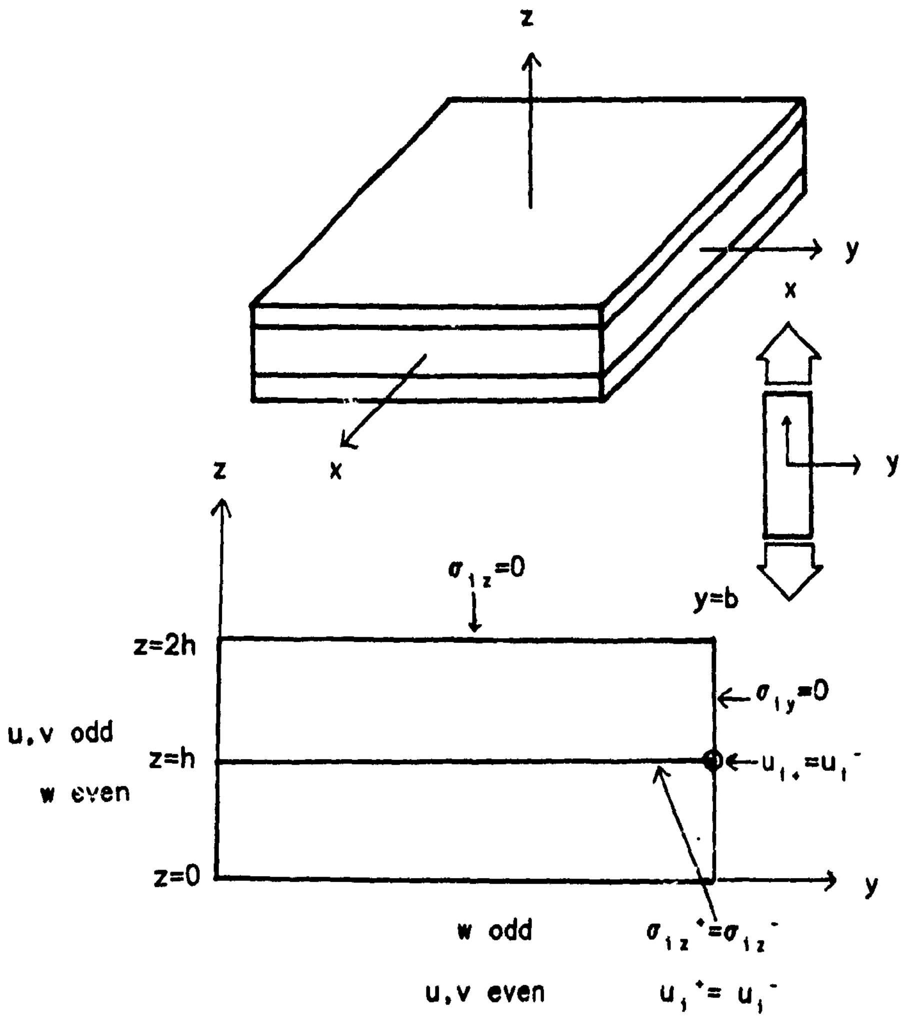

Figure 4.3.3 Uniform extension problem for $[\pm\theta]_s$, $[0/90]_s$, and $[90/0]_s$ laminates.

4.3.2.1 Angle-ply Symmetric Laminates

For the $[\pm\theta]_s$ laminate the displacement functions are:

$$u = \sum_{i=1,7,13..n} \Bigg[\kappa_{u1} \Big[\big(k_i \sinh(\varphi_1 (\psi_z)_{\frac{i+1}{2}} y) \cos((\psi_z)_{\frac{i+1}{2}} z)$$

$$+ k_{i+1} \sinh(\varphi_1 (\psi_z)_{\frac{i+1}{2}} y) \sin((\psi_z)_{\frac{i+1}{2}} z) \Big]$$

$$+ \kappa_{u2} \Big[\big(k_{i+2} \sinh(\varphi_2 (\psi_z)_{\frac{i+3}{2}} y) \cos((\psi_z)_{\frac{i+3}{2}} z)$$

$$+ k_{i+3} \sinh(\varphi_2 (\psi_z)_{\frac{i+3}{2}} y) \sin((\psi_z)_{\frac{i+3}{2}} z) \Big]$$

$$+ \kappa_{u3} \Big[\big(k_{i+4} \sinh(\varphi_3 (\psi_z)_{\frac{i+5}{2}} y) \cos((\psi_z)_{\frac{i+5}{2}} z)$$

$$+ k_{i+5} \sinh(\varphi_3 (\psi_z)_{\frac{i+5}{2}} y) \sin((\psi_z)_{\frac{i+5}{2}} z) \Big] \Bigg]$$

$$v = \sum_{i=1,7,13..n} \Bigg[\kappa_{v1} \Big[\big(k_i \sinh(\varphi_1 (\psi_z)_{\frac{i+1}{2}} y) \cos((\psi_z)_{\frac{i+1}{2}} z)$$

$$+ k_{i+1} \sinh(\varphi_1 (\psi_z)_{\frac{i+1}{2}} y) \sin((\psi_z)_{\frac{i+1}{2}} z) \Big]$$

$$+ \kappa_{v2}\Big[(k_{i+2} \sinh(\varphi_2(\psi_z)_{\frac{i+3}{2}} y) \cos((\psi_z)_{\frac{i+3}{2}} z)$$

$$+ k_{i+3} \sinh(\varphi_2(\psi_z)_{\frac{i+3}{2}} y) \sin((\psi_z)_{\frac{i+3}{2}} z)\Big]$$

$$+ \kappa_{v3}\Big[(k_{i+4} \sinh(\varphi_3(\psi_z)_{\frac{i+5}{2}} y) \cos((\psi_z)_{\frac{i+5}{2}} z)$$

$$+ k_{i+5} \sinh(\varphi_3(\psi_z)_{\frac{i+5}{2}} y) \sin((\psi_z)_{\frac{i+5}{2}} z)\Big]\Big]$$

$$w = \sum_{i=1,7,13..n}\Big[\Big[(k_i \cosh(\varphi_1(\psi_z)_{\frac{i+1}{2}} y) \sin((\psi_z)_{\frac{i+1}{2}} z)$$

$$+ k_{i+1} \cosh(\varphi_1(\psi_z)_{\frac{i+1}{2}} y) \cos((\psi_z)_{\frac{i+1}{2}} z)\Big]$$

$$+ \kappa_2\Big[(k_{i+2} \cosh(\varphi_2(\psi_z)_{\frac{i+3}{2}} y) \sin((\psi_z)_{\frac{i+3}{2}} z)$$

$$+ k_{i+3} \cosh(\varphi_2(\psi_z)_{\frac{i+3}{2}} y) \cos((\psi_z)_{\frac{i+3}{2}} z)\Big]$$

$$+ \kappa_3\Big[(k_{i+4} \cosh(\varphi_3(\psi_z)_{\frac{i+5}{2}} y) \sin((\psi_z)_{\frac{i+5}{2}} z)$$

$$+ k_{i+5} \cosh(\varphi_3(\psi_z)_{\frac{i+5}{2}} y) \cos((\psi_z)_{\frac{i+5}{2}} z)\Big]\Big]$$

in the upper layer and

$$u = \sum_{i=1,4,7..n} \Big[\kappa_{u1}(k_i \ \sinh(\varphi_1(\psi_z)_{\frac{i+1}{2}}\, y)\ \cos((\psi_z)_{\frac{i+1}{2}}\, z)$$

$$+ \kappa_{u2}(k_{i+1} \ \sinh(\varphi_2(\psi_z)_{\frac{i+3}{2}}\, y)\ \cos((\psi_z)_{\frac{i+3}{2}}\, z)$$

$$+ \kappa_{u3}(k_{i+2} \ \sinh(\varphi_3(\psi_z)_{\frac{i+5}{2}}\, y)\ \cos((\psi_z)_{\frac{i+5}{2}}\, z) \Big]$$

$$v = \sum_{i=1,4,7..n} \Big[\kappa_{v1}(k_i \ \sinh(\varphi_1(\psi_z)_{\frac{i+1}{2}}\, y)\ \cos((\psi_z)_{\frac{i+1}{2}}\, z)$$

$$+ \kappa_{v2}(k_{i+1} \ \sinh(\varphi_2(\psi_z)_{\frac{i+3}{2}}\, y)\ \cos((\psi_z)_{\frac{i+3}{2}}\, z)$$

$$+ \kappa_{v3}(k_{i+2} \ \sinh(\varphi_3(\psi_z)_{\frac{i+5}{2}}\, y)\ \cos((\psi_z)_{\frac{i+5}{2}}\, z) \Big]$$

$$w = \sum_{i=1,4,7..n} \Big[k_i \ \cosh(\varphi_1(\psi_z)_{\frac{i+1}{2}}\, y)\ \sin((\psi_z)_{\frac{i+1}{2}}\, z)$$

$$+ k_{i+1} \ \cosh(\varphi_2(\psi_z)_{\frac{i+3}{2}}\, y)\ \sin((\psi_z)_{\frac{i+3}{2}}\, z)$$

$$+ k_{i+2} \cosh(\varphi_3 (\psi_z)_{\frac{i+5}{2}}\, y) \sin((\psi_z)_{\frac{i+5}{2}}\, z)\Big]$$

in the middle layer. The matrix $\bar{G}$ is formed from linear combination of these displacements and their partial derivatives and then summing terms for each k.

The average residual is the root mean square value of the total residual from the collocation points. All applicable boundary conditions are used at each point for simplicity. Collocation allows a choice of the conditions to be applied at the singular point. In practice, it appears that imposing more than displacement continuity, the difference is seen only very near the singularity (e.g. $r/h<.1$) with no set of conditions greatly superior. It was decided that only displacement continuity be imposed. In fact, this will be appropriate for the majority of problems which will be undefined at this point. Because of the point distribution, the average residual taken from these points is strongly weighted at the edge y=b.

In Figure 4.3.4 the average collocation residual is plotted against f_z for n=5,10,20 in both layers. It shows a flat minimum for $f_z \approx 1.3$. Essentially, it appears that the minimum residual w.r.t. f_z ($\approx$1.3) establishes the fundamental frequency which is present in the solution so that increasing f_z has little effect. In Figure 4.3.5 the residual is plotted against n for f_z=1.3. The residual decreases slowly for n>25. The rate of convergence appears to be about O(1/n) for both cases. It is not proven that

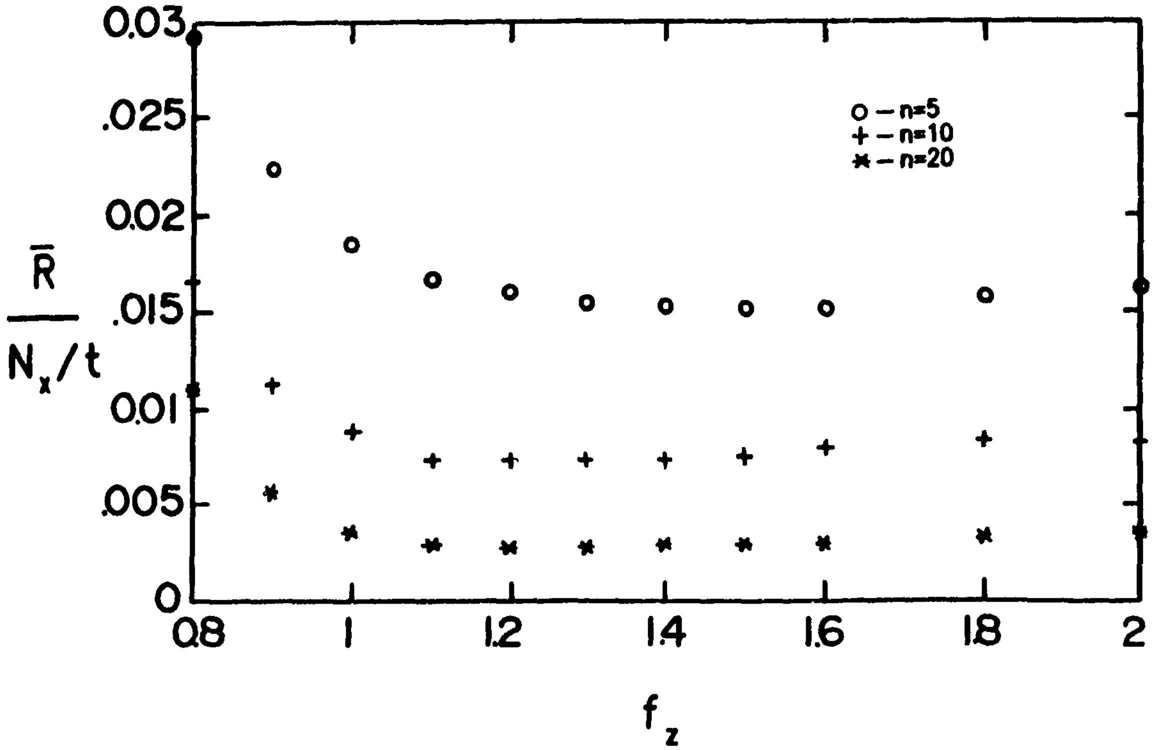

Figure 4.3.4 Average collocation residual vs. f_z for varying number of DOF.

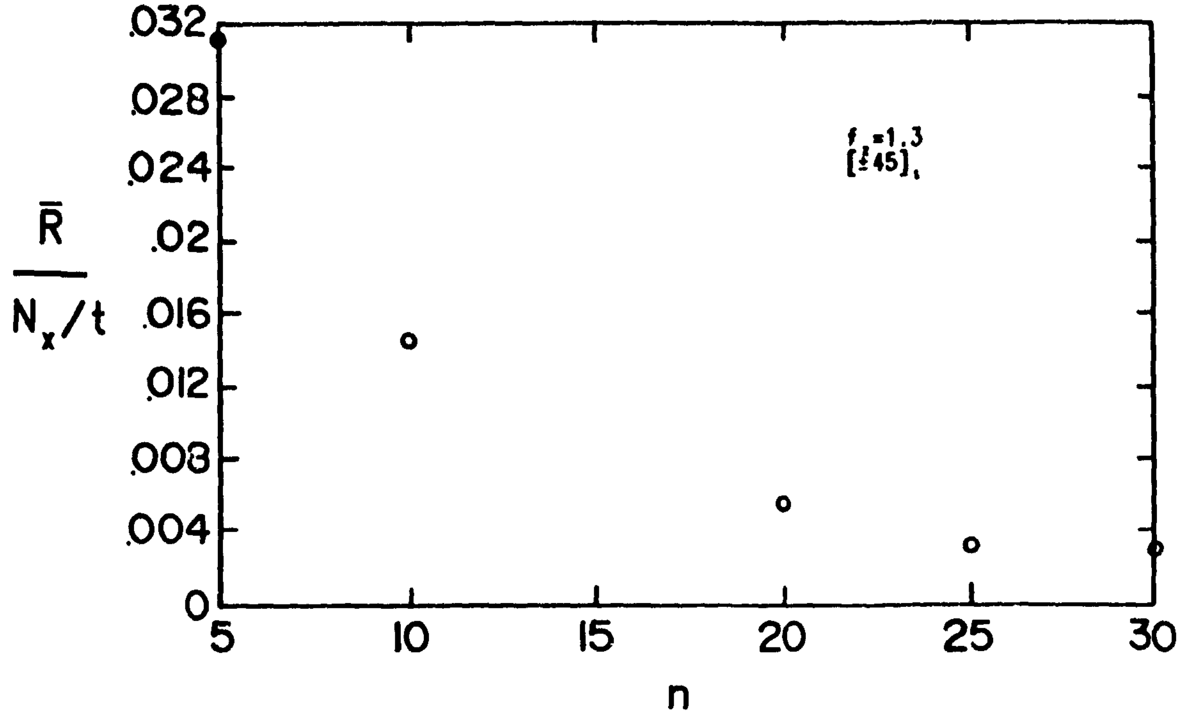

Figure 4.3.5 Average collocation residual vs. number of DOF.

the residual will asymptotically approach zero but does reach a very low value.

In Figures 4.3.6,7 the stresses from various solutions show that solutions are sensitive to changes in the total residual due to varying f_z and n. Most important, it can be seen that although increasing n lowers the residual, it can also be seen that for f_z=.8 the solutions behave badly. For $f_z > f_{z\ opt}$ (>1.3) the solutions are acceptable. The results appear to be stable with respect to small changes in the residual but using a value of $f_z \geq f_{z\ opt}$ seems vital. Fortunately, for this problem at least the minimum region is very flat for $f_z > f_{z\ opt}$; and in fact a higher value of f_z is desirable since fewer collocation points are required for a solution. From the asymptotic approximation of the convergence the exact stresses σ could be approximated from two solutions from different n, i.e. n_1, n_2 by

$$\sigma \approx (\sigma_1 - n_2\sigma_2/n_1)/(1-n_2/n_1). \qquad (4.3.3)$$

Without using equation(4.3.3) solutions obtained are compared with those of other workers in Figure 4.3.8 a-e). The others are:

- a finite difference by Pipes(1970),

- a constant strain 3 node
  finite element solution by Wang and Crossman (1977),

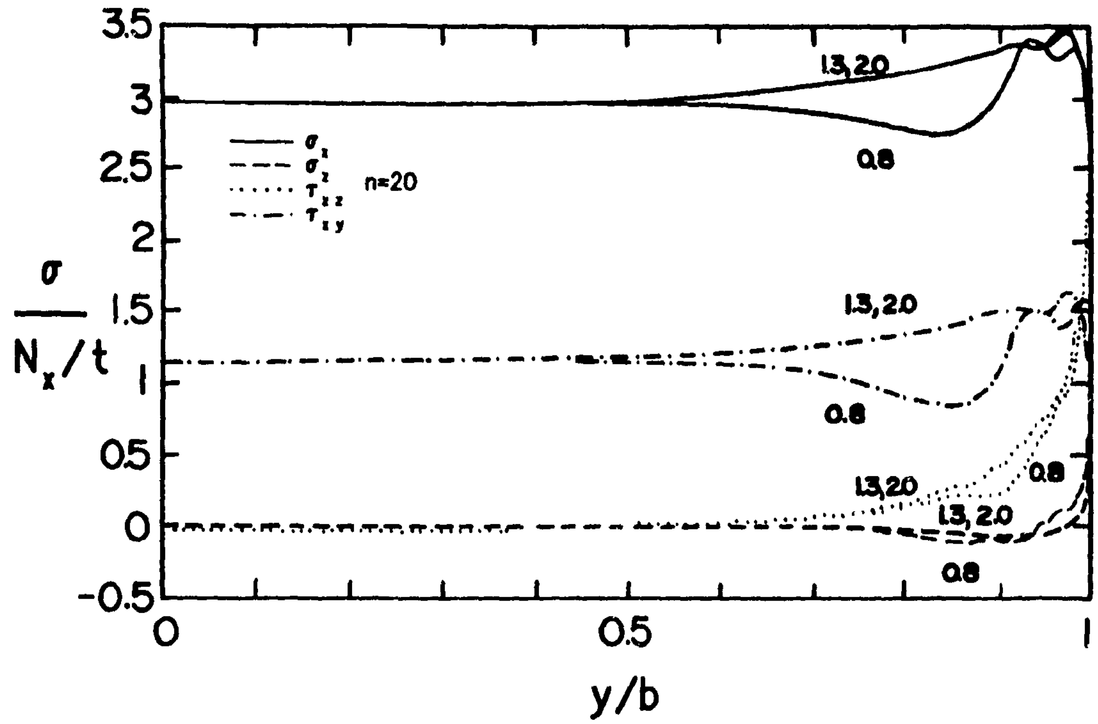

Figure 4.3.6 Influence of f_z on interface stresses for 5 DOF with f_z=.8,1.5,2.0; and 20 DOF with f_z=.8,1.3,2.0.

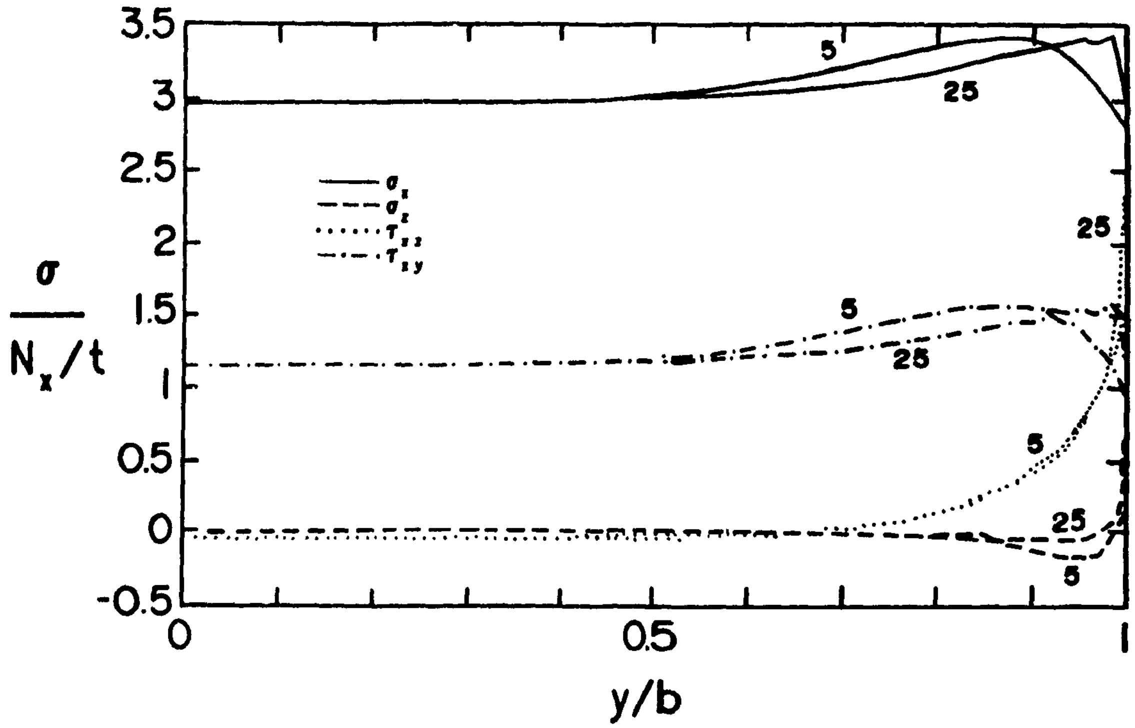

Figure 4.3.7 Interface stresses for 5 and 25 DOF with f_z=1.3.

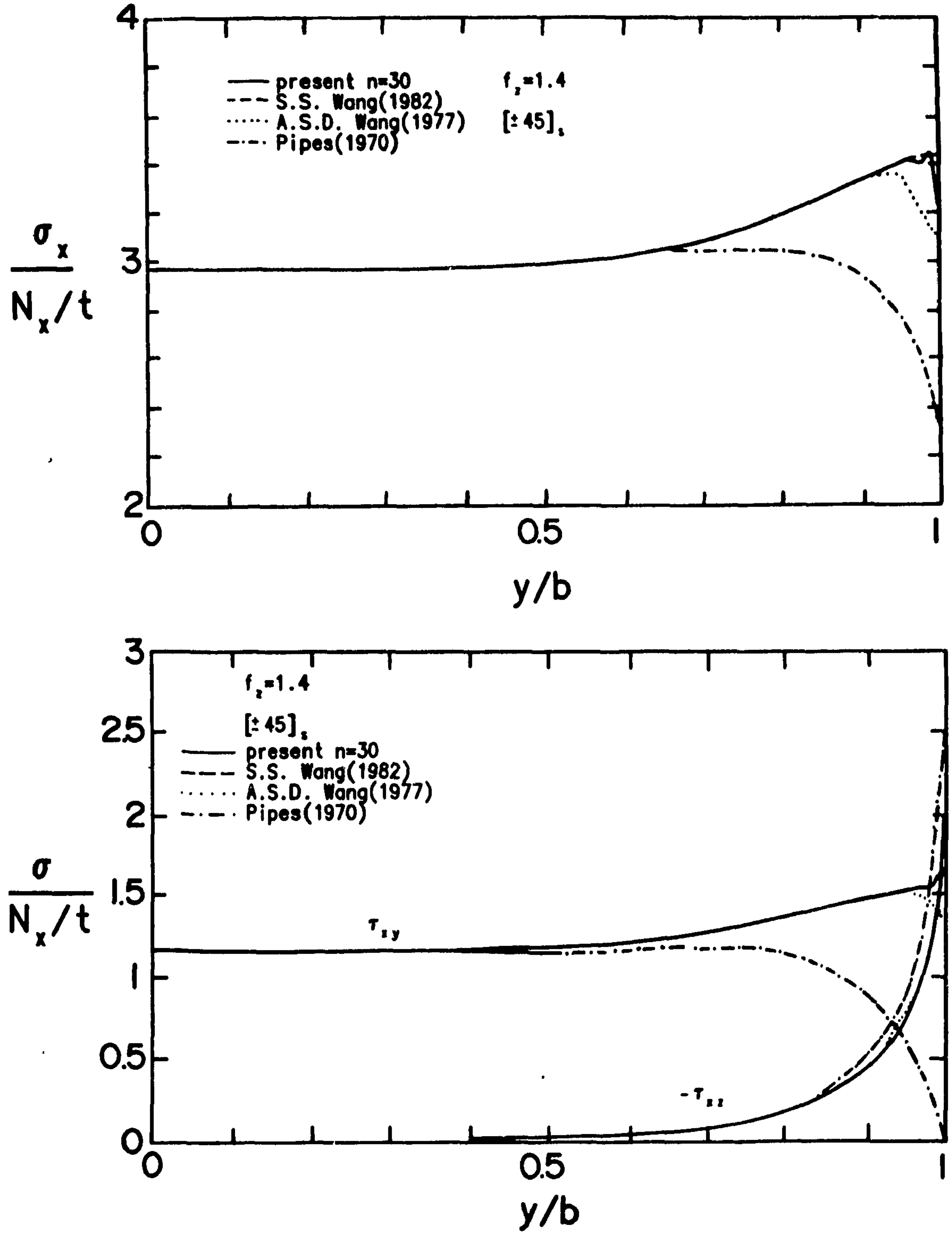

Figure 4.3.8 a,b) Interface stress from present method in comparison with singular, FD, FE solutions.

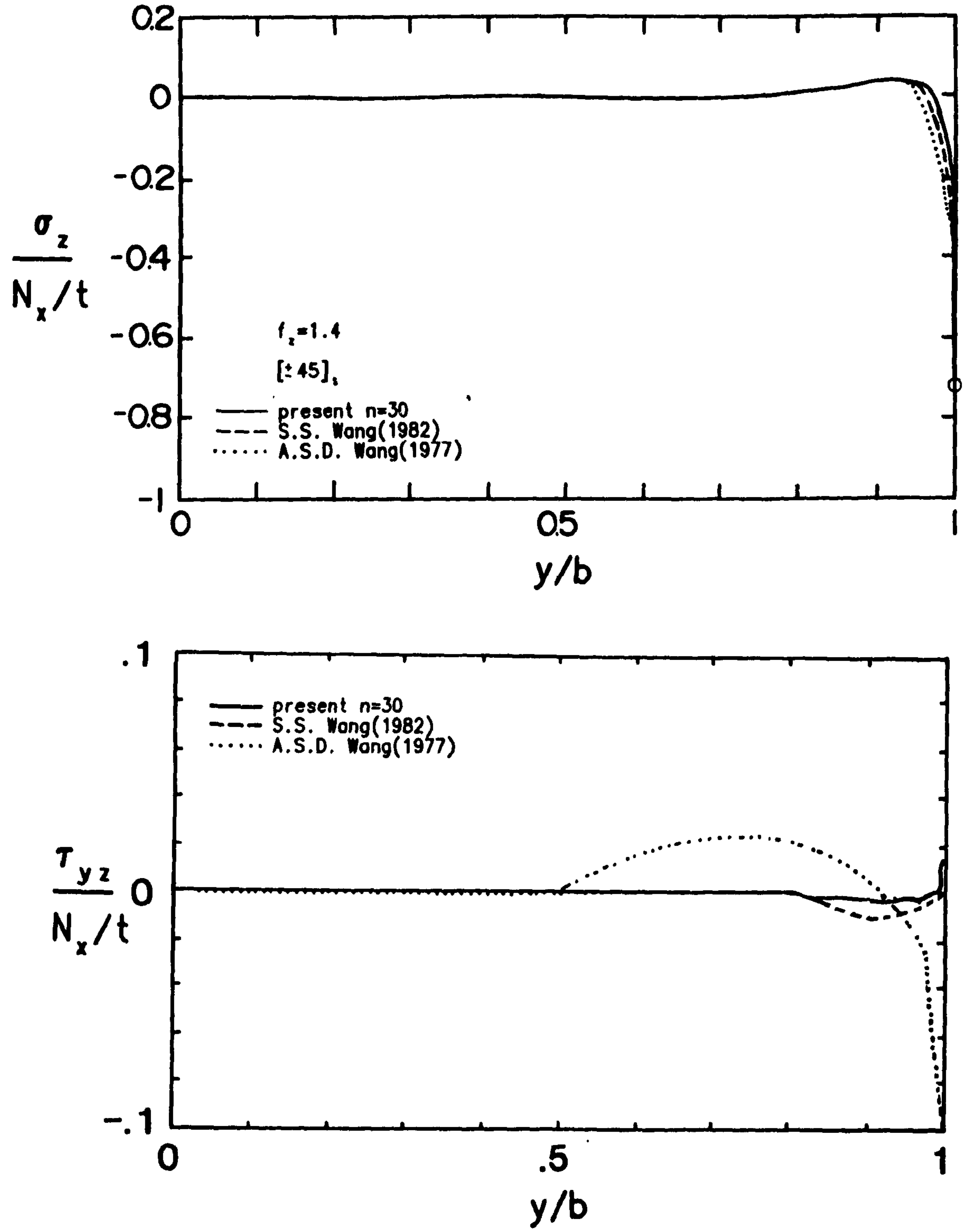

Figure 4.3.8 c,d) Interface interlaminar stresses from the present method in comparison with singular and FE solutions.

- and a collocation solution with singular functions by Wang(1982).

The material properties are listed in Table 4.1.

The finite difference solution used a uniform grid of points throughout the domain and was not dense enough to obtain reasonable accuracy resulting in σ_z and σ_y negligible everywhere. In Wang's(1982) solution all stresses except τ_{yz} are singular. Using n=30 the present method is in excellent agreement with Wang(1982) except very near the singular point for σ_x and τ_{xy} . Using a special storage technique Wang and Crossman's solution required 18 seconds on a Univac-1108 for 678 degrees of freedom (DOF). The results shown for the present method are for 270 DOF and required 243 seconds on a Digital Vax 8800 machine. For results having accuracy comparable to Wang(1977), 108 DOF and 22 seconds on a Vax 8800 were required.

TABLE 4.1 Material Properties and Dimensions for Problems in the Literature

$$E_{11} = 20.0 \text{ Msi } (137.9 \text{ Gpa})$$

$$\nu_{12} = \nu_{13} = \nu_{23} = .21$$

$$E_{22} = E_{33} = 2.1 \text{ Msi } (14.48 \text{ GPa})$$

$$G_{12} = G_{13} = G_{23} = .85 \text{ Msi } (4.98 \text{ GPa})$$

4.3.2.2 Crossplied Symmetric Laminates

For the $[0/90]_s$ and $[90/0]_s$ laminates the displacement functions are:

$$u = \sum_{i=1,4,8..n} \Bigg[\kappa_{u2} \Big[(k_i \sinh(\varphi_2 (\psi_z)_{\frac{i+1}{2}}\, y) \cos((\psi_z)_{\frac{i+1}{2}} z)$$

$$+ k_{i+1} \sinh(\varphi_2 (\psi_z)_{\frac{i+1}{2}}\, y) \sin((\psi_z)_{\frac{i+1}{2}} z) \Big]$$

$$+ \kappa_{u3} \Big[(k_{i+2} \sinh(\varphi_3 (\psi_z)_{\frac{i+3}{2}}\, y) \cos((\psi_z)_{\frac{i+3}{2}} z)$$

$$+ k_{i+3} \sinh(\varphi_2 (\psi_z)_{\frac{i+3}{2}}\, y) \sin((\psi_z)_{\frac{i+3}{2}} z) \Big]$$

$$v = \sum_{i=1,4,8..n} \Bigg[\kappa_{v2} \Big[(k_i \sinh(\varphi_2 (\psi_z)_{\frac{i+1}{2}}\, y) \cos((\psi_z)_{\frac{i+1}{2}} z)$$

$$+ k_{i+1} \sinh(\varphi_2 (\psi_z)_{\frac{i+1}{2}}\, y) \sin((\psi_z)_{\frac{i+1}{2}} z) \Big]$$

$$+ \kappa_{v3} \Big[(k_{i+2} \sinh(\varphi_3 (\psi_z)_{\frac{i+3}{2}}\, y) \cos((\psi_z)_{\frac{i+3}{2}} z)$$

$$+ k_{i+3} \sinh(\varphi_3 (\psi_z)_{\frac{i+3}{2}}\, y) \sin((\psi_z)_{\frac{i+3}{2}} z) \Big] \Bigg]$$

$$w = \sum_{i=1,4,8..n} \Big[\big[(k_i \cosh(\varphi_1 (\psi_z)_{\frac{i+1}{2}} y) \sin((\psi_z)_{\frac{i+1}{2}} z)$$

$$+ k_{i+1} \cosh(\varphi_1 (\psi_z)_{\frac{i+1}{2}} y) \cos((\psi_z)_{\frac{i+1}{2}} z) \big]$$

$$+ \kappa_2 \big[(k_{i+2} \cosh(\varphi_2 (\psi_z)_{\frac{i+3}{2}} y) \sin((\psi_z)_{\frac{i+3}{2}} z)$$

$$+ k_{i+3} \cosh(\varphi_2 (\psi_z)_{\frac{i+3}{2}} y) \cos((\psi_z)_{\frac{i+3}{2}} z) \big]$$

in the upper layer and

$$u = \sum_{i=1,3,5..n} \big[\kappa_{u2} (k_i \sinh(\varphi_2 (\psi_z)_{\frac{i+1}{2}} y) \cos((\psi_z)_{\frac{i+1}{2}} z)$$

$$+ \kappa_{u3} (k_{i+1} \sinh(\varphi_3 (\psi_z)_{\frac{i+3}{2}} y) \cos((\psi_z)_{\frac{i+3}{2}} z) \big]$$

$$v = \sum_{i=1,3,5..n} \big[\kappa_{v2} (k_i \sinh(\varphi_2 (\psi_z)_{\frac{i+1}{2}} y) \cos((\psi_z)_{\frac{i+1}{2}} z)$$

$$+ \kappa_{v3} (k_{i+1} \sinh(\varphi_3 (\psi_z)_{\frac{i+3}{2}} y) \cos((\psi_z)_{\frac{i+3}{2}} z) \big]$$

$$w = \sum_{i=1,3,5..n} \big[k_i \cosh(\varphi_2 (\psi_z)_{\frac{i+1}{2}} y) \sin((\psi_z)_{\frac{i+1}{2}} z)$$

$$+ k_{i+1} \cosh(\varphi_3 (\psi_z)_{\frac{i+3}{2}} y) \sin((\psi_z)_{\frac{i+3}{2}} z)\Big]$$

in the middle layer.

For crossplied laminates the convergence is demonstrated in Figure 4.3.9. It was found that $f_z \approx 1.9$ yields the lowest residual and a flat minimum. The average residual is low in comparison to the $[\pm 45]_s$ initially and reduces at roughly the same relative rate of O(1/n).

Raju and Crews (1981) presented solutions from 8-noded quadrilateral finite elements in three meshes having about 400, 1400 and 3600 DOF. The densest mesh was graded in a radial pattern towards the singularity. The results showed rapid convergence in this respect along z=h for σ_z in the $[0/90]_s$ case; results of all three meshes were not presented for the $[90/0]_s$ case. In Figure 4.3.10 a) results from the present method are shown and compare well with Raju's densest mesh except near the singularity for n=5. Plotted for y=b the same results show excellent agreement except for n=5. It can be seen in this Figure 4.3.10 b) that the magnitude of σ_z near the singularity depends upon the direction of approach. For $[90/0]_s$ in Figure 4.3.11 again there is excellent agreement with Raju except for n=5 which is fair. For n=30 (180 DOF) the solution required 61 CPU seconds.

Wang and Crossman(1977) presented similar FE results

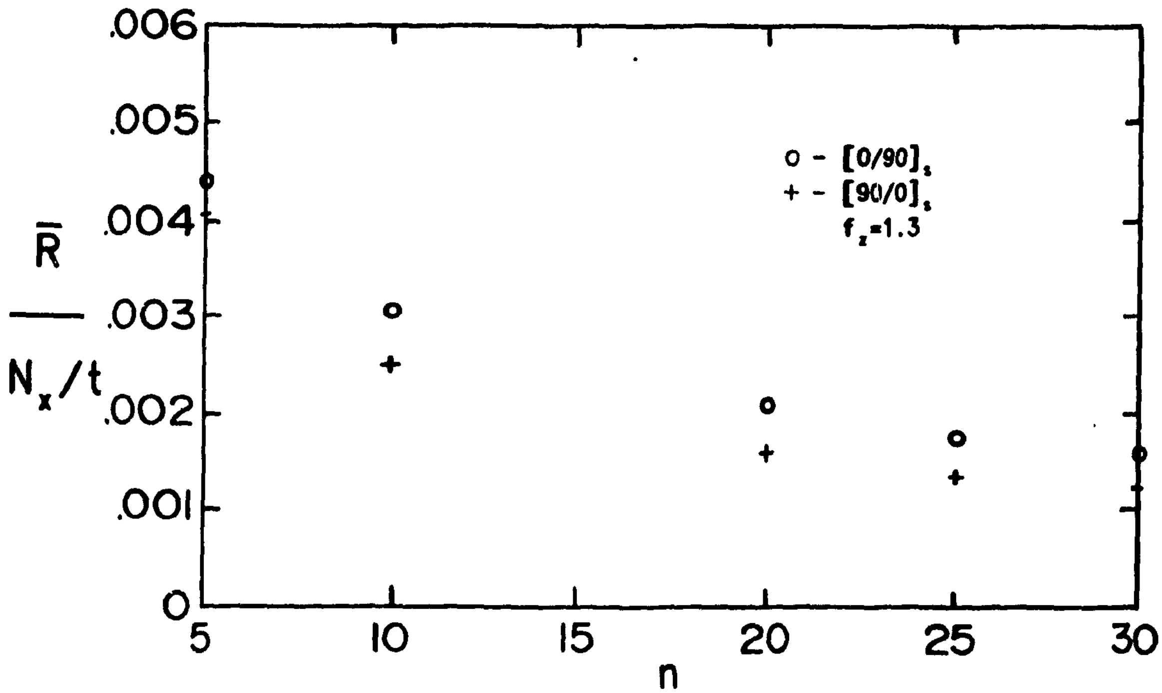

Figure 4.3.9 Average collocation residual for f_z=1.9 vs number of DOF.

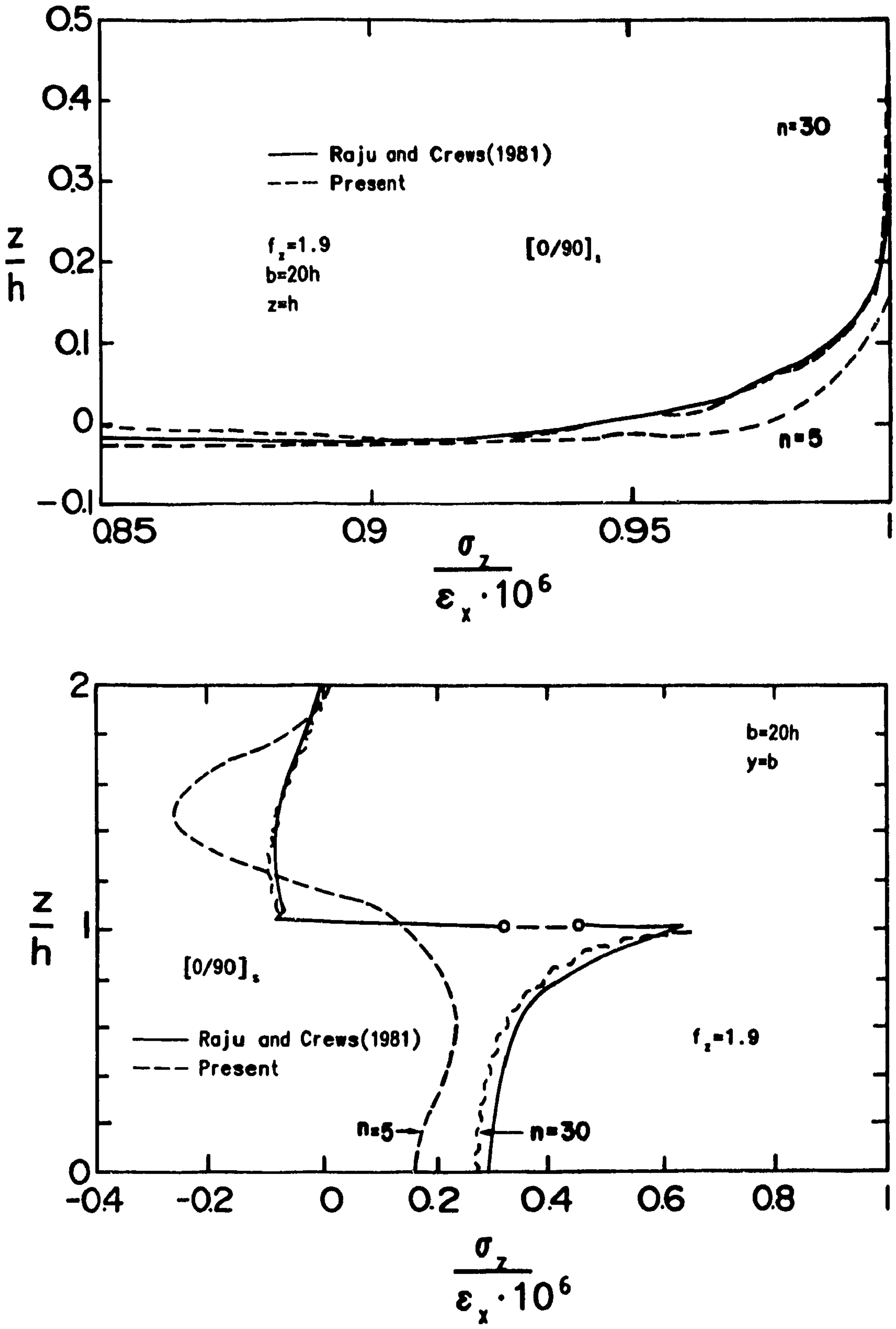

Figure 4.3.10 Interlaminar normal stress compared with FE solution.

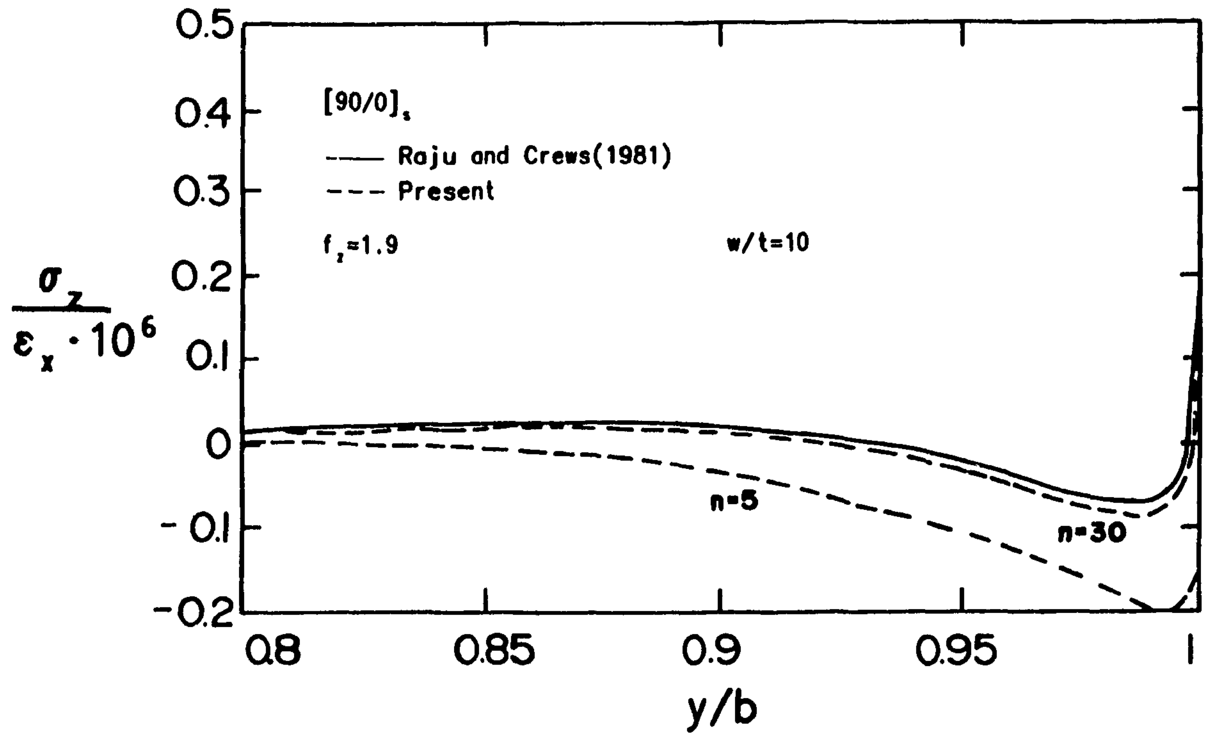

Figure 4.3.11 Interlaminar interface normal stress from present method in comparison with FE solution.

using 3 node triangular elements in a mesh having 678 DOF. For $[90/0]_s$ σ_z in Figure 4.3.12 from the present for n=30 agrees well with Wang except near the singularity where the difference is large; in fact Wang's solution does not show a singularity and σ_z is compressive. The only difference between this laminate and that in Raju(1981) is w/t which should not affect results in the boundary layer. This result demonstrates the extreme refinement that is required for FE accuracy near the singularity.

There is an inherent formulation advantage in using the present method when u=0 as in these problems. The redundant computation of u displacements is easily avoided in the present method resulting in fewer DOF.

4.3.3 Discussion

The method complements other methods in several aspects. Wang's(1982) laminate elasticity collocation solution is believed to be highly accurate and directly yields the order δ of the singularity. As mentioned, it does not include the lnr singularity shown to exist by Zwiers(1982) in the majority of configurations. Wang's method is similar to the present in that it requires collocation. Although Wang's method satifies the free edge, for problems with more than one singularity, collocation points have to be on the same boundaries as in the present. Wang's formulation is more complicated and inflexible for other problems since the boundary conditions across z=h and y=b are formulated exactly for specific geometries. For example, it would require reformulation for a coated edge

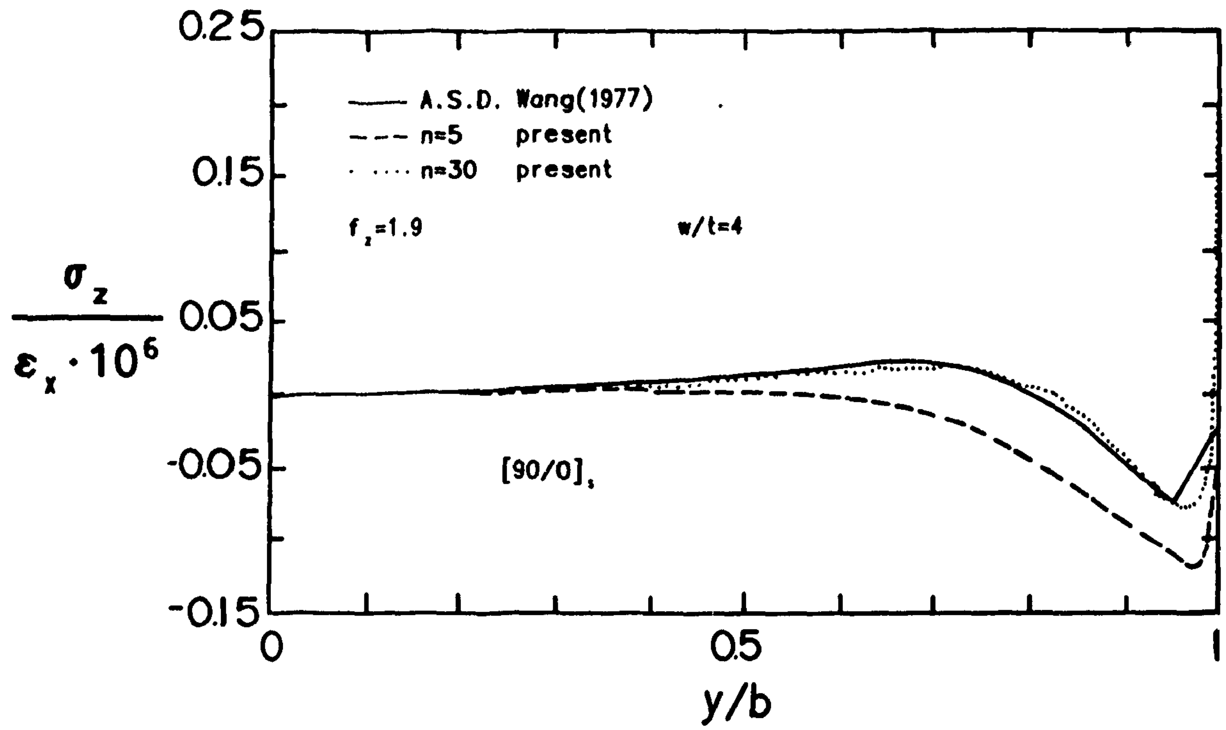

Figure 4.3.12 Interlaminar interface normal stress from present method in comparison with FE solution.

problem. The same applies for singular hybrid elements. In both, the order of the singularity which is approximate for most laminates must be calculated beforehand depending upon the intersection angle and the properties of adjacent plies. This would be cumbersome for modeling multilayer laminates.

Standard finite elements require complex highly refined meshes and show extremely slow *h*-convergence in the vicinity of the singularity. Tong and Pian(1973) showed that *p*-convergence may not be better than *h*-convergence in the vicinity of the singularity. According to Tong and Pian's(1973) estimates the order of convergence will worsen as ω increases, such as for a reentrant corner at the interface. To eliminate complex meshes, optimisation by computer algorithms is a poor approach because of the 'curse of dimension' as more nodal points are included. Further, for multilayer laminates the bandwidth of the final matrix increases. The increase is limited but if complex meshes are used node numbering schemes would be used to minimize the bandwidth.

It has been observed that the FE method requires increasing mesh density towards the singularity. For some three dimensional problems it will not be necessary to have a high element density along the line of the singularity; e.g. for an unloaded hole in the previous chapter. If, for example, there is a line load intersecting the singular line (e.g. a bearing load in a hole) presumably the FE density will have to increase in three dimensions increasing the DOF and complexity of the mesh by an order of magnitude. The rule of discarding two elements adjacent to the singular point will eliminate 32 elements! The FE method will then be computationally inefficient. The present method is potentially better.

The present method offers many problem dependent advantages over other methods.

- The collocation points are simply distributed on the boundary alone which simplifies discretisation over FE and FD procedures.
- The residual provides a meaningful measure of accuracy.
- Relative storage requirements increase only proportional to the number of layers,
- Optimal Ψ may be sought for improved performance.
- trial functions are chosen to satisfy symmetry and only for active DOF easily eliminating redundant DOF.
- extension to three dimensions will potentially amplify the advantages over FE methods.

Foremeost, it is flexible in formulation for material, geometry and loading.

4.3.4. Summary

A simple systematic solution procedure has been developed and examined for performance and compared for common problems with other methods. The results show O(1/n) rate of convergence and lower DOF than the FE results. The present is not a rigourous comparison between methods. The present approach appears to be competitive with other methods depending upon the problem. There also appears to be potential for improvement. On the basis of the demonstrated accuracy and solution checks available the method may be used to study problems other than the test problems.

4.4 Solution of Selected Problems

4.4.1 Description of Problems

In this section the stress state of plates with square free edges is investigated. Selected are problems with straight free edges as in Figure 4.3.3 where CLT stresses are assumed to exist outside the boundary layer. The object is to expand the range of observation, further understanding of edge stresses, and in so doing gain experience and confidence in the mode of solution.

N_x, M_x and M_{xy} make up the loading basis. It should be remembered that CLT bending deformations are for thin plates and do not include the effects of transverse shear. Unless otherwise noted in all the following problems the material properties used are from Table 3.2 for graphite/epoxy. Since the stresses vary across the width actual resultant load would be obtained by integration over the entire domain. However, the CLT value is a good average estimate which improves with increasing width/thickness.

Aspects to study are the effects of ply shuffling and heterogeneous antisymmetric stacking sequences. Ply shuffling (e.g. from $[0_{10}/90_{10}]_S$ to $[0/90]_{10S}$) is attractive to designers because shuffled laminates behave more closely to homogeneous materials having no deformation coupling and effects due to stacking sequence. On the other hand, if coupling is desired heterogeneous laminates must be used. The CLT stresses are affected by changes in stacking sequence; they must equilibrate with interlaminar (IL) stresses in some manner.

The IL stresses equilibrate with the CLT stresses as depicted in Figure 4.4.1. Outside the boundary layer the moment due to σ_y is evaluated; this couple must be balanced by σ_z. Further, equilibrium of τ_{xy} and σ_y directly must be balanced by the net load due to τ_{xz} and τ_{yz} respectively as shown. This analysis does not apply to holes since $\partial\sigma/\partial\theta\neq0$ in general; ignoring this may result in grossly innaccurate

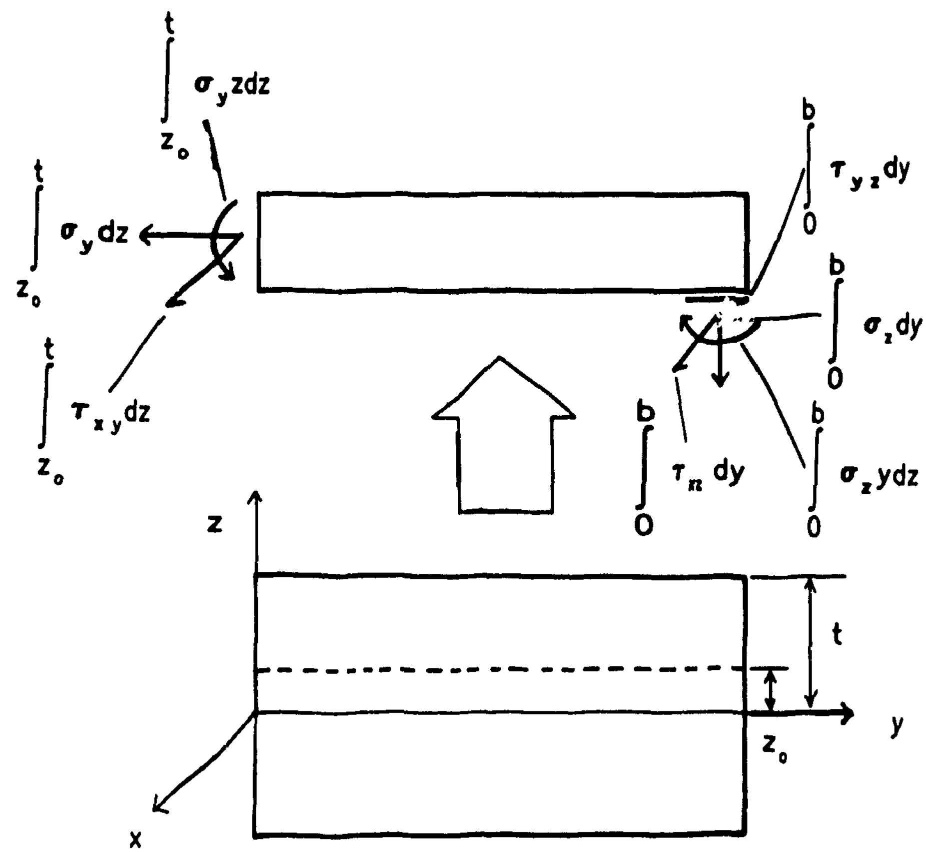

Figure 4.4.1 Stress resultant free body analysis of boundary layer IL and CLT inplane stresses for a section $z_o < z < t$.

and unpredictable estimates.

4.4.2 Crossply Laminates

4.4.2.1 $[90/0]_{ns}$, $[0/90]_{ns}$ Laminates

Shuffling the plies of a symmetric crossply laminate changes the CLT inplane ply stresses without affecting the CLT inplane stiffness matrix $\bar{A}$ (see Appendix A). In response to a load N_x the effect of shuffling plies on the interlaminar edge stresses (at y=b) can be seen in Figure 4.4.2 by comparing $[90/0]_s$ and $[90/0]_{3s}$ laminates. The difference between laminate and sublaminate stresses is barely changed on the edge.

Using the equilibrium analysis it can be seen that the couple on individual plies reduces for repeating sublaminates and the total couple on the midplane is also reduced. If a symmetric laminate in uniform extension has a couple at y=0 on the upper half, then if the symmetric laminate is divided into 2n sublaminates with the same total thickness as in Figure 4.4.3, then the total moment on the upper half becomes 1/n of that in the single sublaminate.

In this case the response to the decreased moment is a decrease in depth of the boundary layer by 1/n (see Figure 4.4.4). The shuffled laminate provides more stress concentration sites which conceivably provides more opportunities to initiate delamination. In both cases σ_z is low (less than 5% of the gross applied stress: $N_x/2t$).

For a bending load M_x the stresses for both crossply stacking sequences $[0/90]_s$ and $[90/0]_s$ are shown in Figure 4.4.5. The displacements w.r.t. z are: u,v - odd and w - even. The two stacking sequences represent highest and lowest bending stiffness for crossply symmetric (i.e. maximum D_{11}). It can be seen in Figure 4.4.5 that the flexible $[90/0]_s$ laminate has the larger interlaminar

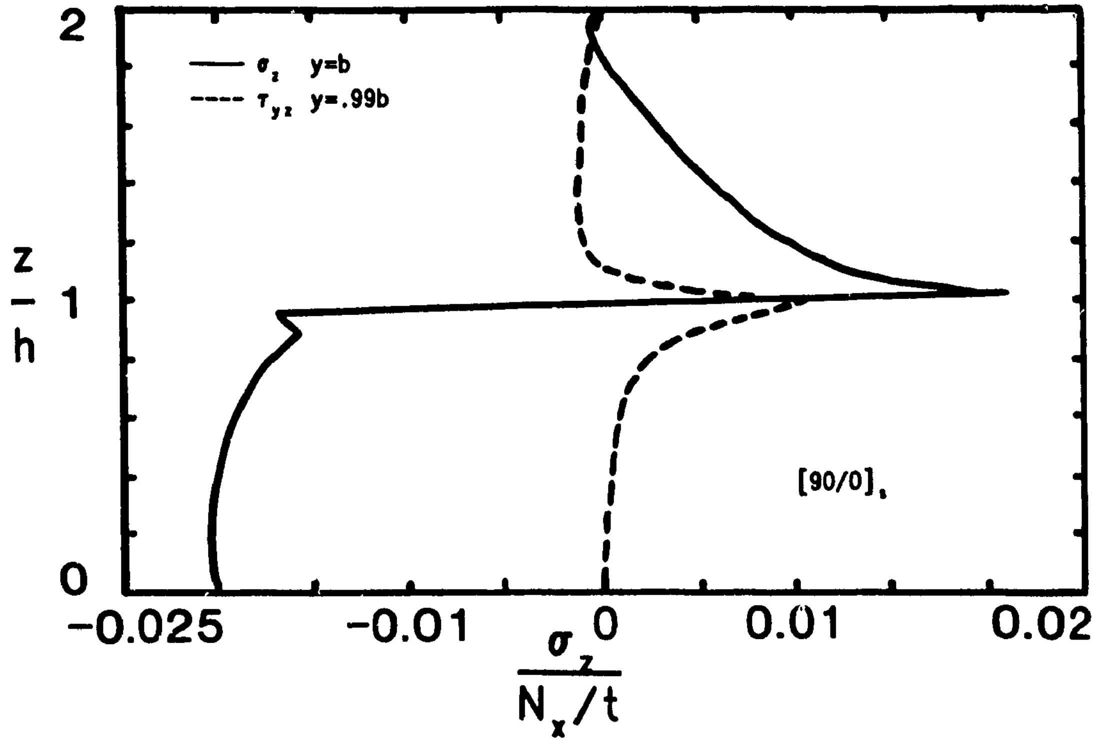

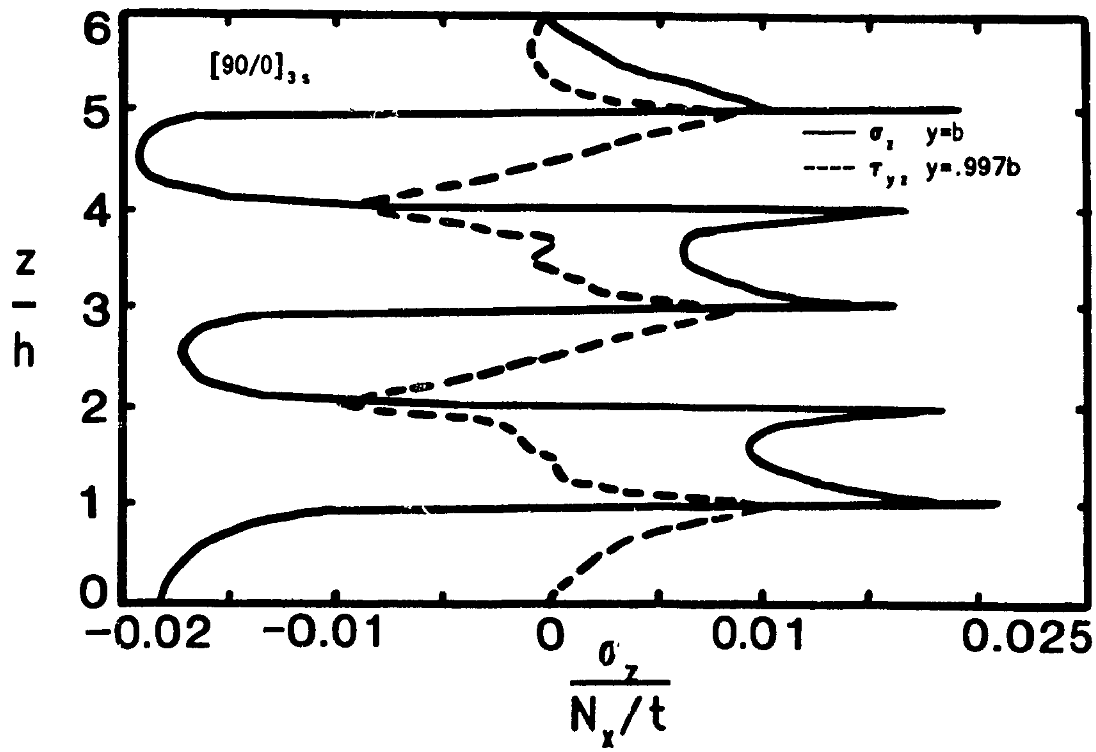

Figure 4.4.2 Il edge stresses for unshuffled and shuffled crossply symmetric laminates with N_x applied. Note: gross applied stress $\sigma_o = N_x/2t$.

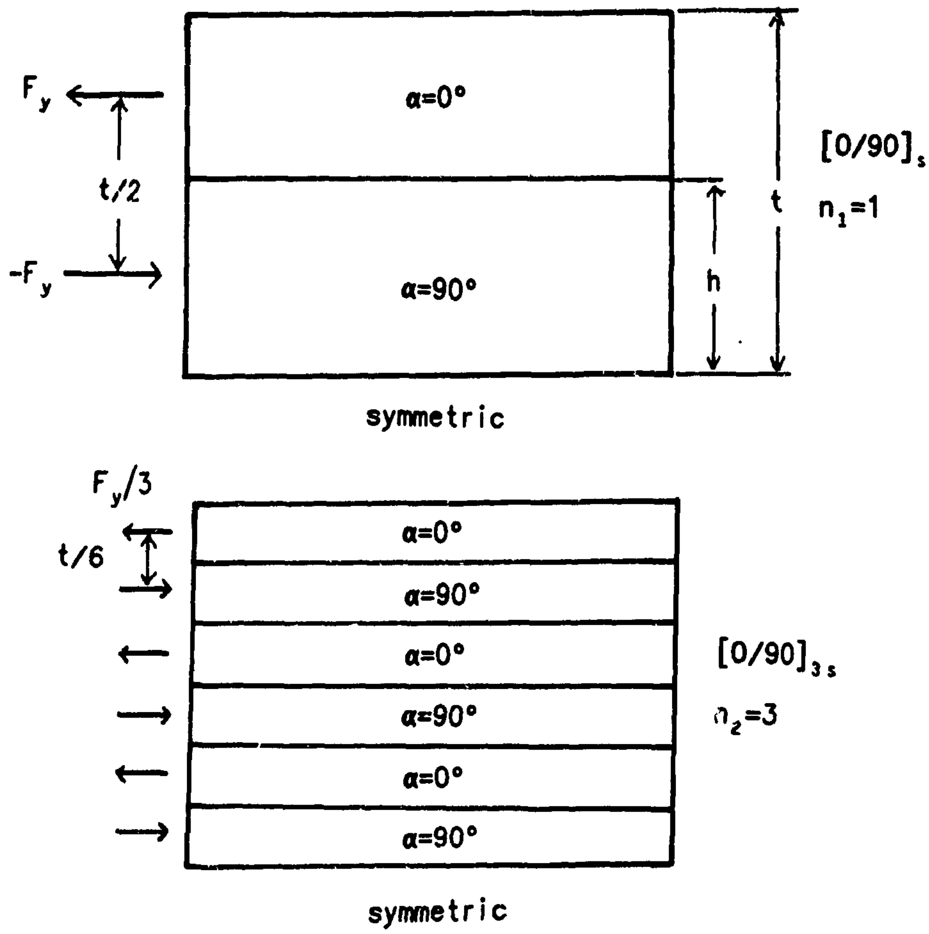

Figure 4.4.3 Shuffling plies from $[0/90]_s$ ($n_1=1$) to $[0/90]_{3s}$ ($n_2=3$) reduces the net couple at y=0 on a ply pair by $(n_1/n_2)^2$ and the couple on the upper half by n_1/n_2 for N_x applied.

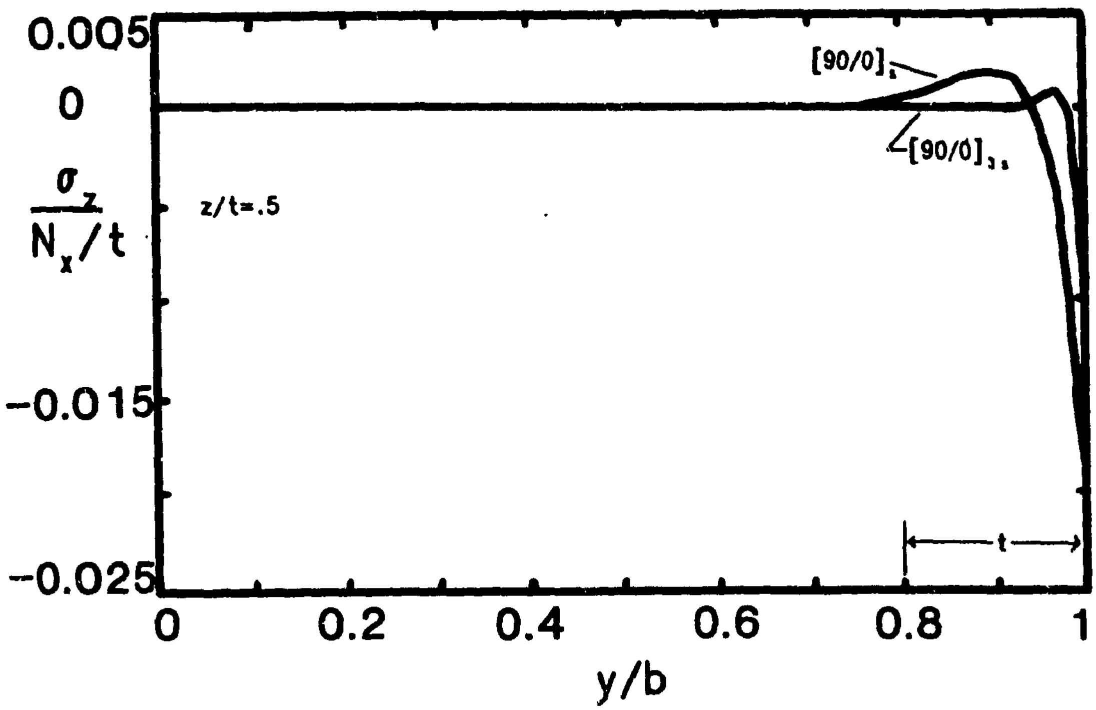

Figure 4.4.4 Il normal stress along the interface at z/t=.5 for unshuffled and shuffled crossply symmetric laminates. Boundary layer depth is reduced by shuffling.

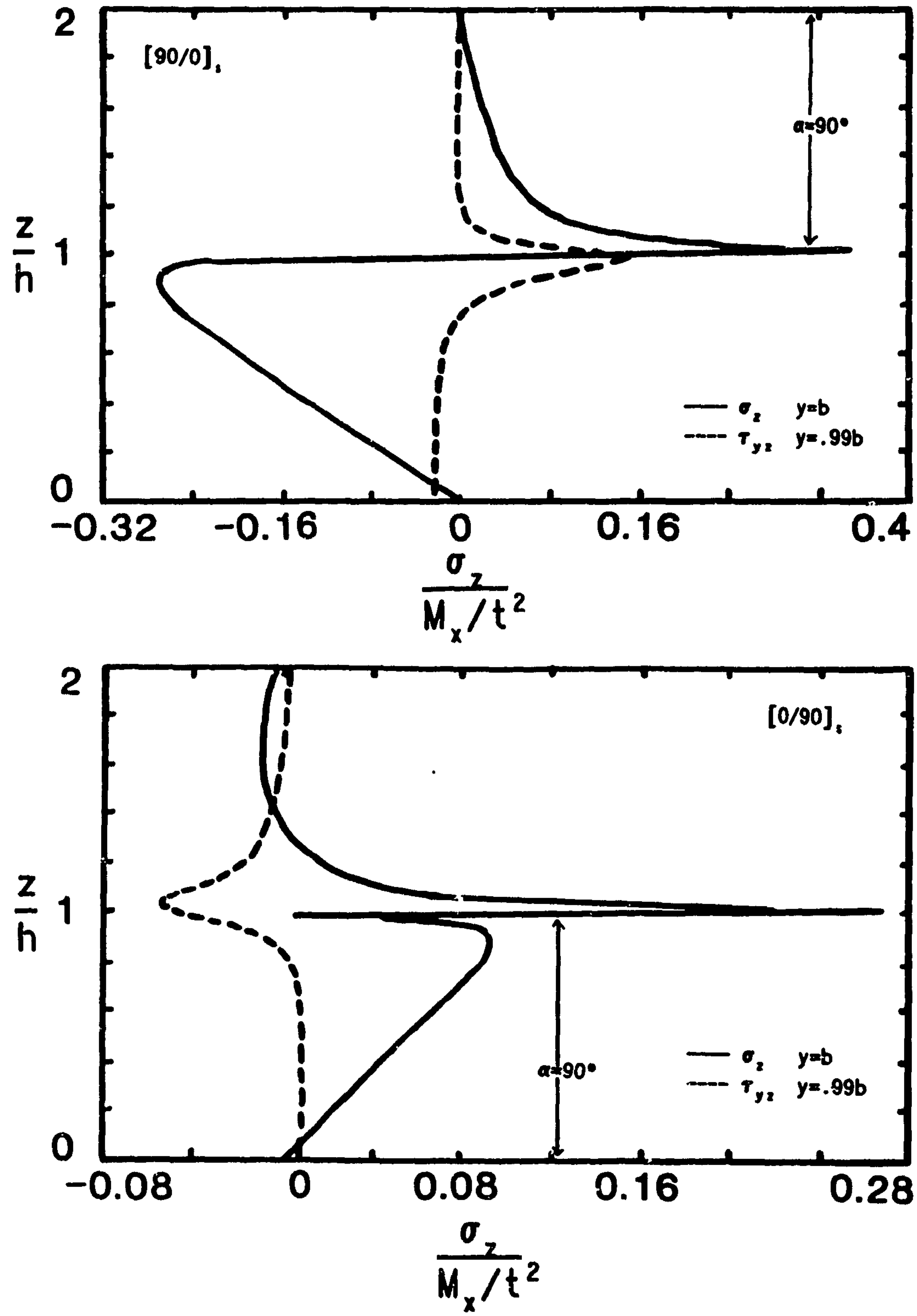

Figure 4.4.5 Il free edge stresses of crossplied symmetric laminates with M_x applied.

stresses. Although not shown, it was noted that the boundary layer in both cases is one laminate thickness, i.e. 2t.

As the layers are shuffled to $[90/0]_{3s}$ and $[0/90]_{3s}$ the bending stiffnesses move closer to those of a quasi-homogeneous lay-up. The edge stresses (see Figures 4.4.6,7) behave in a straightforward manner w.r.t. the CLT stresses. The decreased moments on the interfaces are responded to (see Figure 4.4.8) by a decrease in the BL depth while IL stress maxima increase proportional to the distance from the midplane. Overall, no stacking sequence appears to be clearly superior for reducing the maximum magnitude of the interlaminar stresses relative to load; but, there does appear to be some advantage in having the outer ply oriented 90° to reduce σ_z near the outermost interface. In all cases the boundary layer depth throughout the laminate was about 4h.

4.4.2.2 <u>$[0/90]_n$ and $[90/0]_n$ Laminates</u>

From the class of laminates having equal numbers of alternating 0° and 90° layers of equal thickness the [0/90] exhibits the greatest coupling between bending and extension deformation (i.e. maximum B_{11}). For this problem the displacement functions used in both layers are the same as was used in the upper layer for the symmetric crossplied laminates since there is no symmetry across the midplane. The total thickness of the laminate is denoted by t.

For load N_x the IL stresses are shown in Figure 4.4.9. The interlaminar stresses closely resemble the tension side of the $[90/0]_s$ laminate for M_x applied. This is understandable since their deformation is similar.

For a load M_x the stresses appear in Figure 4.4.10. In this case the IL edge stresses shift from what they are for N_x applied towards compression possibly due to ϵ_x being lower on the midplane than for N_x applied.

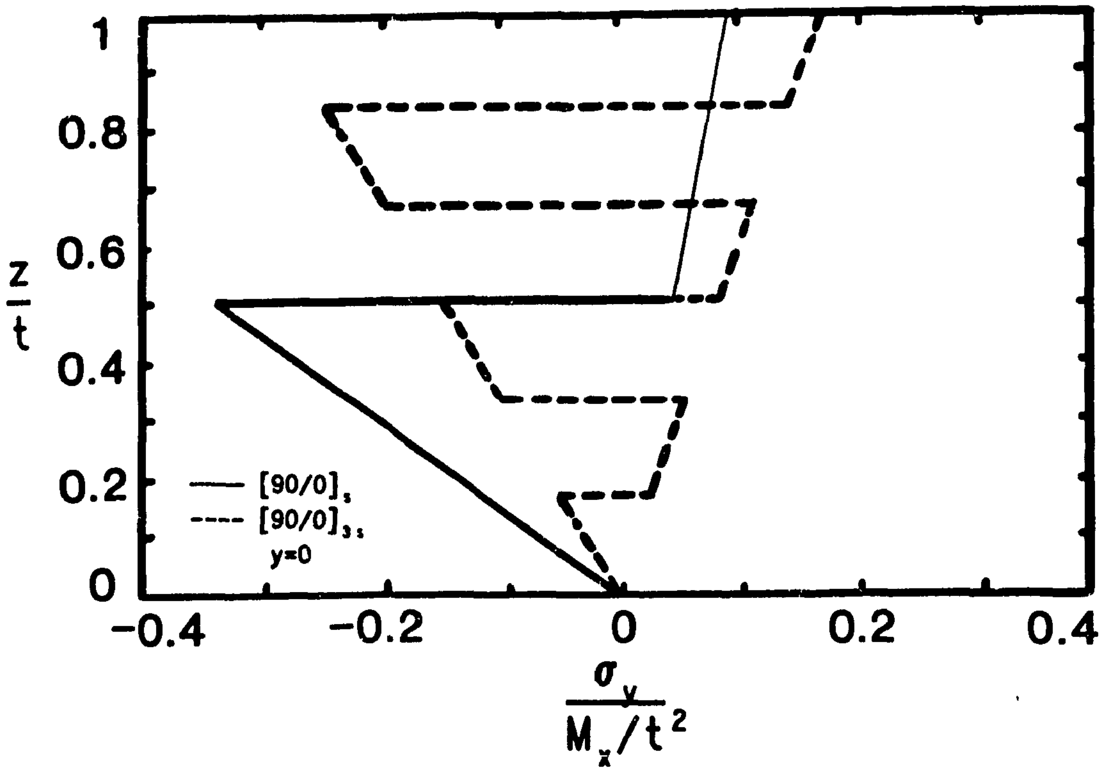

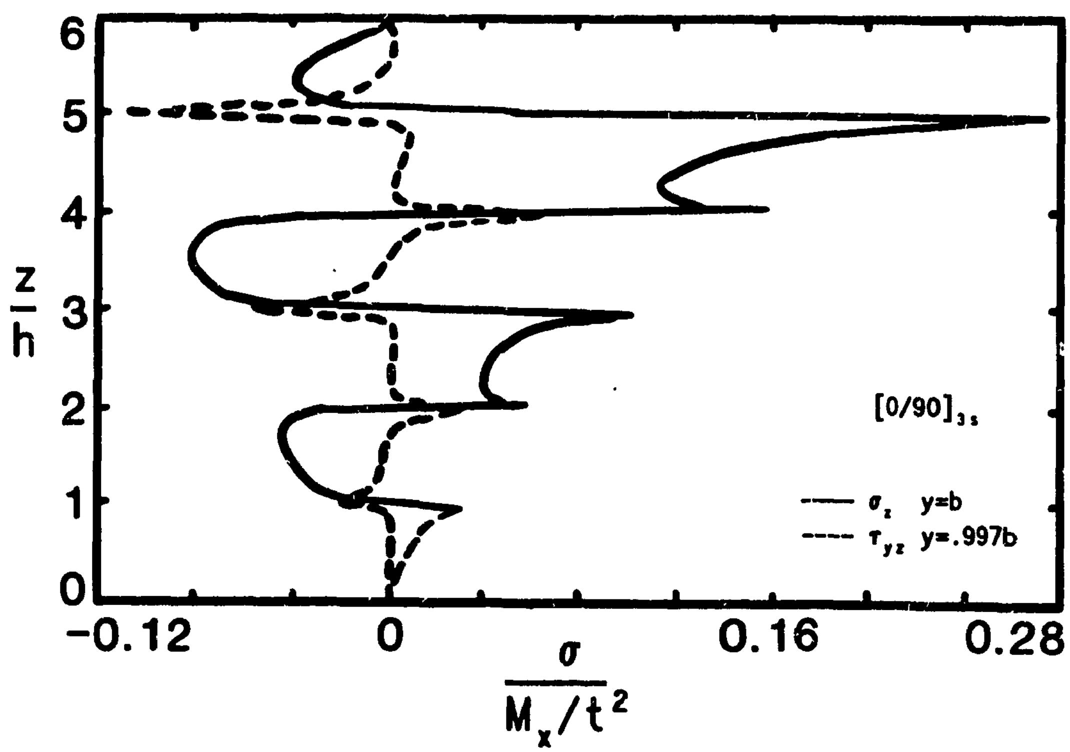

Figure 4.4.6 CLT inplane stresses (top) at y=0 for shuffled and unshuffled crossplied symmetric laminates and (lower) Il free edge stresses for shuffled laminate.

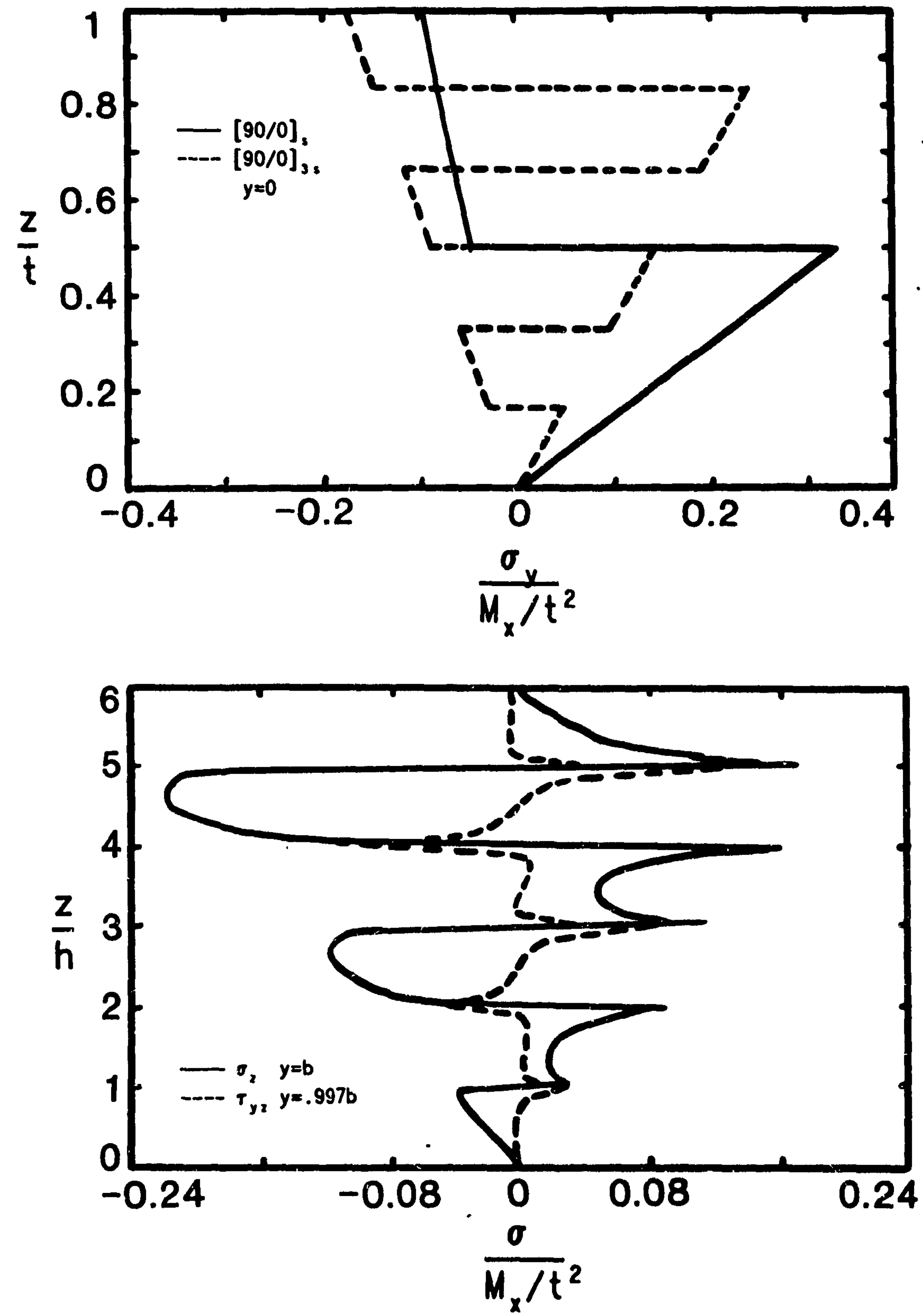

Figure 4.4.7 CLT inplane stresses (top) at y=0 for shuffled and unshuffled crossplied symmetric laminates and (lower) I1 free edge stresses for shuffled laminate.

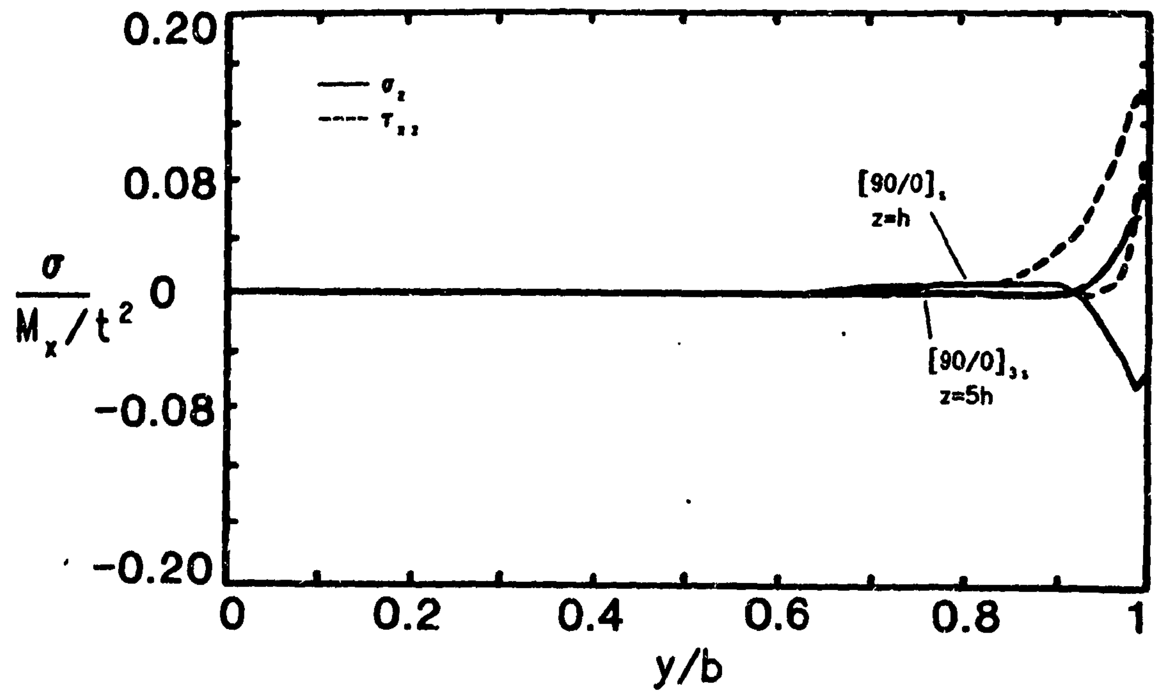

Figure 4.4.8 Il stresses along interfaces of shuffled and unshuffled crossplied symmetric laminates for M_x applied.

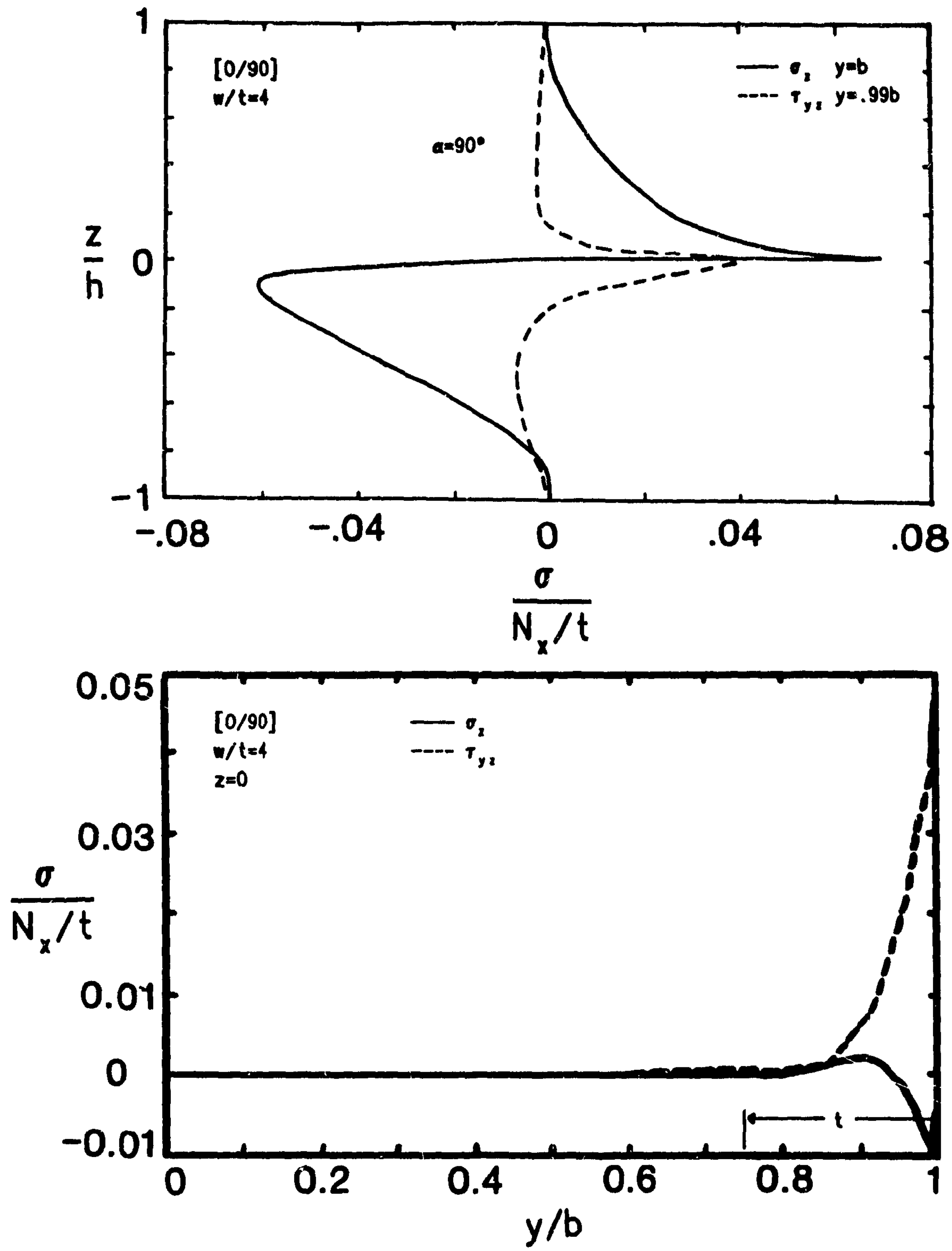

Figure 4.4.9 I1 free edge stresses (top) and interface I1 stresses (lower) of a crossplied asymmetric laminate with N_x applied

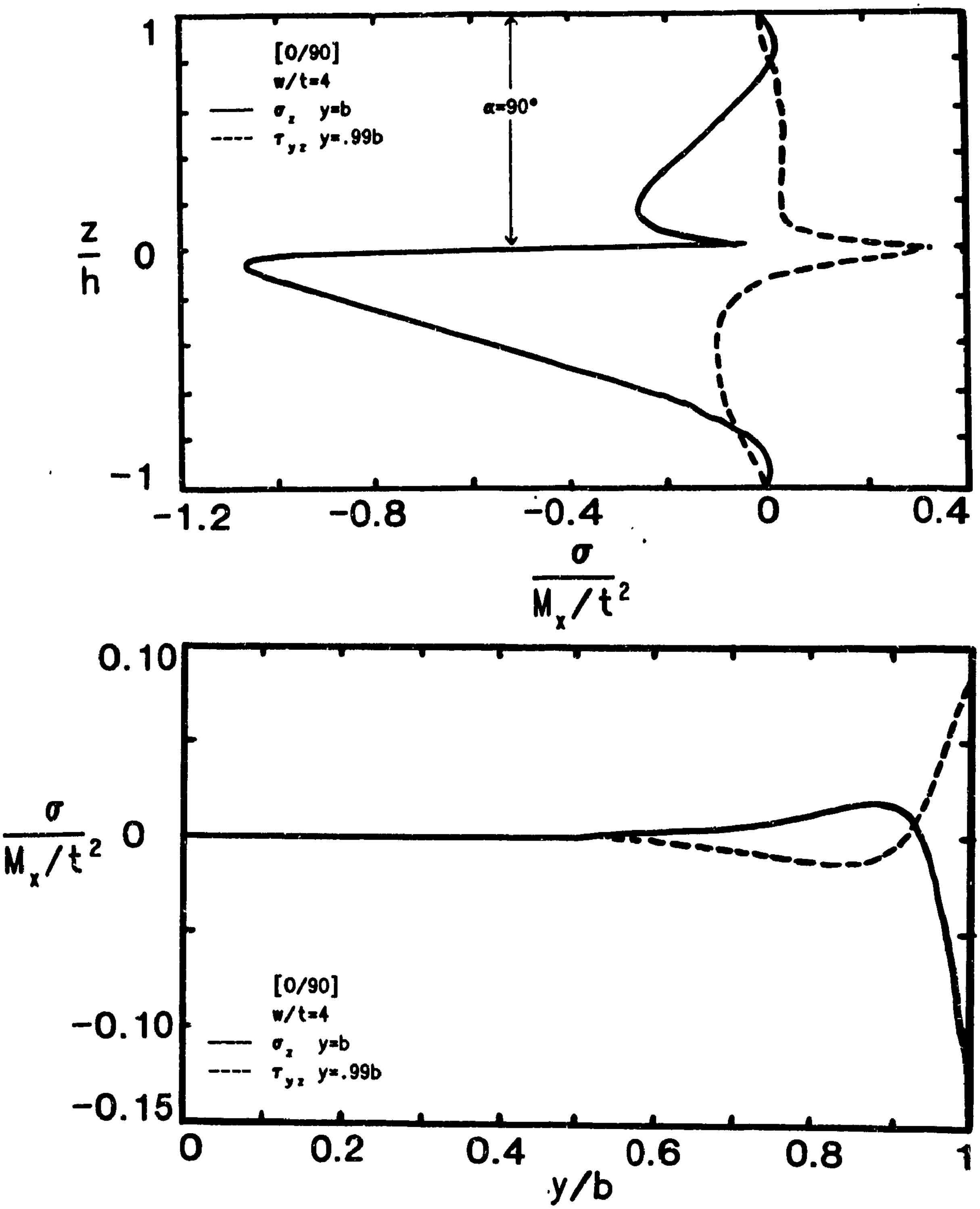

Figure 4.4.10 I1 free edge stresses (top) and interface I1 stresses (lower) for crossplied asymmetric laminate with M_x applied. BL depth is twice the laminate's thickness.

4.4.2.3 Summary

Overall, crossply laminates exhibit weak interlaminar stresses at the interface of less than 10% of the gross average stress. In bending and extension, shuffling the plies alters bending stiffness and reduces the depth of the boundary layer proportional to the decrease in ply thickness. The IL edge stress peaks increase in magnitude roughly proportional to the distance from the midplane.

4.4.3 Angle-Ply Laminates

4.4.3.1 $[\pm\theta]_{ns}$ Laminates

For this laminate in pure bending ($M_x \neq 0$) the displacements w.r.t. z are: u,v - odd, w - even so the trial functions are chosen accordingly in the middle layer. The configuration is as in Figure 4.4.3 with different α's. Shown in Figure 4.4.11 are the results for a $[\pm 45]_s$. As for pure tension σ_z is compressive on the tension side so indicating that delamination would initiate on the compression side. In this case it would be interesting to determine if the delamination would propagate causing buckling of loose plies.

As the configuration is changed to $[\pm 45]_{3s}$ the coupling terms B_{16} and B_{26} decrease in magnitude. In Figure 4.4.11(bottom) it shows that the singular interlaminar stresses on the edge are affected by bending in a straightforward manner. The distributions on the sublaminate edges show IL stress magnitude increasing roughly in proportion to the distance from the midplane. The maximum interface averages are roughly the same in both cases. Shuffling causes a change in the distribution of σ_z along the interface at z/t=.5: there are two zero crossings in the boundary layer. The depth of the boundary layer (see Figure 4.4.12) remains at roughly 4h in both cases decreasing absolutely due to shuffling.

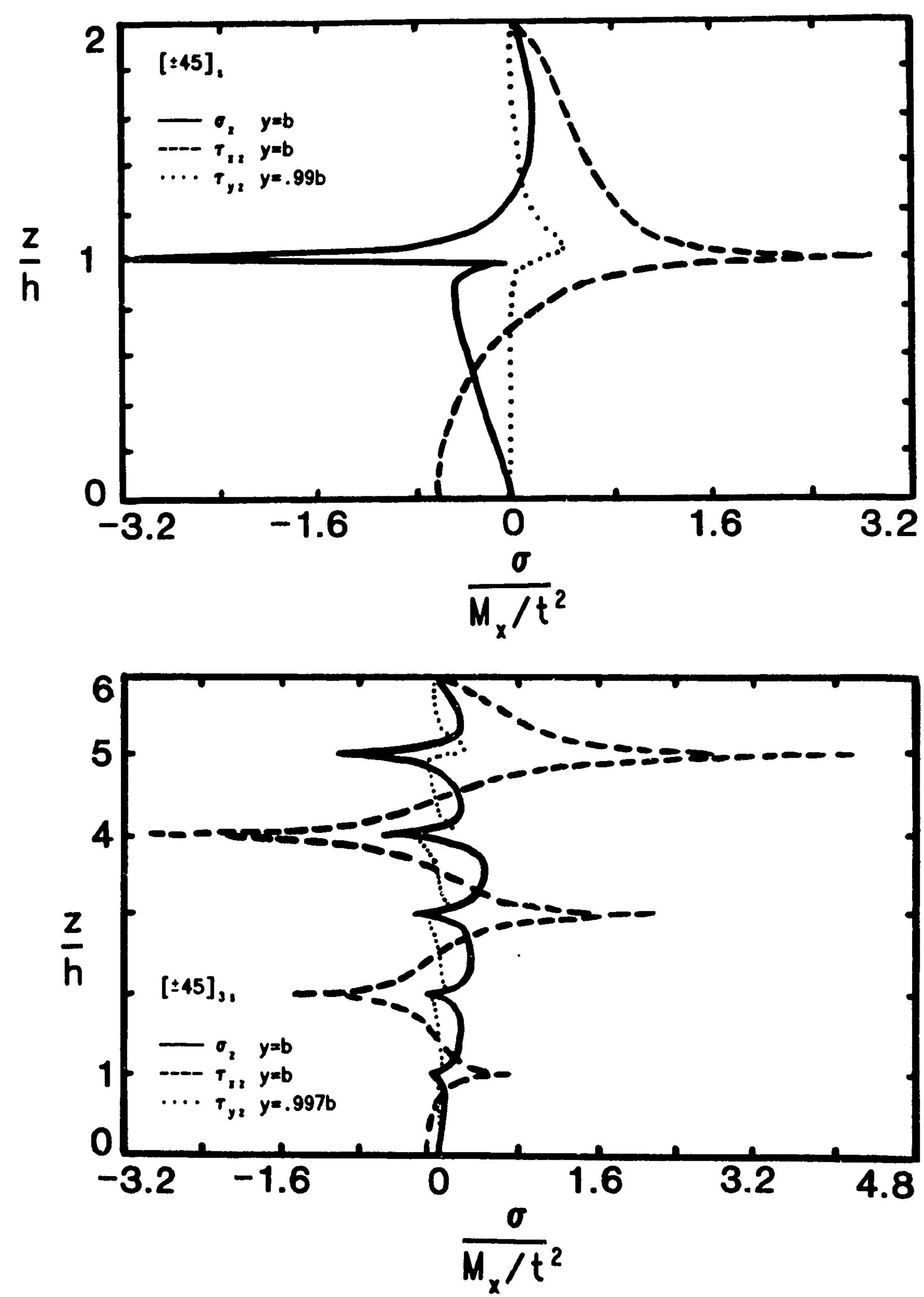

Figure 4.4.11 Il free edge stresses for unshuffled (top) and shuffled (lower) symmetric angle-ply for M_x applied.

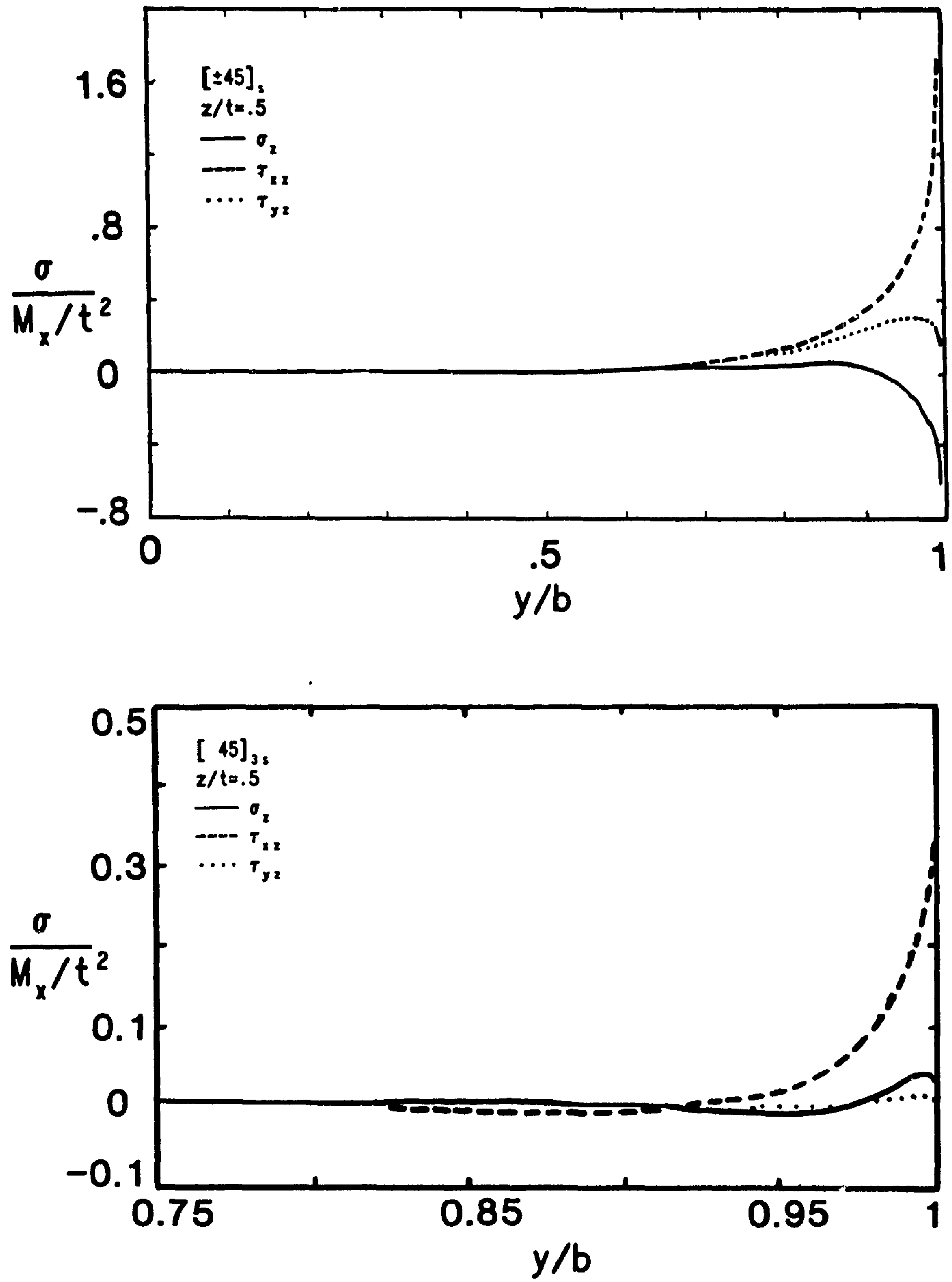

Figure 4.4.12 Il stresses along interface at z/t=.5 for unshuffled (top) and shuffled (lower) angle-plied laminate with M_x applied.

Angle-ply laminates yield a high D_{66} stiffness and so are often used to resist torsion or twisting loads. Symmetric laminates also have a fully populated D matrix and so exhibit bending coupling in response to pure twist loads; the coupling diminishes as the plies are shuffled. The CLT stresses for a $[\pm 45]_s$ with $M_{xy} \neq 0$ are shown in Figure 4.4.13. In this problem, τ_{xz} reapproaches zero near the singularity and is maximum near the midplane.

As the plies are shuffled to $[\pm 45]_{3s}$ so that D_{16} and D_{26} are reduced to one third of their value for $[\pm 45]_s$; the CLT stresses become as shown in Figure 4.4.14. The distribution of τ_{xz} is similar to the unshuffled laminate except that since τ_{xy} at y=0 redistributes slightly reducing the value of $\int_0^t \tau_{xy} dz$ the extremum of τ_{xz} at the midplane is lower in magnitude. At z/t=.5 however, the difference in $\int_{z=.5t}^{z=t} \tau_{xy} dz$ is negligible so the BL depth and distribution of τ_{xz} on the interface do not change (see Figure 4.4.15). Shuffling redistributes σ_y at y=0 so that the maximum of σ_z *and* the BL depth are reduced.

4.4.3.2 $[\pm\theta]_n$ Laminates

Antisymmetric angle-ply laminates have coupling between extension-twist and bending-inplane shear for a finite number of plies i.e. $B_{16}, B_{26} \neq 0$.

The displacements are: u,w - even w - odd. For this problem the solution functions for both layers are the same as for the upper layer in the $[\pm\theta]_s$ problem. It is possible to model only the top layer imposing $u_z, w_z, v, v_{zz}=0$ on z=0; but the entire laminate was modeled so t denotes the laminate thickness. In Figure 4.4.16 for tensile N_x applied

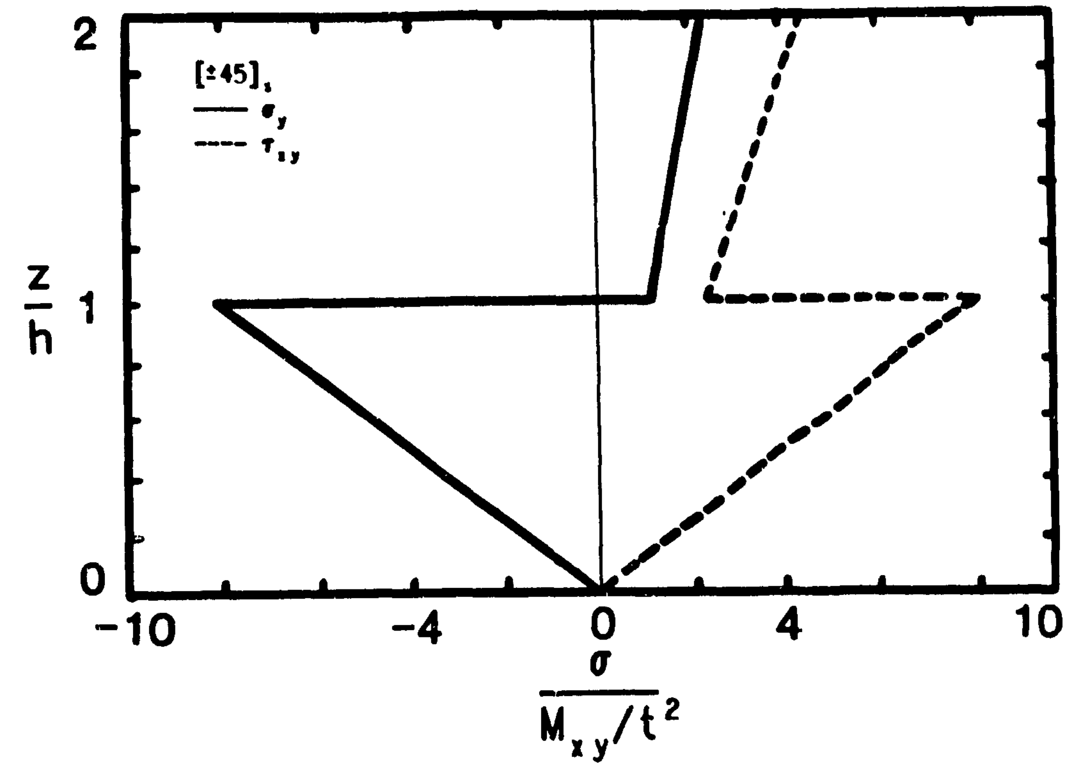

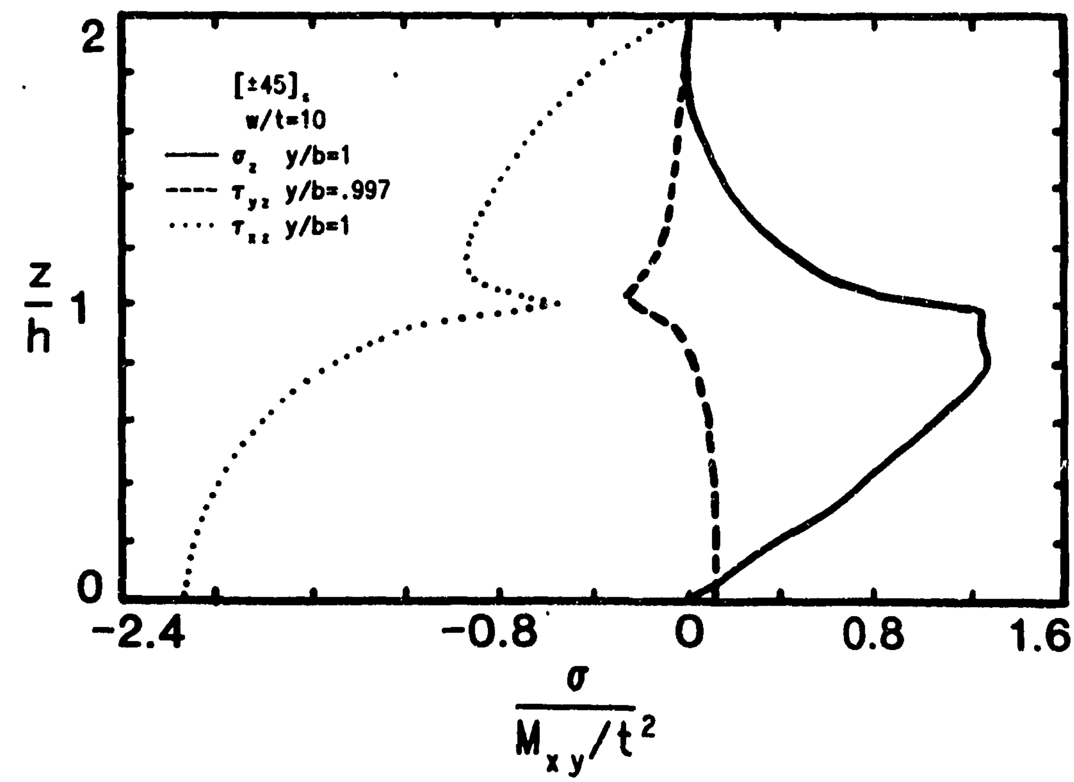

Figure 4.4.13 CLT inplane stresses at y=0 (top) and I1 free edge stresses (lower) for angle-plied symmetric laminate with M_{xy} applied.

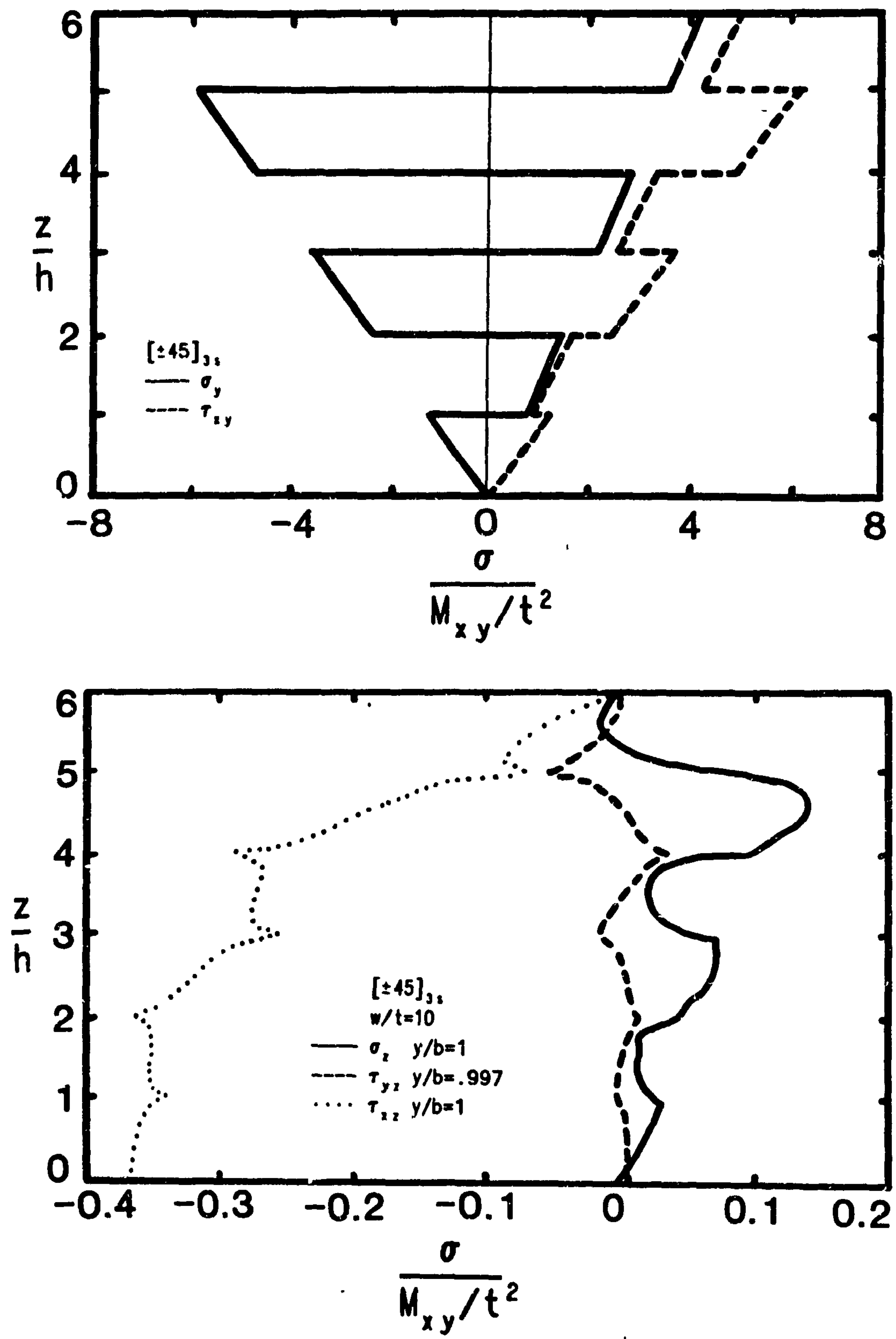

Figure 4.4.14 CLT inplane stresses (top) and resulting I1 free edge stresses (lower) for shuffled angle-plied symmetric laminate with M_{xy} applied.

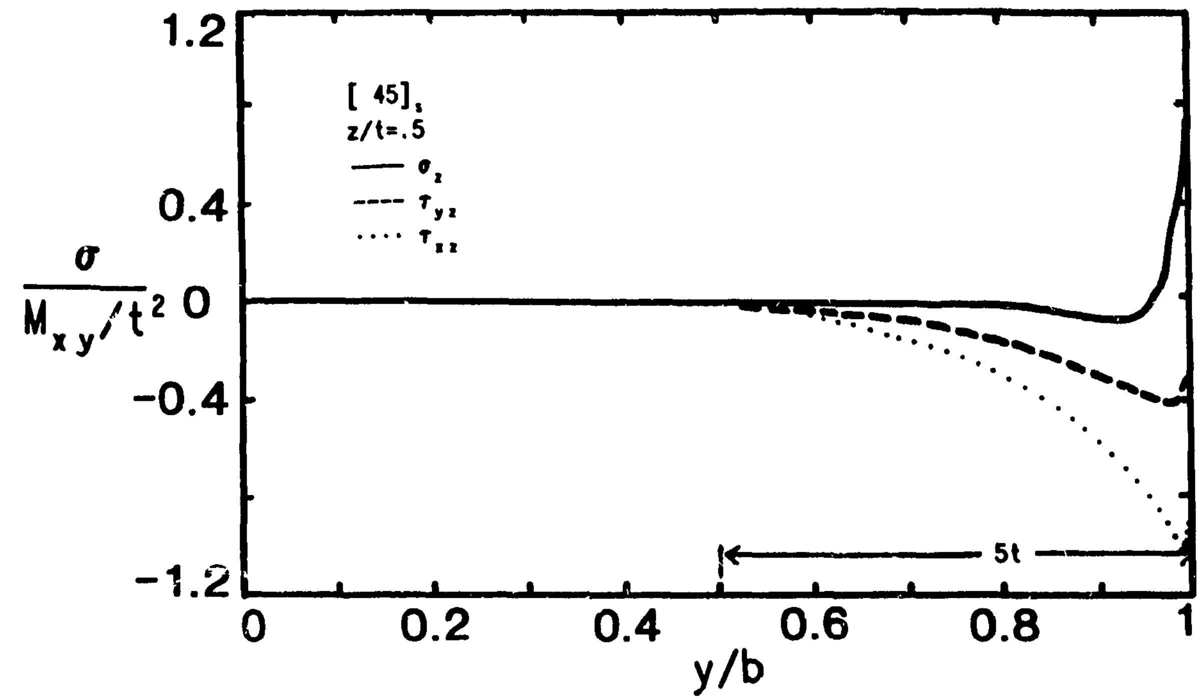

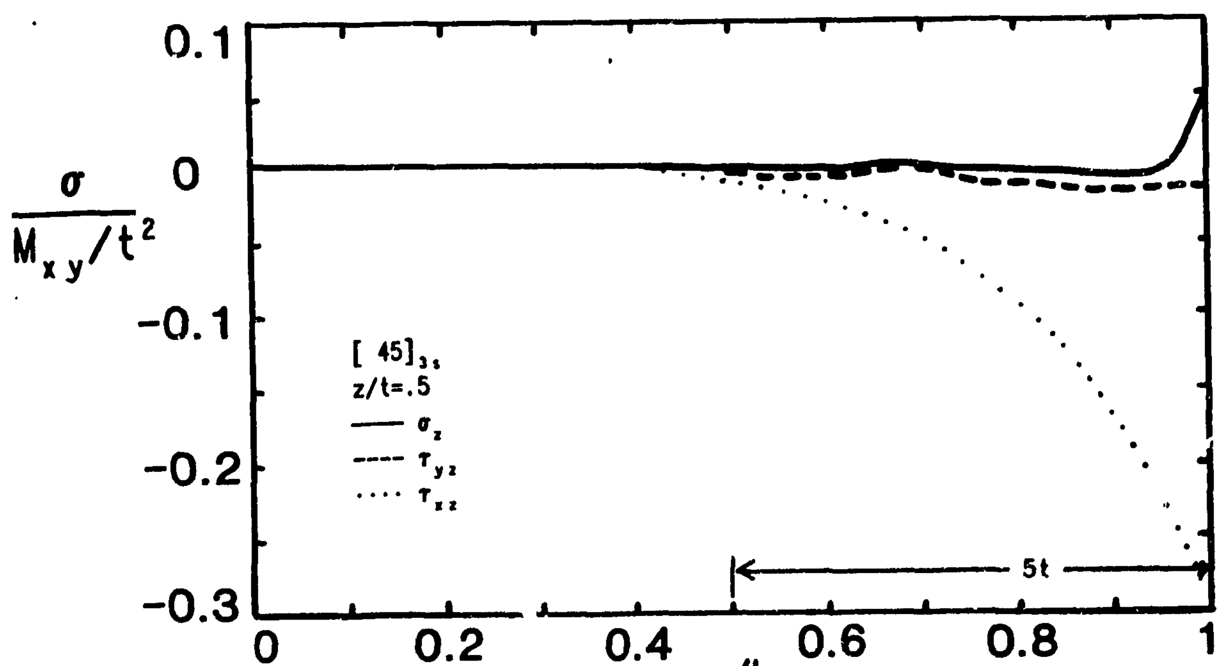

Figure 4.4.15 Il stresses along z/t=.5 interfaces of unshuffled (top) and shuffled (lower) angle-plied symmetric laminates for M_{xy} applied.

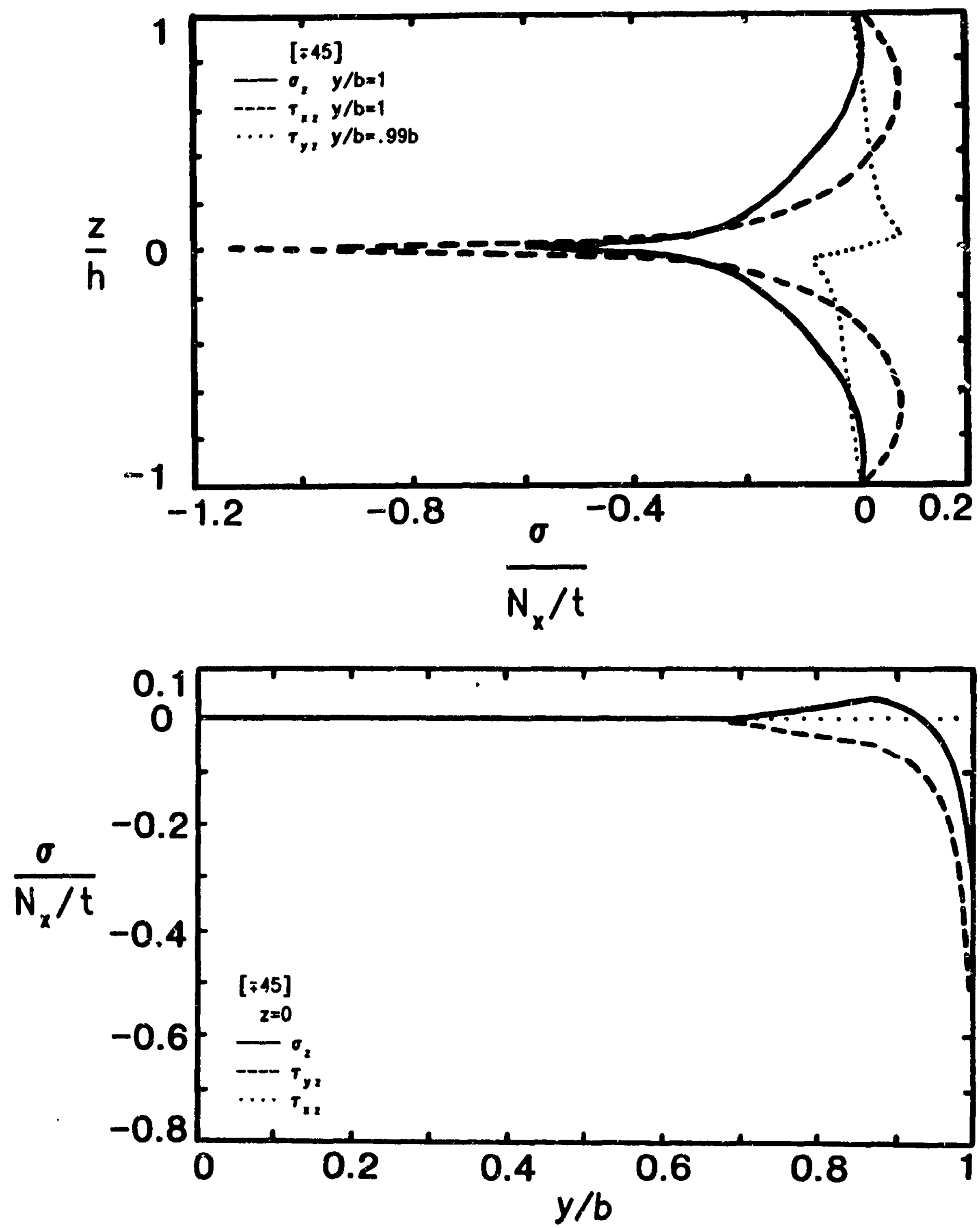

Figure 4.4.16 I1 free edge stresses (top) and interface I1 stresses (lower) of antisymmetric angle-plied laminate for N_x applied.

τ_{xz} is strongest, σ_z is compressive on the free edge, and τ_{yz} is small as in the symmetric laminate.

For M_x applied the results are shown in Figures 4.4.17,18. In this case the displacements across z=0 are: u,v - even and w - odd. Interestingly, in this case near the singularity τ_{yz} dominates while all the other stresses inclusing the inplane stresses vanish. The other interlaminar stresses increase only in the region away from the singularity. For laminates of the same size the maximums of σ_z and τ_{xz} for the antisymmetric dimensions are less than one quarter of the singular stresses of symmetric laminate.

For M_{xy} applied the displacements w.r.t. z are: u,v - odd and w - even. The B_{16} term couples twist to extension in this laminate. In Figure 4.4.19 it can be seen that the IL tensile normal stress at the midplane/interface is very large and dependent upon the sign of M_{xy}. This configuration appears to be very susceptible to delamination for a twisting load which causes a negative ϵ_x by coupling.

4.4.3.3 Summary

The IL edge stresses increase in proportion to the distance from the midplane in shuffled laminates. The BL depth is strongly related to the CLT forces and moment at y=0. Antisymmetric [±45] show IL stresses similar to the symmetric case for N_x applied, much lower for bending, but are worse for twist.

4.4.4 Quasi-Isotropic Laminates

As a replacement for conventional materials this class of laminates is heavily used. The angles in the laminate progress in a π/n increment e.g. $[0/60/-60....]_s$, $[0/45/90/-45....]_s$, $[0/36/72/-18/-54...]_s$.. $([0/90...]_s$ is orthotropic). Stacking sequence does not influence inplane

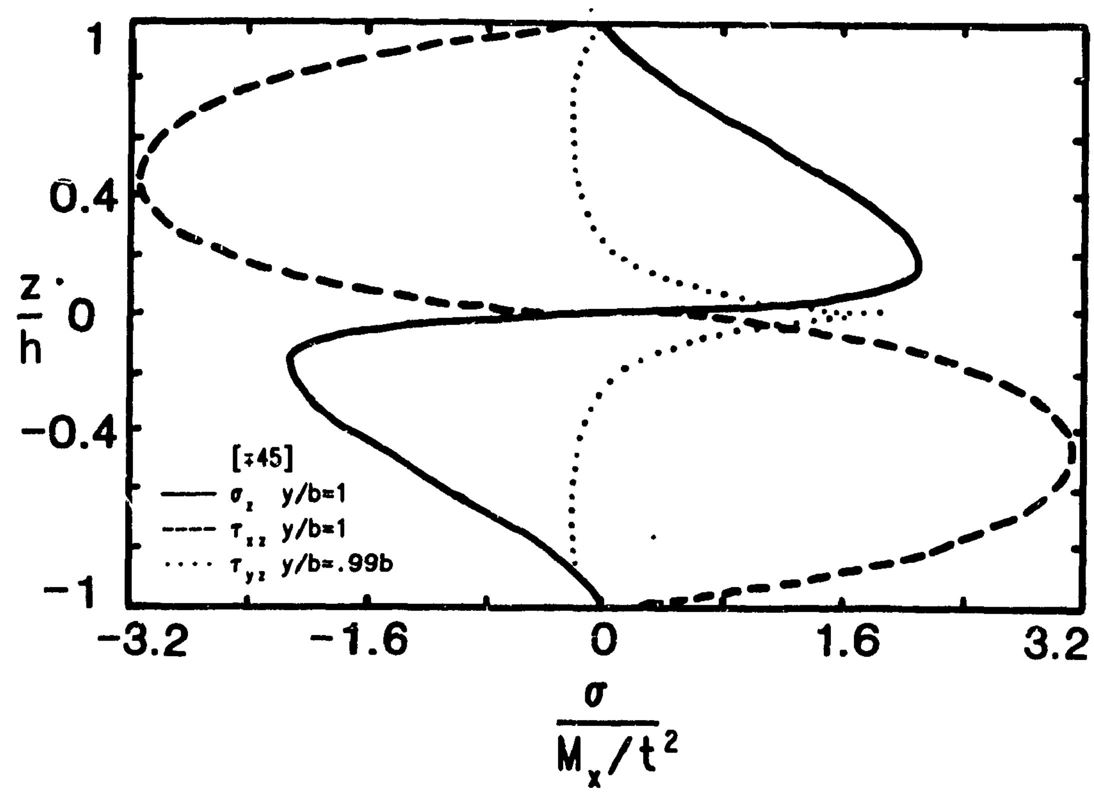

Figure 4.4.17 I1 free edge stresses for antisymmetric angle-plied with M_x applied.

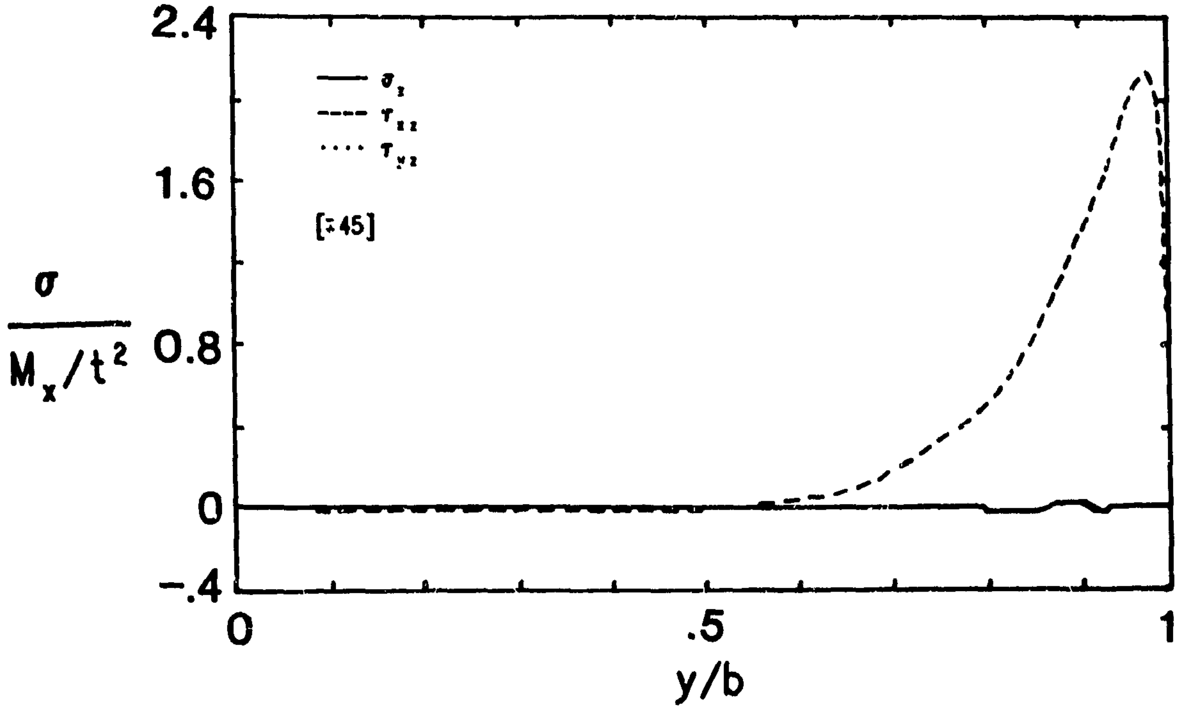

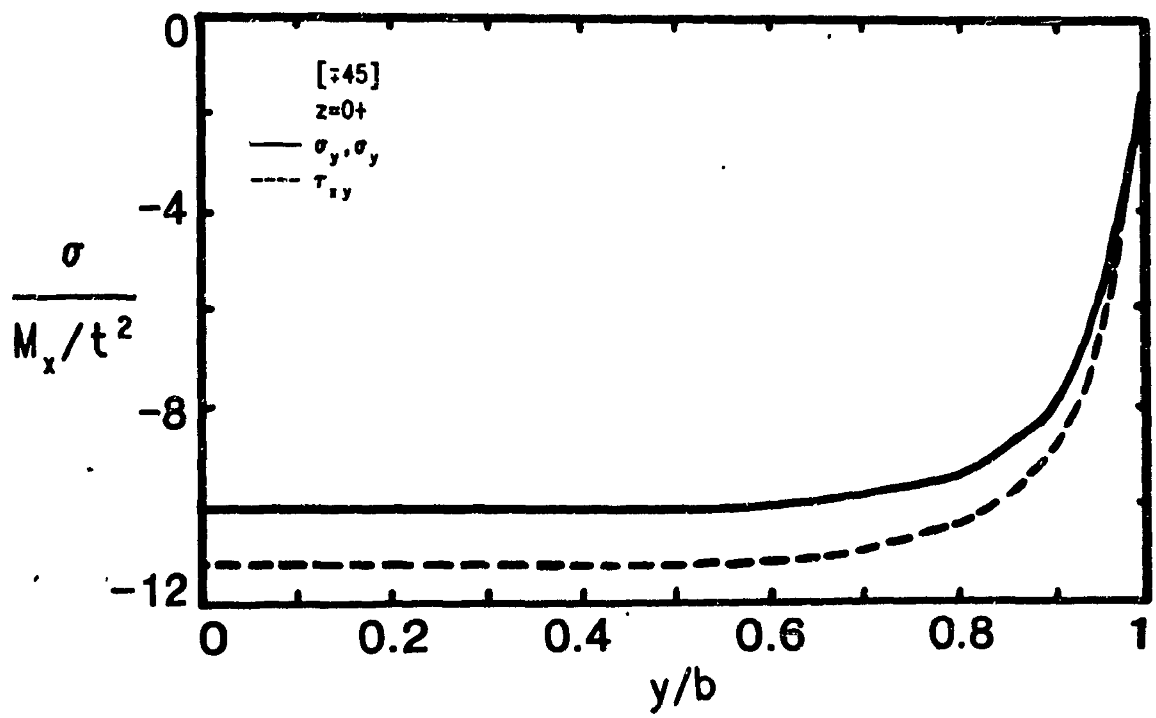

Figure 4.4.18 Il free edge stresses (top) and inplane stresses (lower) of antisymmetric angle-plied laminate for M_x applied.

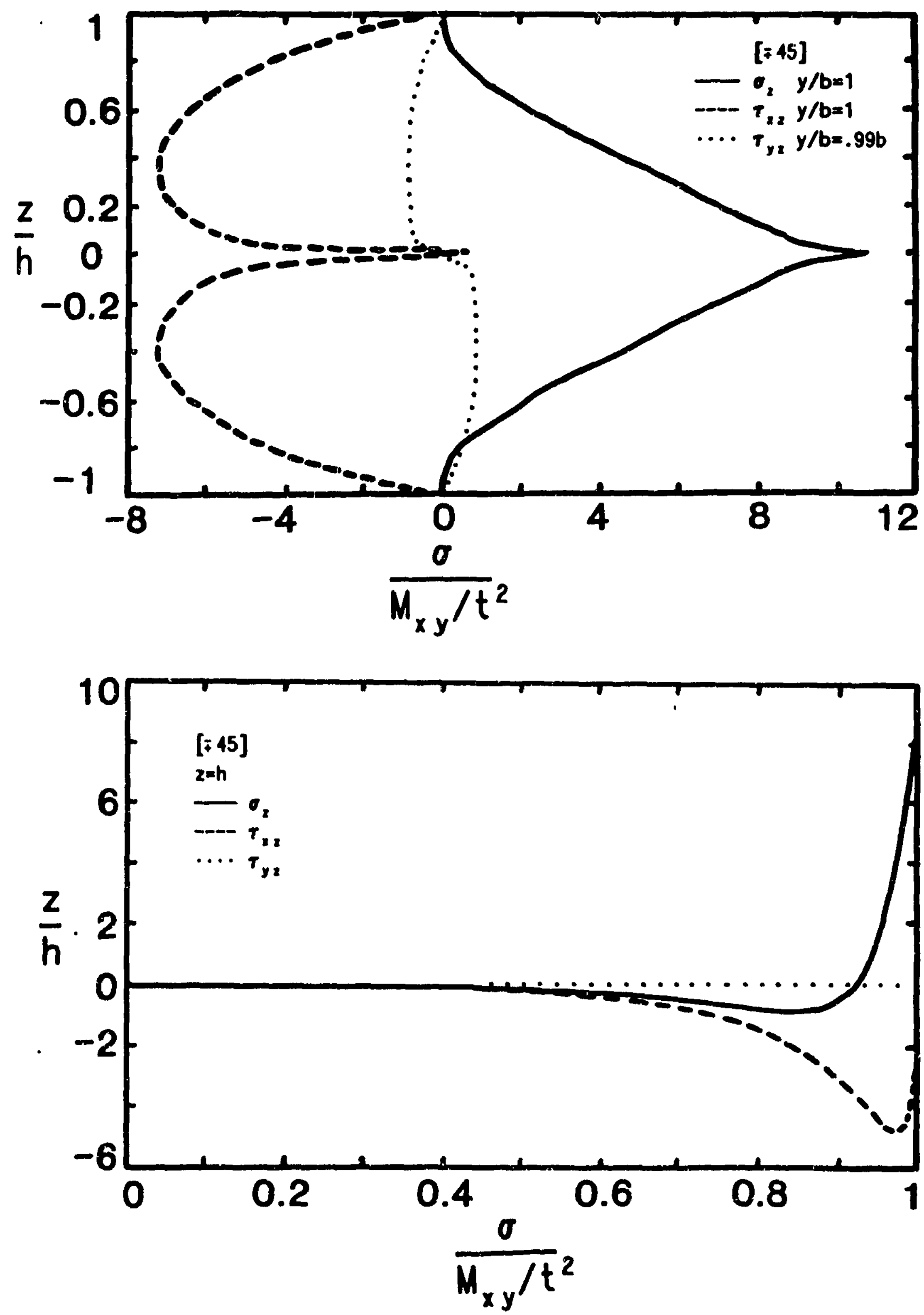

Figure 4.4.19 Il free edge stresses (top) and Il interface stresses (lower) of antisymmetric angle-plied laminate for M_{xy} applied.

stiffness or CLT ply stresses for N_x applied but does affect the moments at y=0. These laminates have also received much attention for uniform extension of symmetric laminates using FE solutions(e.g. see Whitcomb(1984)). In this brief subsection the effects of stacking sequence for N_x applied are examined.

$\pi/3$ laminates exhibit negligible free edge stresses in uniform extension so $\pi/4$ are investigated. In order to minimize the midplane moment the plies can be stacked in a "spiral" sequence i.e. $[0/+45/90/-45]_s$ (but not $[45/90/-45/0]_s$) which minimizes the pure couple due to σ_y. By this measure the worst possible case would be $[\pm 45/0/90]_s$ for a $\pi/4$. These and various other cases are shown in Figure 4.4.20 with the inplane couples and the free edge stresses are shown in Figure 4.4.21.

The σ_y couple influences the midplane edge value of σ_z predictably. In Figure 4.4.22 the midplane distributions of σ_z show boundary layer depth and maximum stress predicted by the magnitude and sign of the couple. Unless the 90^o ply is placed on the upper surface, the edge magnitude is not greatly influence by stacking sequence. The BL depth changes in response to changing moment.

There are two basic stacking sequences distinguished by whether the 45^o layers are adjacent. When they are adjacent τ_{yz} is significant while it is negligible when they are not grouped. Also, τ_{xz} is stronger at ± 45 interfaces than at 90/45 or 90/-45 interfaces even though the net shear force is the same.

The couple at y=0 predicts the sign of σ_z at y=b and it's magnitude is a balance of the magnitude of σ_z and the depth of the boundary layer. The maximum IL edge stress depends upon the orientation of the adjacent layers. It is better to consider the possible interaction between adjacent plies due to poisson and shear coefficient mismatch (e.g. $\eta_{16}=\varepsilon_6/\varepsilon_1$ for $N_x \neq 0$) than the couple at y=0 to estimate IL

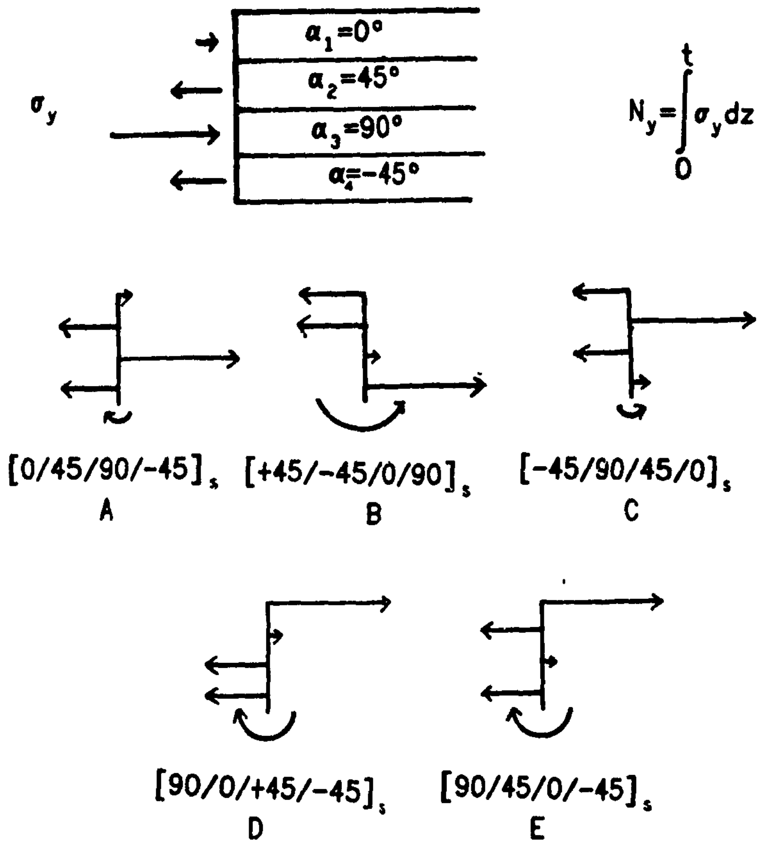

Figure 4.4.20 Influence of stacking sequence on the resultant couple of a half laminate. In order from largest couple causing compressive Il normal edge stress to tensile they are D,E,A,C,B.

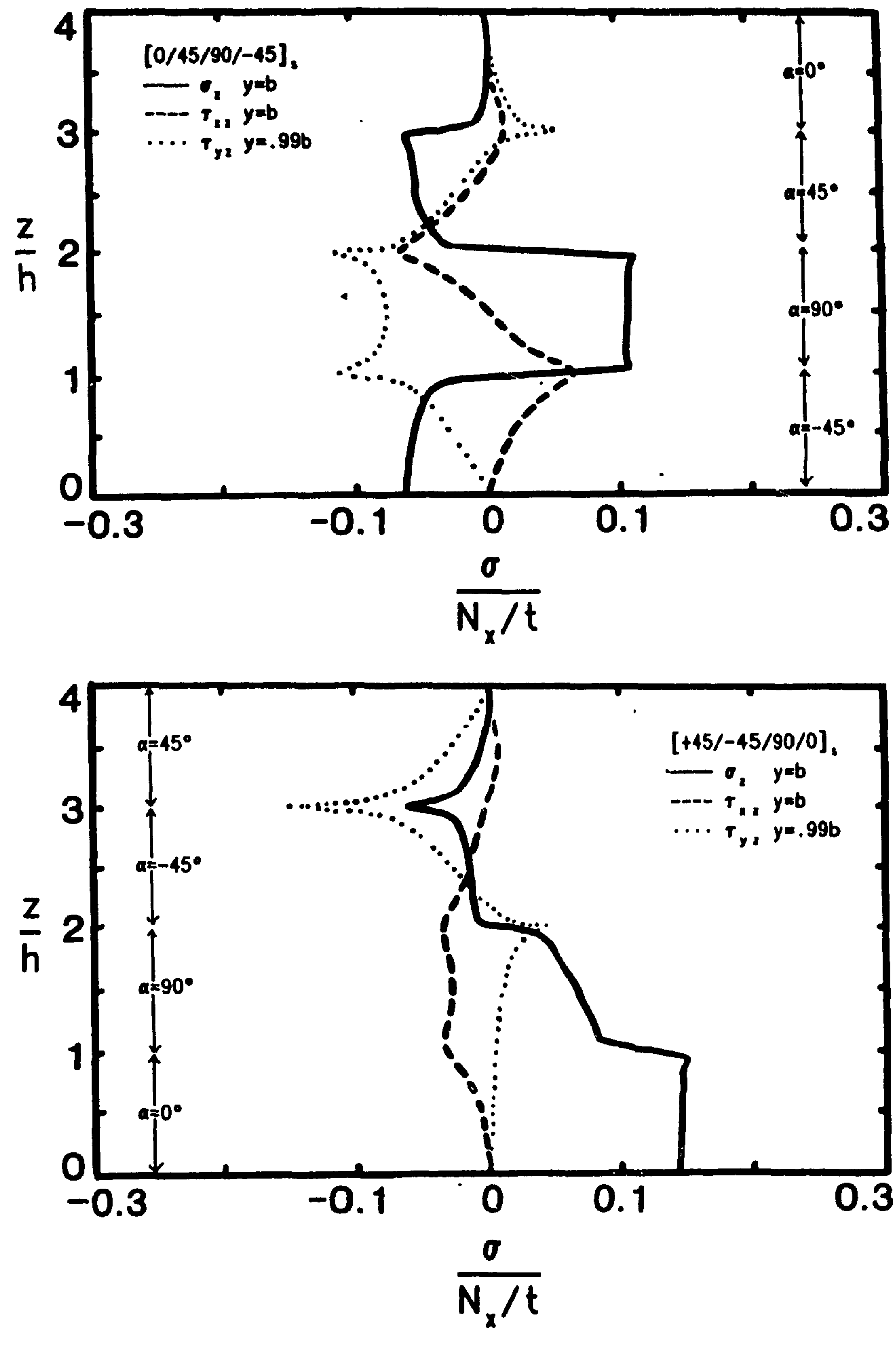

Figure 4.4.21 a) Il edge stresses for stacking sequence A (top) and B.

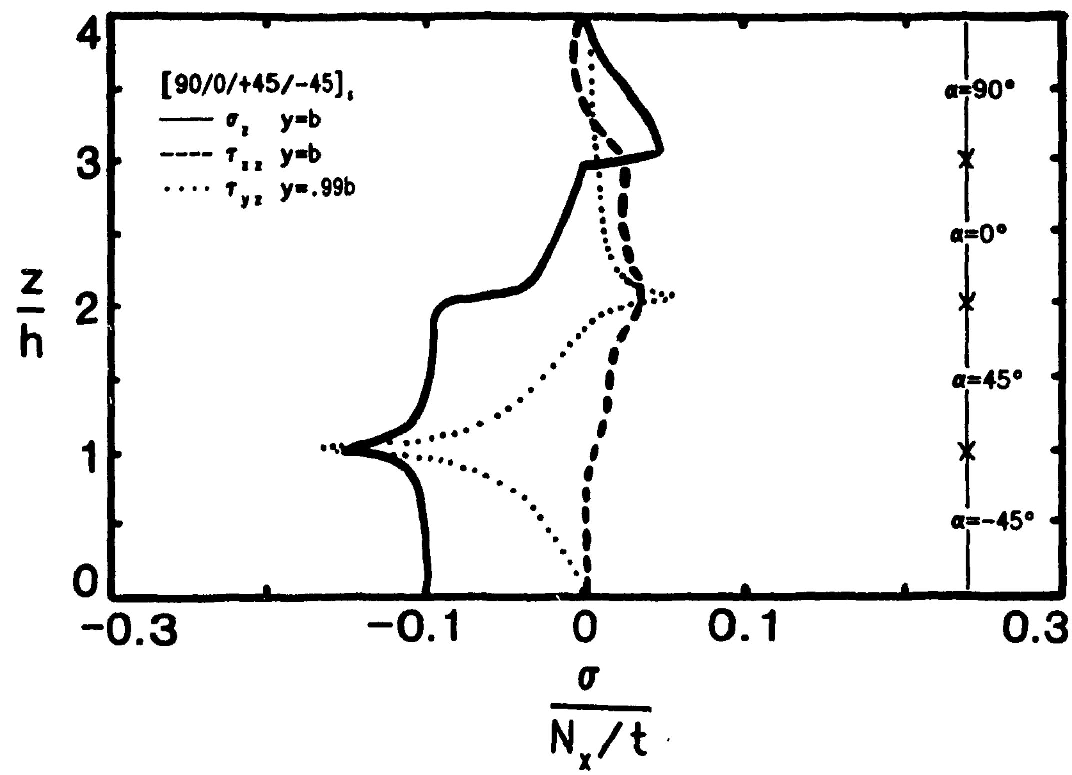

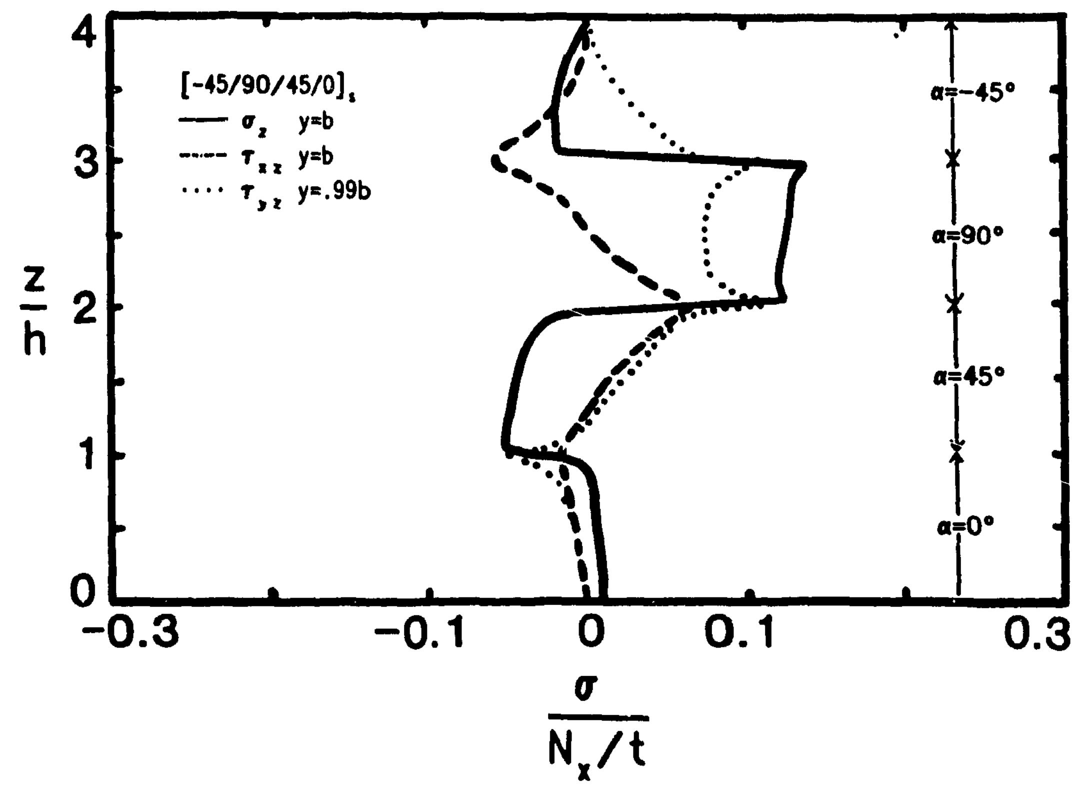

Figure 4.4.21 b) Il edge stresses for stacking sequence D (top) and C.

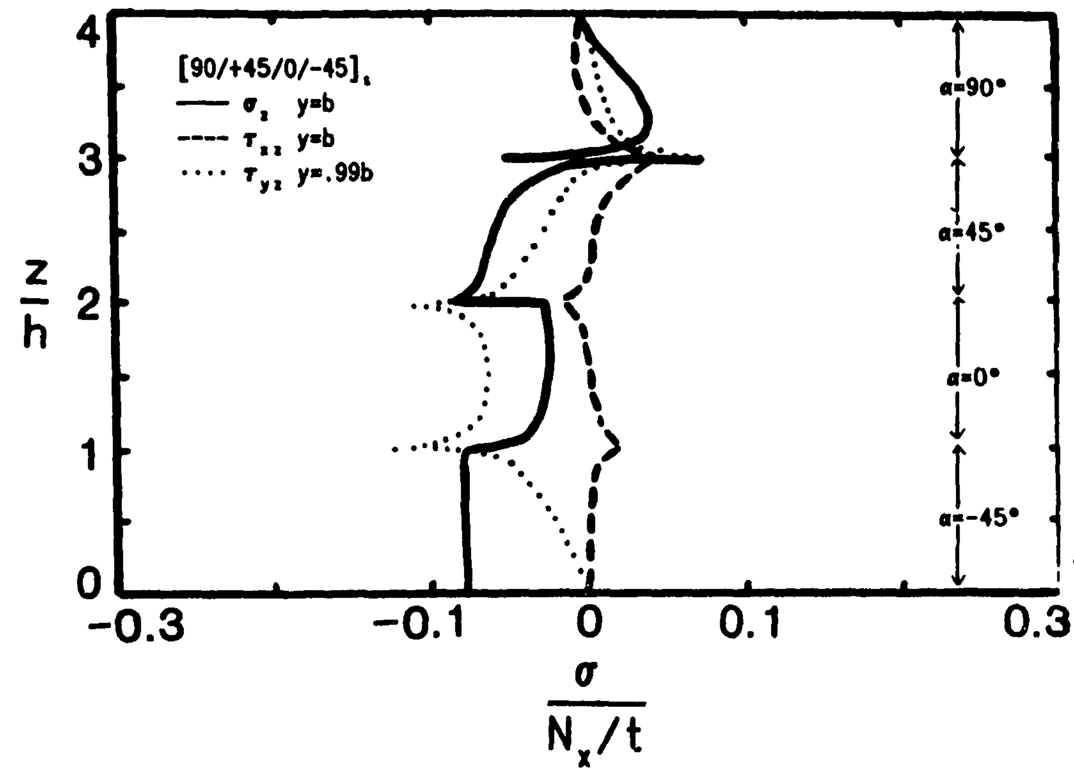

Figure 4.4.21 c) I1 edge stresses for stacking sequence E.

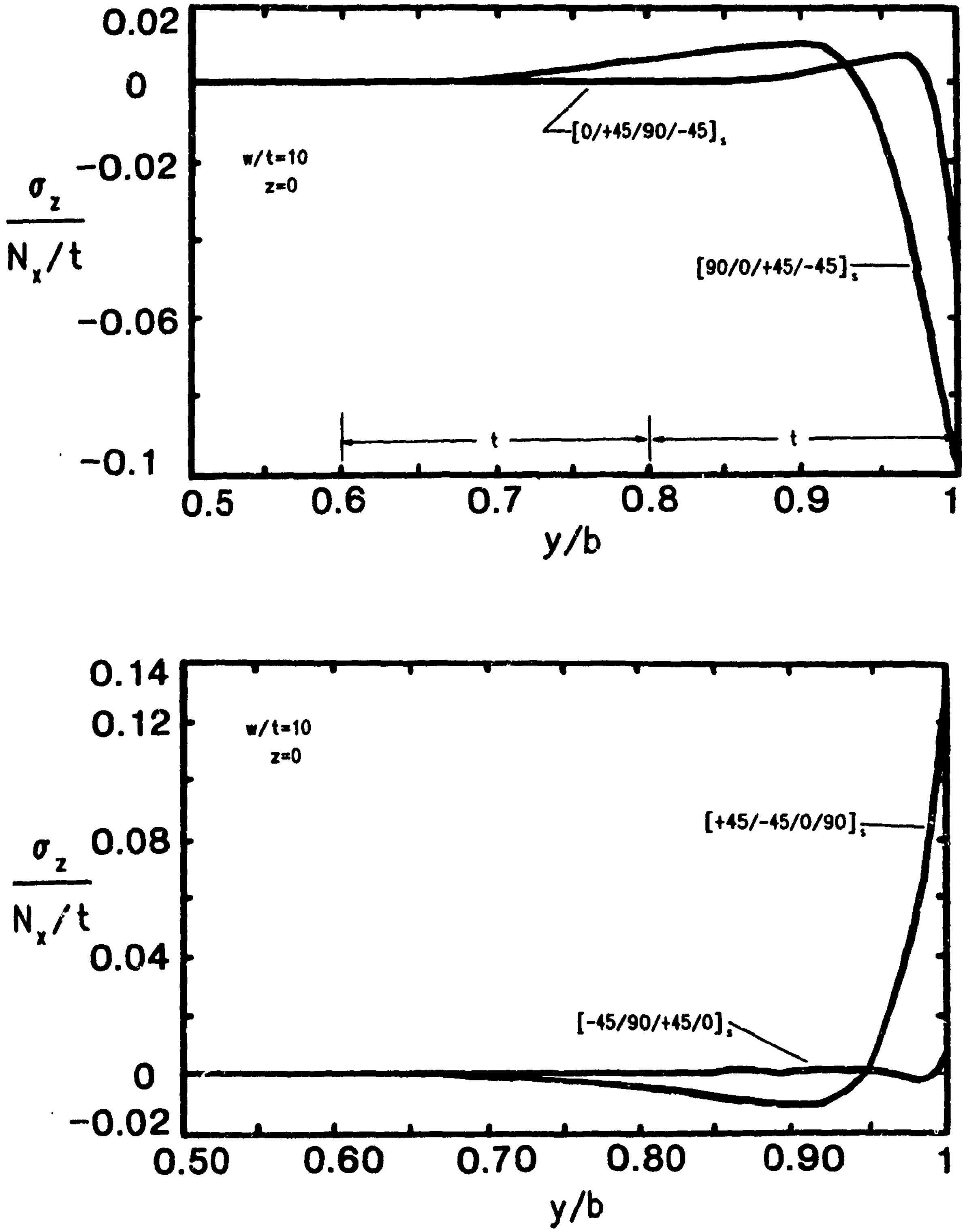

Figure 4.4.22 Il normal stress on the midplane of quasi-isotropic laminates shows relation of couple to BL depth and stress magnitude.

edge stresses.

4.4.5 Discussion and Conclusions

From a simple equilibrium analysis it can be seen that both the maximum IL stress and depth of the boundary layer change to equilibrate the CLT stresses occurring outside the boundary layer. Laminate and sublaminate thickness determines boundary layer depth only insofar as it affects the far field CLT stresses; IL stresses are highly problem dependent. Equilibrium analysis has only limited use for predicting the IL stresses since, for example, the σ_z couple depends upon maximum stress, the BL depth and also the number of zero crossings in the BL which is often more than two. This equilibrium analysis cannot be used for circular holes without potentially gross error since $\partial\sigma/\partial\theta \neq 0$ for holes.

For all loads and cases, the maximum stresses on the edge of shuffled laminates were not reduced. For bending and twisting the stresses of shuffled laminates increased in proportion to the distance from the midplane so that the maximum was shifted towards the laminate surface.

The boundary layer depth was less than 5 laminate thicknesses in all cases.

Finally, on the mode of solution, shortcuts to accurate solutions are not obvious. From observations, solutions to the complete boundary value problem without assumptions beyond those made here will consistently yield results of sufficient accuracy.

CHAPTER 5

CLOSURE

5.1 Summary

Using the classical linear elastic material model of a fiber-reinforced composite, the stresses in composite laminates near edges have been investigated by approximate solution of the equations of elasticity for static loads and by measurement. The investigation was undertaken based on the assumption that free edge stresses play a significant role in the failure processes of laminates and will contribute to the understanding and prevention of free edge failures.

Finite element solutions for plates with holes using standard displacement-formulated isoparametric elements showed h-dependence of stresses in the region near the surmised singularity but using a substructuring scheme acceptable results overall in the boundary layer were obtained with reasonable computer resources. However, the h-dependence of stresses near the singularity cannot be neglected for the effect on magnitude while distributions (or shape) were less dependent.

Measurements of hole surface normal strains were in good agreement with FE results for the plates investigated having large values of Rt/a^2. For ϵ_z, near the singularity the measured strains were shown in FE solutions for models of instrumented plates to have been significantly influenced by the mechanical behaviour of the gages. From limited data, the measured strains support the predictions of the model only when the gages are included. From these results, any method using coatings in a similar situation should be suspected of effects on the measurements.

FE solutions showed on the hole surface of $[0/90]_s$, $[90/0]_s$, and [90/0] Graphite/Epoxy plates that $\tau_{z\theta}$ is the strongest interlaminar stress and is maximum at the interface but everywhere less than the applied stress. The interlaminar stresses do not vanish as R/t increases but, in fact, can increase although a state appears to be approached asymptotically with increasing R/t; very thick plates were not modeled so no similar statement can be made for very low R/t. The [90/0] plates had the largest maximum of σ_z for all cases. R/t did not appear to significantly alter σ_z at the interface in any case. R/t and stacking sequence dramatically affects the distribution of σ_z on the midplane of symmetric plates although the maximum on the hole surface was observed to be less than 20% of the applied stress. Overall the most severe hole stress state occurred for the [90/0] laminate where the hole surface intreface stresses were very large.

From observations on the FE results a method of estimating the circumferential stress on the hole surface of a laminate using plane stress and plate theory formulas for single layers is proposed. When compared with FE results for both symmetric and unsymmetric plates, the two dimensional solutions bounded the maximum σ_θ for the range of R/t 1-25. An heuristic explanation is that the methods roughly model bonded and unbonded layers and the effects of bonding are relatively more localized near the interface as R/t increases. This method, after further verfication, may provide easy estimates, increase understanding and so benefit designers.

Reinforcement of a hole with an elastic ring can mitigate the interlaminar stresses and reduce the maximum stress concentration in the plate. In the process the overall stress state is altered as radial stresses emerge. The stress state in the plate may be tailored by varying ring thickness and rigidity.

A procedure for solving problems involving laminates with certain anisotropy of the layer material properties valid for cases where $\partial\sigma/\partial x=0$ was developed and used to investigate angle-ply and cross-ply; shuffled and unshufffled; symmetric, asymmetric, and antisymmetric Gr/Ep laminates for CLT loadings M_x, N_x and M_{xy}. In comparison to other approaches successfully taken in the literature this method is very competitive in terms simplicity, flexibility, and computing resources.

While interlaminar stresses must satisfy equilibrium with stresses outside the boundary layer, the BL depth and stress distribution are too variable and problem dependent for estimates using the CLT stress resultants to be accurate. Therefore, IL stresses are adequately determined at present only by solution of the complete boundary value problem.

5.2 Recommendations for Future Work

Although the severity of the stress state is determined by failure criteria which is material dependent generally the high stresses at the surmised singularity appear to be most serious. Paradoxically, it is in this region that the verity of the model and measurements are most doubtful. From what has been observed in the present investigation, more detailed work in measurement, more solution accuracy in modeling, and better interpretation of the results will be required to understand and predict the behaviour at the interface/edge intersection.

Although the results were valuable, the FE method of solution used in Chapter 3 was inefficient and so is of limited use. Therefore it is not recommended that any further work (e.g. convergence studies) be done in developing the method for three-dimensional laminate edge problems.

Enlarged models is the approach recommended for measurement. Measurement of $\gamma_{z\theta}$, which was not feasible in the present work, should be attempted since $\tau_{z\theta}$ is observed to be a significant stress.

Prevention of delamination may be possible by mitigating the stress state in the boundary layer. Hole reinforcing rings appear promising. Experimental work could be based on the results presented here. Coatings should be investigated for straight edges as well. Coatings could be used for configurations which might otherwise be avoided due to severe free edge stresses.

The mode of solution in Chapter 4 requires: further work on the use of the residual as an error estimate, analysis of the homogeneous solution functions as approximation functions, and to exploit the low number of degrees of freedom in solutions in terms of computing resources. As a suggestion, other collocation point distribution schemes and frequency distributions may lead to a reduction in the computing resources required.

References

1) Aderholdt R.W, Berghaus D.G, (1976),"Model Design and Fabrication for Stress Analysis in Multilaminar Composites", Experimental Mechanics, January, pages 32-37.

2) Altus E., Bar-Yoseph P.,(1983), "A 3-D Finite Difference Solution for Orthotropic Laminated Composites Using Curvilinear Coordinates", Computers and Structures, volume 17, number 4, page 573.

3) Altus E., Rotem A., Shmueli M.,(1980),"Free Edge Effect in Angle-Ply Laminates-A New Three Dimensional Finite Difference Solution", Journal of Composite Materials, volume 14, January, page 21.

4) Ayres F.,(1974), "Schaum's Outline of Theory and Problems of Matrices", MacGraw-Hill, New York.

5) Bar-Yoseph P.,Avrashi J.,(1985a), "Interlaminar Stress Analysis for Laminated Plates Containing a Curvilinear Hole", Computers and Structures, volume 21, number 5, pages 917-932.

6) Bar-Yoseph P., Siton G., (1985b), "The Effect of Material Non-linearity on the Interlaminar Stress Field in Composite Laminates", Computers and Structures, volume 21, number 6, pages 1105-1108.

7) Bar-Yoseph, P.,(1983),"On the Accuracy of Interlaminar Stress Calculation in Laminated Plates", Computer Methods in Applied Mechanics and Engineering, volume 36, pages 309-329.

8) Bar-Yoseph P., Pian T.H.H.,(1981), "Calculation of Interlaminar Stress Concentration in Composite Laminates", Journal of Composite Materials, volume 15, May, page 225.

9) Bathe K.J., Wilson E.W., Peterson F.E., (1974), "Sap IV-A Structural Analysis Program for Static and Dynamic Response of Linear Systems", Report No. EERC 73-11 from College of Engineering, University of California at Berkeley to National Science Foundation, April.

10) Beatty M.F., Chewning S.W.,(1979), "Numerical Analysis of the Reinforcement Effect of a Strain Gage Applied to a Soft Material", International Journal of Engineering Science, volume 17, page 907.

11) Berghaus D.G., Aderholdt R.W.,(1975), "Photoelastic Analysis of Interlaminar Matrix Stresses in Fibrous Composite Models", Experimental Mechanics, November, pages 409-417.

12) Bogy D.B., (1968), "Edge-Bonded Dissimilar Orthogonal Elastic Wedges Under Normal and Shear Loading", Journal of Applied Mechanics, September, pages 460-466.

13) Brinson H.F., Yeow Y.T., (1977), "An Experimental Study of the Fracture Behaviour of Laminated Graphite/Epoxy Composites", Comosite Materials: Testing and Design (Fourth Conference), ASTM STP 617, American Society for Testing and Materials, pages 18-38.

14) Ci-Da,Xu,(1985), " Weighted Residual Methods (WRM) in Solid Mechanics, Recent Advances in China", Dailan, June.

15) Collatz L., (1960), "The Numerical Treatment of Differential Equations", Springer-Verlag, New York.

16) Cook R.D.,(1974), "Concepts and Applications of Finite Element Analysis ",John Wiley and Sons, page 346.

17) Crandall S., (1956), "Engineering Analysis- A Survey of Numerical Procedures", MacGraw-Hill, New York.

18) Czarnek R., Post D, and Herakovitch C,(1983), "Edge Effects in Composites by Moire Interferometry", Experimental Techniques, January, page 18.

19) Dana J.R.,(1973)," Three Dimensional Finite Element Analysis of Thick Laminated Composites- Including Interlaminar and Boundary Effects Near Circular Holes", Phd Thesis, Virginia Polytechnic and State University, Blacksburg, Virginia.

20) Daniel I.M.,(1980),"Behaviour of Graphite-Epoxy Plates with Holes Under Biaxial Loading " , Experimental Mechanics, page 1.

21) Daniel I.M.,(1978), "Strain and Failure Analysis of Graphite-Epoxy Plates with Cracks", Experimental Mechanics, July, page 246.

22) Daniel I.M., Rowlands R.E, and Whiteside J.B.,(1974), "Effects of Material and Stacking Sequence on Behaviour of Composite Plates with Holes", Experimental Mechanics, January, page 1.

23) Daniel I.M., Rowlands R.E., and Whiteside J.B.,(1973), "Deformation and Failure of Boron-Epoxy Plate with Circular Hole", Analysis of the Test Methods for High Modulus Fibers and Composites, ASTM STP 521, American Society for Testing and Materials, page 143.

24) Findlay B.A., Scriven L.E., (1966), "The Method of Weighted Residuals- A Review", Applied Mechanics Reviews, volume 19, number 9, September, page735.

25) Fletcher R., (1980), " Practical Methods of Optimisation, Volume 1: Unconstrained Optimisation", John Wiley and sons.

26) Ford J.L., Patel H.P., and Turner J.L,(1982), "Interlaminar Shear Effects in Cord-Rubber Composites", Fiber Science and Technology, volume 17, pages 255-271.

27) Given W., (1958), "Computation of Plane Unitary Rotations Transforming a General Matrix to Triangular Form", SIAM J. App. Math, volume 6, pages 26-50.

28) Green A.E., Zerna W.,(1954), "Theoretical Elasticity", Oxford at the Clarendon Press.

29) Gresczcuk L.B.,(1972),"Stress Concentrations and Failure Criteria for Orthotropic and Anisotropic Plates with Circular Openings", Composite Materials: Testing and Design (Second Conference), ASTM STP 497, 1972, pages 363-381.

30) Halpin J.C.,(1984), "Primer on Composite Materials", Technomic Publishers, Lancaster, Pennsylvania.

31) Hamming R.W.,(1973),"Numerical Methods for Engineers and Scientists", MacGraw-Hill, New York.

32) Hashin Z., (1983), "Analysis of Composite Materials-A Survey", Journal of Applied Mechanics, September, volume 50, pages 481-505.

33) Hashin Z.,(1972)," Theory of Fiber Reinforced Materials", NASA Report CR-1974, March.

34) Herakovich C.T., Post D., Buczek M.B., and Czarnek R.,(1985), "Free Edge Strain Concentration in Real Composite Laminates: Experimental-Theoretical Correlation", American Society of Mechanical Engineers Paper 85-WA/APM-10.

35) Herakovich C.T.,(1980),"Composite Laminates with Negative Through-the Thickness Poisson's Ratios", Journal of Composite Materials, volume 18, September, pages 447-455.

36) Hsu P.W., Herakovich C.T,(1977),"Edge Effects in Angle-Ply Composite Laminates", Journal of Composite Materials, volume 11, October, page 422.

37) Jaeger L.G.,(1966), "Cartesean Tensors in Engineering Science", Pergamon Press, New York.

38) Kassapoglou C., Lagace P.A.,(1986), "An Efficient Method for the Calculation of Interlaminar Stresses in Composite Materials", Journal of Appled Mechanics, volume 53, pages 744-749.

39) Kriz R.D.,(1977),"Effect of Material Properties on Interlaminar Stresses in Angle-Ply Composite Laminates",

VPI-E-77-16.

40) Langhaar H.,(1951),"Dimensional Analysis and Theory of Models", John Wiley and Sons.

41) Lawson C.L, Hanson R.J.,(1974), "Solving Least Squares Problems", Prentice-Hall, New Jersey.

42) Lee J.D., (1982), "Three Dimensional Finite Element Analysis of Damage Accumulation in Composite Laminate", Computers and Structures, volume 15, number 3, pages 335-350.

43) Lee J.D., (1980), "Three Dimensional Finite Element Analysis of Layered Fiber-Reinforced Composite Materials", Computers and Structures, volume 12, pages 319-339.

44) Lekhnitskii S.G.,(1977),"Theory of Elasticity of an Anisotropic Body" , Translated from the 1977 Russian 2nd Edition, Mir Publishers, Moscow.

45) Lekhnitskii S.G.,(1968),"Anisotropic Plates", Gordon and Breach Publishers, New York.

46) Levy A., Armen H., Whitside J.,(1971), " Elastic and Plastic Interlaminar Shear Deformation in Laminated Composites Under Generlized Plane Stress", Presented at the October 1971 Air Force 3rd Conference on Matrix Methods in Structural Mechanics held at the Wright Patterson Air Force base, Ohio.

47) Lou A.Y.C, Walter J.D., (1978), "Interlaminar-Shear-Strain Measurements in Cord-Rubber

Composites", Experimental Mechanics, December, pages 457-463.

48) Love A.E.H.,(1944),"A Treatise on the Mathematical Theory of Elasticity", Fourth Edition, Dover, New York.

49) Lucking W.M., Hoa S.V., Sankar T.S., (1984)," The Effect of Geometry on Interlaminar Stresses of $[0/90]_s$ Composite Laminates with Circular Holes", Journal of Composite Materials, Volume 18, number 2, March, pages 188-198.

50) Mandel J.,(1964) "The Statistical Analysis of Experimental Data", Dover, New York.

51) Micro-Measurements Tech Note,(1982), "Errors due to Transverse Sensitivity in Strain Gages," M-M Tech. Note TN-509, Micro Measurements Division, Measurement Group, Inc., Raleigh, NC.

52) Micro-Measurements Tech Note, (1979), "Optimizing Strain Gage Excitation Levels," M-M Tech. Note TN-502, Micro Measurements Division, Measurement Group, Inc., Raleigh, NC.

53) Oplinger D.W.,Parker B.S., and Chiang F.P.,(1974), "Edge Effect Studies in Fiber-Reinforced Laminates", Experimental Mechanics, September, pages 347-354.

54) Pagano N.J., Soni S.R., (1982), Elastic Response of Composite Laminates, Mechanics of Composite Materials-Recent Advances, Proceedings of the IUTAM Symposium on Mechanics of Composite Materials, VPISU, Blacksburg VA, August 16-19, pages 227-242.

55) Pagano N.J.,(1974), On the Calculation of Interlaminar Normal Stress in Composite Laminate, Journal of Composite Materials, volume 8, pages 65-82.

56) Pagano N.J., Rybicki E.F.,(1976)," A Study on the Influence of Microstructure on the Modified Effective Modulus Approach for Composite Laminates", Proc. 1975 Int. Conf. Comp. Mat. 2, page 149.

57) Pagano N.J.,(1975), "The Role of Effective Modulus in the Elastic Analysis of Composite Laminates", Mechanics of Composite Materials, G.P. Sendeckyj,Ed., Academic Press, New York.

58) Pagano N.J., Rybicki E.F.,(1974), "On the Significance of Effective Modulus Solutions for Fibrous Composites", Journal of Composite Materials, volume 8, July, page 214.

59) Pipes R.B.,(1979),"Notched Strength of Composite Materials", Journal of Composite Materials, volume 13, page 148.

60) Pipes R.B.,(1972),"Solution of Certain Problems in the Theory of Elasticity for Laminated Anisotropic Systems", PhD. Thesis, University of Texas at Arlington, Texas.

61) Pipes R.B., Daniel I.M.,(1971),"Moire Analysis of the Interlaminar Shear Edge Effect in Laminated Composites", Journal of Composite Materials, volume 5, April 1971, page 255.

62) Pipes R.B., Pagano N.J.,(1970), "Interlaminar Stresses

in Composite Laminates Under Uniform Axial Extension", Journal of Composite Materials, October, volume 4, page 539.

63) Post D., Czarnek R., and Joh D.,(1987),"Shear Strains in a Graphite/PEEK Beam by Moire Interferometry with Carrier Fringes", Experimental Mechanics, volume 27, number 3, September, pages 246-9.

64) Raju I.S., Crews J.H.,(1982a), Three Dimensional Analysis of $[0/90]_s$ and $[90/0]_s$ Laminates with a Central Circular Hole, Composites Technology Review, volume 4, number 4, page 116.

65) Raju I.S., Crews J.H.(1982b),"Three Dimensional Analysis of [0/90]s and [90/0]s Laminates with a Central Circular Hole", NASA-TM-83300 April.

66) Raju I.S., Crews J.H.,(1981), Interlaminar Stress Singularities at a Straight Free Edge in Composite Laminates, Computers and Structures, volume 14, number 1-2, pages 21-28.

67) Reifsneider K.L., Henneke E.G., and Stinchcomb W.W., (1977), "Delamination in Quasi-Isotropic Graphite-Epoxy Laminates", Composite Materials: Testing and Design (Fourth Conference), ASTM STP 617, American Society for Testing and Materials, pages 93-105.

68) Rowlands R.E., Daniel I.M., Whitside J.B.(1974), "Geometric and Loading Effects on Strength of Composite Plates with Cutouts", Composite Materials and Testing and

Design (3rd Conf) ASTM STP 546, page 361.

69) Rowlands R.E., Daniel I.M., and Whiteside J.B., (1973), " Stress and Failure Analysis of a Glass-Epoxy Composite Plate with a Circular Hole", Experimental Mechanics, January, page 31.

70) Rybicki E.F., Schmeuser D.W.,(1978), "Effect of Stacking Sequence and Lay-up Angle on Free Edge Stresses Around a Hole in a Laminated Plate Under Tension", Journal of Composite Materials, page 300.

71) Rybicki E.F., Kanninen M.F., (1977a), " A Finite Element Calculation of Stress Intensity Factors by a Modified Crack Closure Integral", Engineering Fracture Mechanics, volume 9, pages 931-938.

72) Rybicki E.F., Pagano N.J.,(1977b), "On the Significance of Effective Modulus Solutions for Fibrous Composites",Journal of Composite Materials, volume 8 ,page 214.

73) Rybicki E.R., Hopper A.T.,(1973)," Analytical Investigation of Stress Concentrations Due to Holes in Fiber Reinforced Plastic Laminated Plates, Three Dimensional Models", Tech Report, AFML TR73 100, June.

74) Salamon N., (1980), " An Assessment of the Interlaminar Stress Problem", Supplement to the Journal of Composite Materials, January, page 1.

75) Sandorff P.E.,(1982)," Tranverse Shear Stiffness of T300/5208 Graphite/Epoxy in Simple Bending", Journal of

Reinforced Plastics and Composites, volume 1, October, page 335.

76) Savin G.N.,(1961), "Stress Distributions Around Holes", Pergamon Press, London.

77) Stalnaker D.O., Kennedy R.H., and Ford J.L.,(1980), "Interlaminar Shear Strain on a Two-ply Balanced Cord-Rubber Composite", Experimental Mechanics, March, page 87.

78) Stehlin P.,(1972),"Strain Distribution Around Strain Gages", Journal of Strain Analysis, volume 7, number 3, page 228.

79) Sternberg E., Sadowsky M.A.,(1949), " Three Dimensional Solution for the Stress Concentration Around a Circular Hole in a Plate of Arbitrary Thickness", Journal of Applied Mechanics, March, pages 27-38.

80) Strang G., Fix G.J.,(1973)," An Analysis of the Finite Element Method", Prentice Hall.

81) Tang S.,(1977), "Interlaminar Stresses Around Circular Cutouts in Composite Plates Under Tension" AIAA Journal, November, page 1631.

82) Tong P, Pian H.H,(1973) On the Convergence of the Finite Element Method for Problems with Singularity, International Journal of Solids and Structures, volume 9, page 313.

83) Tsai S.W. and Hahn H.T., (1980), "Introduction to Composite Materials", Technomic Publishers, Lancaster PA.

84) Tuttle M.M., Brinson H.F.,(1984), "Resistance-Foil Strain- Gage Technology as Applied to Composite Materials", Experimental Mechanics, volume 24, number 1, March, pages 54-65.

85) Wang A.S.D.,Crossman F.W.,(1977),"Some New Results on Edge Effects in Symmetric Composite Laminates, Journal of Composite Materials, volume 11, page 92.

86) Wang A.S.D., Crossman, W.F.,(1978), "Calculation of Edge Stresses in Multilayer Laminates by Substructuring", Journal of Composite Materials, volume 12, January, page 76.

87) Wang S.S.,(1985), "Three-Dimensional Hybrid-Stress Finite Element Analysis of Composite Laminates with Cracks and Cutouts", Pressure Vessel and Piping Conference and Exhibition, New Orleans, June, Sponsored by ASME.

88) Wang S.S., (1984),"Edge Delamination in Angle-Ply Composite Laminates", AIAA Journal, volume 22, number 2, February, pages 256-264.

89) Wang S.S. and Stango R.J., (1983a)," Optimally Discretized Finite Elements for Boundary-Layer Stresses in Composite Laminates", AIAA Journal, V21, April, pages 614-620.

90) Wang S.S., Choi I.,(1983b),"Boundary-layer Effects in Composite Laminates: Part III - The Influence of Lamination Variables on Free-Edge Stresses", (was to have appeared in the Journal of Applied Mechanics).

91) Wang S.S., Yuan F.G.,(1983c), " A Hybrid Finite Element

Approach to Composite Laminate Elasticity Problems with Singularities", Journal of Applied Mechanics, volume 50 number 4A, pages 835-844.

92) Wang S.S., (1982), "Elasticity Solutions for a Class of Composite Laminate Problems with Stress Singularities", Mechanics of Composite Materials-Recent Advances, Proceedings of the IUTAM Symposium on Mechanics of Composite Materials, VPISU, Blacksburg VA, August 16-19, pages 259-282.

93) Whitcomb J.D., Raju I.S.,(1984),"Analysis of Interlaminar Stresses in Thick Composite Laminates with and without an Edge Delamination", NASA Technical Memorandum 85738, January.

94) Whitcomb J.D., Raju I.S., Goree J.G., (1982), "Reliability of the Finite Element Method for Calculating Free Edge Stresses in Composite Laminates", Computers and Structures, volume 15 , number 1, page 23.

95) Zienkiewicz O.C.,(1977), "The Finite Element Method", MacGraw-Hill, New York.

96) Zwiers R.I., Ting T.C.T.,(1983),"Singularity of Contact-Edge Stress in Laminated Composites Under Uniform Extension", Journal of Composite Materials, volume 17, January, pages 49-63.

97) Zwiers R.I., Ting T.C., Spilker R.L.,(1982),"On the Logarithmic Singularity of Free-Edge Stress in Laminated Composites Under Uniform Extension", Journal of Applied Mechanics, volume 49, September, pages 561-569.

Appendix A: Equations of Classical Lamination Theory

Following Kirchoff's hypothesis that in any deformation plane sections remain plane the laminate displacements are given by

$$u = u_0 - z\, w_x$$
$$v = v_0 - z\, w_y$$

where u_0, v_0 are the displacements at z=0. The strains are then

$$\varepsilon_x = \varepsilon_{x0} - z\, k_x$$
$$\varepsilon_y = \varepsilon_{y0} - z\, k_y$$
$$\gamma_{xy} = \gamma_{xy} - z\, k_{xy}$$

where

$$k_x = w_{xx} \qquad k_y = w_{yy} \qquad k_{xy} = 2w_{xy}$$

And finally, the stresses are related to the strains by

$$\begin{bmatrix} N \\ M \end{bmatrix} = \begin{bmatrix} A & B \\ B & D \end{bmatrix} \begin{bmatrix} \varepsilon \\ k \end{bmatrix}^{0} \qquad \text{where}$$

$$[N\ M]^T = [\ N_x\ N_y\ N_{xy}\ M_x\ M_y\ M_{xy}]$$

$$[\varepsilon_0\ k] = [\ \varepsilon_{x0}\ \varepsilon_{y0}\ \gamma_{xy0}\ k_x\ k_y\ k_{xy}]$$

$$A_{ij} = \sum_{k=1}^{n} (Q_{ij})^k (z_k - z_{k-1}) \qquad B_{ij} = \frac{1}{2} \sum_{k=1}^{n} (Q_{ij})^k (z_k^2 - z_{k-1}^2)$$

and
$$D_{ij} = \frac{1}{3} \sum_{k=1}^{n} (Q_{ij})^k (z_k^3 - z_{k-1}^3)$$

and $\bar{A}, \bar{B}, \bar{D}$ are called the laminate stiffnesses. Compliances are given by

$$\bar{a}=\bar{A}^{-1} \qquad \bar{b}=\bar{B}^{-1} \qquad \bar{d}=\bar{D}^{-1}.$$

For a symmetric laminate $\bar{B}=0$ (a 3x3 matrix of zeroes) and there is no bending-membrane coupling. If for every α there is a $-\alpha$ included then $A_{i6}=0$.

Appendix B: Evaluation of Specimen Effective Moduli

In order to make the FE results relevant to the experimental work EM constants were determined for the specimen plates. $[0_8]$ for E_{11}, ν_{12}; $[90_8]$ for $E_{22}, \nu_{21}, \nu_{23}$; and $[\pm 45_2]_s$ for G_{12} strips were characterized to obtain the values listed in Table 4.1. Along with fiber volume content of the characterization specimens these moduli are used for evaluating the EM properties as a function of the fiber volume. The relations between the constituent and composite properties are given by the following equations due to Hashin(1972)

B1) $$E_{11} = \eta_m E_m + \eta_f E_{f1} + \delta_e$$

B2) $$\nu_{12} = \nu_m \eta_m + \eta_f \nu_{f1} + \delta_\nu$$

B3) $$G_{12} = \frac{G_m (G_m \eta_m + G_{f1}(1+\eta_f))}{(G_m(1+\eta_f) + G_{f1}\eta_m)}$$

B4) $$G_{23} = \frac{G_m(1+(1+\beta_1)\eta_f)}{(R-\eta_f(1+3\beta_1{}^2\eta_f{}^2/(\alpha\eta_f{}^3+1)))}$$

B5) $$E_{22} = \frac{4K_s G_{23}}{K_s + MG_{23}}$$

where the matrix properties are ν_m, E_m and $G_m = E_m/2(1+\nu_m)$, the fiber properties are E_{ft}, ν_{ft} and $G_{ft} = E_{ft}/2(1+\nu_{ft})$ in the transverse plane so that the fiber is transversely isotropic , and E_{fl}, ν_{fl} and G_{fl} in the longitudinal direction. Also

$$\delta_e = \frac{(4(\nu_{fl}-\nu_m)^2 \eta_f \eta_m}{\dfrac{\eta_f}{K_f} + \dfrac{\eta_m}{K_m} + \dfrac{1}{G_m}} \qquad \delta_\nu = \frac{(\eta_f - \eta_m)(\ 1/K_m - 1/K_f)\eta_f \eta_m}{\dfrac{\eta_m}{K_f} + \dfrac{\eta_f}{K_m} + \dfrac{1}{G_m}}$$

which are almost negligible, and

$$G_m = \frac{E_m}{2(1+\nu_m)} \qquad K_m = \frac{G_m}{(1-2\nu_m)} \qquad K_f = \frac{G_{ft}}{(1-2\nu_{ft})}$$

$$\beta_1 = \frac{K_m}{(K_m + 2G_m)} \qquad \beta_2 = \frac{K_f}{(K_f + 2G_{ft})}$$

$$G = \frac{G_{ft}}{G_m} \qquad \alpha = \frac{(\beta_1 - G\ \beta_2)}{(1 + G\ \beta_2)} \qquad R = \frac{(G + \beta_1)}{(G - 1\ )}$$

$$K_s = \frac{(K_m(K_f+G_m)\eta_m + K_f(K_m+G_m)\eta_f}{((K_f+G_m)\eta_m + (K_m+G_m)\eta_f)} \qquad M = 1 + \frac{4K_s \nu_{12}^2}{E_{11}}$$

The unknown values of the constituent moduli satisfy these equations when the EM values and η_f in each are fixed. After finding the constituent moduli equations B1-5 yield the EM values as functions of η_f only.

There are seven constituent properties while only five EM properties were measured. At these high fiber volume contents the matrix properties have very little influence on the calculated composite properties. Therefore, the manufacturer's values for E_m and ν_m were estimated so that a numerical search could be made for the other constituent properties. A simple manual routine was used which searches for the minimum of the sum of squared differences between the measured EM values and the values calculated using the equations.

To begin the procedure initial values of the fiber properties are required. Beyond this, since E_{11}, ν_{12}, and G_{12} are , aside from the matrix properties, weakly coupled to each other and to ν_{23} and E_{22}, then using the manufacturer's values for ν_m and E_m and the experimental data for E_{11}, ν_{12}, and G_{12} the constituent properties G_{fl}, E_{fl}, and ν_{fl} can be determined approximately. Further, by setting ν_{ft} and G_{ft} simultaneously the properties E_{22}, G_{23}, and ν_{23} can be estimated. These are the values used to initialize the numerical method.

After reducing the error in B1-5 to less than the number of decimal places shown in the EM properties it was observed that changes of up to 10% in the matrix properties influenced, at worst, the 4th floating point digit in all the resulting final EM properties for the test plates.

Appendix C: Experimental Measurement Data

In the following tables C1 and C2 the slopes of stress/gage output curves are presented as the raw data. The measurements identified in the tables by gage length in thousandths of an inch (the gages are classified in Imperial units by the manufacturer) , angular position θ, direction of measurement (T-transverse, C-circumferential), and position through the thickness (i-interface, m-midplane).

Table C1: Slopes in $\mu\varepsilon$/MPa for $[0/90]_s$ Specimen

Gage length	Gage position & type	Replication # 1 measured	Replication # 1 corrected	Replication # 2 measured	Replication # 2 corrected
031	22.5 Ti	1.45	1.47	1.33	1.34
031	45 Ti	-3.81	-3.52	-4.19	-3.89
031	67.5 Ti	-29.25	-28.38	-30.18	-29.30
015	90 Cm	46.24	46.28	46.08	46.11
015	67.5 Cm	44.58	44.54	44.64	44.59
015	45 Cm	21.39	21.33	21.40	21.34
015	22.5 Cm	-4.99	-5.01	-4.27	-4.29
015	0 Cm	-22.50	-22.47	-22.59	-22.55
		7.01	7.21	5.54	5.74
		2.31	2.52	2.08	2.30
015	0 Ti	3.33	3.54	0.03	0.25
015	22.5 Ti	-1.22	-1.17	-1.05	-1.00
015	45 Ti	-11.42	-11.70	-11.45	-11.73
015	67.5 Ti	-29.68	-30.58	-29.41	-30.30
015	90 Ti	-52.79	-53.54	-52.87	-53.62
015	90 Tm	-17.81	-18.42	-18.41	-19.03
015	67.5 Tm	-4.67	-5.32	-4.94	-5.59
015	45 Tm	4.07	3.73	4.16	3.82
015	22.5 Tm	5.61	5.55	4.84	4.89
015	0 Tm	0.75	1.08	1.12	1.45
015	90 Ci	63.76	63.97	64.13	64.34
		88.82	88.85	89.56	89.59
015	67.5 Ci	46.56	46.66	46.66	46.76
		26.63	26.66	26.40	26.43
		20.90	20.94	20.14	20.18
015	45 Ci	22.66	22.69	23.01	23.04
015	22.5 Ci	-2.31	-2.30	-3.41	-3.40
015	0 Ci	-15.05	-15.04	-15.46	-15.45
		5.46	5.69	6.12	6.35
088	0 Ti	4.61	4.85	2.20	2.45
		3.65	3.68	3.32	3.35
008	22.5 Ti	0.95	1.00	0.24	0.29
		-5.23	-5.59	-5.51	-5.87
008	45 Ti	-7.48	-7.83	-9.40	-9.73
008	67.5 Ti	-44.92	-45.84	-46.44	-47.35
		-28.17	-29.14	-29.35	-30.31
008	90 Ti	-19.27	-20.30	-18.65	-19.69

Table C1 cont'd

Gage length	Gage Position & type	Replication # 3 measured	3 corrected	4 measured	4 corrected
031	22.5 Ti	1.28	1.30	1.99	2.00
031	45 Ti	-4.23	-3.93	-2.51	-2.22
031	67.5 Ti	-29.97	-29.10	-29.97	-29.10
015	90 Cm	46.03	46.06	46.06	46.09
015	67.5 Cm	44.55	44.50	44.94	44.90
015	45 Cm	21.03	20.97	22.01	21.95
015	22.5 Cm	-4.39	-4.42	-4.51	-4.54
015	0 Cm	-22.84	-22.81	-22.07	-22.04
		6.24	6.44	5.13	5.33
		2.55	2.76	4.34	4.55
015	0 Ti	-0.77	-0.54	-0.77	-0.54
015	22.5 Ti	-1.15	-1.10	-0.65	-0.60
015	45 Ti	-11.87	-12.16	-11.75	-12.03
015	67.5 Ti	-29.84	-30.74	-29.89	-30.79
015	90.0 Ti	-53.14	-53.89	-52.70	-53.45
015	90 Tm	-18.54	-19.15	-18.45	-19.07
015	67.5 Tm	-4.57	-5.22	-4.55	-5.20
015	45 Tm	4.07	3.73	4.20	3.86
015	22.5 Tm	4.90	4.94	5.00	5.05
015	0 Tm	0.78	1.11	1.15	1.48
015	90.0 Ci	64.94	65.15	66.28	66.49
		88.71	88.75	89.14	89.17
015	67.5 Ci	47.52	47.62	49.35	49.45
		26.40	26.43	26.67	26.69
		20.70	20.74	22.11	22.14
015	45 Ci	23.99	24.02	24.04	24.07
015	22.5 Ci	-2.85	-2.84	-3.45	-3.43
015	0.00 Ci	-14.86	-14.85	-14.63	-14.62
		5.12	5.35	5.01	5.25
008	0 Ti	4.72	4.96	5.94	6.17
		2.74	2.78	2.74	2.78
008	22.5 Ti	2.54	2.58	-2.91	-2.84
		-5.79	-6.15	-5.77	-6.13
008	45 Ti	-6.63	-6.98	-4.82	-5.19
008	67.5 Ti	-44.23	-45.15	-42.94	-43.87
		-26.83	-27.81	-25.76	-26.75
008	90 Ti	-20.08	-21.11	-19.30	-20.33

Table C1 cont'd

Gage length	Gage position & type	average	corrected average	corrected variance	Std. dev'n
031	22.5 Ti	1.51	1.53	0.10	0.32
031	45 Ti	-3.68	-3.39	0.64	0.80
031	67.5 Ti	-29.84	-28.97	0.16	0.40
015	90 Cm	46.10	46.14	0.01	0.10
015	67.5 Cm	44.68	44.63	0.03	0.18
015	45 Cm	21.46	21.40	0.16	0.41
015	22.5 Cm	-4.54	-4.56	0.10	0.32
015	0 Cm	-22.50	-22.47	0.10	0.32
		5.98	6.18	3.21	
		2.82	3.03	0.31	
		0.45	0.68	3.53	
015	0.00 Ti	3.08	3.30	7.05	2.65
015	22.5 Ti	-1.02	-0.97	0.06	0.25
015	45 Ti	-11.62	-11.91	0.05	0.22
015	67.5 Ti	-29.71	-30.60	0.05	0.22
015	90.0 Ti	-52.87	-53.62	0.04	0.19
015	90 Tm	-18.30	-18.92	0.11	0.33
015	67.5 Tm	-4.68	-5.33	0.03	0.18
015	45 Tm	4.12	3.78	0.00	0.07
015	22.5 Tm	5.09	5.13	0.12	0.35
015	0 Tm	0.95	1.28	0.05	0.21
015	90.0 Ci	64.78	64.99	1.24	1.11
		89.06	89.09	245.72	
		47.52	47.62	246.37	
015	67.5 Ci	68.29	68.36	492.09	22.18
		26.52	26.55	6.80	
		20.96	21.00	0.74	
		23.43	23.46	0.68	
015	45 Ci	22.19	22.23	8.22	2.87
015	22.5 Ci	-3.00	-2.99	0.29	0.54
015	0.00 Ci	-15.00	-14.99	0.12	0.35
		5.43	5.66	0.26	
		4.37	4.61	1.19	
008	0.00 Ti	4.90	5.13	1.46	1.21
		3.11	3.15	1.28	1.13
		0.20	0.26	3.41	1.85
008	22.5 Ti	1.66	1.70	4.68	2.16
		-5.58	-5.94	0.35	
		-7.08	-7.43	1.85	
008	45.0 Ti	-6.33	-6.68	2.20	1.48
008	67.5 Ti	-44.63	-45.55	2.10	1.45
		-27.53	-28.50	24.54	
		-19.32	-20.36	22.46	
008	90.0 Ti	-23.43	-24.43	23.50	4.85

Table C2: Slopes in $\mu\varepsilon$/MPa for $[90/0]_s$ Specimen

Gage Length	Gage Position & type	Replication #			
		1		2	
		measured	corrected	measured	corrected
031	22.5 Ti	0.02	0.13	-0.44	-0.32
		-3.96	-3.82	-4.19	-4.05
031	45 Ti	-10.74	-11.42	-11.97	-12.64
		-13.51	-14.17	-13.72	-14.38
031	67.5 Ti	-19.25	-20.55	-20.05	-21.35
		-18.67	-19.97	-18.80	-20.10
015	90 Cm	77.82	77.78	77.23	77.19
015	67.5 Cm	63.25	63.27	61.95	61.97
015	45 Cm	25.59	25.62	24.49	24.53
015	22.5 Cm	-6.05	-6.01	-7.33	-7.30
015	0 Cm	-12.09	-12.10	-12.79	-12.80
015	22.5 Tm	-2.88	-2.76	-3.94	-3.82
015	45 Tm	-12.10	-12.41	-12.02	-12.33
015	67.5 Tm	-20.20	-21.03	-20.41	-21.24
015	90 Tm	-12.88	-13.98	-13.42	-14.52
015	0.00 Ti	5.68	5.97	5.61	5.90
015	22.5 Ti	-29.07	-28.88	-29.09	-28.89
		-25.99	-25.81	-26.20	-26.02
015	45 Ti	-19.78	-20.19	-20.18	-20.58
		-17.9[illegible]	-18.33	-18.35	-18.76
015	67.5 Ti	-3.35	-4.27	-3.54	-4.46
		-6.27	-7.17	-6.44	-7.34
015	90.0 Ti	-27.28	-28.24	-27.67	-28.63
015	0 Tm	6.96	7.12	5.82	5.99
015	90.0 Ci	71.60	71.65	71.45	71.50
015	67.5 Ci	68.83	68.75	69.33	69.25
		55.81	55.75	55.24	55.19
0[illegible]	45 Ci	33.57	33.64	33.58	33.64
015	22.5 Ci	-5.52	-5.39	-5.14	-5.02
		-3.44	-3.32	-4.22	-4.10
015	0.00 Ci	-21.29	-21.29	-21.46	-21.46
008	0.00 Ti	6.58	6.91	6.77	7.10
008	22.5 Ti	-0.50	-0.41	-0.59	-0.50
008	45.0 Ti	-13.36	-13.85	-13.12	-13.62
008	67.5 Ti	-19.33	-20.31	-18.90	-19.89
008	90.0 Ti	-15.26	-16.45	-15.47	-16.66

Table C2 cont'd

Gage Length	Gage Position & type	Replication # 3 measured	Replication # 3 corrected	Replication # 4 measured	Replication # 4 corrected
		0.49	0.60	0.09	0.20
031	22.5 Ti	-3.88	-3.74	-4.27	-4.13
		-12.58	-13.25	-12.60	-13.27
031	45 Ti	-13.62	-14.28	-13.59	-14.25
		-20.58	-21.87	-21.58	-22.87
031	67.5 Ti	-19.42	-20.72	-19.22	-20.52
015	90 Cm	76.06	76.02	76.07	76.03
015	67.5 Cm	60.29	60.31	60.37	60.40
015	45 Cm	23.61	23.65	23.35	23.39
015	22.5 Cm	-7.89	-7.86	-8.38	-8.34
015	0 Cm	-12.40	-12.41	-14.07	-14.08
015	22.5 Tm	-4.64	-4.51	-5.45	-5.32
015	45 Tm	-13.38	-13.69	-13.91	-14.21
015	67.5 Tm	-21.48	-22.31	-21.91	-22.74
015	90 Tm	-14.58	-15.67	-15.12	-16.20
015	0.00 Ti	5.98	6.27	5.29	5.58
		-29.98	-29.78	-30.81	-30.61
015	22.5 Ti	-27.00	-26.81	-26.73	-26.54
		-20.63	-21.03	-21.48	-21.38
015	45 Ti	-18.87	-19.28	-18.31	-18.72
		-4.64	-5.55	-5.24	-6.15
015	67.5 Ti	-7.32	-8.22	-7.26	-8.16
015	90.0 Ti	-28.59	-29.55	-28.00	-28.96
015	0 Tm	5.32	5.49	4.42	4.59
015	90.0 Ci	72.65	72.70	71.87	71.92
		69.21	69.13	69.16	69.08
015	67.5 Ci	55.05	55.00	53.62	53.56
015	45 Ci	31.99	32.06	31.38	31.44
		-4.97	-4.85	-4.74	-4.62
015	22.5 Ci	-6.04	-5.92	-5.13	-5.01
015	0.00 Ci	-20.67	-20.67	-20.66	-20.66
008	0.00 Ti	5.84	6.18	5.92	6.26
008	22.5 Ti	-1.17	-1.07	-0.34	-0.25
008	45.0 Ti	-13.92	-14.41	-13.17	-13.67
008	67.5 Ti	-20.75	-21.72	-20.15	-21.13
008	90.0 Ti	-16.35	-17.53	-15.77	-16.95

Table C2 cont'd

Gage length	Gage Position & type	average	corrected average	corrected variance	Std. dev'n
		0.04	0.15	2.45	
		-4.08	-3.94	2.40	
031	22.5 Ti	-2.02	-1.89	4.85	2.20
		-11.97	-12.64	0.70	
		-13.61	-14.27	0.38	
031	45 Ti	-12.79	-13.46	1.08	1.04
		-20.37	-21.66	0.66	
		-19.03	-20.33	0.30	
031	67.5 Ti	-19.70	-20.99	0.96	0.98
015	90 Cm	76.79	76.75	0.77	0.88
015	67.5 Cm	61.46	61.49	1.99	1.41
015	45 Cm	24.26	24.30	1.02	1.01
015	22.5 Cm	-7.41	-7.38	1.01	1.00
015	0 Cm	-12.84	-12.85	0.76	0.87
015	22.5 Tm	-4.23	-4.10	1.18	1.09
015	45 Tm	-12.85	-13.16	0.88	0.94
015	67.5 Tm	-21.00	-21.83	0.68	0.82
015	90 Tm	-14.00	-15.09	1.05	1.02
015	0.00 Ti	5.64	5.93	0.08	0.28
		-29.74	-29.54	1.80	
		-26.48	-26.30	1.60	
015	22.5 Ti	-28.11	-27.92	3.39	1.84
		-20.52	-20.92	0.88	
		-18.36	-18.77	0.72	
015	45 Ti	-19.44	-19.85	1.60	1.27
		-4.20	-5.11	1.32	
		-6.82	-7.72	1.10	
015	67.5 Ti	-5.51	-6.41	2.42	1.56
015	90.0 Ti	-27.88	-28.84	0.30	0.55
015	0 Tm	5.63	5.80	1.11	1.06
015	90.0 Ci	71.89	71.94	0.28	0.53
		69.13	69.05	28.74	
		54.93	54.88	29.09	
015	67.5 Ci	62.03	61.96	57.83	7.60
015	45 Ci	32.63	32.69	1.25	1.12
		-5.09	-4.97	0.07	
		-4.71	-4.59	0.56	
015	22.5 Ci	-4.90	-4.78	0.63	0.79
015	0.00 Ci	-21.02	-21.02	0.17	0.42
008	0.00 Ti	6.28	6.61	0.21	0.46
008	22.5 Ti	-0.65	-0.56	0.13	0.36
008	45.0 Ti	-13.39	-13.89	0.13	0.36
008	67.5 Ti	-19.78	-20.76	0.68	0.82
008	90.0 Ti	-15.71	-16.90	0.22	0.47

Appendix D: Listing of Computer Program and I/O Files for Chapter 4

The following pages contain the program and input files used in Chapter 4 for the method of weighted residuals solutions. The program is coded in Digital Vax Fortran v 4.0 language.

```
*+++++++++++++++++++++++++++++++++++++++++++++++++++++++++++++++++++++++++++C

C METHOD OF WEIGHTED RESIDUALS PROGRAM                                       C

C+++++++++++++++++++++++++++++++++++++++++++++++++++++++++++++++++++++++++++C

       implicit real*8 (a-h,o-z)

       integer n,iprint,intype,maxcal,ibound,lh,istate(100),iw(100),
     +liw,lw,ifail,mt(100),md(100),mn(100)
       real*8 gx(801,3003),gy(3003,501),
     +a(6,6),q(6,6),
       yy(100)

      common/stuff/ z(3003),y(3003),THeta(100),ex(100,12),SO(100),
     +g3(19001),b(19001),wkarea(6),
     +fz(100),e11,e22,e33,g12,g13,g23,v12,v13,v23,
     +rts(100,3),RL(3,3),CKm(100,3),clm(100,3),cmm(100,3),
     +R(19001),qb(6,6),
     +c(100,6,6),FW(8),thick,width

      common/int/ N2(2,12,11),N3(19001),n4(100),N5(100,3),N6(2,15),
     +n5i(100),nb(100),nf(100,2),np3l(10,100),n5j(100),
     +np3,np4,np3d,np4d,np1,nc,kn,nfz

      COMMON e(1,2100),PK(2,4,3003),PM(2,4,3003),PL(2,4,3003),
     +g1(1,3003),c11,C12,C13,C23,C22,C33,C66,c55,c44


       open (unit=1, file='mwrin.dat', status='old')
       open (unit=5, file='mwr.dat', status='old')
       open (unit=2, file='file2.dat', status='old')
       open (unit=3, file='file3.dat', status='old')
       open (unit=6, file='mwrout.dat', status='old')

c   input data for housekeeping tasks from file mwr.dat

      read(5,90)(((N2(K,I,J),J=1,11),I=1,12),K=1,2)
      read(5,91)((N6(K,J),J=1,15),K=1,2)
      read(5,92)((Q(i,j),i=1,6),j=1,6)
      read(5,93)((CKM(i,j),j=1,3),i=1,5)
      read(5,93)((CLM(i,j),j=1,3),i=1,5)
      read(5,94)((rl(i,j),j=1,3),i=1,3)
      read(5,93)((rts(i,j),j=1,3),i=1,5)
      read(5,95)(NB(I),I=1,10)
      read(5,96)((NP3L(I,J),J=1,6),I=1,10)

      read(5,97)((NF(I,K),k=1,2
     +),I=1,10)
      read(5,99)((ex(i,j),j=1,12),i=1,2)

       PI=3.14159265358979323846D00
90    format(24(/11i3))
91    format(2(/15i3))
92    format(2(/18f3.0))
93    format(/15f3.0)
```

```
94    format(/9f3.0)
95    format(/10i3)
96    format(3(/18i3),/6i3)
97    format(10(/2i3))
99    format(2(/12f3.0))

C-----------computational dimensions

      NP3D=501
      NFUNC=0
      NP4D=801
      N5D=2001
      NP1D=100
      NCD=300
      NG=50000
      NEQ=2100

      NQ1=1
      REWIND6
      IF(NQ1.EQ.1)WRITE(6,604)(((N2(K,I,J),J=1,11),I=1,12),K=1,2)
 604  FORMAT(/'           N2 ARRAY'/
     +2(12(11I4/)/))
      WRITE(6,605)(NB(I),I=1,10),((NF(I,K)
     +,K=1,2),I=1,10),
     +((NP3L(I,J),J=1,2),I=1,10)
 605  FORMAT(/'  NBOTTOM'//10I3//
     +'  NFUNCTION '//10(/3I3,4X,3I3)//
     +'  NP3L   '//10(/2I3)//
     +'  NP3U   '//10(/2I3,4X,2I3,4X,2I3))


c -------> Input problem data from mwrin.dat

      REWIND1
      read(1,*)
      READ(1,*)NP1
      do 992 i=1,10
      do 992 j=1,np1
      np31(i,j)=0
 992   continue
      read(1,*)NPTY
      READ(1,*)NPTZz

      READ(1,*)(N5I(1))
      n5x=n5i(1)

       IF(NP1.GT.NP1D)GOTO 1004
      IF(NP1*21.GT.NEQ)GOTO 1006
      READ(1,*)
      READ(1,*)(THETA(I),I=1,NP1)
      READ(1,*)WIDTH
      READ(1,*)SK
      READ(1,*)THICK
      READ(1,*)EXx
      read(1,*)(s0(i),i=1,6)
      READ(1,*)E11
      READ(1,*)E22
      READ(1,*)E33
```

```
      READ(1,*)V12
      READ(1,*)V23
      READ(1,*)V13
      READ(1,*)G12
      READ(1,*)G23
      READ(1,*)G13
      READ(1,*)FWEIGHT
      READ(1,*)NC
      IF(NF(NC,1).EQ.2.AND.NC.EQ.1.AND.N5I(1)/2
     +.NE.FLOAT(N5I(1))/2.)GOTO 1200
      READ(1,*)
      READ(1,*)(FW(I),I=1,8)
      READ(1,*)MWRSOLV
      READ(1,*)N5J(1),n5j(2)
      read(1,*)ffz
      Read(1,*)ee

      ex(1,1)=exx
           RATT=WIDTH/THICK
           RATW=THICK/WIDTH
      nptz=nptzz*np1+1
      ZH=THICK/(nptz-1.)
      yy(1)=0


      jj=2
 67   yy(jj)=((jj-1.)/(nptzz/2.-1.))**sk*width
      jj=jj+1
      if(yy(jj-1).lt.width)goto 67
      yy(jj-1)=width
      npty=jj-1
      print*,npty

      WRITE(6,234)THETA(1),THeta(100),width,THICK,ex(1,1)
 234  FORMAT(
     +/' THETA(1)=',E12.5,'    THeta(100)=',E12.5,
     +/'     W=',E12.5,'     T=',E12.5,'    EX=',E12.5)


C-------- EVALUATE STIFFNESS MATRIX IN PRINCIPAL COORDINATES

      CALL STIFF

C---------> Get stiffness matrices for layers and calculate
           roots of charateristic equations

       kn=2
      do 412 j=1,np1
       IF(THETA(J).ne.0.and.theta(j).ne.90)KN=1
 412  continue

      DO 411 J=1,NP1
      CALL EDGE(J)
      IF(NQ1.EQ.1)WRITE(6,45)((C(J,KK,LL),LL=1,6),KK=1,6)
 45   FORMAT(/'    C MATRIX     '//6(6E12.4/)/)

      IF(N5I(1).EQ.0)GOTO 411
      CALL ROOTS(J)
```

```
 411   CONTINUE

 443  FORMAT(/'    L IJ MATRIX'/3(/3E12.5))
      WRITE(6,444)(((RTS(II,JJ)),JJ=1,3),II=1,NP1)
 444  FORMAT(/'    ROOTS1'/5(/3E12.5))
      WRITE(6,445)(((CKM(II,JJ)),JJ=1,3),II=1,NP1),
     +(((CLM(II,JJ)),JJ=1,3),II=1,NP1)
 445  FORMAT(/'    CKM AND CLM   '/10(/3E12.5))


      DO 23 I=1,NP1
      IF(N5(I,1)+N5(I,2)+N5(I,3)+NP3L(NC,I).GT.N5D)GOTO 1018
 23   CONTINUE

      WRITE(6,446)((N5(KK,LL),LL=1,3),KK=1,NP1)
 446     FORMAT(//'      N5'/5(/3I4))


  c-------> Get laminate strains and stiffness matrices

      CALL FLEx(a,q)
      if(np3l(nc,1).eq.0)goto 454
      do 453 kk=2,12
      do 453 jj=1,np1
      ex(jj,kk)=0.0
 453  continue

      ex(1,1)=exx
 454  continue
      SIGMAXO=ex(1,1)*E22

      IF(MWRSOLV.EQ.2)GOTO 998
      WRITE(6,47)ex(1,1),SIGMAXO
      PRINT47,ex(1,1),SIGMAXO
      WRITE(6,47) ex(1,1),A(1,1),SIGMAXO
 47   FORMAT(' EX=',E12.5,' A(1,1)=',E12.5,'  SIGMA XO=',E12.5)

C-------> Generate collocation points

      WRITE(6,186)NPTY,NPTZ
 186  FORMAT(/'  NPTY=',I5,10X,'  NPTZ=',I5/)

C-------> Calculate total number of points: npts

      N62=(NPTZ-NP1-1)/NP1
      IF(NPTZ.EQ.0)N62=0
      NPTS=(NP1+NB(NC))*NPTY+NPTZ-NP1-NB(NC)
      IF(NPTZ.EQ.0)NPTS=NPTS+NP1+NB(NC)
      WRITE(6,183)NPTS
 183  FORMAT(/'   NPTS=',I5/)


C--------> Fill N4 Matrix

      N4(1)=2*NPTY+N62
      N99=N4(1)
      IF(NP1.EQ.2)GOTO 43
```

```
      DO 42 IJ=2,NP1
      N4(IJ)=NPTY+N62
      IF(IJ.NE.NP1)N99=N99+N4(IJ)
42    CONTINUE
43    CONTINUE
      N4(NP1)=N62+1+NB(NC)*(NPTY-1)
      N99=N99+N4(NP1)
      PRINT6789,NPTS,N99
6789  FORMAT( //'  NPTS=',I5,'  N99=',I5)

      IF(SK.GT.0)X0=WIDTH/((1+SK)**(NPTY-1)-1)/SK

      zhh=zh
      IF(NPTZ.EQ.0)ZH=THICK/npi
      I5=1

      Z1=THICK/(NB(NC)+1.)
      DO 69 I=1,NP1+NB(NC)
      Y1=0.
      YH=width/(npty-1)
      jj=npty
      DO 68 J=1,NPTY-1
      IF(SK.le.0)Y(I5)=Y1
      y(i5)=width-yy(jj)
      jj=jj-1

      Y1=Y1+YH
      Z(I5)=Z1
      i5=i5+1
68    CONTINUE
      Z(I5)=Z1
      Y(I5)=WIDTH
      I5=I5+1
      IF(N62.EQ.0)GOTO 79
      DO 71 J=1,N62
      Z1=Z1-ZH
      Y(I5)=WIDTH
      Z(I5)=Z1
      IF(I.EQ.NP1+NB(NC).AND.NB(NC).NE.0)GOTO 826
      I5=I5+1
71    CONTINUE
79    CONTINUE
      Z1=Z1-ZH
69    CONTINUE
      Y(NPTS)=WIDTH
      Z(NPTS)=0.

826      CONTINUE

C-------> Fill N3 matrix-equations at a point


      N3(1)=9
      DO 70 I=2,NPTY-1
      N3(I)=2
70    CONTINUE

      N3(NPTY)=5
      mt(1)=n6(kn,9)+(npty-2)*n6(kn,2)+n6(kn,5)+
```

```
     +n6(kn,3)*n62
c      IF(NPTZ.EQ.0)N3(NPTY)=2
      I5=NPTY+1
      IF(N62.EQ.0)GOTO 86
      DO 74 I=1,N62
      N3(I5)=3
      I5=I5+1
 74   CONTINUE
 86   CONTINUE
      DO 76 I=2,NP1
      N3(I5)=11
      I5=I5+1
      DO 75 J=2,NPTY-1
      N3(I5)=4
      I5=I5+1
 75   CONTINUE
      N3(I5)=6
      IF(NPTZ.EQ.0)N3(I5)=4
      I5=I5+1

      IF(N62.EQ.0)GOTO 87
      DO 77 II=1,N62
      N3(I5)=3
      I5=I5+1
 77   continue
      md(i-1)=n6(kn,11)+(npty-2)*n6(kn,4)+n6(kn,6)
      mt(i)=n6(kn,3)*n62
 76   CONTINUE
 87   CONTINUE
      IF(NB(NC).EQ.0)THEN
      mt(np1)=mt(np1)+n6(kn,10)
      N3(NPTS)=10
      ELSE
      N3(I5)=9
      mt(np1)=mt(np1)+n6(kn,9)+(npty-2)*n6(kn,2)+n6(kn,5)
      I5=I5+1
      DO 181 I=2,NPTY-1
      N3(I5)=2
      I5=I5+1
 181   CONTINUE
      N3(I5)=5
      IF(NPTZ.EQ.0)N3(I5)=2
       ENDIF
        write(6,177)(mt(jj),jj=1,np1),(md(jj),jj=1,np1),
     +(mn(jj),jj=1,np1)

C-------> Evaluate the total number of equations: NP4

      NP4=0
      I89=1
       DO 416 I87=1,NP1
      DO 416 I88=1,N4(I87)
      IF(N3(I89).EQ.0)GOTO 416
      NP4=NP4+N6(KN,N3(I89))
       I89=I89+1
 416  CONTINUE

      PRINT417,NP4
      WRITE(6,417)NP4
```

```
      WRITE(6,442)(N4(IJ),IJ=1,NP1)
 442  FORMAT(/' N4 ARRAY---->',20(5I5/))
 417  FORMAT(/'   NP4=',I5/)



      WRITE(6,188)
 188  FORMAT(/'      N3 ARRAY  '/)
      WRITE(6,187)(N3(I),I=1,NPTS)
 187  FORMAT(/24I5/)
      WRITE(6,190)
 190  FORMAT(/'                N6 ARRAY'/)
      WRITE(6,101)((N6(II,I),I=1,15),II=1,2)
 101  FORMAT(15I5)
      WRITE(6,9999)
 9999    FORMAT(//)
      WRITE(6,9999)

      I2=1
      DO 80 I=1,NPTS
      WRITE(6,81)I,Z(I),Y(I),I2,N3(I),(N2(KN,N3(I),J),J=1,N6(
     +KN,N3(I)))
      I2=I2+N6(KN,N3(I))
 80   CONTINUE
 81   FORMAT(I5,2E12.5,13I5)


      NP3D=501
      NP4D=801
       ih0=0
 123  continue
      ih0=ih0+1
      n=1

        do 602 kj=1,3
      DO 602 KL=1,NP1
      n5(kl,kj)=0
      if(kj.ge.kn)N5(KL,KJ)=N5I(1)
602   continue

      do 603 kj=1.3
      n5(np1,kj)=n5i(1)/(2-nb(nc))
 603  continue

C-------> Evaluate the total number of DOF: NP3

      NP3=0
      DO 41 I=1,NP1
      mn(i)=0
      DO 40 J=1,3
      NP3=NP3+N5(I,J)
      mn(i)=mn(i)+n5(i,j)
 40   CONTINUE
      mn(i)=mn(i)+np3l(nc,i)
      NP3=NP3+NP3L(NC,I)
 41   CONTINUE
      if(mn(1)*2.gt.np3d)goto 2031
      PRINT186,NP3
```

```
 177  format(/' mt'/10i5/'md'/10i5/'mn'/10i5)
      WRITE(6,185)NP3
 185  FORMAT(/'  NP3=',I5/)
c      IF(NP3.GT.NP3D)GOTO 1002
      if(n5i(1).eq.0)goto 660

c-------> Set initial frequency vector

      j=1
      RYZ=(PI/Thick/(2.-nb(nc))/ffz*np1)
      do 31 k=1,n5i(1)/nf(nc,1)
      fz(k)=k*ryz
 31   continue
      nfz=n5i(1)/nf(nc,1)
      n=nfz

c-------> Get initial G matrix and r vector

         DO 904 I=1,NP3
           G3(I)=0.0
 904       CONTINUE

          DO 903 I=1,NP4
           R(I)=0.0
 903       CONTINUE

 660   continue

      call funct(iflag,n,mt,md,mn,gx,gy,xran,zh,yh)
 12   continue


c-------> Minimize r2 with respect to the k vector

      do 991 i=1,np4
      b(i)=r(i)
991   continue

      call givens(mt,md,mn,gx,gy)
         r2=0.
       do 456 ii=np3+1,np4
       r2=r2+r(ii)**2
 456   continue
       r2=sqrt(r2/np4)
       print133,r2
c      print133,sqrt(sig**2*(np4-ir)/np4),ir
133    format(//' residual :',f10.5, ' rank',i3)
      ffz=ffz+.1
      if(ih0.le.0)goto 123
      WRITE(6,124)
 124  FORMAT(/'    R VECTOR (OUTPUT)'/)
      WRITE(6,105)(B(KO),KO=1,NP3)
 105  FORMAT(E22.12/)
      rewind3

      WRITE(3,*)(B(I),I=1,NP3)
      if(nfz.ne.0)write(3,*)(fz(i),i=1,nfz)
      write(3,*)(y(i),i=1,npty)
      ijk=npty+(nptz-1)/2
```

```
      write(3,*)(z(i),i=npty,ijk),
     +(z(i),i=ijk+npty,ijk+npty+(nptz-1)/2)
      close (unit=3, status='save')

C--------------> OUTPUT TO FILE TAPE 2 FOR POSTPROCESSING

      REWIND2
      WRITE(2,*)NP1,NPTY,NPTZ,NP3,NP4,width,SK,THICK,
     +((ex(i,j),i=1,np1),j=1,12)
     +,A(1,1),
     +SIGMAX0,E11,E22,E33,V12,V13,V23,G12,G13,G23,
     +(THFTA(I),I=1,NP1),((((C(I,J,K)),K=
     +1,6),J=1,6),I=1,NP1),((N5(I,J),J=1,3),I=1,NP1),
     +(((RTS(I,J)),J=1,3),I=1,NP1),
     +(((CKM(I,J)),J=1,3),I=1,NP1),
     +(((CLM(I,J)),J=1,3),I=1,NP1),
     +(((CMM(I,J)),J=1,3),I=1,NP1),
     +KN,NFUNC,(NB(I),I=1,10),((NF(I,K),
     +K=1,2),
     +I=1,10),((NP3L(I,J),J=1,np1),I=1,10),
     +NC,MWRSOLV,(N5J(I),I=1,2),(nfz,j=1,np1),
     +(s0(i),i=1,6),0,0,0,0,0

            GOTO 997

  998 CONTINUE

      REWIND2
      WRITE(2,*)NP1,NPTY,NPTZ,NP3,NP4,width,SK,THICK,ex(1,1),
     +A(1,1),
     +SIGMAX0,E11,E22,E33,V12,V13,V23,G12,G13,G23,
     +(THETA(I),I=1,NP1),((((C(I,J,K)),K=
     +1,6),J=1,6),I=1,NP1),((N5(I,J),J=1,3),I=1,NP1),
     +(((RTS(I,J)),J=1,3),I=1,NP1),
     +(((CKM(I,J)),J=1,3),I=1,NP1),
     +(((CLM(I,J)),J=1,3),I=1,NP1),
     +(((CLM(I,J)),J=1,3),I=1,NP1),
     +KN,NFUNC,(NB(I),I=1,10),((NF(I,K),
     +K=1,2),
     +I=1,10),((NP3L(I,J),J=1,np1),I=1,10),
     +NC,MWRSOLV,(N5J(I),I=1,2)
  997       CONTINUE

      close (unit=2, status='save')

C-------> Error messages

      GO TO 999
 1000 FORMAT('    ERROR NOT ENOUGH EQUATIONS!!!!!!!')
 2000 CONTINUE
      PRINT1000
      WRITE(6,1000)
      GOTO 999
 1001 FORMAT('     ERROR TOO MANY EQUATIONS!!!!!')
 1002 PRINT1003,NP3,NP3D
      WRITE(6,1003)NP3,NP3D
 1003 FORMAT('  NP3 EXCEEDS DIMENSION NP3D! NP3=',I5,'  NP3D=',I5)
      GOTO 999
```

```
 1200 WRITE(6,2200)
 2200 FORMAT('      ERROR   N5I(1) MUST BE EVEN!!!')
      GOTO 999
 1004 PRINT1005,NP1,NP1D
      WRITE(6,1005)NP1,NP1D
 1005 FORMAT('NP1=',I5,' EXCEEDS DIMENSION NP1D=',I5)
      GOTO 999
 1006 PRINT1007,NP1*21,NEQ
      WRITE(6,1007)NP1*21,NEQ
 1007 FORMAT(' NP1*21=',I5,'  EXCEEDS DIMENSION NEQ=',I5)
      GOTO 999
 1008 PRINT1009,N99,NCD
      WRITE(6,1009)N99,NCD
 1009 FORMAT('  # COORDINATE POINTS=',I5,
     +'   EXCEEDS DIMENSION NCD=',I5)
      GOTO 999
 1010 PRINT1011,mt(1)+2*md(1),2*mn(1),NP3D,NP4D
      WRITE(6,1011)NP4,NP3,NP3D,NP4D
      GOTO 999
 1012 PRINT1013,NPTZ
      WRITE(6,1013)NPTZ
 1013 FORMAT(/'  ERROR------NPTZ=',I5,'   NPTZ MUST BE AN ODD #!'/)
 1011 FORMAT(/'  DIMENSIONS ARE TOO SMALL: NP4,NP3=',2I5,
     +' NP3D,NP4D=',2I5)
      GOTO 999
 1016 PRINT1017,NP4,NP4D
      WRITE(6,1017)NP4,NP4D
      GOTO 999
 1020 PRINT2020,NP3,I10
 2020 FORMAT(///'   ERROR I10=',I3,'  GT  NP3=',I3,'!!!!')
      GOTO 999
 1018 PRINT1019
 1019 FORMAT(/'  ERROR N5 IS TOO BIG!!!!'/)
      GOTO 999
 1017 FORMAT(/'  ERROR!    NP4=',I4,' > NP4D=',I4/)
 1021 WRITE(6,2021)NPTZ,N5I(KL)
 2021 FORMAT(//'  ERROR: ALIASING ERROR....INCREASE NPTZ!!',2I3)
      goto 999
 2031 write(6,1031)2*mn(1),np3d
 1031 format(//' ERROR: GY EXCEEDS DIMENSION 2*MN='
     +,i5,'  NP3D=',i5//)
 999  CONTINUE
      stop
      end

c*********************************************************************
      Subroutine funct(iflag,n,mt,md,mn,gx,gy,xran,zh,yh)
c*********************************************************************
      implicit real*8 (a-h,o-z)
      integer*4 iran
      real*8 gx(801,3003),gy(3003,501),xran(10)
      Integer md(100),mt(100),mn(100)
      common/stuff/ z(3003),y(3003),THeta(100),ex(100,12),S0(100),
     +G3(19001),b(19001),wkarea(6),
     +fz(100),e11,e22,e33,g12,g13,g23,v12,v13,v23,
     +rts(100,3),RL(3,3),CKm(100,3),clm(100,3),cmm(100,3),
     +R(19001),qb(6,6),
     +c(100,6,6),FW(8),thick,width
      common/int/ N2(2,12,11),N3(19001),n4(100),N5(100,3),N6(2,15),
```

```
     +n5i(100),nb(100),nf(100,2),np31(10,100),n5j(100),
     +np3,np4,np3d,np4d,np1,nc,kn,nfz
      COMMON e(1,2100),PK(2,4,3003),PM(2,4,3003),PL(2,4,3003),
     +g1(1,3003),c11,C12,C13,C23,C22,C33,C66,c55,c44

      iran=12345
      I1=1
      I10=0
      NPT=0
      I6=0
      I7=0
      I8=1
      ixx=0
      k0=1
      i1min=9999999
      i1max=0
      DO 1 K=1,NP1
      i0=1
      i2=0
      mdx=0
      if(k.ne.1)mdx=md(k-1)
      DO 4 I=1,N4(K)
      if(i0.gt.mt(k).and.k.ne.np1)i2=1
      NPT=NPT+1
      I3=NPT

C-------> LOOP FOR # EQNS FOR CASE OF POINT I3

C-------> CALCULATE P MATRICES FOR POINT I3

      I4=N3(I3)
      rw1=1
      if(width-y(i3).gt.4*thick/np1)rw1=thick/np1/
     +(width-4*thick/np1)
c       if(k.ne.1)rw1=1./(1+i2)

      DO 2 J=1,11

      if(int(z(i3)/np1).eq.z(i3)/np1
     +.and.y1.ne.width)then
 56   y1=y(i3)+(y(i3+1)-y(i3))/n6(kn,n3(i3))*(j-1)

      else
      Y1=Y(I3)
      endif
      IF(N3(I3).EQ.0) GOTO 4
      z1=z(i3)
      if(int(z(i3)/np1).ne.z(i3)/np1)Z1=z(i3)+zh*(2.*ran(iran)-1.)

       CALL TFUNC(K,Z1,Y1)
      IF(N2(KN,I4,J).EQ.0.AND.J.GT.N6(KN,I4))GOTO 4
      N11=N2(KN,I4,J)
      IF(N11.LT.9.OR.N11.GT.11)GOTO 568
      I10=I10+1
c      N10(I10)=I1
```

```
 568  CONTINUE
C-------> GET E VECTOR FOR POINT CASE
      N1=N2(KN,I4,J)
      CALL EQNS(K,N1,I1,RW,RW1,z1)
 102  FORMAT(4(9E8.2/)/)

C-------> GET G1 VECTOR FOR POINT CASE [G1]=[E][P]
      CALL MATMULT(K)
C-------> PUT G1 VECTOR INTO ROW OF G
      rt=0
      do 12 kk=k0,k0+mn(k)+i2*mn(k+1)-1
      rt=rt+g1(1,kk)**2
   12 continue
      rt=sqrt(rt)
      G2=0
      DO 3 K1=k0,k0+mn(k)+i2*mn(k+1)-1
      if(i1.le.k1)then
      k1y=k1-int((i1-.1)/mn(1))*mn(1)
      gy(i1,k1y)=g1(1,k1)/rt
      else
      if(k1.gt.k0+mn(k)-1)then
      i1x=i1-ixx-mt(k)-mdx
      else
      i1x=i1-ixx
      endif
      if(i1x.gt.np4d)goto 2031
      if(i1x.gt.i1max)i1max=i1x
      if(i1x.lt.i1min)i1min=i1x

      gx(i1x,k1)=g1(1,k1)/rt
      endif
      G3(K1)=G3(K1)+G1(1,K1)
      IF(G1(1,K1).NE.0.)I6=I6+1
      G2=G2+ABS(G1(1,K1))
 3    CONTINUE
      I7=I7+1
      IF(G2.EQ.0.)PRINT2002,I1
      IF(G2.EQ.0.)WRITE(6,2002)I1
 2002 FORMAT('  ROW #',I3,' IS ALL ZEROES! ')
      r(i1)=r(i1)/rt
      I1=I1+1
      i0=i0+1
 2    CONTINUE
 4    continue
      ixx=ixx+mt(k)+mdx
      k0=k0+mn(k)
 1    CONTINUE
      print*
      print*,i1min,i1max

      DO 5 I=1,NP3
```

```
      IF(G3(I).EQ.0.)PRINT 2003,I
      IF(G3(I).EQ.0.)WRITE(6,2003)I
 5    CONTINUE


 2003 FORMAT('   COLUMN #',I5,' IS ALL ZEROES!!')

C----------> END OF [G] FORMULATION LOOP

      IF(I1.LT.(NP4+1))PRINT1000
      IF(I1.LT.(NP4+1))WRITE(6,1000)
      IF(I1.GT.(NP4+1))PRINT1001
      IF(I1.GT.(NP4+1))WRITE(6,1001)
66    continue

C--------------- ERROR MESSAGES
         GO TO 9999
 1000 FORMAT('    ERROR NOT ENOUGH EQUATIONS!!!!!!!')
 2000 CONTINUE
      PRINT1000
      WRITE(6,1000)
      GOTO 999
 1001 FORMAT('     ERROR TOO MANY EQUATIONS!!!!!')
 1002 PRINT1003,NP3,NP3D
      WRITE(6,1003)NP3,NP3D
 1003 FORMAT('  NP3 EXCEEDS DIMENSION NP3D! NP3=',I5,'  NP3D=',I5)
      GOTO 999
 1200 WRITE(6,2200)
 2200 FORMAT('      ERROR   N5I(1) MUST BE EVEN!!!')
      GOTO 999
 1004 PRINT1005,NP1,NP1D
      WRITE(6,1005)NP1,NP1D
 1005 FORMAT('NP1=',I5,' EXCEEDS DIMENSION NP1D=',I5)
      GOTO 999
 1006 PRINT1007,NP1*21,NEQ
      WRITE(6,1007)NP1*21,NEQ
 1007 FORMAT(' NP1*21=',I5,'  EXCEEDS DIMENSION NEQ=',I5)
      GOTO 999
 1008 PRINT1009,N99,NCD
      WRITE(6,1009)N99,NCD
 1009 FORMAT('  # COORDINATE POINTS=',I5,
     +'   EXCEEDS DIMENSION NCD=',I5)
      GOTO 999
 1010 PRINT1011,NP4,NP3,NP3D,NP4D
      WRITE(6,1011)NP4,NP3,NP3D,NP4D
      GOTO 999
 1012 PRINT1013,NPTZ
      WRITE(6,1013)NPTZ
 1013 FORMAT(/'  ERROR-----NPTZ=',I5,'   NPTZ MUST BE AN ODD #!'/)
 1011 FORMAT(/'  DIMENSIONS ARE TOO SMALL: NP4,NP3=',2I5,
     +' NP3D,NP4D=',2I5)
      GOTO 999
 1016 PRINT1017,NP4,NP4D
      WRITE(6,1017)NP4,NP4D
      GOTO 999
 1020 PRINT2020,NP3,I10
 2020 FORMAT(///'   ERROR I10=',I3,'  GT  NP3=',I3,'!!!!')
      GOTO 999
 1018 PRINT1019
```

```
 1019 FORMAT(/'  ERROR N5 IS TOO BIG!!!!'/)
      GOTO 999
 1017 FORMAT(/'  ERROR!    NP4=',I4,' > NP4D=',I4/)
 1021 WRITE(6,2021)NPTZ,N5I(KL)
 2021 FORMAT(//'  ERROR: ALIASING ERROR....INCREASE NPTZ!!',2I3)
      goto 999
 2031 write(6,1031)i1x,np4d
 1031 format(//' ERROR: rows EXCEED DIMENSION FOR GX-
     +I1X=',i5,'  NP4D=',i5)
 999  stop
 9999 return
      END

C******************************************************************************C
      SUBROUTINE EDGE(N)
C******************************************************************************C

      IMPLICIt real*8 (A-H,O-Z)

      common/stuff/ z(3003),y(3003),THeta(100),ex(100,12),S0(100),
     +G3(19001),b(19001),wkarea(6),
     +fz(100),e11,e22,e33,g12,g13,g23,v12,v13,v23,
     +rts(100,3),RL(3,3),CKm(100,3),clm(100,3),cmm(100,3),
     +R(19001),qb(6,6),
     +c(100,6,6),FW(8),thick,width
      COMMON e(1,2100),PK(2,4,3003),PM(2,4,3003),PL(2,4,3003),
     +g1(1,3003),c11,C12,C13,C23,C22,C33,C66,c55,c44
        common/int/ N2(2,12,11),N3(19001),n4(100),N5(100,3),N6(2,15),
     +n5i(100),nb(100),nf(100,2),np31(10,100),n5j(100),
     +np3,np4,np3d,np4d,np1,nc,kn,nfz

      PI=3.14159265358979323846
      T=THETA(N)*PI/180.
      C4=cos(T)**4
      S4=sin(T)**4
      S2=sin(T)**2
      C2=cos(T)**2
      C1=cos(T)
      S1=sin(T)
      C3=cos(T)**3
      S3=sin(T)**3

      DO 10 I=1,6
      DO 10 J=1,6
      C(N,I,J)=0.0
 10    CONTINUE

      C(N,1,1)=C11*C4+C22*S4+2*(C12+2*C66)*C2*S2
      C(N,1,2)=(C11+C22-4*C66)*S2*C2+C12*(S4+C4)
      C(N,1,3)=C2*C13+C23*S2
      C(N,1,6)=(C11-C12-2*C66)*S1*C3+(C12-C22+2*C66)*S3*C1
      C(N,2,2)=C11*S4+C22*C4+2*(C12+2*C66)*S2*C2
      C(N,2,3)=C23*C2+C13*S2
      C(N,2,6)=(C11-C12-2*C66)*S3*C1+(C12-C22+C66*2)*S1*C3
      C(N,3,3)=C33
      C(N,3,6)=(C13-C23)*C1*S1
      C(N,4,4)=C44*C2+C55*S2
      C(N,4,5)=-C44*C1*S1+C55*S1*C1
      C(N,5,5)=C44*S2+C55*C2
```

```
      C(N,6,6)=C11*S2*C2+C22*C2*S2-2*C12*S2*C2+C66*(C4-2*S2*C2+S4)
      IF(THETA(N).EQ.90.)THEN
      C(N,1,1)=C(N,3,3)
      C(N,1,2)=C(N,2,3)
      C(N,4,4)=C(N,6,6)
      C(N,1,6)=0.
      C(N,2,6)=0.
      C(N,3,6)=0.
      C(N,4,5)=0.
      ELSE
      IF(THETA(N).NE.0)GOTO 22
      C(N,2,2)=C(N,3,3)
      C(N,1,2)=C(N,1,3)
      C(N,5,5)=C(N,6,6)
      C(N,1,6)=0.
      C(N,2,6)=0.
      C(N,3,6)=0.
      C(N,4,5)=0.
 22   CONTINUE
      ENDIF

C        TRANSPOSE FOR SYMMETRY

      DO 1 I=2,6
      DO 1 J=1,I-1
      C(N,I,J)=C(N,J,I)
 1    CONTINUE
      RETURN
      END


C*****************************************************************
      SUBROUTINE EQNS(K,N1,N,RW,RW1,z1)
C*****************************************************************
      IMPLICIt real*8 (A-H,O-Z)

      common/stuff/ z(3003),y(3003),THeta(100),ex(100,12),S0(100),
     +G3(19001),b(19001),wkarea(6),
     +fz(100),e11,e22,e33,g12,g13,g23,v12,v13,v23,
     +rts(100,3),RL(3,3),CKm(100,3),clm(100,3),cmm(100,3),
     +R(19001),qb(6,6),
     +c(100,6,6),FW(8),thick,width
      COMMON e(1,2100),PK(2,4,3003),PM(2,4,3003),PL(2,4,3003),
     +g1(1,3003),c11,C12,C13,C23,C22,C33,C66,c55,c44
      common/int/ N2(2,12,11),N3(19001),n4(100),N5(100,3),N6(2,15),
     +n5i(100),nb(100),nf(100,2),np31(10,100),n5j(100),
     +np3,np4,np3d,np4d,np1,nc,kn,nfz

      nN2=(K-1)*21
      RW=1.

      DO 22 I=1,NP1*21
      E(1,I)=0.0
 22   CONTINUE
      GOTO(1,2,3,4,5,6,7,8,9,10,11,12,13,14,15,16)N1
C GOVERNING EQN #1
 1    E(1,nn2+5)=C(K,5,5)
      E(1,nn2+12)=C(K,4,5)
```

```
      E(1,nn2+6)=C(K,6,6)
      E(1,nn2+13)=C(K,2,6)
      E(1,nn2+21)=C(K,3,6)+C(K,4,5)
      GOTO 999
C GOVERNING EQN #2
 2    E(1,nn2+5)=C(K,4,5)
      E(1,nn2+12)=C(K,4,4)
      E(1,nn2+6)=C(K,2,6)
      E(1,nn2+13)=C(K,2,2)
      E(1,nn2+21)=C(K,2,3)+C(K,4,4)
      GOTO 999
C GOVERNING EQN #3
 3    E(1,nn2+19)=C(K,3,3)
      E(1,nn2+20)=C(K,4,4)
      E(1,nn2+7)=C(K,3,6)+C(K,4,5)
      E(1,nn2+14)=C(K,2,3)+C(K,4,4)
      GOTO 999
C BC #1 SIGMA Z=0
 4    E(1,nn2+3)=c(k,3,6)
      E(1,nn2+8)=C(K,3,6)
      E(1,nn2+10)=C(K,2,3)
      E(1,nn2+18)=C(K,3,3)
      E(1,nn2+1)=C(K,1,3)
      CALL EMULT(K,3,RX,Z1)
      R(N)=-RX
      RW=FW(5)
      GOTO 999
C BC #2 TAU XZ=0
 5    E(1,nn2+11)=C(k,4,5)
      E(1,nn2+17)=C(K,4,5)
      E(1,nn2+4)=c(k,5,5)
      E(1,nn2+15)=C(K,5,5)
      RW=FW(7)
      GOTO 999
C BC #3 TAU YZ=0
 6    E(1,nn2+11)=c(k,4,4)
       E(1,nn2+17)=C(K,4,4)
      RW=FW(8)
      E(1,nn2+4)=c(k,4,5)
      E(1,nn2+15)=C(K,4,5)
      GOTO 999
C BC #4 SIGMA Y=0
    7 CALL EMULT(K,2,RX,Z1)
      R(N)=-Rx
      E(1,nn2+1)=C(K,1,2)
      RW=FW(4)
      E(1,nn2+3)=c(k,2,6)
      E(1,nn2+8)=C(K,2,6)
      E(1,nn2+10)=C(K,2,2)
      E(1,nn2+18)=C(K,2,3)
      GOTO 999
C BC #5 TAU YX=0
   8  CALL EMULT(K,6,RX,Z1)
      R(N)=-RX
      E(1,nn2+1)=C(K,1,6)
      RW=FW(6)
      E(1,nn2+3)=c(k,6,6)
      E(1,nn2+8)=C(K,6,6)
      E(1,nn2+10)=C(K,2,6)
```

```
      E(1,nn2+18)=C(K,3,6)
      GOTO 999
C BC#6 (U+)-(U-)=0
 9    E(1,nn2+2)=1.0
      RW=FW(1)
      E(1,nn2+21+2)=-1.0
      GOTO 999
C BC#7 (V+)-(V-)=0
 10   E(1,nn2+9)=1.0
      RW=FW(2)
      E(1,nn2+9+21)=-1.0
      GOTO 999
C BC#8 (W+)-(W-)=0
 11   E(1,nn2+16)=1.0
      RW=FW(3)
      E(1,nn2+16+21)=-1.0
      GOTO 999
C BC #9 (SIGMA Z+)-(SIGMA Z-)=0
 12     E(1,nn2+3)=c(k,3,6)
        E(1,nn2+8)=C(K,3,6)
      E(1,nn2+1)=C(K,1,3)
      RW=FW(5)
      E(1,nn2+10)=C(K,2,3)
      E(1,nn2+18)=C(K,3,3)
      CALL EMULT(K,3,RX,Z1)
      E(1,nn2+18)=C(K,3,3)
      R(N)=-RX*1.0D00
      E(1,nn2+3+21)=-c(k+1,3,6)
      E(1,nn2+8+21)=-C(K+1,3,6)
      E(1,nn2+1+21)=-C(K+1,1,3)
      E(1,nn2+10+21)=-C(K+1,2,3)
      E(1,nn2+18+21)=-C(K+1,3,3)
      CALL EMULT(K+1,3,RX,Z1)
      R(N)=R(N)+RX*1.0D00
      GOTO 999
C BC # 10 (TAU XZ+)-(TAU XZ-)=0
 13     E(1,nn2+11)=c(k,4,5)
        E(1,nn2+17)=C(K,4,5)
      RW=FW(7)
      E(1,nn2+4)=c(k,5,5)
      E(1,nn2+15)=C(K,5,5)
      E(1,nn2+4+21)=-c(k+1,5,5)
      E(1,nn2+15+21)=-C(K+1,5,5)
      E(1,nn2+11+21)=-c(k+1,4,5)
      E(1,nn2+17+21)=-C(K+1,4,5)
      GOTO 999
C BC# 11 (TAU YZ+)-(TAU YZ-)=0
 14   E(1,nn2+11)=c(k,4,4)
      E(1,nn2+17)=C(K,4,4)
      RW=FW(8)
      E(1,nn2+4)=c(k,4,5)
      E(1,nn2+15)=C(K,4,5)
      E(1,nn2+4+21)=-c(k+1,4,5)
      E(1,nn2+15+21)=-C(K+1,4,5)
      E(1,nn2+11+21)=-c(k+1,4,4)
        E(1,nn2+17+21)=-C(K+1,4,4)
      GOTO 999
C BC #12 (SIGMA Y+)-(SIGMA Y-)=0
 15   CALL EMULT(K,2,RX,Z1)
```

```
        R(N)=-RX*1.0D00
       E(1,nn2+1)=C(K,1,2)
       RW=FW(4)
       E(1,nn2+3)=c(k,2,6)
       E(1,nn2+8)=C(K,2,6)
       E(1,nn2+10)=C(K,2,2)
       E(1,nn2+18)=C(K,2,3)
       E(1,nn2+3+21)=-c(k+1,2,6)
       E(1,nn2+8+21)=-C(K+1,2,6)
       E(1,nn2+10+21)=-C(K+1,2,2)
       E(1,nn2+1+21)=-C(K+1,1,2)
       E(1,nn2+18+21)=-C(K+1,2,3)
       CALL EMULT(K+1,2,RX,Z1)
       R(N)=R(N)+RX*1.0D00
       GOTO 999
C BC #13 (TAU YX+)-(TAU YX-)=0

 16    CALL EMULT(K,6,RX,Z1)
        R(N)=-RX*1.0D00
       E(1,nn2+1)=C(K,1,6)
       RW=FW(6)
       E(1,nn2+3)=c(k,6,6)
       E(1,nn2+8)=C(K,6,6)
       E(1,nn2+10)=C(K,2,6)
       E(1,nn2+18)=C(K,3,6)
       E(1,nn2+3+21)=-c(k+1,6,6)
       E(1,nn2+8+21)=-C(K+1,6,6)
       E(1,nn2+10+21)=-C(K+1,2,6)
       E(1,nn2+18+21)=-C(K+1,3,6)
       CALL EMULT(K+1,6,RX,Z1)
       R(N)=R(N)+RX*1.0D00
       E(1,nn2+1+21)=-C(K+1,1,6)
       GOTO 999
 999   CONTINUE
       DO 100 I=1,NP1*21
       E(1,I)=RW*E(1,I)*RW1
 100   CONTINUE
       R(N)=RW*R(N)*RW1
       RETURN
       END



C**********************************************************************************C

       SUBROUTINE TFUNC(K,Z1,Y1)
C**********************************************************************************

       IMPLICIt real*8 (A-H,O-Z)

       common/stuff/ z(3003),y(3003),THeta(100),ex(100,12),SO(100),
      +G3(19001),b(19001),wkarea(6),
      +fz(100),e11,e22,e33,g12,g13,g23,v12,v13,v23,
      +rts(100,3),RL(3,3),CKm(100,3),clm(100,3),cmm(100,3),
      +R(19001),qb(6,6),
      +c(100,6,6),FW(8),thick,width

       COMMON e(1,2100),PK(2,4,3003),PM(2,4,3003),PL(2,4,3003),
```

```
     +gl(1,3003),c11,C12,C13,C23,C22,C33,C66,c55,c44

        common/int/ n2(2,12,11),N3(19001),n4(100),N5(100,3),N6(2,15),
     +n5i(100),nb(100),nf(100,2),np31(10,100),n5j(100),
     +np3,np4,np3d,np4d,npl,nc,kn,nfz


      PI=3.14159265358979323846D00
      yy=Y1
      zz=Z1

C INITIALIZE P MATRICES

      DO 66 I=1,2
      DO 66 J=1,4
      DO 66 J1=1,NP3
      PK(I,J,J1)=0.
      PL(I,J,J1)= 0.
      PM(I,J,J1)=0.
 66   CONTINUE


      K1=1
      DO 19 KK=K,K+1


C---------------> LINEAR TERMS
      iu=0.
      iv=0.
      iw=0.
      i1=1
      in2=0
      i3=1
      I2=1
      I4=1
      DO 27 L=kn,3
      in2=0
      IF(N5(KK,L).EQ.0)GOTO 27
      NNX=N5(KK,L)
      kkk=1
      if(kk.eq.npl)kkk=2
      IF(NF(NC,KKk).EQ.2)NNX=NNX/2

      DO 1 I=1,NNX
      in2=in2+1
      cz=fz(in2)
      CY=(SQRT(abs(RTS(KK,L)))*CZ)
      IF(NF(NC,KKk).EQ.1.and.nc.ne.4)GOTO 31

      A=exp(-I2*CY*(yy+width))

      bB=exp(I2*CY*(yy-width))

      SNH=Bb-A
      SN=sin(I2*CZ*zz)
      CSH=bB+A
      CS=cos(I2*zz*CZ)
C- U
```

```
      PK(K1,2,I1+IU)=-SN*SNH*(CKM(KK,L))
C U,Y
      PK(K1,3,I1+IU)=-I2*CY*SN*CSH*
     +(CKM(KK,L))
C U,Z

      PK(K1,4,I1+IU)=-I2*CZ*CS*SNH
     +*(CKM(KK,L))
C-  V

      PL(K1,2,I1+IV)=-SN*SNH*(CLM(KK,L))
C  V,Y
      PL(K1,3,I1+IV)=-I2*CY*SN*CSH*
     +(CLM(KK,L))
C V,Z

      PL(K1,4,I1+IV)=-I2*CZ*CS*SNH
     +*(CLM(KK,L))
C W
      PM(K1,2,I1+IW)=
     +CS*CSH*cmm(kk,1)
C W,Y

      PM(K1,3,I1+IW)=I2*CY*CS*SNH*cmm(kk,1)
C W,Z

      PM(K1,4,I1+IW)=-I2*CZ*SN*CSH*cmm(kk,1)


      I1=I1+1


      IF(NF(NC,KKk).EQ.2)GOTO 31
      GOTO 1

 31   CONTINUE
      CZ=fz(in2)
      CY=(SQRT(abs(RTS(KK,L)))*CZ)

      A=exp(-I3*CY*(yy+width))

      Bb=exp(I3*CY*(yy-width))

      SNH=Bb-A
      SN=sin(I3*CZ*zz)
      CSH=bB+A
      SN=sin(CZ*zz*I3)
      CS=cos(I3*CZ*zz)

C  U
```

```
      PK(K1,2,I1+IU)=CS*SNH*(CKM(KK,L))

C U,Y
      PK(K1,3,I1+IU)=I3*CY*CS*CSH*
     +(CKM(KK,L))

C U,Z

      PK(K1,4,I1+IU)=-I3*CZ*SN*SNH*(CKM(KK,L))

C- V

      PL(K1,2,I1+IV)=CS*SNH*(CLM(KK,L))

C  V,Y
      PL(K1,3,I1+IV)=I3*CY*CS*CSH*
     +(CLM(KK,L))

C  V,Z

      PL(K1,4,I1+IV)=-I3*CZ*SN*SNH*(CLM(KK,L))


C W
      PM(K1,2,I1+IW)=
     +SN*CSH*cmm(kk,1)

C W,Y

      PM(K1,3,I1+IW)=I3*CY*SN*SNH*cmm(kk,1)

C W,Z

      PM(K1,4,I1+IW)=I3*CZ*CS*CSH*cmm(kk,1)



      I1=I1+1
c       I3=I3+1

 1    CONTINUE
 27   CONTINUE
      IF(KK.EQ.NP1)GOTO 999
      K1=2
 19   CONTINUE
 999  CONTINUE
      RETURN
      END

C**********************************************************************
      SUBROUTINE STIFF
C*********************************************************************
      IMPLICIt real*8 (A-H,O-Z)

      COMMON e(1,2100),PK(2,4,3003),PM(2,4,3003),PL(2,4,3003),
     +gl(1,3003),c11,C12,C13,C23,C22,C33,C66,c55,c44

      common/int/ N2(2,12,11),N3(19001),n4(100),N5(100,3),N6(2,15),
```

```
     +n5i(100),nb(100),nf(100,2),np31(10,100),n5j(100),
     +np3,np4,np3d,np4d,npl,nc,kn,nfz

      common/stuff/ z(3003),y(3003),THeta(100),ex(100,12),SO(100),
     +G3(19001),b(19001),wkarea(6),
     +fz(100),e11,e22,e33,g12,g13,g23,v12,v13,v23,
     +rts(100,3),RL(3,3),CKm(100,3),clm(100,3),cmm(100,3),
     +R(19001),qb(6,6),
     +c(100,6,6),FW(8),thick,width

      V32=V23*E33/E22
      V31=V13*E33/E11
      V21=V12*E22/E11
      DET=1-V12*V21-V31*V13-V23*V32-V21*V13*V32-V31*V12*V23
      C11=E11*(1-V32*V23)/DET
      C12=E22*(V12+V13*V32)/DET
      C13=E33*(V13+V12*V23)/DET

      C22=E22*(1-V31*V13)/DET
      C23=E22*(V32+V31*V12)/DET
      C33=E33*(1-V21*V12)/DET

      C44=G23
      C55=G13
      C66=G12
      WRITE(6,1)C11,C12,C13,C22,C23,C44,C55,C66
 1    FORMAT('C11=',E12.5,' C12=',E12.5,' C13=',E12.5/
     +' C22=',E12.5,' C23=',E12.5/' C44=',E12.5,
     +' C55=',E12.5,' C66=',E12.5)
      RETURN
      END

C*****************************************************************************C

      SUBROUTINE FLEx(q,a)
C*****************************************************************************C
C CALCULATE THE GROSS LAMINATE FLEXIBILITY MATRIX                             C
C*****************************************************************************C
        IMPLICIt real*8 (A-H,O-Z)

      real*8  q(6,6),a(6,6),qq(3,3)
      common/stuff/ z(3003),y(3003),THeta(100),ex(100,12),SO(100),
     +G3(19001),b(19001),wkarea(6),
     +fz(100),e11,e22,e33,g12,g13,g23,v12,v13,v23,
     +rts(100,3),RL(3,3),CKm(100,3),clm(100,3),cmm(100,3),
     +R(19001),qb(6,6),
     +c(100,6,6),FW(8),thick,width

      common/int/ N2(2,12,11),N3(19001),n4(100),N5(100,3),N6(2,15),
     +n5i(100),nb(100),nf(100,2),np31(10,100),n5j(100),
     +np3,np4,np3d,np4d,npl,nc,kn,nfz

      COMMON e(1,2100),PK(2,4,3003),PM(2,4,3003),PL(2,4,3003),
     +gl(1,3003),c11,C12,C13,C23,C22,C33,C66,c55,c44

      DO 45 I=1,3
      DO 45 J=1,3
      QQ(I,J)=0.
```

```
45    CONTINUE
      V21=E22*V12/E11

      Q11=E11/(1-V21*V12)
      Q22=E22/(1-V21*V12)
      Q12=V21*E11/(1-V21*V12)
       Q66=G12
      H=Thick/NP1
      PI=asin(1.)*2
      DO 1 L=1,NP1
      I=NP1-L+1
      CS=cos(THETA(L)*PI/180.)
      SN=sin(THETA(L)*PI/180.)
      QQ(1,1)=Q11*CS**4+2*(Q12+2*Q66)*SN**2*CS**2+Q22*SN**4
      QQ(2,2)=Q11*SN**4+2*(Q12+2*Q66)*SN**2*CS**2+Q22*CS**4
      qi= (Q11+Q22-4*Q66)*SN**2*CS**2+Q12*(SN**4+CS**4)
      QQ(2,1)=qi
      QQ(1,2)=qi

      QQ(3,3)=(Q11+Q22-2*q12-2*Q66)*SN**2*CS**2+Q66*(SN**4+CS**4)
      qi=(Q11-Q12-2*Q66)*SN*CS**3+(Q12-Q22+2*Q66)
     +*SN**3*CS
      QQ(1,3)=qi
      QQ(3,1)=qi
      qi=(Q11-Q12-2*Q66)*SN**3*CS+(Q12-Q22+2*Q66)*SN*CS**3
      QQ(3,2)=qi
      QQ(2,3)=qi

      DO 1 J=1,6
      DO 1 K=1,6
      IF(K.GT.3)THEN
      K1=K-3
      ELSE
      K1=K
      ENDIF
      IF(J.GT.3)THEN
      J1=J-3
      ELSE
      J1=J
      ENDIF
      IF(J.LT.4)THEN
      IF(K.LT.4)THEN
      Q(J,K)=Q(J,K)+QQ(J1,K1)*H*(2-NB(NC))
      ELSE
      Q(J,K)=Q(J,K)+QQ(J1,K1)*((I-np1/2*NB(NC))**2-
     +(I-1-np1/2*NB(NC))**2)
     +*H**2/2
      Q(J,K)=Q(J,K)*(NB(NC))
      ENDIF
      ELSE
      IF(K.LT.4)THEN
      Q(J,K)=Q(J,K)+QQ(J1,K1)*((I-np1/2*NB(NC))**2-
     +(I-1-np1/2*NB(NC))**2)*H**2/2
      Q(J,K)=Q(J,K)*(NB(NC))
      ELSE
      Q(J,K)=Q(J,K)+QQ(J1,K1)*(2-NB(NC))*
     +((I-np1/2*NB(NC))**3-(I-1-np1/2*NB(NC))**3)*H**3/3.
      ENDIF
      ENDIF
```

```
 1      CONTINUE
        IFAIL=0
        WRITE(6,122)((q(ii,kk),kk=1,6),ii=1,6)
122      format(///6(/6E12.5))
        CALL F01AAF(Q,6,6,A,6,WKAREA,ifail)
        print*,ifail
        WRITE(6,122)((a(ii,kk),kk=1,6),ii=1,6)
        DO 5 I=1,6
        if(np31(nc,1).ne.0)goto 4
        do 5 k=1,np1
        ex(k,I)=0.
 4      continue
        DO 5 J=1,6
        ex(k,I)=ex(k,I)+A(I,j)*SO(J)
 5      CONTINUE
        DO 12 I=1,NP1
        ex(i,12)=ex(i,6)
        ex(i,7)=ex(i,4)
        ex(i,8)=ex(i,5)
        ex(i,6)=ex(i,3)
        ex(i,3)=0.
        ex(i,4)=0.
        ex(i,5)=0.
        ex(i,9)=0.
        ex(i,10)=0.
        ex(i,11)=0.
 12     CONTINUE
        DO 10 I=1,NP1
        ex(i,3)=-(C(I,1,3)*ex(i,1)+C(I,2,3)*
       +ex(i,2)+C(I,3,6)*ex(i,6))/C(I,3,3)
        ex(i,9)=-(c(i,1,3)*ex(i,7)+c(i,2,3)*ex(i,8)+c(i,3,6)
       +*ex(i,12))/c(i,3,3)
  10    CONTINUE
        print*,((ex(i,j),j=1,12),i=1,np1)
        write(6,*)((ex(i,j),j=1,12),i=1,np1)
        RETURN
        END


C+++++++++++++++++++++++++++++++++++++++++++++++++++++++++++++++++++++++++++++++++C

        SUBROUTINE ROOTS(K)
C+++++++++++++++++++++++++++++++++++++++++++++++++++++++++++++++++++++++++++++++++C

        IMPLICIt real*8 (A-H,O-Z)

        common/stuff/ z(3003),y(3003),THeta(100),ex(100,12),SO(100),
       +G3(19001),b(19001),wkarea(6),
       +fz(100),e11,e22,e33,g12,g13,g23,v12,v13,v23,
       +rts(100,3),RL(3,3),CKm(100,3),clm(100,3),cmm(100,3),
       +R(19001),qb(6,6),
       +c(100,6,6),FW(8),thick,width

        COMMON e(1,2100),PK(2,4,3003),PM(2,4,3003),PL(2,4,3003),
       +g1(1,3003),c11,C12,C13,C23,C22,C33,C66,c55,c44

        common/int/ N2(2,12,11),N3(19001),n4(100),N5(100,3),N6(2,15),
       +n5i(100),nb(100),nf(100,2),np31(10,100),n5j(100),
       +np3,np4,np3d,np4d,np1,nc,kn,nfz
```

```
      AA=C(K,4,4)*C(K,6,6)*C(K,2,2)-
     +C(K,4,4)*C(K,2,6)**2.

      BB=C(K,6,6)*C(K,2,2)*C(K,3,3)+
     +C(K,4,4)**2.*C(K,6,6)+
     +C(K,4,4)*C(K,5,5)*C(K,2,2)+
     +2.*C(K,2,6)*(C(K,3,6) C(K,4,5))*(C(K,2,3)+C(K,4,4))-
     +C(K,6,6)*(C(K,2,3)+C(K,4,4))**2.-
     +C(K,2,2)*(C(K,3,6)+C(K,4,5))**2.-
     +C(K,3,3)*C(K,2,6)**2.-
     +2.*C(K,4,4)*C(K,4,5)*C(K,2,6)
      IF(AA.EQ.0)GOTO 999


      CC=C(K,6,6)*C(K,3,3)*C(K,4,4)+
     +C(K,2,2)*C(K,3,3)*C(K,5,5)+
     +C(K,4,4)**2.*C(K,5,5)+
     +2.*C(K,4,5)*(C(K,3,6)+C(K,4,5))*(C(K,2,3)+C(K,4,4))-
     +C(K,5,5)*(C(K,2,3)+C(K,4,4))**2.-
     +C(K,4,4)*(C(K,3,6)+C(K,4,5))**2.-
     +C(K,4,4)*C(K,4,5)**2.-
     +2.*C(K,3,3)*C(K,4,5)*C(K,2,6)

      DD=C(K,3,3)*C(K,5,5)*C(K,4,4)-
     +C(K,3,3)*C(K,4,5)**2.
      WRITE(6,100)AA,BB,CC,DD
 100  FORMAT(//'   CHARATERISTIC COEFFICIENTS ARE:',2(/4E12.5/))
      PRINT100,AA,BB,CC,DD,1.,BB/AA,CC/AA,DD/AA

      IF(THETA(K).NE.0.AND.THETA(K).NE.90)THEN
      cmm(k,1)=1.0
      cmm(k,2)=1.0
      cmm(k,3)=1.0
C----------> SEARCH FOR THE FIRST REAL ROOT

      Xx=0.D00
      DX=1.D7
      LL=1
 400  CONTINUE
      FX=DD+xX*(CC+xX*(BB+AA*xX))
      IF(abs(FX).GT.1E-15.OR.abs(DX).GT.1E-15)GOTO 404
      GOTO 826
 404  CONTINUE
      IF(abs(FX).EQ.0.)GOTO 826
      FPX=CC+Xx*(2.*BB+Xx*3.*AA)
      FPPX=BB*2.+6.*AA*xX
      DX=(FX*FPX)/(FPX**2.-FX*FPPX)
      Xx=Xx-DX
      LL=LL+1
      IF(LL.EQ.1000)PRINT 607
      IF(LL.EQ.1000)WRITE(6,607)
      GOTO 400
 826  CONTINUE
 607  FORMAT(/'   ROOT FINDER HAS PASSED 1000 ITERATIONS!!'/)
      PRINT606,FX,DX
      WRITE(6,606)FX,DX
 606  FORMAT(/' FX,DX='/2D12.5/)
      RTS(K,1)=xX
```

```
      CALL CHECK(K,1,R1,AA,BB,CC,DD)
C-----------> FIND OTHER TWO (POSSIBLY IMAGINARY!)

C-------> REDUCE BY SYNTHETIC DIVISION

      C2=BB+Xx*AA
      C3=CC+Xx*C2
      C4=DD+Xx*C3
      XR=-C2/2./AA
      XM=C2**2.-4.*AA*C3
      IF(XM.LT.0.)PRINT8801
      IF(XM.LT.0.)WRITE(6,8801)
      PRINT*,XR,XM
      WRITE(6,*)XR,XM
 8801 FORMAT(/'   ERROR !! IMAGINARY ROOT!!!!'/)
      RTS(K,2)=XR-sqrt(XM)/2./AA
      RTS(K,3)=XR+sqrt(XM)/2./AA
      CALL CHECK(K,1,R1,AA,BB,CC,DD)
      CALL CHECK(K,2,R2,AA,BB,CC,DD)
      CALL CHECK(K,3,R3,AA,BB,CC,DD)
c       PRINT80,R1,R2,R3
      WRITE(6,80)R1,R2,R3
 80   FORMAT(/'            RESIDUALS'/,3E22.14)


C-----------> SOLVE FOR EIGENVECTORS

      CALL EIGEN(K,1)

      WRITE(6,333)CLM(K,1),CKM(K,1),RTS(K,1)
 333  FORMAT(/'  CLM=',E12.5,' CKM=',E12.5,'  RTS=',E12.5)
      CALL EIGEN(K,2)

      WRITE(6,333)CLM(K,2),CKM(K,2),RTS(K,2)
      CALL EIGEN(K,3)

      WRITE(6,333)CLM(K,3),CKM(K,3),RTS(K,3)
      ELSE
      cmm(k,2)=1.0
      cmm(k,3)=1.0
      if(kn.eq.1)then
      clm(k,1)=0.0
      cmm(k,1)=0.0
      ckm(k,1)=1.0
      else
      clm(k,1)=0.0
      cmm(k,1)=0.0
      ckm(k,1)=0.
      endif
         RTS(K,1)=-C(K,5,5)/C(K,6,6)*1.0D00
      CKM(K,2)=0.0
      CKM(K,3)=0.0

      clm(k,1)=0.0
```

```
      WRITE(6,333)CLM(K,1),CKM(K,1),RTS(K,1)
      AA=C(K,2,2)*C(K,4,4)
      BB=C(K,2,2)*C(K,3,3)+C(K,4,4)**2-(C(K,2,3)+C(K,4,4))**2
      CC=C(K,3,3)*C(K,4,4)
      XM=SQRT(BB**2-4*AA*CC)
      XL=-BB/2/AA
      RTS(K,2)=XL+XM/2/AA
      RTS(K,3)=XL-XM/2/AA
      IF(RTS(K,2).EQ.RTS(K,3))N6(K,2)=0
      CLM(K,2)=(C(K,2,3)+C(K,4,4))*sqrt(abs(RTS(K,2)))/
     +(C(K,2,2)*RTS(K,2)+C(K,4,4))
      CLM(K,3)=(C(K,2,3)+C(K,4,4))*sqrt(abs(RTS(K,3)))/
     +(C(K,2,2)*RTS(K,3)+C(K,4,4))

      WRITE(6,333)CLM(K,2),CKM(K,2),RTS(K,2)

      WRITE(6,333)CLM(K,3),CKM(K,3),RTS(K,3)
      CALL EIGCHK(K,1)
      CALL EIGCHK(K,2)
      CALL EIGCHK(K,3)
      ENDIF
  999 RETURN
      END

C*****************************************************************
      SUBROUTINE CHECK(N,M,RR,AA,BB,CC,DD)
C*****************************************************************
      IMPLICIt real*8 (A-H,O-Z)

      common/stuff/ z(3003),y(3003),THeta(100),ex(100,12),SO(100),
     +G3(19001),b(19001),wkarea(6),
     +fz(100),e11,e22,e33,g12,g13,g23,v12,v13,v23,
     +rts(100,3),RL(3,3),CKm(100,3),clm(100,3),cmm(100,3),
     +R(19001),qb(6,6),
     +c(100,6,6),FW(8),thick,width

        common/int/ N2(2,12,11),N3(19001),n4(100),N5(100,3),N6(2,15),
     +n5i(100),nb(100),nf(100,2),np31(10,100),n5j(100),
     +np3,np4,np3d,np4d,npl,nc,kn,nfz

      Xx=RTS(N,M)
      RR=DD+Xx*(CC+Xx*(BB+Xx*AA))
      RETURN
      END
C*****************************************************************
      SUBROUTINE EIGEN(N,M)
C*****************************************************************
      IMPLICIt real*8 (A-H,O-Z)

      common/stuff/ z(3003),y(3003),THeta(100),ex(100,12),SO(100),
     +G3(19001),b(19001),wkarea(6),
     +fz(100),e11,e22,e33,g12,g13,g23,v12,v13,v23,
     +rts(100,3),RL(3,3),CKm(100,3),clm(100,3),cmm(100,3),
     +R(19001),qb(6,6),
     +c(100,6,6),FW(8),thick,width

      COMMON e(1,2100),PK(2,4,3003),PM(2,4,3003),PL(2,4,3003),
     +g1(1,3003),c11,C12,C13,C23,C22,C33,C66,c55,c44
```

```
        common/int/ N2(2,12,11),N3(19001),n4(100),N5(100,3),N6(2,15),
     +n5i(100),nb(100),nf(100,2),np31(10,100),n5j(100),
     +np3,np4,np3d,np4d,npl,nc,kn,nfz

      xX=RTS(N,M)
      ri=-(C(N,6,6)*xX+C(N,5,5))
      RL(1,1)=ri
      ri=-(C(N,2,6)*xX+C(N,4,5))
      RL(1,2)=ri

      RL(2,1)=ri
      ri=(C(N,3,6)+C(N,4,5))
      RL(1,3)=ri
       RL(3,1)=ri
      RL(2,2)=-(C(N,2,2)*xX+C(N,4,4))
      ri=(C(N,2,3)+C(N,4,4))
      RL(3,2)=ri
       RL(2,3)=ri
      RL(3,3)=-(C(N,4,4)*Xx+C(N,3,3))
      CLM(N,M)=(RL(1,2)*RL(1,3)/RL(1,1)-RL(2,3))/(RL(2,2)-
     +RL(1,2)**2./RL(1,1))
      CLM(N,M)=CLM(N,M)*sqrt(abs(RTS(N,M)))
      CKM(N,M)=(RL(1,2)*RL(2,3)/RL(2,2)-RL(1,3))/(RL(1,1)
     +-RL(1,2)**2./RL(2,2))
      CKM(N,M)=CKM(N,M)*sqrt(abs(RTS(N,M)))
      RTY=sqrt(abs(RTS(N,M)))

C-----------> ERROR CHECK

      ERR1=RL(1,1)*CKM(N,M)+RL(1,2)*CLM(N,M)+RL(1,3)*RTY
      ERR2=RL(2,1)*CKM(N,M)+RL(2,2)*CLM(N,M)+RL(2,3)*RTY
C NOTE NEGATIVE DUE TO IMAGINARY CONSTANTS IN RTY AND CLM,CKM
      ERR3=-RTY*RL(3,1)*CKM(N,M)-RTY*RL(3,2)*CLM(N,M)+RL(3,3)

      WRITE(6,400)ERR1,ERR2,ERR3
 400  FORMAT(/' GOV EQ RESIDUALS'/3E22.12/)
      RETURN
      END
C*****************************************************************
      SUBROUTINE EIGCHK(N,M)
C*****************************************************************
      IMPLICIt real*8 (A-H,O-Z)

      COMMON e(1,2100),PK(2,4,3003),PM(2,4,3003),PL(2,4,3003),
     +g1(1,3003),c11,C12,C13,C23,C22,C33,C66,c55,c44

        common/int/ N2(2,12,11),N3(19001),n4(100),N5(100,3),N6(2,15),
     +n5i(100),nb(100),nf(100,2),np31(10,100),n5j(100),
     +np3,np4,np3d,np4d,npl,nc,kn,nfz
      common/stuff/ z(3003),y(3003),THeta(100),ex(100,12),SO(100),
     +G3(19001),b(19001),wkarea(6),
     +fz(100),e11,e22,e33,g12,g13,g23,v12,v13,v23,
     +rts(100,3),RL(3,3),CKm(100,3),clm(100,3),cmm(100,3),
     +R(19001),qb(6,6),
     +c(100,6,6),FW(8),thick,width

      xX=RTS(N,M)
      ri=-(C(N,6,6)*xX+C(N,5,5))
      RL(1,1)=ri
```

```
      ri=-(C(N,2,6)*xX+C(N,4,5))
      RL(1,2)=ri
      RL(2,1)=ri
      ri=(C(N,3,6)+C(N,4,5))
      RL(1,3)=ri
      RL(3,1)=ri
      RL(2,2)=-(C(N,2,2)*xX+C(N,4,4))
      ri=(C(N,2,3)+C(N,4,4))
      RL(3,2)=ri
      RL(2,3)=ri
      RL(3,3)=-(C(N,4,4)*xX+C(N,3,3))
      RTY=sqrt(abs(RTS(N,M)))

C-----------> ERROR CHECK

      ERR1=RL(1,1)*CKM(N,M)+RL(1,2)*CLM(N,M)+RL(1,3)*RTY
      ERR2=RL(2,1)*CKM(N,M)+RL(2,2)*CLM(N,M)+RL(2,3)*RTY
C NOTE NEGATIVE DUE TO IMAGINARY CONSTANTS IN RTY AND CLM,CKM
      ERR3=-RTY*RL(3,1)*CKM(N,M)-RTY*RL(3,2)*CLM(N,M)+RL(3,3)

      WRITE(6,400)ERR1,ERR2,ERR3
 400  FORMAT(/' GOV EQ RESIDUALS'/3E22.12/)
      RETURN
       END
C*****************************************************************
      SUBROUTINE MATMULT(N1)
C*****************************************************************
      IMPLICIt real*8 (A-H,O-Z)

      common/stuff/ z(3003),y(3003),THeta(100),ex(100,12),S0(100),
     +G3(19001),b(19001),wkarea(6),
     +fz(100),e11,e22,e33,g12,g13,g23,v12,v13,v23,
     +rts(100,3),RL(3,3),CKm(100,3),clm(100,3),cmm(100,3),
     +R(19001),qb(6,6),
     +c(100,6,6),FW(8),thick,width
      COMMON e(1,2100),PK(2,4,3003),PM(2,4,3003),PL(2,4,3003),
     +g1(1,3003),c11,C12,C13,C23,C22,C33,C66,c55,c44
        common/int/ N2(2,12,11),N3(19001),n4(100),N5(100,3),N6(2,15),
     +n5i(100),nb(100),nf(100,2),np3l(10,100),n5j(100),
     +np3,np4,np3d,np4d,npl,nc,kn,nfz
      NN2=0
      DO 34 I=1,NP3
      G1(1,I)=0.000
 34   CONTINUE
      IF(N1.EQ.1)GOTO 109

      DO 1 I=1,N1-1
      NN2=NN2+(N5(I,1)+N5(I,2)+N5(I,3))+NP3L(NC,I)
 1    CONTINUE
 109   CONTINUE
      I1=1
      DO 2 K=N1,N1+1

      I6=1
      if(np3l(nc,k).eq.0)goto 303
      DO 302 L=1,NP3L(NC,K)
      DO 361 J=1,4
      G1(1,NN2+I6)=G1(1,NN2+I6)+E(1,(K-1)*21+J)
     +*PK(I1,J,L)
```

```
    ++E(1,(K-1)*21+J+7)*PL(I1,J,L)+E(1,(K-1)*21+14+J)
    +*PM(I1,J,L)
361       CONTINUE
      I6=I6+1
302    CONTINUE
303    continue

      NN2=NN2+NP3L(NC,K)
      NN1=(N5(K,1)+N5(K,2)+N5(K,3))
      IF(NN1.EQ.0)GOTO 33
      DO 3 I=1,NN1
      DO 4 J=1,4
         II=I+NP3L(NC,K)
      G1(1,NN2+I)=G1(1,NN2+I)+E(1,(K-1)*21+J)*PK(I1,J,II)
     ++E(1,(K-1)*21+J+7)*PL(I1,J,II)+
     +E(1,(K-1)*21+J+14)
     +*PM(I1,J,II)
4     CONTINUE
3     CONTINUE
33    CONTINUE
      NN2=NN2+NN1
      I1=2
      IF(K.EQ.NP1)GOTO 999
2     CONTINUE
999   RETURN
      END
c*********************************************************************
      SUBROUTINE EMULT(K,N,RX,Zz)
c*********************************************************************
      IMPLICIt real*8 (A-H,O-Z)

      common/stuff/ z(3003),y(3003),THeta(100),ex(100,12),S0(100),
     +G3(19001),b(19001),wkarea(6),
     +fz(100),e11,e22,e33,g12,g13,g23,v12,v13,v23,
     +rts(100,3),RL(3,3),CKm(100,3),clm(100,3),cmm(100,3),
     +R(19001),qb(6,6),
     +c(100,6,6),FW(8),thick,width

      COMMON e(1,2100),PK(2,4,3003),PM(2,4,3003),PL(2,4,3003),
     +g1(1,3003),c11,C12,C13,C23,C22,C33,C66,c55,c44

      common/int/ N2(2,12,11),N3(19001),n4(100),n5(100,3),N6(2,15),
     +n5i(100),nb(100),nf(100,2),np31(10,100),n5j(100),
     +np3,np4,np3d,np4d,np1,nc,kn,nfz

      RX=0
      DO 1 I=1,6
      RX=RX+C(K,N,I)*(Ex(k,I)+Zz*Ex(k,I+6))
1     CONTINUE
      RETURN
      END

c***************************************************************
       subroutine givens(mt,md,n,gx,gy)
c***************************************************************
      implicit real*8(a-h,o-z)
      real*8 gx(801,3003),gy(3003,501)
      integer md(100),mt(100),n(100)
      common/stuff/ z(3003),y(3003),THeta(100),ex(100,12),S0(100),
```

```
+g3(19001),b(19001),wkarea(6),
+fz(100),e11,e22,e33,g12,g13,g23,v12,v13,v23,
+rts(100,3),RL(3,3),CKm(100,3),clm(100,3),cmm(100,3),
+R(19001),qb(6,6),
+c(100,6,6),FW(8),thick,width

 common/int/ N2(2,12,11),N3(19001),n4(100),N5(100,3),N6(2,15),
+n5i(100),nb(100),nf(100,2),np31(10,100),n5j(100),
+np3,np4,np3d,np4d,npl,nc,kn,nfz

  i0=0
  k0=0
  i2=0
  k2=0

  do 10 l1=1,npl

  mdx=0
  if(l1.gt.1)mdx=md(l1-1)

  do 20 k1=1,mt(l1)
  k=k0+k1
  ik=int((k-.1)/n(1))*n(1)
  kxx=k-i0-1
  kx=k-k2

  if(i0+n(l1).le.k-1)kxx=n(l1)

  do 21 i1=1,kxx

  i=i0+i1
  ii=int((i-.1)/n(1))*n(1)
  iiy=i-ii
  iky=i-ik
  if(k.gt.i)then
  gki=gx(kx,i)
  else
  gki=gy(k,iky)
  endif
  if(gki.eq.0.)then
  cc=1.
  ss=0.
  else
  if(abs(gki).ge.abs(gy(i,iiy)))then
  t=gy(i,iiy)/gki
  ss=1./sqrt(1+t**2)
  cc=ss*t
  else

     t=gki/gy(i,iiy)
     cc=1./sqrt(1+t**2)
     ss=cc*t

   endif
   endif

     do 22 j1=i,i0+n(l1)
     j=j1
     jky=j-ik
```

```
      jiy=j-ii
      v=gy(i,jiy)

      if(k.gt.j)then
      w=gx(kx,j)
      else
      w=gy(k,jky)
      endif

      gy(i,jiy)=cc*v+ss*w

      if(k.gt.j)then

      gx(kx,j)=-ss*v+cc*w
      else
      gy(k,jky)=-ss*v+cc*w
      endif
22    continue

       ri=r(i)
       r(i)=cc*r(i)+ss*r(k)
       r(k)=-ss*ri+cc*r(k)
21     continue
20     continue

   if(l1.eq.np1)goto 10
   k0=k0+mt(l1)

   do 30 k1=1,md(l1)
   k=k0+k1
   ik=int((k-.1)/n(1))*n(1)
   kxx=k-i0-1
   if(i0+n(l1)+n(l1+1).le.k-1)kxx=n(l1)+n(l1+1)

   do 31 i1=1,kxx

   if(i1.gt.n(l1))then
   kx=k-k2-mt(l1)-mdx
   else
   kx=k-k2
   endif


   i=i0+i1
   ii=int((i-.1)/n(1))*n(1)
   iiy=i-ii
   iky=i-ik
   if(k.gt.i)then

   gki=gx(kx,i)
   else
   gki=gy(k,iky)
   endif
   if(gki.eq.0.)then
   cc=1.
   ss=0.
   else
   if(abs(gki).ge. abs(gy(i,iiy)))then
   t=gy(i,iiy)/gki
```

```
      ss=1./sqrt(1+t**2)
      cc=ss*t
       else

         t=gki/gy(i,iiy)
         cc=1./sqrt(1+t**2)
         ss=cc*t

       endif
       endif

         do 32 j1=i,i0+n(l1)+n(l1+1)
          j=j1
          jiy=j-ii
          jky=j-ik

          v=gy(i,jiy)

          if(k.gt.j)then
          kx=k-k2
          if(j.gt.i0+n(l1))kx=k-k2-mt(l1)-mdx
          w=gx(kx,j)
          else
          w=gy(k,jky)
          endif

          gy(i,jiy)=cc*v+ss*w

          if(k.gt.j)then
          gx(kx,j)=-ss*v+cc*w
          else
          gy(k,jky)=-ss*v+cc*w
          endif

 32       continue
          ri=r(i)
          r(i)=cc*r(i)+ss*r(k)
          r(k)=-ss*ri+cc*r(k)
 31       continue
 30       continue
          i0=i0+n(l1)
          k0=k0+md(l1)
          k2=k2+mt(l1)+mdx
 10        continue


c-------> backwards substitution

              i0=np1
              nx=np3
              do 60 i=np3,1,-1
              b(i)=r(i)
              ii=int((i-.1)/n(1))*n(1)
              do 50 j=i+1,nx
              b(i)=b(i)-gy(i,j-ii)*b(j)
 50           continue
              if(nx-i.ge.n(i0)-1.and.i0.ne.np1)then
              nx=nx-n(i0)
              i0=i0-1
```

```
            else
            endif

            if(nx-i.ge.n(np1)+n(np1-1)-1.and.i0.eq.np1)then
            nx=nx-n(np1)
            i0=i0-1
            else
            endif

            b(i)=b(i)/gy(i,i-ii)
60          continue
           return
           end
```

```
************** MWR INPUT FILE ***********************
2     : NP1---- HALF OF # OF LAYERS IN HALF LAMINATE
 51   : NPTY
 51   : NPTZ
60 60 :N5I # TERMS IN SERIES/ROOT/LAYER 1ST EVEN IF NC=1
********* LAY-UP ANGLES ********************
-45 45  90 0 30 0 90 30 -30 0 90 30 -30 90 45 -45 45 -45 45 -45 45 0 90 0 90
4.0   : WIDTH
.05   :SK DISTRIBUTION PARAMETER FOR Y AXIS
1.0   : THICKNESS
1.0E-6: UNIFORM AXIAL STRAIN AT CENTER
.0 0.0 0.0 1.0 .0 .0    load vector nx,ny,nxy,mx,my,mxy
21.   : E11
1.55  : E22
1.55  : E33
 .31  : V12
0.49  : V23
 .31  : V13
.65   : G12
0.52  : G23
0.65  : G13
0     : FLAG FOR WEIGHTING (1 FOR WEIGHTING, 0 NOT)
3     : CASE NUMBER SEE PROGRAM HEADER   NC
********* WEIGHTING VALUES FOR U,V,W,SY,SZ,TXY,TXZ,TYZ ******
1.0E2,1.0E2,1.0E2,1.,1.,1.,1.,1.
0     :MWRSOLV/0 FOR COLL/2 FOR CG/3 FOR BOTH
 00 00 00 :ADDITIONAL DOF FOR CG METHOD
1.4   :ffz scaling for frequencies
1.00  :exponent for frequencies (set to 1)
0     : ncoat  1 for edge coating, 0 for free edge
.05   : cthick thickness of coating
.12   .3  : elastic modulus and poisson ratio for coating
9     : number of points across the coating thickness
200   : number of points on coating face
0     : maxcal max no of iterations
```

Input File for Mwr Program: MWR.DAT

```
((N2(K  I   J)  J=1   11)  I=1   12)  K=1   2)
   1  2  3  0  0  0  0  0  0  0  0
   4  5  6  0  0  0  0  0  0  0  0
   6  7  8  0  0  0  0  0  0  0  0
   9 10 11 12 13 14  0  0  0  0  0
   4  5  6  7  8  0  0  0  0  0  0
   9 10 11  0  0  0  0  0  0  0  0
   1  2  0  0  0  0  0  0  0  0  0
   3  0  0  0  0  0  0  0  0  0  0
   4  0  0  0  0  0  0  0  0  0  0
   7  8  0  0  0  0  0  0  0  0  0
  11 12  0  0  0  0  0  0  0  0  0
   9 10 11  0  0  0  0  0  0  0  0
   1  2  3  0  0  0  0  0  0  0  0
   4  6  0  0  0  0  0  0  0  0  0
   7  6  0  0  0  0  0  0  0  0  0
  11 12 10 14  0  0  0  0  0  0  0
   4  6  7  0  0  0  0  0  0  0  0
  11 10  0  0  0  0  0  0  0  0  0
   1  2  0  0  0  0  0  0  0  0  0
   3  0  0  0  0  0  0  0  0  0  0
   4  0  0  0  0  0  0  0  0  0  0
   7  0  0  0  0  0  0  0  0  0  0
  11 12  0  0  0  0  0  0  0  0  0
  10 11  0  0  0  0  0  0  0  0  0
((N6(K   J)   J=1   15)  K=1   2)
   3  3  3  6  5  3  2  1  1  2  2  3  0  0  0
   3  2  2  4  3  2  2  1  1  1  2  2  0  0  0
Q
   0.  0.  0.  0.  0.  0.  0.  0.  0.  0.  0.  0.  0.  0.  0.  0.  0.  0.
   0.  0.  0.  0.  0.  0.  0.  0.  0.  0.  0.  0.  0.  0.  0.  0.  0.  0.
   CKM
   0.  0.  0.  0.  0.  0.  0.  0.  0.  0.  0.  0.  0.  0.  0.
   CLM
   0.  0.  0.  0.  0.  0.  0.  0.  0.  0.  0.  0.  0.  0.  0.
   RL
   0.  0.  0.  0.  0.  0.  0.  0.  0.
  RTS
   0.  0.  0.  0.  0.  0.  0.  0.  0.  0.  0.  0.  0.  0.  0.
(NB(I)  I=1   10)
 0  0  1  0  0  0  0  0  0  0
  ((NP3L(I   J)  J=1   6)  I=1   10)
   0  0  0  0  0  0  0  0  0  0  0  0  0  0  0  0  0  0
   0  0  0  0  0  0  0  0  0  0  0  0  0  0  0  0  0  0
   0  0  0  0  0  0  0  0  0  0  0  0  0  0  0  0  0  0
   0  0  0  0  0  0
(((NF(I  J  K)  J=1   3)  K=1   6)  I=1   10)
   2  1
   2  2
   2  2
   2  1
   2  2
   0  0
   0  0
   0  0
   0  0
   0  0
```

ex
0. 0. 0. 0. 0. 0. 0. 0. 0. 0. 0. 0.
0. 0. 0. 0. 0. 0. 0. 0. 0. 0. 0. 0.